COMMUNICATIONS OF THE GEOLOGICAL SURVEY OF NAMIBIA

Volume 27

MINISTRY OF MINES AND ENERGY

2024

GEOLOGICAL SURVEY OF NAMIBIA

MINISTRY OF MINES AND ENERGY

Deputy Permanent Secretary: Gloria Simubali

COMMUNICATIONS OF THE GEOLOGICAL SURVEY OF NAMIBIA

VOLUME 27

Reviewers: T. Füllgraf, H. Mocke,
P. Schreck, U. M. Schreiber, G. Shaanika

Manuscript handling: U. M. Schreiber, M. Pickford

Obtainable from
Geological Survey of Namibia
Private Bag 13297, Windhoek, Namibia
and
https://www.mme.gov.na/publications/?designation=gsn

ISSN 1026-2954

COMMUNICATIONS OF THE GEOLOGICAL SURVEY OF NAMIBIA

VOLUME 27
2024

CONTENTS

Cover image: View into the Fish River Canyon, farm Hobas (Photo: P. Macey)

Foreword

Apart from a number of original research papers, Volume 27 of the "Communications of the Geological Survey of Namibia" features such varied items as a couple of post-graduate studies carried out at the University of Namibia, a review of one of the Geological Survey's flagship projects of recent years and a report on a novel initiative to improve geoscience education and outreach. In addition to these current topics, in this issue we would like posthumously to pay our respects to an eminent colleague and for many years fixture of the Namibian geological scene, with an exposition on a little-known aspect of Namibia's multi-faceted geology lately discovered among his manuscripts. A tribute to Professor Klaus Weber of Göttingen, Germany, and an introduction to this so far unpublished part of a lifetime's work spent largely among the lower regions of the stratigraphic column, has kindly been provided by J. Walter and T. Becker (Füllgraf), themselves connoisseurs of Namibian geology.

Ute Schreiber, Martin Pickford (Editors)
Windhoek, July 2024

Professor Klaus Weber *4. 12. 1936 † 18. 10. 2010

When Prof Dr Klaus Weber passed away in October 2010 at the age of 73, the geosciences lost a passionate and, up to the end, curious disciple who during his career initiated and played a key role in many important research projects. His work on the Rhenish Massif of western Germany, the German Continental Deep Drilling Programme (KTB), and, above all, the numerous research projects he headed in Namibia are amongst the most important milestones of his professional career. Even after his retirement from the Chair of Structural Geology and Geodynamics at the Georg-August-University of Göttingen, he remained committed to the geosciences. Never loath to explore new fields or propound unorthodox and "original" theories, he now widened his scope beyond structural geology and the Proterozoic.

Klaus Weber was introduced to the geology of Namibia and in particular to the Southern Margin of the Damara Orogen by Henno Martin during a joint research trip in 1975, as part of the University of Göttingen's Special Research Programme entitled "Earth's Crust" (SFB 48). This excursion turned out to be a crossroads, both scientifically and personally, for Namibia became his favourite destination and stamping ground. Henceforth, he initiated numerous research programmes on the geodynamic development of the Damara Orogen, supervising more than fifteen mapping projects as part of diploma (M.Sc.) and doctoral theses, which are now to be made available to the Geological Survey of Namibia.

Upon retiring, Klaus Weber's special passion for the Gamsberg motivated him to carry out the preliminary investigation of the supracrustal deposits of the Gamsberg Plateau presented in this volume - thus continuing the work on the Gamsberg earthquake cracks by Reinhold Wittig, another Göttingen geology guru. Initially, the results of this study, which sheds new light on the composition and stratigraphy of the younger rocks forming the plateau of this ancient granitic landmark, were shared only with a small but enthusiastic community of amateur and professional geologists on scientific excursions Klaus Weber guided in Namibia after his retirement, occasionally in rather audacious circumstances.

The original German text of this excursion guide has been translated into English to make it accessible to a wider readership, while annotated Google Earth images and a locality map were appended to provide a better overview of the study area. By publishing this part of his latter activities, we would like to commemorate Klaus, who was an important mentor for many Göttingen graduates of our generation, and who in the course of a distinguished career made a significant contribution to Namibian geology.

Jens Walter and Thomas Becker (Füllgraf), January 2024

The sedimentary and volcanic rocks of the Gamsberg Plateau

K. Weber †2010

(translated and modified extract from unpublished excursion guide, 2003)

Abstract :- This excursion guide describes and proposes an interpretation of hitherto little or unknown sedimentary and volcanic rocks of probably Early Cretaceous age, which overlie Mesoproterozoic granites on the Gamsberg Plateau, together with their major element composition and a preliminary radiometric age. Much of this erstwhile thick package of supracrustal rocks, for which the name Gamsberg Plateau Formation is suggested, has subsequently been eroded, and only isolated remnants and scree cover are available for study today. Furthermore, clays of probably Neogene to Quaternary age, which in turn overlie the quartzites and rhyolites, their mineralogy and pollen content are described.

Keywords :- Gamsberg, Quartzite, Rhyolite, Earthquake fissures, Clay, Neogene, Early Cretaceous

To cite this paper :- Weber, K. 2024. Sediments and volcanic rocks of the Gamsberg Plateau. *Communications of the Geological Survey of Namibia*, **27**, 2-18.

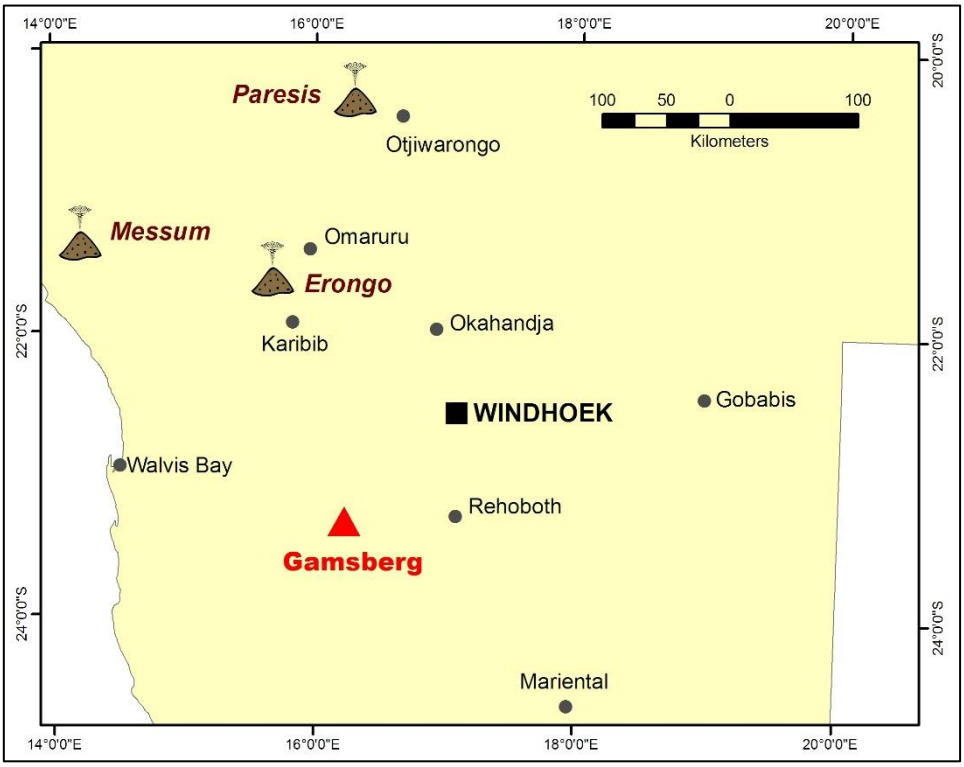

Figure 1. Locality map of central Namibia showing the relative positions of Gamsberg and Early Cretaceous eruptive centres of felsic volcanism (Erongo, Messum and Paresis)

Gamsberg quartzite

Gamsberg is a 2347 m high table mountain in central Namibia (Fig. 1), whose plateau is formed by quartzite (Fig. 2). These rocks have been lithostratigraphically correlated with the ca. 200 Ma Lower Jurassic Etjo Formation, which is similarly developed at Mount Etjo and Waterberg. However, for a number of reasons explained below, it seems more likely now that the Gamsberg quartzite is a correlate of the Twyfelfontein Formation of the Lower Cretaceous Etendeka Group in northwestern Namibia.

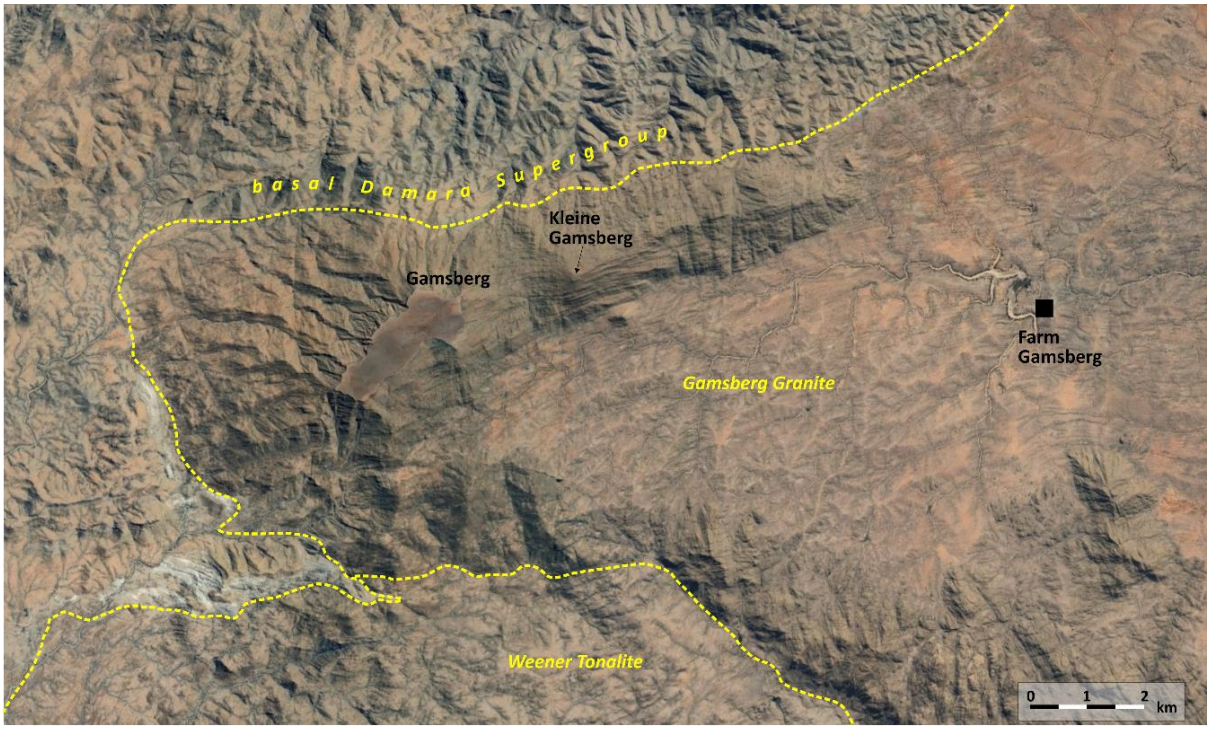

Figure 2. Aerial view of the Gamsberg area: the Gamsberg quartzite unconformably overlies Mesoproterozoic ca. 1.2 Ga granite gneiss of the Gamsberg Suite. The basal Damara metasediments west of the Gamsberg are outlined by bright bands of folded marble of the Samara Formation, while the pronounced foliation in the vicinity of Gamsberg and Klein Gamsberg results from differential weathering and erosion of the numerous intercalated, ca. 30° NW-dipping amphibolite dykes transposed parallel to the gneissic foliation.

At its base, the Gamsberg quartzite is developed as a medium- to coarse-grained, limnic-fluviatile, matrix-supported, conglomeratic sandstone with angular to poorly rounded, centimetre-sized clasts of the underlying Gamsberg granite and vein quartz. Apart from mudcracks (Fig. 3A), newly discovered trace fossils in the form of tubes and burrows (Fig. 3B) are present in places. There are also vertical tubular casts and carbonate-cemented cylindrical forms (Fig. 3C), which indicate temporary plant growth. Towards the hanging wall, the limnic-fluviatile sandstone changes into aeolian sandstone with large foresets typical of dunes (Fig. 3E). Numerous casts of gypsum crystals (Fig. 3D), such as those found in the Namib today, suggest an arid climate during the deposition of the upper levels of the Gamsberg quartzite, although the origin of the sulphur is unclear. Like many other sandstones formed in desert climates, the quartzite at the top of Gamsberg is strongly silicified (Fig. 3F), which probably contributed to the fact that this plateau right on the edge of the escarpment has survived to this day.

Gamsberg volcanic rocks

However, the intense silicification of the Gamsberg quartzite cannot be ascribed solely to palaeoclimatic conditions. In several places the sedimentary rocks are overlain by remnants of felsic volcanics, which to date had been unknown from the Gamsberg Plateau. They are very SiO_2-rich rhyolites, whose silica content probably also results from secondary silicification by a thicker package of originally overlying, now eroded, felsic volcanics.

The Gamsberg volcanic rocks are observed at the margins of three pans in the central and north-eastern parts of the plateau; in the satellite image they stand out in colour and texture from their surroundings (Fig. 4). In the interior of the pans they are covered by clays of Neogene age, or occur as angular fragments and blocks in and on top of these overlying, limnic-fluviatile deposits.

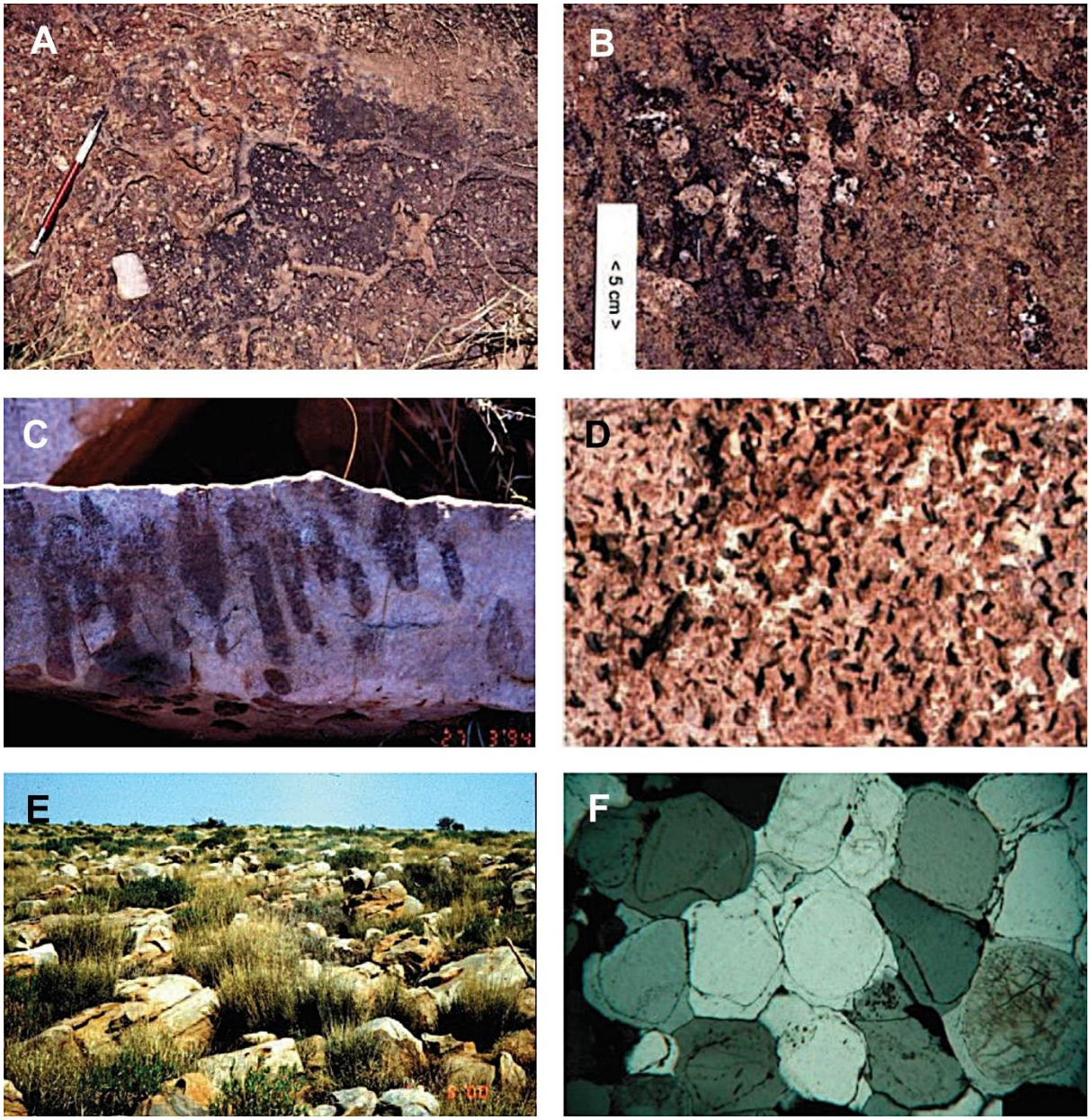

Figure 3. A) Mudcracks in the basal conglomeratic Gamsberg quartzite. In the lower left corner a large, rectangular vein quartz fragment can be seen; B) Trace fossils (burrowing and digging traces of worms, crabs or mussels) in the basal, limnic-fluviatile part of the Gamsberg quartzite; C) Dark, cylindrical forms of carbonate-rich sandstone, with a diameter of 1 to 2 cm, probably representing plant stalks. The colour results from weathering and the oxidation of traces of iron; D) Gypsum casts in Gamsberg quartzite (image width: 6 cm); E) Fossil dune cross-stratification in Gamsberg quartzite; F) Photomicrograph of the Gamsberg quartzite showing well-rounded quartz grains with opaque rims (iron oxides and hydroxides) typical of aeolianites. The grains are cemented by diagenetic quartz (image width: 3 mm).

The most conspicuous volcanic rock type is an autoclastic and/or hyaloclastic breccia (Figs 5, 6). Fine-grained, laminated pyroclastics locally show flow-banding (Figs 5A, B) or flow-folding (Fig. 5C). Flow-lamination is generally poorly developed, but in places can be very pronounced. All the Gamsberg pyroclastic deposits are extremely fine-grained and free of macroscopic pyro- and lithoclasts, suggesting deposition distal to the eruptive centre(s). The auto- or hyaloclastic breccias and the fluidal fabric of the silicified rhyolites indicate high temperatures of the fine-grained volcanic material, resulting in flow-deformation during or immediately after deposition. These deposits are interpreted as rheomorphic vitrified ash tuffs whose flow-foliation originated at an advanced stage of welding (McPhie *et al*., 1993). Further

movement during subsequent cooling is recorded by synthetic Riedel shear planes, which developed under semi-ductile conditions (Fig. 5). These rocks and structures form in the internal, hottest parts of pyroclastic layers, while autoclastic and hyaloclastic breccias develop at the cooler surfaces and in aquatic environments, respectively.

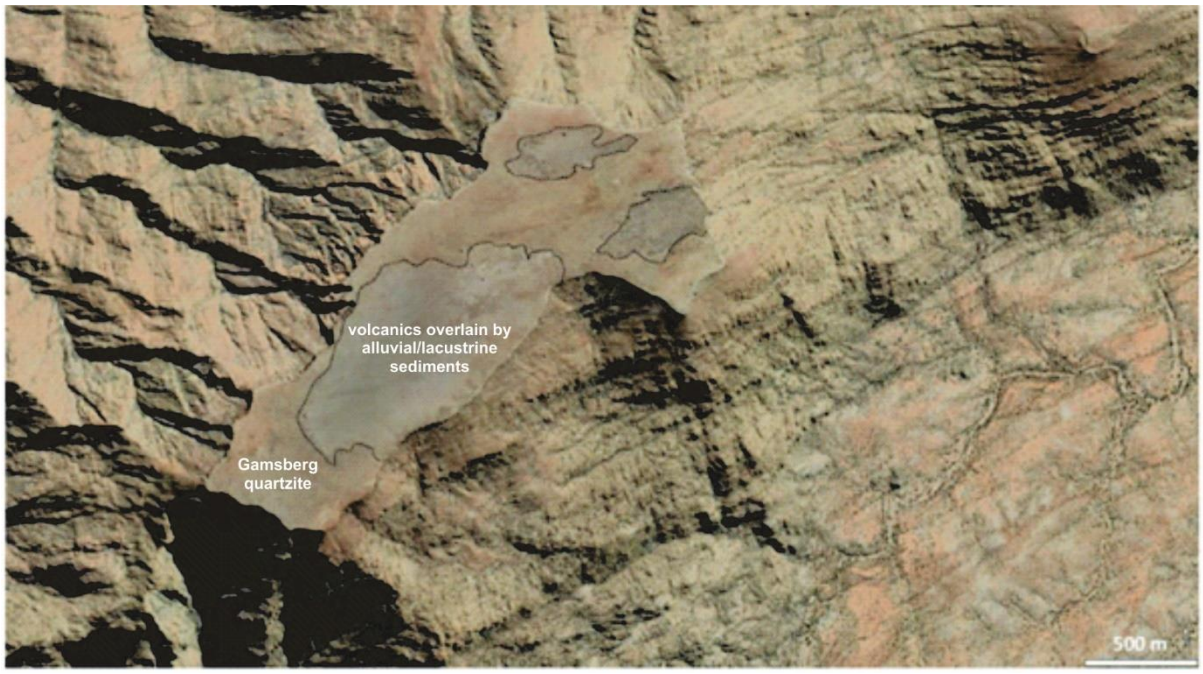

Figure 4. Satellite image (Google Earth) showing the distribution of rhyolitic volcanic rocks on the Gamsberg plateau, overlying Gamsberg quartzite and covered by Neogene limnic-alluvial sediments

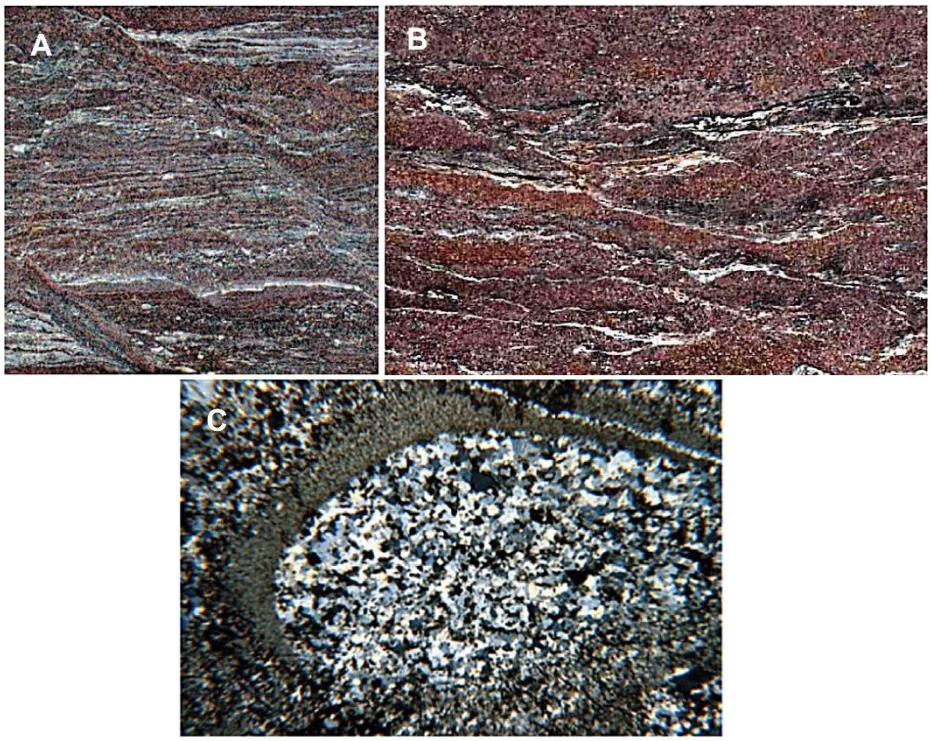

Figure 5. A-B) Gamsberg rhyolite with high-temperature flow-banding and Riedel shear planes developed under semi-ductile conditions during cooling. The light-coloured layers are rich in devitrified volcanic glass (pumice), image width B: 6 cm; C) Drop-shaped fluidal structure in Gamsberg rhyolite. The dark layer consists of devitrified glass (Xn λ/4, image width: 4.5 mm).

The Gamsberg volcanics often show lithophysae concentrically filled with chalcedony and clear idiomorphic quartz crystals up to several centimetres in size. In addition, nests occur of millimetre-sized, translucent actinolite (Fig. 7E), indicating temperatures of around 300°C in the meteoric fluids circulating through the volcanic rock. Patchy, post-magmatic actinolite is also found in less strongly welded, more porous parts (Fig. 7C), and in the matrix of the rhyolitic pyroclastic deposits (Fig. 7D). The relatively high post-magmatic temperature implies a considerable thickness of the volcanic pile that once must have overlain the Gamsberg quartzite; it is also responsible for the fine, recrystallised grain size, sericitisation of the glass fragments (Fig. 8), and the absence of Y-cracks in thin section. These conclusions are consistent with the result of apatite fission track analysis, according to which some 2000 m of Mesozoic rocks once lay on top of the Gamsberg granite.

In one rhyolite sample (Fig. 9) with a relatively weak flow texture, red-brown veinlets occur parallel to the flow. According to petrographic and geochemical analysis, the vein consists of silicified rhyolite which does not differ from the host rhyolite in terms of major and trace element composition. The development of such veins with short apophyses into and containing small fragments of the lighter-coloured host rhyolite, argues for an intrusive association, which, however, to my knowledge is unusual in rheomorphic welded tuffs, and cannot be readily explained.

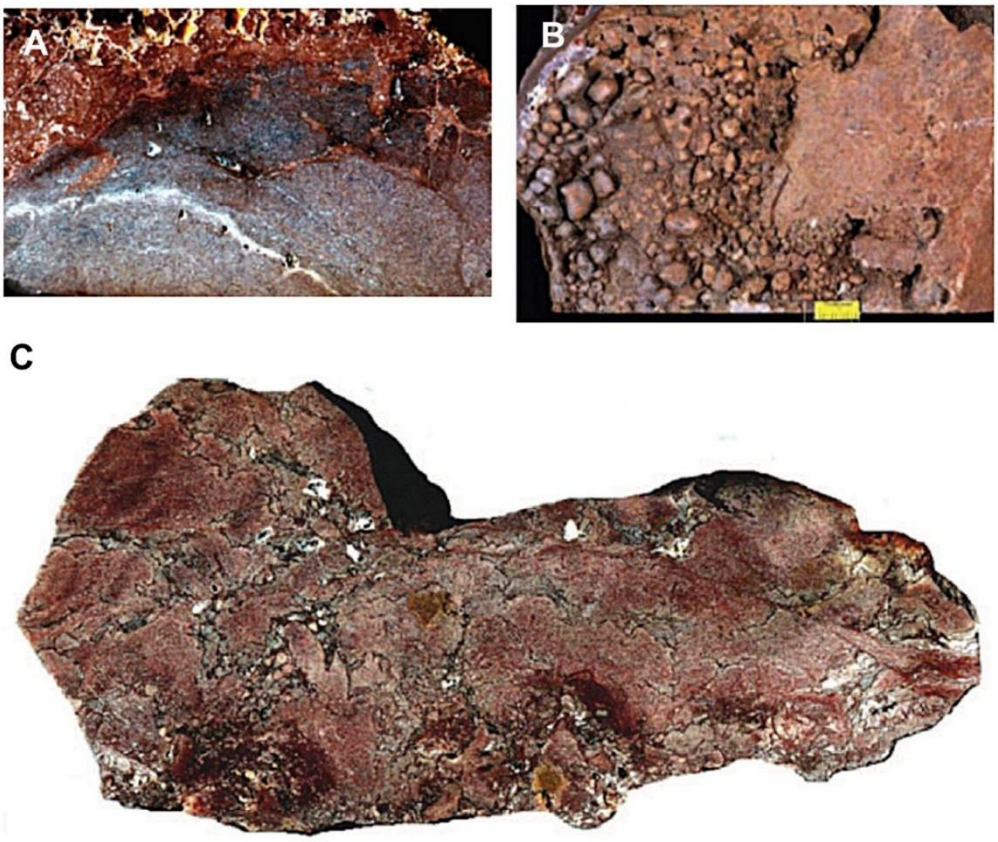

Figure 6. A) Auto- or hyaloclastic brecciation at the surface of Gamsberg rhyolite under a strongly altered pumice-like breccia (image width: 15 cm); B) Surface of an auto- or hyaloclastic breccia; C) Auto- or hyaloclastic breccia with quartz-mineralised vugs (white; sample length: 24 cm)

The volcanic rocks are underlain by one to two metre-thick, strongly silicified tuffitic sandstones, which in turn grade into the Gamsberg quartzite. The tuffitic sandstones are medium-grey when fresh and beige to reddish-brown on weathered surfaces. They are usually massive rocks that tend to show woolsack weathering, and because of their well-rounded (aeolian) grains and intense silicification have been considered part of the Gamsberg quartzite. However, petrographic studies show them to have a significantly higher feldspar content than

the underlying quartzite, and also a high proportion of extremely fine-grained crystallised pumice and glass fragments; this is also expressed by geochemical composition (see 'Geochemistry of the Gamsberg rocks'). The proportion of clastic quartz grains in these tuffitic sediments varies from very high to very low, resulting in a complete transition from silicified tuffitic sandstone to silicified rhyolitic tuff, with scattered aeolian sand grains. The tuffitic sandstones presumably stem from aquatic mixing of aeolian sands and rhyolitic glass-ash tuffs, which is supported by the absence of aeolian cross-bedding in these epiclastic sediments. It is suggested that the aeolian sand grains originate from dunes in the area of the phreatic explosion and were transported together with the fine-grained ignimbrites to the place of deposition. In the Etendeka area, such aeolian sediments interlayered with volcanic rocks are common (Jerram *et al*., 2000), although they have not yet been reported from the rhyolitic volcanics of the Erongo Mountain, which is thought to be the probable source region of the Gamsberg rhyolites (Fig. 1).

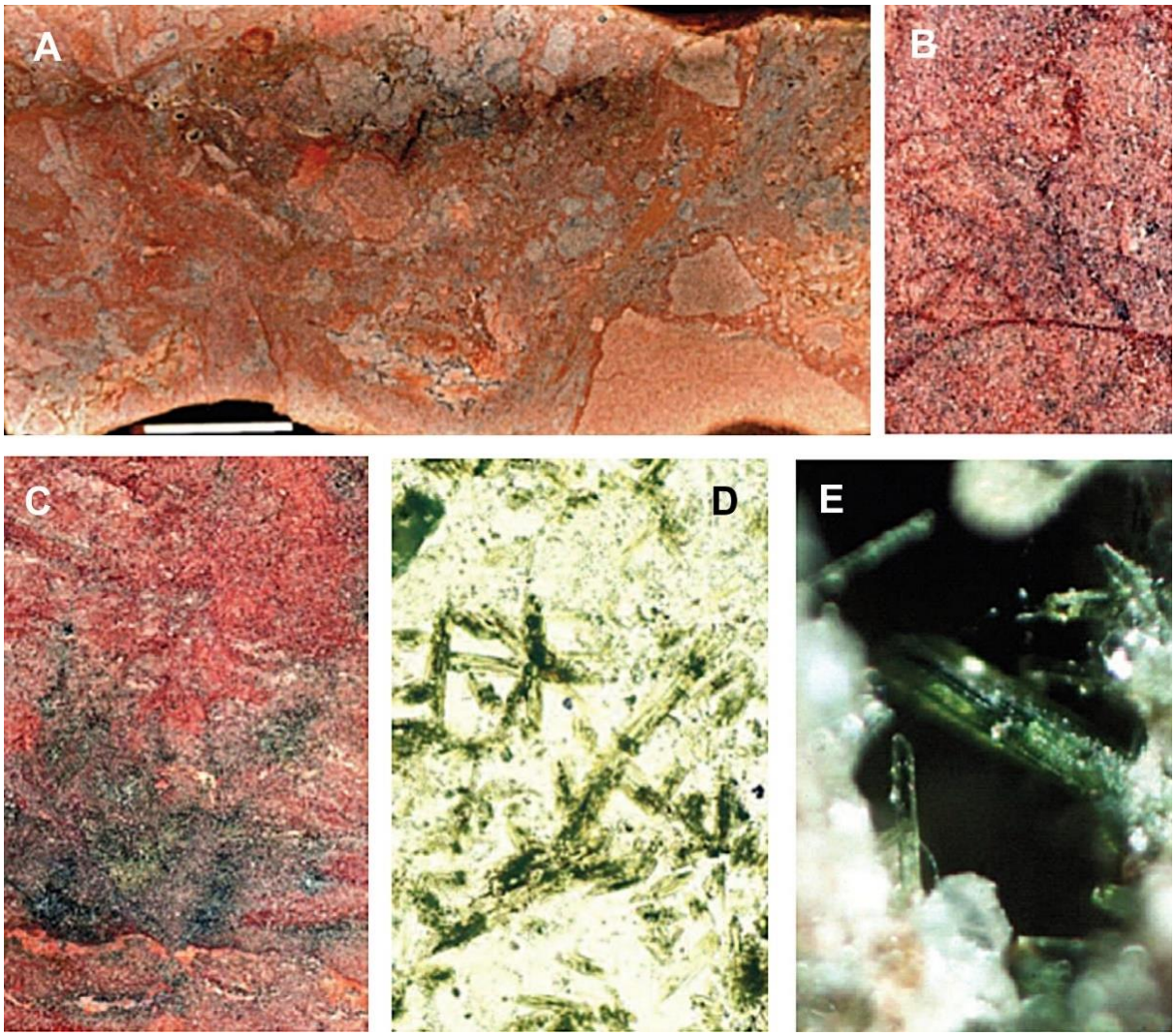

Figure 7. A) Rhyolite breccia from the Gamsberg; B) Incipient brecciation due to volume loss during cooling and devitrification of the welded tuff. The cracks are healed with quartz (chert; image width: 3 cm. C) Fine-grained rhyolitic tuff with light-coloured, devitrified pumice fragments and layers of pumice (fiamme; image width: 4 cm). Post-magmatic actinolite has grown in the grey-green and somewhat more porous, less welded parts of the pyroclastite; D) Photomicrograph of post-magmatic actinolite in rhyolitic tuff (Xn, image width: 2 mm); E) Photomicrograph of lithophysae with post-magmatic actinolite and quartz in Gamsberg rhyolite (image width: 2 mm)

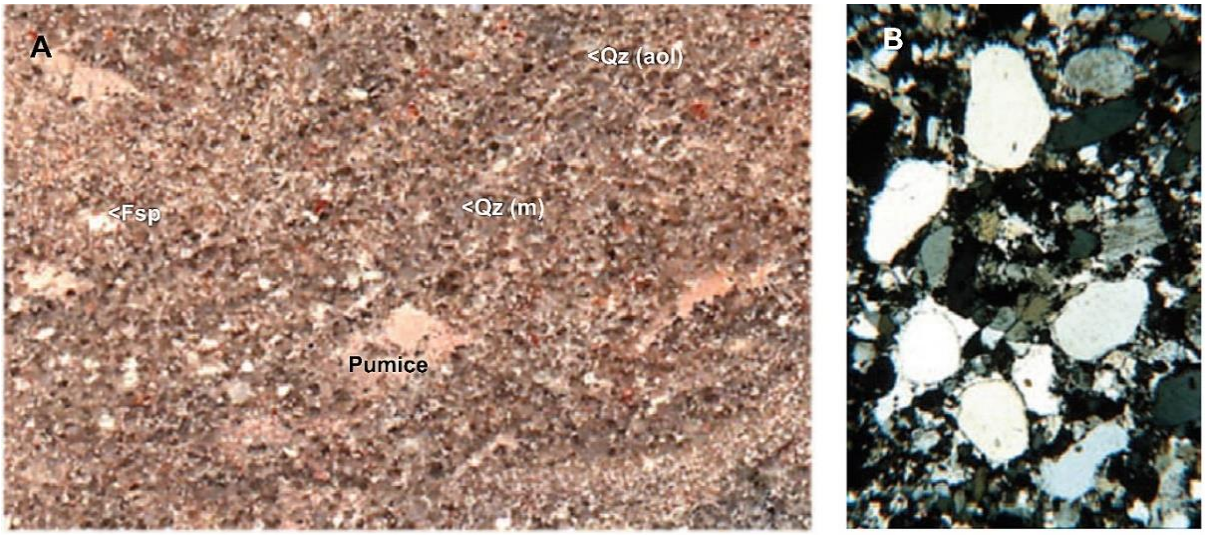

Figure 8. A) Silicified tuffitic sandstone from the uppermost part of the Gamsberg deposits with irregular, beige pumice fragments, white magmatic feldspar (Fsp), well-rounded aeolian (Qz aol) and angular, probably magmatic quartz grains (Qz m). Milky vein quartz grains are usually well-rounded; the very fine-grained, light-coloured grains are mostly feldspar and devitrified, variably sericitised glass fragments (image width: 17 mm, sample 22.8.00/5); B) Photomicrograph of aeolian quartz grains with opaque fringes in a finely crystalline, feldspar-rich rhyolitic matrix (Xn, image width: 2.15 mm)

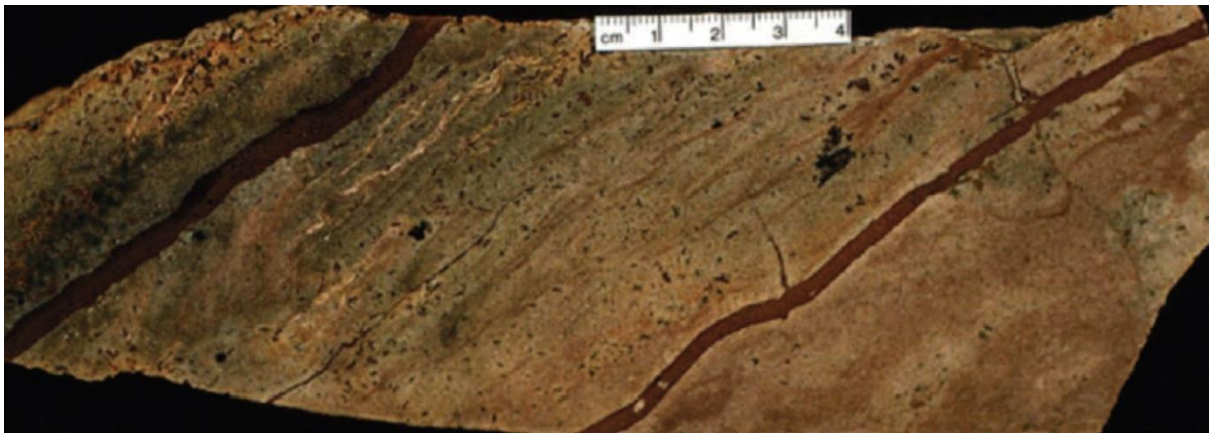

Figure 9. Fine-grained, red rhyolite veinlets within Gamsberg rhyolite, probably representing flow-parallel sills. From the sill on the right, small apophyses extend into the host rock. Also, two small fragments of the lighter-coloured host rhyolite occur within the right-hand sill (lower margin of the picture). The two rhyolites do not differ in geochemical composition.

Clastic dykes

Wittig (1976) described clastic dykes from the Gamsberg quartzite and the underlying Gamsberg granite (Figs 10-12). These dykes, which appear up to 240 m below the base of the quartzite in the Gamsberg granite, are interpreted as infill of earthquake fissures and divided into two types: a) dykes cross-cutting the basal (limnic-fluviatile) Gamsberg quartzite and the Gamsberg granite and filled with detritus of basal Gamsberg quartzite, and b) dykes cross-cutting the overlying aeolian, cross-bedded Gamsberg quartzite, filled with material from a higher, now eroded level. The garnet-rich dyke cutting the Gamsberg granite on farm Weener described by Wittig (1976) and cited by Schalk (1984) is not a clastic dyke with a garnet-rich sand-filling, but an igneous dyke with microcline, garnet and quartz as its main components.

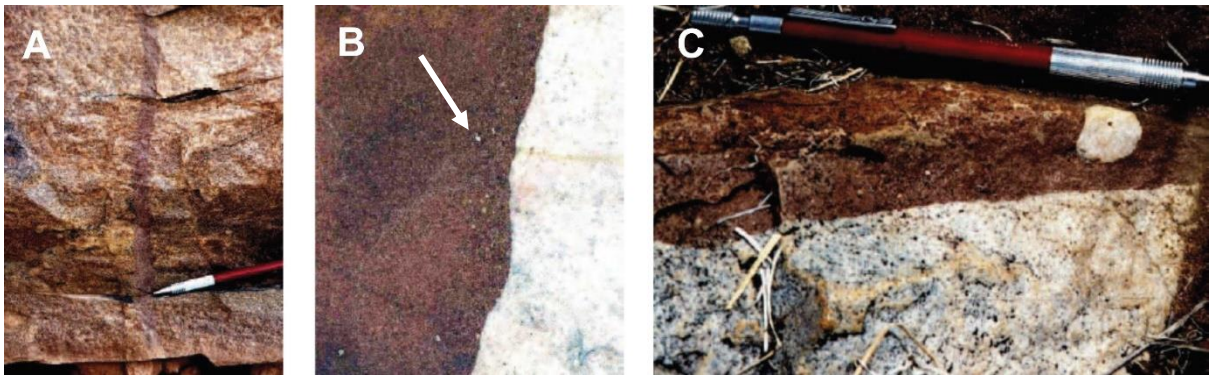

Figure 10. A) Clastic dyke of red tuffitic sandstone cross-cutting Gamsberg quartzite; B) Close-up of the contact between a clastic dyke (red) and light-coloured Gamsberg quartzite. The small, bright clasts in the clastic dyke are rhyolitic fragments (arrow, image width: 6 cm); C) Clastic vein (red) in Gamsberg quartzite with a large clast of light-coloured Gamsberg quartzite, demonstrating that the latter was already lithified at the time the clastic dyke formed.

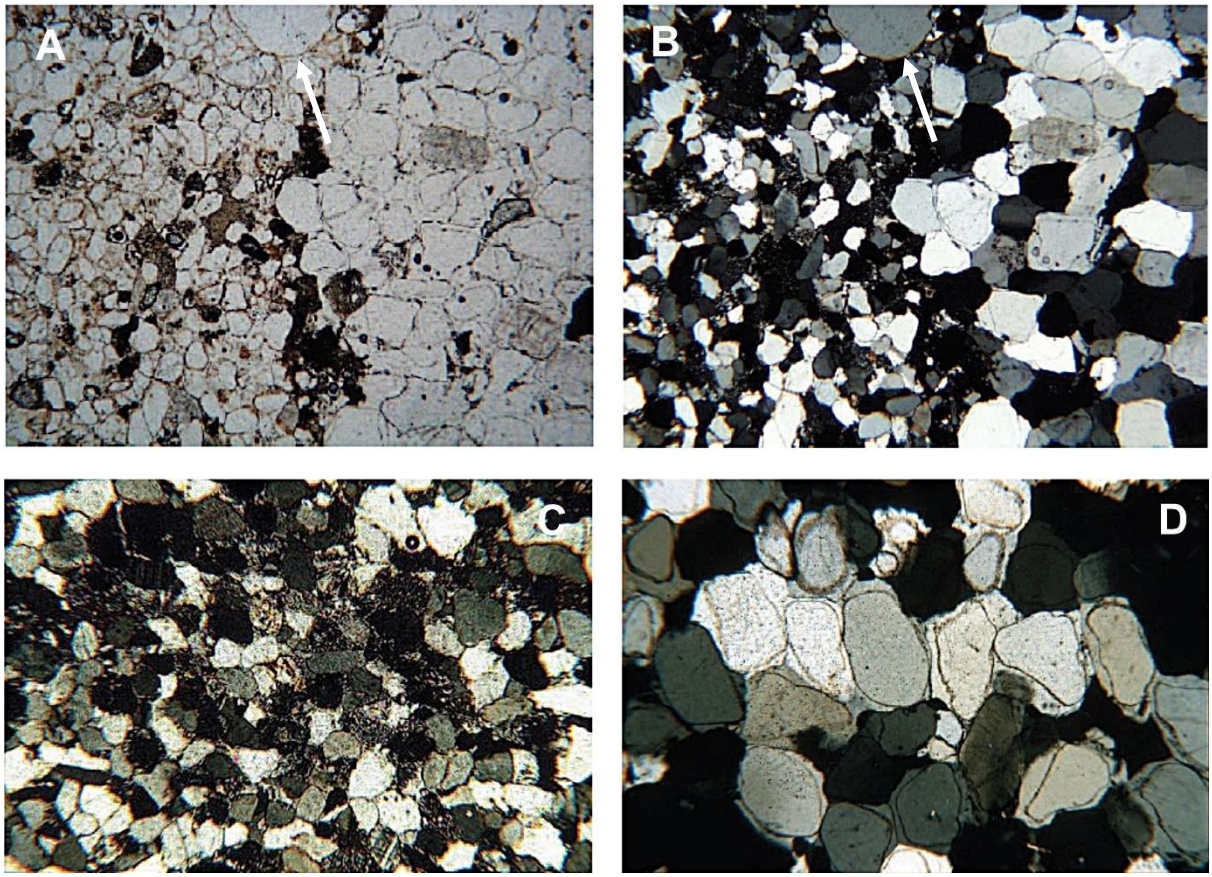

Figure 11. Photomicrographs of the contact between Gamsberg quartzite (on the right in each photo) and a clastic dyke (on the left) in A) planar-polarised light-PPL and B) cross-polarised light-Xn: grain size in the clastic dykes ranges from silt to fine sand. Aeolian grains (arrows) differ from the fluviatile ones by being larger and better rounded (image: width 5 mm.); C) Sample from the deepest clastic dyke below the top of the Gamsberg granite displaying fractured and subrounded quartz grains cemented by microcrystalline quartz (chert; image width: 2.15 mm); D) Gamsberg quartzite cemented by authigenic quartz (image width: 2.15 mm) for comparison with C)

The clastic dykes are clearly distinguishable from the hosting Gamsberg quartzite by their red to deep red colour (Fig. 10). Well-rounded, aeolian sand grains ca. 0.5 mm in size, as are present in the Gamsberg quartzite, also occur in varying proportions within the clastic dykes. However, most clastic grains are angular, range in size from silt to fine sand, and are

of fluviatile rather than aeolian origin. While the Gamsberg quartzite - apart from the tuffitic transition layers below the rhyolitic tuffs - is a pure quartzite, the clastic dykes consist exclusively of tuffitic sandstones with high proportions of fine-grained feldspar and devitrified pumice and glass fragments, which excludes their derivation from the Gamsberg quartzite. Moreover, clasts of Gamsberg quartzite (Fig. 10C) occur within the tuffitic sandstone of the clastic dykes proving that it was already lithified at the time of dyke formation. The latter are massive and unstratified, locally displaying cloudy textures. Low-temperature meteoric waters probably circulated throughout the predominantly vertical fissure system, which according to Wittig (1976) has a preferred north - south orientation; these waters are thought to have washed in the sand fill, as well as provided the microcrystalline quartz (chert) cement. Microcrystalline quartz mineralisation is characteristic of low-temperature hydrothermal systems, while authigenic quartz, as in the Gamsberg quartzite, is of diagenetic origin. The deepest clastic dyke, with a width of 5 to 10 cm, was encountered some 240 m below the base of the quartzite in the granite.

Similar clastic dykes have also been found in the Etendeka volcanic rocks of northwestern Namibia, where they consist of aeolian and fluviatile tuffitic intertrap sandstones. Therefore, the intercalated red, tuffitic sandstones, which clearly differ from the Gamsberg quartzite in colour, petrographic composition, grain size and grain shape, are likewise interpreted as intertrap sandstones within the Gamsberg volcanics, which were deposited on top of the quartzite. Locally, larger vein quartz clasts are found in the clastic dykes, suggesting the presence of conglomeratic intercalations, similar to the ones observed in the Etendeka lavas, within the now eroded Gamsberg volcanics. These clastic dykes of tuffitic sandstone also are found in the Gamsberg rhyolites (Fig. 12A).

Figure 12. A) Clastic dyke of tuffitic sandstone with rhyolite clasts and numerous sericitised pumice fragments in brecciated Gamsberg rhyolite; B) Feldspar-rich clastic dyke (small light-coloured grains: feldspar and pumice fragments) in the Gamsberg quartzite with a large vein quartz clast, and smaller fragments of red rhyolite, devitrified volcanic glass (arrow) and silicified mudstone (image width: 6 cm); C) Clastic dyke cross-cutting Gamsberg granite

The clastic dykes which cross-cut the remnants of the Gamsberg rhyolites, the underlying tuffitic sandstones and Gamsberg quartzite, as well as the Gamsberg granite, are an archive of the sediments which once covered the Gamsberg Plateau. Grain size and shape show them to be of both fluviatile and aeolian origin, and it is likely that they belong to the Etendeka Group.

Geochemistry of the Gamsberg rocks

The Gamsberg volcanic rocks were analysed for main and trace elements. Further geochemical investigations were not carried out because of the strong silicification, hydrothermal overprinting and aeolian contamination. Results are shown in the tables and diagrams below. According to petrographic studies, samples with SiO_2 contents of 85 to ~88 wt% are volcanic rocks, including sample 9.4.90/4a (Fig. 9; 85.6 wt% SiO_2) from a fine-grained rhyolite vein within Gamsberg rhyolite sample 9.4.90/4. Sample 9.4.90/13b (89.9 wt% SiO_2) represents a clastic dyke of tuffitic sandstone with rhyolite clasts and sericitised pumice fragments cross-cutting Gamsberg rhyolite (Fig. 12A). The sand grains are predominantly of aeolian origin and were washed into the crack together with the tuffitic material. Table 1 shows the mean geochemical composition of the eighteen analysed Gamsberg rhyolites as compared to rhyolites from the Erongo Mountain (Emmermann, 1976) and average rhyolite (Duncan *et al*., 1984).

Comparison with the Erongo rhyolites was chosen as this Cretaceous volcano, located some 200 km to the north (Fig. 1), is the nearest source from which the Gamsberg rhyolites could have been derived. Geochemical composition of the Gamsberg rhyolites, together with petrography and magmatic texture, suggest a very silica-rich magmatic parent rock, which geochemically could have been a rhyolite (possibly rhyolitic glass ash tuff), as the Gamsberg rhyolites are free of magmatic phenocrysts. Of note is the relatively strong depletion of Al_2O_3, which, however, is probably due to the subsequent intense silicification (Table 1, Column B).

	A	B	C	D
SiO_2	87.10	73.00	73.10	72.82
TiO_2	0.23	0.51	0.40	0.28
Al_2O_3	5.60	12.47	13.40	13.27
Fe_2O_3	1.08	2.41	2.87	2.59
MnO	0.01	0.02	0.04	0.06
MgO	0.15	0.33	0.45	0.39
CaO	0.10	0.22	0.98	1.14
Na_2O	0.71	1.58	2.79	3.55
K_2O	3.58	7.97	5.24	4.30
P_2O_5	0.03	0.07	0.23	0.07
	98.59	**98.59**	**99.5**	**98.47**

	A	B
Nb	7	
Zr	224	214
Y	28	
Sr	30	80
Rb	24	303
Pb	10*	
Ga	6	
Zn	13*	
Cu	25*	
Ni	18	
Co	*<5**	
Cr	27	
V	30	
Ba	611	420
Sc	6*	

Table 1. Geochemical composition of the Gamsberg (Barge, 2001) and Erongo rhyolites (Emmermann, 1976). Left: major element composition (wt %) of A) Gamsberg rhyolite, mean values of 18 samples; B) Gamsberg rhyolite, values of column A recalculated to 73% SiO_2 due to silicification; C) Erongo rhyolite, mean values of 11 samples; D) Average rhyolite (after Duncan *et al*., 1984); right: trace element composition (ppm) of A) Gamsberg rhyolite, mean values of 18 samples (complete analytical results shown in Appendix I, *values below detection limit omitted as unreliable), and B) Erongo rhyolite, mean values of 11 samples (complete analytical results shown in Appendix II)

Aluminium, iron, titanium and sodium and potassium exhibit an almost linear decrease with increasing SiO_2-content (Fig. 13), i. e. from the volcanic rocks to the tuffitic sandstone of the Gamsberg fissures and the Gamsberg quartzite. This linear decrease is most obvious for Al_2O_3. Recalculation of the analysed average Al_2O_3-content (Table 1, column A) to 73 wt% SiO_2 (Table 1, column B) results in an Al_2O_3-content of 12.47 wt%. From this a "dilution factor" of 2.227 (12.47:5.6=2.227) for 73 wt% SiO_2 was determined, which is applied to

the other major elements. Results show the immobile elements iron and titanium to be in relatively good agreement with the Erongo rhyolites, while sodium and calcium are depleted and potassium enriched relative to the Erongo rocks (Table 1, columns B and C). This can be attributed to the higher mobility of the alkali and earth-alkali elements during secondary alteration. As only Zr, Rb, Sr and Ba were analysed from the Erongo rhyolites (Emmermann, 1976; Table 1 & Appendix II), a comparison of trace element concentrations remains inconclusive.

SiO_2-contents between 90 (89.7 wt%) and 95 wt% have been determined for samples from a) clastic dykes, b) rhyolitic pyroclastic rocks with isolated aeolian quartz grains and c) tuffitic sandstones. Thus, the clastic dykes in the Gamsberg quartzite and the granitic basement differ from the quartzite geochemically as well as in terms of mineral content, grain size and grain shape, which excludes the latter, as already concluded from other evidence, as the source of the clastic dykes. The Gamsberg sedimentary and volcanic rocks show a continuous transition from silicified rhyolitic tuffs to pure quartzite. Between these end members the silicified tuffitic sandstones and clastic dykes occupy intermediate positions.

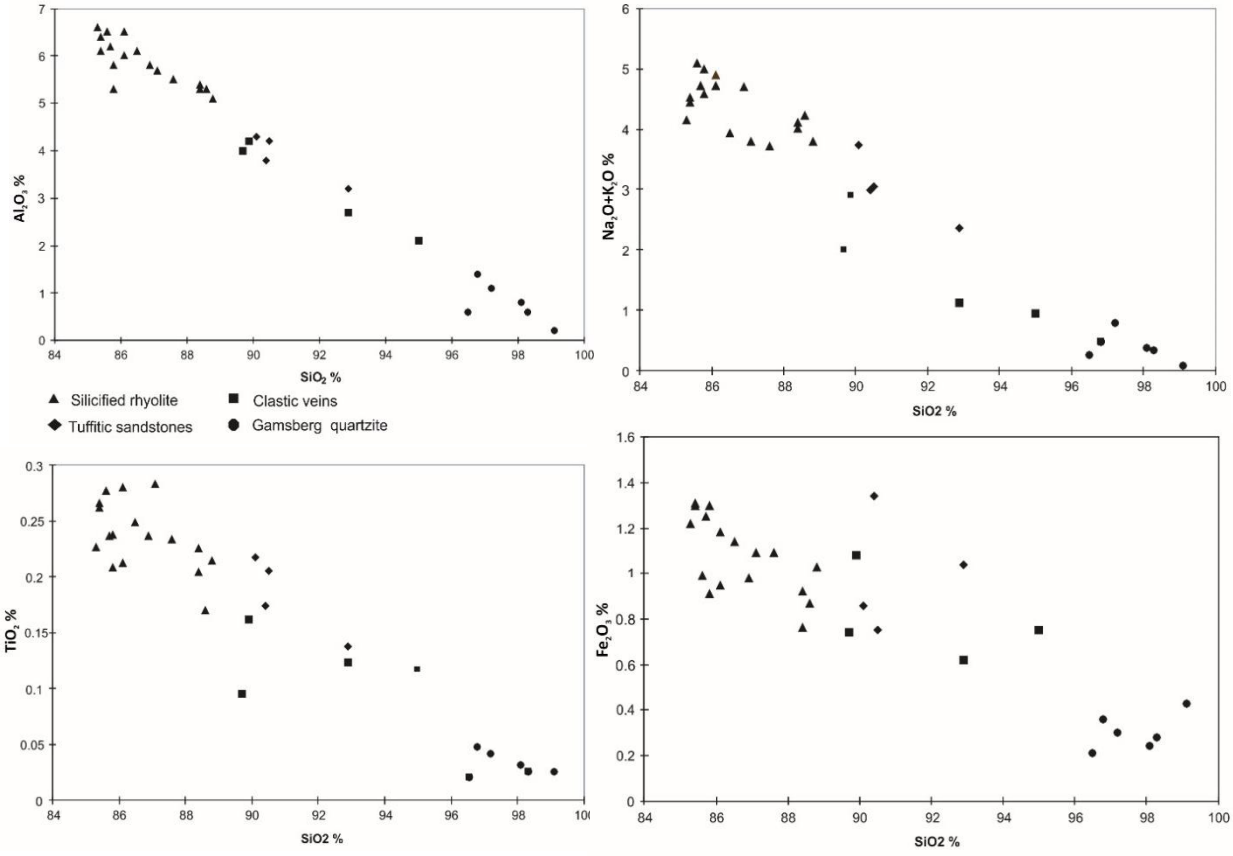

Figure 13. Harker (1909) diagram representation for some major elements of the Gamsberg rhyolite

Radiometric ages

Some 50 kg of a silicified rhyolite sample were processed for zircon separation but without success. Presumably, the expected very fine-grained zircons could not be isolated due to the strong silicification of the volcanic rocks. An attempt to prepare magnetically enriched fractions with diluted hydrofluoric acid also remained unsuccessful.

On sample 9.4.90/3, K/Ar ages were determined for the grain fractions <2 µm and < 0.2 µm (Table 2). The samples were crushed with a jaw crusher and briefly ground with a vibrating disc mill; the above grain fractions were obtained by the Atterberg process.

Compared to the total sample (K_2O = 3.91%), the K_2O-content of the grain fraction

<2 µm is significantly higher and probably results from an enrichment of potassium feldspar, as no mica was found in the fine fractions by X-ray diffraction. The preserved age (Table 2) is inconclusive and corresponds neither to the Karoo volcanics (170 to 180 Ma) nor to the Etendeka volcanics (132 Ma), but lies in between.

Due to the failed zircon dating and the uncertain K/Ar ages, reliable dating of the Gamsberg rhyolites is still pending. Assuming, however, that the Gamsberg volcanics, due to their rhyolitic chemistry, more likely correlate with felsic rocks of the Etendeka Group than with (the predominantly mafic) Karoo igneous province, one has to conclude that the Gamsberg rocks are younger than originally thought, i. e. that they are Lower Cretaceous in age. Recently found trace fossils in the limnic-fluviatile basal part of the Gamsberg quartzite on the other hand suggest a correlation with the older limnic-fluviatile layers of the Jurassic Etjo Formation, on the basis of which an unlikely duration of ca. 70 Ma would have to be assumed for the deposition of the rocks on the Gamsberg Plateau (Lower Jurassic to Lower Cretaceous).

Sample	Fraction	K_2O (wt%)	40 Ar*(nl/g) STP	40 Ar* (%)	Age (Ma)	2s- error (Ma)	2s-error (%)
09.04.90 / 03	<2 µm	7.46	41.46	94.35	164.7	3.5	2.1
09.04.90 / 04	<0.2 µm	5.62	30.13	88.47	159.1	6	3.8

Table 2. K-Ar geochronology of the Gamsberg rhyolite

Another conclusion, i. e. that both the Gamsberg quartzite and the overlying rhyolitic volcanics are younger than the Etjo Formation seems the more probable. This would suggest a correlation of the quartzite with the Twyfelfontein Formation, which Stollhofen (1999) places at the base of the Etendeka Group. The Twyfelfontein Formation also contains limnic-fluviatile deposits below the aeolian sediments (Jerram *et al*., 1999), for instance in the Huab Basin, which previously had been correlated with the Etjo Formation. Moreover, the very good Gamsberg outcrops give no indication of a hiatus between the deposition of the quartzite and the rhyolite. Rather, the outcrops as well as the geochemical data show that there is a continuous transition from pure quartzite via tuffitic sandstone to rhyolitic tuff. The tuffitic /epiclastic sediment fill of the clastic dykes further supports the existence of now eroded volcanic rocks as well as fluviatile and aeolian sediments, which, based on the presence of post-magmatic actinolites and apatite fission track analysis, must have had a considerable thickness. Therefore, the here described sedimentary and volcanic rocks should be awarded formation status (proposed name: Gamsberg Plateau Formation), and the unit tentatively placed in the basal Etendeka Group.

Cenozoic limnic-fluviatile sediments

The (provisional) Gamsberg Plateau Formation is overlain by grey clays, with a few intercalated gravel lenses of well-rounded vein quartz. The distribution of the clays on the Gamsberg Plateau, which largely coincides with that of the rhyolites, can be seen on the satellite image in Figure 4. The preserved thickness of these deposits is at least 1.20 m in the central area of their occurrence, as I was able to show by trenching. However, the original thickness must have been much greater, as indicated by the dense scree layer of well-rounded vein quartz clasts (Fig. 14A), compared to their prevalence in the *in situ* sediment. As there are no quartz veins on the isolated inselberg of the Gamsberg and the rounding of the vein quartz pebbles implies considerable transport distances, they are thought to belong to a limnic-fluviatile depositional environment connected with the metamorphic basement. As this question is of particular interest for the climate development, I took samples of these clays for pollen analysis and mineralogical investigation.

Asteraceae pollen dominate in the Gamsberg clays, but their proportion decreases very sharply in the lower part of the profile (Table 3). As the phylogenetic development of the *Asteraceae* only started during the Late Palaeogene, a Neogene maximum age of the clays is assumed. The samples contain numerous fungal spores, fungal oogonia and fungal hyphae, a number of algal cysts, some spores that cannot be identified, and a narrow spectrum of pollen. Particularly remarkable is the almost universal occurrence of *Asteraceae* pollen, especially of an extremely small form (generally < 10 µm). Much rarer are similarly small tricolpate and tricolporate forms (*Tricolpopollites liblarensis pusillus*-type or *Tricolporopollanites cingulum oviformis*-type). A few faecal pellet-like agglomerates of the former have been identified in the sample taken 75 cm below surface (insect faecal pellets?). A more detailed systematic determination is not possible. The two forms probably originate from the large family of Fagaceae.

Figure 14. A) Scree layer on top of the Gamsberg clay; B) Deflation plane with alluvial gravel on the Gamsberg Plateau

An important problem is whether the collected pollen represent recent contamination or a sediment-borne fossil record. The occurrence in the samples of forms such as *Betula* (birch) and *Alnus* (alder), which are not native to Namibia and also contain remnants of protoplasm, proves that there are impurities. However, in the case of the *Asteraceae* pollen contamination in the laboratory or during sample handling is unlikely. Although they may stem from the recent vegetation on Gamsberg, I would like to rule out contamination in the field, as the samples were collected from a fresh trench and immediately packed in plastic bags with zip fasteners. It remains to be noted that the pollen which cannot be clearly attributed to impurities, probably represent an *in situ* fossil record; thus, a Neogene to Quaternary age is assigned to the Gamsberg clays, as *Asteraceae* only form a notable component of the vegetation since the Neogene.

With more than 20,000 species, the daisy family is currently one of the most diversified families of seed plants worldwide. Vertical trends in the distribution of palynofacies elements are difficult to identify in the Gamsberg profile, excepting only the *Asteraceae* pollen which show a maximum in the middle and a sharp decrease in the lower part (Table 3). To a lesser extent the latter also applies to the pollen content as a whole. It is noteworthy that the fern spores (small trilete verrucate forms and monolete *Polypodiaceae* spores) are restricted to the uppermost four samples (< 65 cm depth), while mushroom spores and mushroom oogonia occur throughout the entire profile. Fungal hyphae also are common, especially in its upper part. Heavy minerals occur more frequently in the footwall than in the hanging wall.

Prof. Dr. Grüger of the Botanical Institute, University of Göttingen, who helped with the determination of the pollen, stated that the samples do not represent Quaternary or recent forms known to him. Also, the pollen associations found are not typical of today's local flora on the Gamsberg Plateau. Table 3 lists the results of the pollen analysis, which is thought to represent the fossil record in each of the samples.

The <2 µm and <0.2 µm fractions from the Gamsberg clays were isolated using the Atterberg method and examined by X-ray diffraction. Glycolised and non-glycolised oriented sections were used for clay mineral anal-

ysis. The Gamsberg clays contain very little illite in the particle size fraction <2 µm. Apart from kaolinite, they consist predominantly of expansive clay minerals (smectites). The quartz content in the fraction <2 µm is also very low, while the <0.2 µm particle size fraction is entirely free of quartz. The greyish colour of the clays, together with the predominant kaolinite and smectites, indicate a humid climate at the time of deposition. This would argue for a pre- to Early Miocene age, i. e. before the onset of the Benguela Current and the formation of the Namib Desert, with markedly arid climatic conditions.

Depth	15-20 cm	40 cm	50 cm	65 cm	75 cm	85 cm	93-96 cm	95-100 cm	100-105 cm
***Asteraceae* pollen <10 µm**	39	X	70	2	22	14		11	1
***Asteraceae* pollen >10 µm**	9	X	3	1		2		2	1
***T. cingulum oviformis* -type**			1	1	10		1		
***T. liblarensis pusillus* -type**	7	X	1		1 as faecal pellets				
***Betula* (recent)**					1				
***Alnus* (recent)**						1			
***Chenopodiaceae* pollen**	2								
small trilete verrucate spores	14	XX		1					
monolete spores (*Polypodiaceae*)	2	X	1						
reticulate cysts	1	X	9	1		2			2
rugulate cysts	12	X	1						
algal cysts		X	XX	XX	XX	X			
fungi spores/ fungi oogonies		XX		XX		XX	X		XX
fungal hyphae		XXX		XX					X
resinite splinter		XX		XX		X	X	X	X
heavy minerals			XX	XX	XX	X	X	XX	XX
other pollen	3	X	2	2				3	
undetermined forms	3	3							
***Pterosphaeridia* - similar cysts**	3								
fine material		XX	XX						
Pinus								1	

Table 3. Fossil record of each profile section (cm below ground level). Numbers in the table represent counts per slide. In each case one slide was counted, which was screened completely. X = present, XX = common, XXX = very common

While digging the trench it was noted that the entire profile contained very few fragments of the underlying quartzite and volcanic rock, whereas the surface was covered by such rubble. The reason for this is the high smectite content of the Gamsberg clays. After the peri-

odic rains, they swell so much as to make the terrain barely passable for vehicles. When it dries, deep hexagonal systems of shrinkage cracks form, the alternating volume increase and decrease leading to large rock fragments being transported to the surface, as happens also in periglacial soils. Due to this mechanism the volcanic rocks of the Gamsberg Plateau underlying the clays are frequently encountered as large fragments on the surface. However, it also reduces the reliability of the pollen analysis, as it allows contamination with recent pollen at least of the upper 20 to 30 cm of the profile by way of these deep shrinkage cracks.

References

Barge, S. 2001. Untersuchungen zur mesozoisch-känozoischen Entwicklung des Großen Gamsberges (Namibia). Diplom Thesis, University of Göttingen, Germany.

Duncan, A. R., Erlank, A. J. and Marsh, J. S. 1984. Regional geochemistry of the Karoo Igneous Province. *In*: Erlank, A. J. (Ed.) *Petrogenesis of the volcanic rocks of the Karoo Province. Special Publication Geological Society South Africa*, **13**, 355-388.

Emmermann, R. 1976. Die Magmenabfolge des Erongo und ihre genetische Deutung. *Fortschritte Mineralogie*, **54**, Beiheft 1, 18 pp.

Harker, A. 1909. *The Natural History of Igneous Rocks*. Methuen, London, 344 pp.

Jerram, D., Mountney, N., Holzförster, F. and Stollhofen, H. 1999. Internal stratigraphic relationships in the Etendeka Group in the Huab Basin, NW Namibia: understanding the onset of flood volcanism. *Journal of Geodynamics*, **28**, 393–418.

Jerram, D. A., Mountney, N. P., Howell, J. A., Long, D. and Stollhofen, H. 2000. Death of a sand sea: an active aeolian erg systematically buried by the Etendeka flood basalts of NW Namibia. *Journal of the Geological Society, London*, **157**, 513-516.

McPhie, J., Doyle, M. and Allen, R. 1993. *Volcanic textures. A guide to the interpretation of textures in volcanic rocks. Centre for ore deposit and exploration studies*. University of Tasmania, Hobart, Australia, 197 pp.

Schalk, K.E.L. 1984. Geologische Geschichte des Gamsberggebietes. *Journal of the Southwest African Scientific Society*, **38**, 7-15.

Stollhofen, H. 1999. Karoo Synrift-Sedimentation und ihre tektonische Kontrolle am entstehenden Kontinentalrand Namibias. *Zeitschrift deutsche Geologische Gesellschaft*, **149**, 519-632.

Wittig, R. 1976. Die Gamsberg-Spalten (SW-Afrika) - Zeugen Karroo-zeitlicher Erdbeben. *Geologische Rundschau.*, **65**, 1019-1034.

Appendix I. Major and trace element composition of the Gamsberg rhyolites analysed by X-Ray Fluorescence (Barge, 2001)

Sample No	09.04.90/ 01	09.04.90/ 03	09.04.90/ 04a	09.04.90/ 08	09.04.90/ 12	09.04.90/ 13a	09.04.90/ 20	17.08.92/ 08	14.09.94/ 1+1	14.09.94/ 1+2	14.09.94/ 1+3	12.04.00/ 05	12.04.00/ 06	12.04.00/ 08	12.04.00/ 11	12.04.00/ 12	12.04.00/ 13
Major elements (wt. %)																	
SiO2	85.4	85.4	85.6	87.1	90.1	86.9	85.8	85.8	87.6	88.8	88.4	88.6	85.7	86.5	88.4	86.1	90.4
TiO2	0.262	0.266	0.277	0.283	0.218	0.237	0.208	0.238	0.234	0.214	0.204	0.17	0.237	0.249	0.226	0.212	0.174
Al2O3	6.1	6.4	6.5	5.7	4.3	5.8	5.3	5.8	5.5	5.1	5.3	5.3	6.2	6.1	5.4	6	3.8
Fe2O3	1.3	1.31	0.99	1.09	0.86	0.98	1.3	0.91	1.09	1.03	0.76	0.87	1.25	1.14	0.92	1.18	1.34
MnO	0.007	0.007	0.009	0.02	0.006	0.01	0.009	0.013	0.009	0.009	0.01	0.004	0.004	0.006	0.005	0.004	0.05
MgO	0.17	0.25	0.13	0.16	0.03	0.06	0	0.91	0.23	0.09	0.05	0.04	0.05	0.15	0.07	0.03	0.05
CaO	0.19	0.11	0.2	0.13	0.03	0.11	0.03	0.21	0.11	0.06	0.04	0.06	0.05	0.17	0.03	0.03	0.08
Na2O	0.72	0.61	1.13	0.8	0.17	0.58	0.3	1.46	0.87	0.91	0.76	0.94	0.61	0.83	0.6	0.82	0.34
K2O	3.73	3.91	3.95	2.99	3.57	4.12	4.27	3.54	2.85	2.88	3.35	3.28	4.1	3.11	3.41	4.08	2.65
P2O5	0.045	0.032	0.029	0.045	0.018	0.015	0.018	0.031	0.017	0.012	0.016	0.021	0.014	0.053	0.022	0.013	0.016
Total	*97.92*	*98.30*	*98.82*	*98.32*	*99.30*	*98.81*	*97.24*	*98.91*	*98.51*	*99.11*	*98.89*	*99.29*	*98.22*	*98.31*	*99.08*	*98.47*	*98.90*
Trace elements (ppm)																	
Nb	12	9	6	7	7	9	6	5	7	6	8	5	7	7	5	5	12
Zr	233	225	286	290	280	267	134	274	235	213	159	161	201	228	251	235	141
Y	52	31	16	19	19	20	23	22	15	8	15	10	12	19	15	16	105
Sr	65	27	24	21	14	33	28	37	31	25	35	25	15	36	33	31	29
Rb	15	25	18	20	29	29	26	25	14	14	18	20	29	52	47	17	21
Pb	7	2	10	20	<5	10	2	7	3	3	8	0	0	0	0	9	18
Ga	8	7	7	6	4	6	5	7	6	8	7	5	6	7	6	6	3
Zn	10	14	15	11	9	16	11	21	0	9	16	3	1	3	0	7	11
Cu	16	26	29	29	12	31	20	30	<5	4	32	0	0	0	0	0	42
Ni	19	17	13	16	15	14	14	19	15	14	13	16	25	18	17	34	17
Co	3	3	<5	<5	<5	<5	1	3	<5	5	<5	2	1	1	1	0	0
Cr	33	30	23	23	26	24	30	24	26	23	26	24	35	32	26	27	26
V	34	20	26	33	16	48	33	21	10	16	24	23	13	31	17	37	91
Ba	1837	625	178	124	499	644	1059	522	626	459	878	286	344	278	250	773	732
Sc	2	1	4	3	4	6	4	6	2	1	1	3	2	3	6	0	7

Appendix II. Major and trace element composition of the Erongo rhyolites (Emmermann, 1976)

	Sills							Ignimbrites			Tuff
Sample No	**82**	**108**	**115**	**120**	**131**	**140**	**146**	**40**	**41**	**141**	**42**
Major elements (wt %)											
SiO_2	70.6	72.3	75.2	72.8	72.6	72.0	74.8	72.6	74.5	73.8	72.5
TiO_2	0.69	0.46	0.26	0.38	0.42	0.29	0.34	0.42	0.33	0.37	0.4
Al_2O_3	13.5	13.7	13.0	13.9	12.8	13.5	13.3	13.3	13.4	13.6	13.2
Fe_2O_3	4.00	3.22	1.72	2.50	2.80	4.20	2.59	2.86	2.34	2.43	2.96
MnO	0.03	0.06	0.01	0.05	0.04	0.05	0.05	0.03	0.04	0.03	0.03
MgO	0.76	0.80	0.25	0.58	0.30	0.22	0.35	0.50	0.37	0.46	0.40
CaO	1.65	0.95	0.91	0.67	1.06	1.4	1.04	0.62	0.95	0.86	0.62
Na_2O	2.87	2.85	2.95	2.57	2.74	3.10	2.70	2.69	2.44	2.64	3.10
K_2O	4.77	5	5.5	5.82	6.78	5.12	4.02	5.4	5.2	4.88	5.11
P_2O_5	0.23	0.26	0.24	0.22	0.2	0.06	0.26	0.26	0.3	0.25	0.25
LOI	0.96	0.73	0.42	0.69	0.52	0.54	0.58	1.22	0.48	0.72	1.37
Total	*100.06*	*100.33*	*100.46*	*100.18*	*100.26*	*100.48*	*100.03*	*99.90*	*100.35*	*100.04*	*99.94*
Trace elements (ppm)											
Rb	213	350	364	320	284	376	339	189	365	342	194
Sr	137	82	78	55	68	33	81	122	63	50	116
Zr	272	175	142	155	208	425	139	268	180	167	225
Ba	730	480	260	355	440	220	370	480	450	370	460

Rare Earth Element Geochemistry of the Epembe Carbonatite Dyke, Opuwo Area, North-western Namibia

Ester Kapuka

Geological Survey of Namibia, 6 Aviation Road, Windhoek
<Ester.Kapuka@mme.gov.na>

Abstract :- The Epembe carbonatite dyke was emplaced along a northwest-trending fault zone into syenites and nepheline syenites of the Epembe Subsuite (Epembe-Swartbooisdrift Alkaline Suite). It extends for approximately 6.5 km in a northwest - southeast direction, with a maximum outcrop width of 400 m. The Epembe carbonatite has a Mesoproterozoic age of 1184 ± 10 Ma; field relationships support that it is younger than the enclosing nepheline syenites dated at 1216 ± 2.4 Ma. This study examines geochemical and mineralogical variations within the carbonatite dyke, with special emphasis on rare earth elements (REE). Analytical and petrographic results show that it primarily consists of coarse-grained calcite, with accessory apatite, pyrochlore, aegirine, feldspar and iron oxide, and therefore classifies as calcio-carbonatite. Although the concentration of REE (total REE+Y) in the Epembe carbonatite dyke ranges from 406 to 912 ppm, no REE-minerals were observed in the analysed samples, except for monazite in trace amounts. It is concluded that REE are either contained in accessory minerals, such as apatite and pyrochlore, and/or gangue minerals (e. g. silicates and carbonates). The Epembe carbonatite is enriched in light rare earth elements (LREE) compared to heavy rare earth elements (HREE), which is attributed to fractional crystallisation and chemical substitution primarily affecting former.

Keywords :- Geochemistry, Rare earth elements (REE), Epembe carbonatite dyke

To cite this paper :- Kapuka, E. 2024. Rare Earth Element Geochemistry of the Epembe Carbonatite Dyke, Opuwo Area, Kunene Region, North-western Namibia. *Communications of the Geological Survey of Namibia*, **27**, 19-39.

Introduction

Owing to a globally increased demand, rare earth elements have attracted the attention of numerous exploration companies and researchers to examine potential host rocks, including monazite ± apatite veins, carbonatites, pegmatites, peralkaline igneous rocks, ion-adsorption clays, placers, and certain deep-ocean sediments (Kanazawa and Kamitani, 2006). Currently, most light rare earth elements (LREE) are extracted from carbonatite-related deposits, while heavy rare earth elements (HREE) are mostly derived from REE-bearing ion-adsorption clays (Wall, 2014). Accordingly, carbonatites have become prime exploration targets for junior companies across the globe as they are the principal suppliers of REE and niobium, which are essential raw materials for important economic sectors, such as the manufacture of electric vehicles, permanent magnets and solar panels (European Commission, 2014).

This investigation focuses on the analysis of major and trace elements, including REE, across the Epembe carbonatite, Kunene Region, north-western Namibia, with the aim of establishing and understanding their distribution within the dyke. The study area is situated roughly 95 km northwest of the regional capital Opuwo, between the villages of Ohamaremba and Epembe (Fig. 1).

Regional Geology

The regional geology of the area is characterised by gneisses of the Epupa Metamorphic Complex, intruded by two igneous alkaline suites/complexes, i. e. the Mesoproterozoic rocks of the Kunene Anorthosite Complex with a concordant U-Pb single zircon age of 1370 Ma (Mayer *et al*., 2004) and the Epembe–Swartbooisdrift Alkaline Suite with a

minimum age of 1100 Ma (nepheline syenite and lamprophyre; U-Pb zircon / K-Ar biotite; Menge, 1986); the latter encompasses the Epembe and Swartbooisdrif Subsuites. The metamorphic and igneous units are partly overlain by (meta)-sedimentary rocks of the Neoproterozoic Damara and the Palaeozoic Karoo Supergroup, which, however, in the study area are present only as isolated, transported boulders (Falshaw, 2012). An overview of the intrusive and metamorphic units of the study area is given in Table 1.

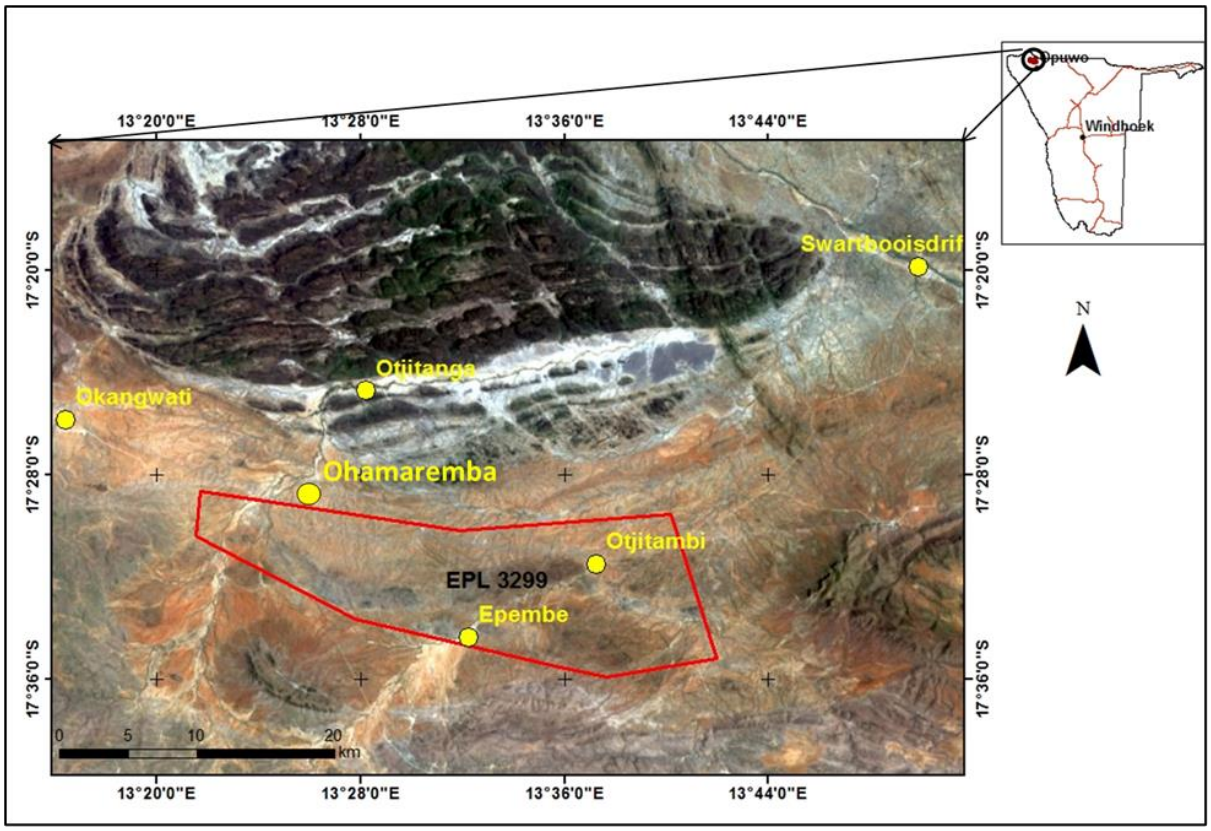

Figure 1. Satellite image (Landsat 8, sharpened) showing the location of the study area and Exclusive Prospecting Licence (EPL) 3299, which covers the Epembe carbonatite dyke (satellite image: National Aeronautics and Space Administration, USA)

Epupa Metamorphic Complex

The metamorphic and igneous rocks of the Epupa Metamorphic Complex (EMC) represent the oldest Palaeo- to Mesoproterozoic basement in the area, which was intruded by the anorthosites of the Kunene Igneous Complex (Maier *et al*., 2008). The EMC is composed of upper amphibolite facies and ultrahigh-temperature granulite facies rocks (Brandt, 2003), which have been subdivided into two distinctive units based on petrology, metamorphic grade, structure, and field relationship (Brandt *et al*., 1999), i. e. the Orue and Epembe units (Fig. 2).

Following the work of Martin (1965) and Köstlin (1967), the Orue unit consists mainly of a widely migmatised volcano-sedimentary sequence, intruded by large volumes of granitic magma. The rocks exhibit uniform upper amphibolite facies metamorphic grade, as well as structural similarities. The Epembe unit encompasses a 50 km long, E-W trending and up to 10 km wide, well-defined terrane of ultrahigh-temperature granulite facies ortho- and paragneisses. The central part of this unit comprises volcano-sedimentary successions of interlayered mafic and felsic granulites, and subordinate migmatitic metasedimentary granulite (Brandt, 2003; Brandt *et al*., 2000, 2007). Both volcano-sedimentary sequences, separated by a subvertical E-W trending fault known as the Otjitambi-Ehomba Fault (Fig. 2), have undergone substantial burial to mid-crustal levels (Brandt, 2003). Subsequently, the Epembe unit was intruded by small stocks and dykes of carbonatite, nephe-

line syenite and lamprophyre of the Epembe Subsuite (Maier *et al*., 2008). While the Orue unit has been dated at 1334 ± 21 Ma (Seth *et al*., 2003), a protolith age of up to 1810 Ma (Drüppel *et al*., 2001; Seth *et al*., 2003) is assigned to the Epembe unit.

Lithology	Intrusive unit	Sub-Unit	Suite/Complex	Age
Carbonatite	Epembe carbonatite, Swartbooisdrift carbonatite		Epembe-Swartbooisdrift Alkaline Suite	
Syenite				± 1100 Ma
Nepheline syenite	Otjitanga-Epembe nepheline syenite			± 1250 Ma
Serpentinite, hornblendite, anorthosite, troctolite	Otjitambi hyperite	Satellite intrusions	Kunene Anorthosite Complex	
Anorthosite	Marginal Zone			
Anorthosite (subordinate olivine anorthosite)	Upper Zone	Zebra Moutains succession		
Troctolite (subordinate anorthosite)	Lower Zone			± 1370 Ma
Granite gneiss, amphibolite			Epupa Metamorphic Complex	± 1470 Ma

Table 1. Stratigraphy of the study area (modified after Menge, 1986, 1996; Seth *et al*., 2003)

Kunene Igneous Complex

The EMC is intruded by the Mesoproterozoic anorthosites of the Kunene Igneous Complex (KIC), which straddles the Namibian/Angolan border, and, with ca. 20 000 km^2, is the largest anorthosite complex of the world (Drüppel, 1999). The southern part of the KIC was first described by Beetz (1933), who established the presence of gabbro, norite, anorthosite and pyroxenite. These rocks were divided into three distinct intrusive successions (e. g. Menge, 1996); 1) massive, light-coloured anorthosite intercalated with 2) dark leucotroctolite - anorthosite in the northwest ("Zebra Mountains"), and 3) a small unit of anorthosite and subordinate, locally olivine-bearing, leucogabbro. The emplacement age of the KIC has been well constrained at around 1370 Ma by various authors (U–Pb single zircon/baddeleyite dating; e. g. Drüppel *et al*., 2007; McCourt *et al*., 2013; Bybee *et al*., 2019).

Swartbooisdrift - Epembe Alkaline Suite

Two successions of alkaline rocks occur in the Epembe – Swartbooisdrift area. The Epembe Subsuite consists mainly of nepheline syenite plugs, the Epembe carbonatite dyke, marginal syenite, and minor syenite and lamprophyre dykes, which intruded Epupa Complex gneisses (Figs 2, 3). Dolerite and quartz dolerite dykes of unknown age are present in the same area and generally follow the same regional trends. The Swartbooisdrift Subsuite, located in the vicinity of Swartbooisdrift on the Namibian/Angolan border, comprises dykes of banded sodalite, analcite, ankerite, cancrinite, albite and magnetite, which intruded mostly Kunene anorthosites and cross-cut older lamprophyres and syenite dykes. The Swartbooisdrift sodalite has been exploited for semi-precious stone and dimension stone.

The Epembe carbonatite dyke, some 40 km southwest of Swartbooisdrift, is distinctly younger than both the anorthosite and the syenites / nepheline syenites. While the latter were dated at 1213 ± 2.5 Ma (Seth *et al*., 2003), a concordant U-Pb age of 1184 ± 10 Ma was obtained for the former (Simon *et al*., 2017); for comparison, the age of the Swartbooisdrift carbonatite has been given as 1140 – 1120 Ma (Drüppel, 2003).

Local geology of the study area

The Epembe carbonatite dyke was emplaced along a northwest-trending fault zone into syenite and nepheline syenites (Menge, 1996); it extends for 6.5 km in a northwest-southeast direction (Figs 3, 4) and dips steeply (70° to 80°) towards the southwest. The

Epembe carbonatite has a maximum outcrop width of 200-400 m; the partially soil-covered dyke is thought to pinch out towards the east-southeast, where it forms several discontinuous veins. The carbonatite dyke is flanked by fenitised metamorphic rocks and alkaline intrusions of shonkinite and nepheline syenite (Fig. 3), with the degree of fenitisation being generally stronger in the fractured and jointed rocks adjoining the intrusions; farther away it becomes more erratic.

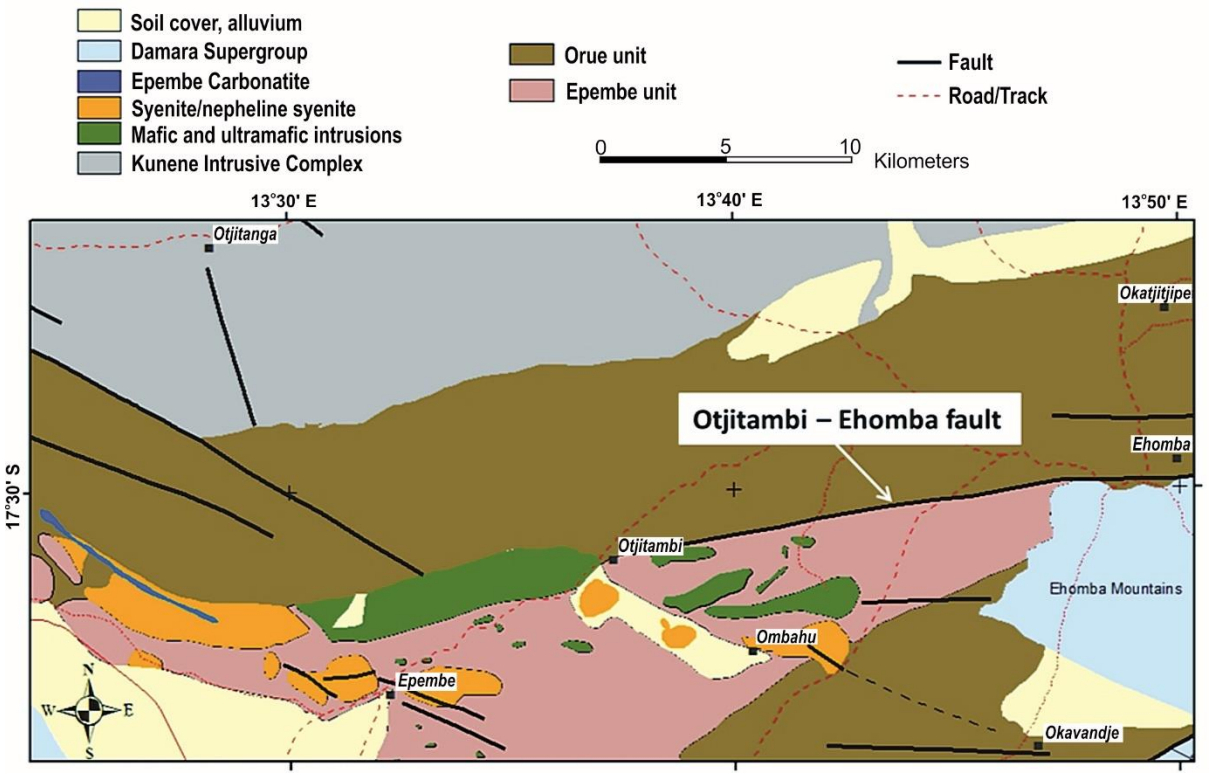

Figure 2. Geological overview of the southern part of the Kunene Intrusive Complex and the adjoining Epupa Metamorphic Complex (after Menge, 1996)

Methodology

Field work was undertaken to study the intrusive relationship between the carbonatites and their host rocks, and to collect representative samples for geochemical and petrographic analysis. Sixteen fresh rock samples (EPB1–EPB16) were collected along the Epembe carbonatite dyke and from the surrounding syenites and fenites (Fig. 5). Hand specimen images (Fig. 6) and thin section photographs (Fig. 7) illustrate mineralogy and texture of rock types present; detailed descriptions are given in Table 2.

A desk top study, including a review of existing publications, maps and miscellaneous documents, such as mineral exploration reports, provided the background for the current investigation. A total of sixteen rock samples was analysed for major and trace elements, and ten carbonatite thin sections, prepared at the Geological Survey of Namibia (GSN) laboratories, were studied to identify component mineral phases. Sample preparation for geochemical analysis was also carried out at the GSN labs. Whole rock samples were crushed to 0.5–15 mm size fraction and milled to a powder finer than 64 microns. A barren quartz flush was pulverised between each sample to minimise the risk of contamination. The sixteen pulp samples were sent to the laboratory of the University of the Witwatersrand (Johannesburg, South Africa) for major and trace element analysis. No control or duplicate samples were analysed due to financial constraints.

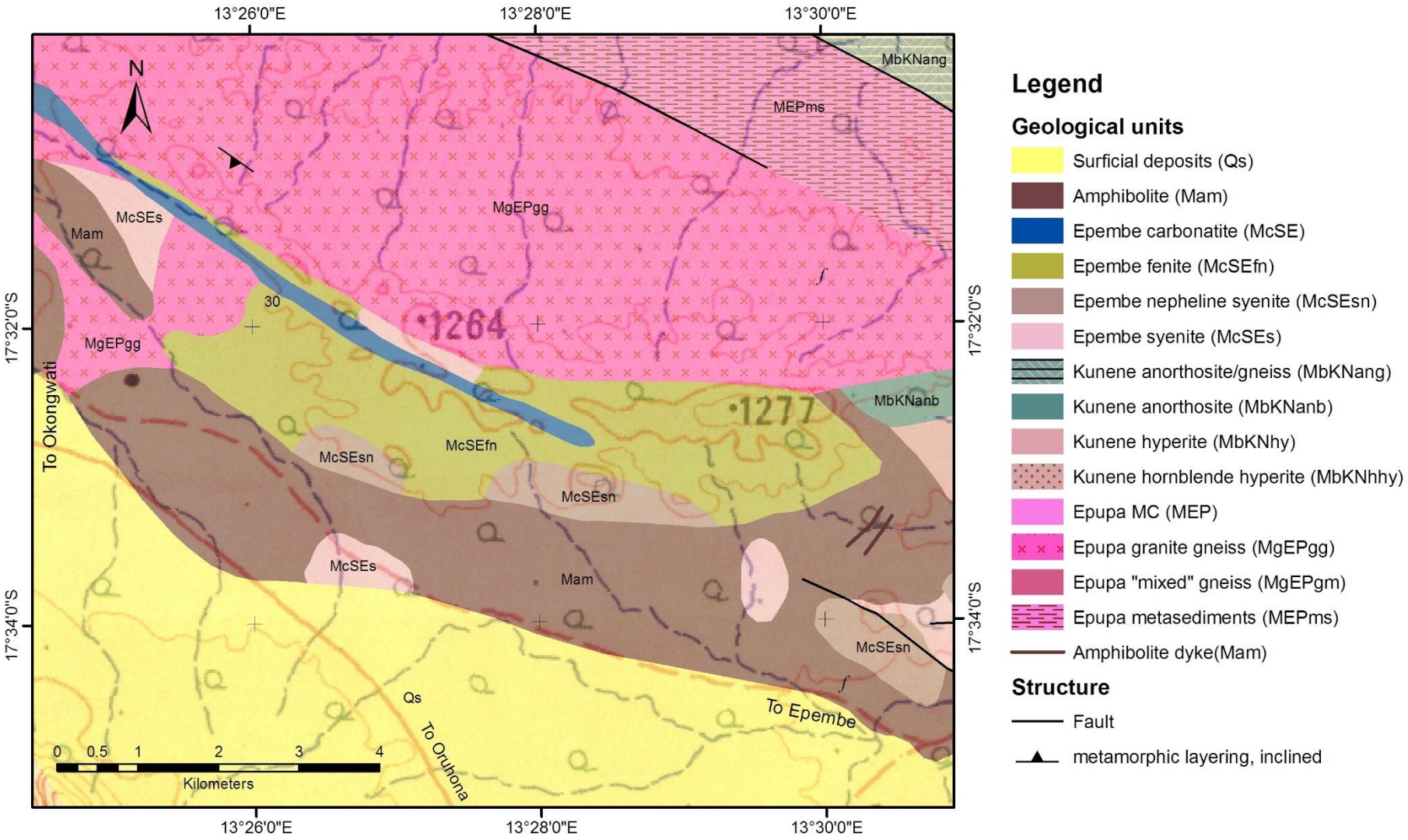

Figure 3. Geological map of the Epembe Subsuite showing the Epembe carbonatite dyke and surrounding rocks (Data source: Menge, 1996)

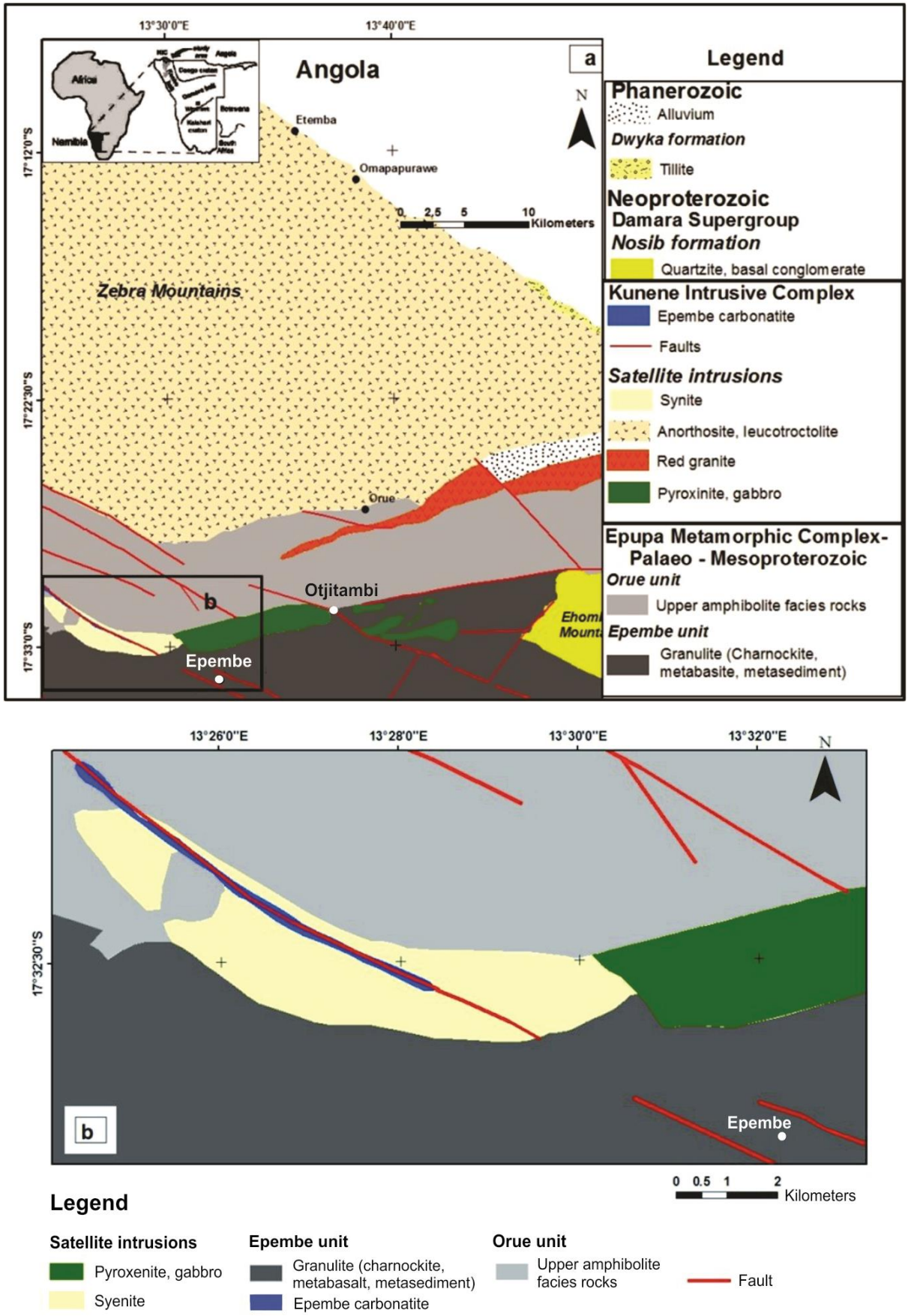

Figure 4. a) Simplified map of part of the Kunene Igneous Complex (KIC) showing location of the study area (black box); b) Sketch map of the study area showing the Epembe carbonatite dyke (after Simon *et al*., 2017)

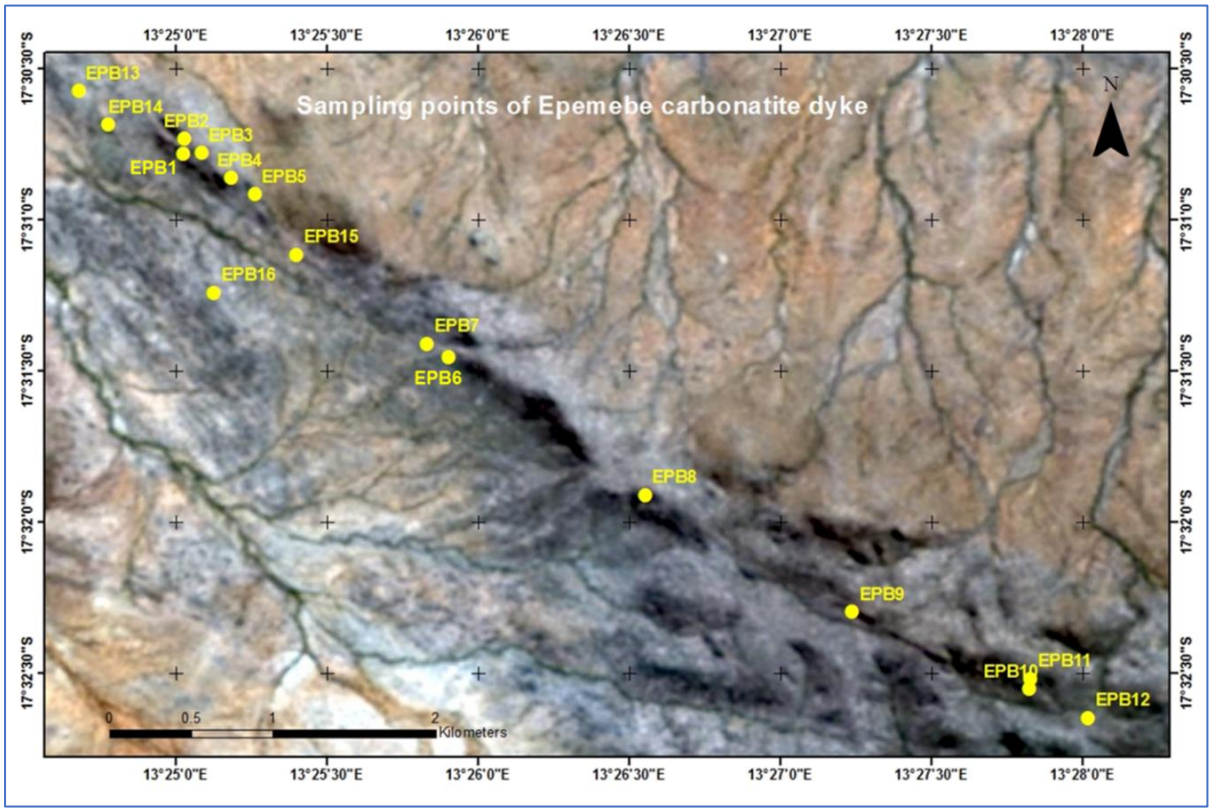

Figure 5. Google Earth image (Landsat 8, sharpened) of the Epembe carbonatite dyke showing sample locations

Major element oxides and trace elements were determined by the Norrish Fusion technique (Norrish and Hutton, 1969); analyses were carried out with a Panalytical (Philips PW2404) X-ray fluorescence spectrometer, using in-house correction procedures. Glass discs for major element analysis were fused with Johnson Matthey Spectrol flux 105 at 1100°C. Sample mass was 0.35 gram and flux mass 2.5 gram. Standard calibration was carried out with synthetic oxide mixtures and international standard rocks as well as in-house controls. Precision is set at 1% for elements making up more than 5% of the mass, and at 5% for elements forming less than 5% of the mass.

Pressed powder pellets for trace element analysis were produced with a Moviol alcohol solution binder. Standardisation was carried out using International Reference Materials of the United States Geological Survey and the NIM (National Institute of Metrology, China) series. Precision was determined based on time counts and is taken as 5% for elements in abundances greater than 100 ppm and 10% for elements in abundances from 10 to 100 ppm.

For rare earth element determination 50 mg of the sample were dissolved with high purity HF-HNO_3 in a MARS microwave digester, before being analysed by ICP-MS (Perkin Elmer DRC-e), using certified primary solution standards. International reference materials AGV-2, BCR-1 and BR-1 were analysed with every run. Agreement to accepted values of the standards was better than 10% for all elements, and often better than 5%.

Mineral identification was carried out on milled rock samples by a Bruker AXS D8 Advance X-ray Diffraction (XRD) Spectrometer. The "Eva" software (Bruker) was employed to identify characteristic peaks of the mineral phases present.

Petrography

The mineralogy of the Epembe Carbonatite-Syenite Subsuite is simple. Major minerals observed are calcite, apatite, biotite, K-feldspar, plagioclase, magnetite and aegirine. Hand specimens from weathered carbonatite outcrops are brown, while fresh surfaces

are a light tan in colour (Fig. 6E). The brown colouration is probably due to ferruginous staining through oxidation. The reddish-brown to white-grey carbonatites show some variation in grain size, ranging from fine- to coarse-grained (0.5 – 5.0 mm); locally the massive rocks are intruded by late-stage hydrothermal calcite veins (Figs 6A & E), which can be observed at outcrop level.

Calcite is the dominant carbonate mineral in all studied samples. Composition varies from almost monomineralic pure calcite (Fig. 6B) to aggregates with accessory apatite, pyrochlore, K-feldspar and minor aegirine, forming interlocking and hypidiomorphic textures. Yellowish-green apatite is found consistently throughout the Epembe carbonatite dyke, making up between 3 to 7 wt. %. Apatite occurs as subrounded or hexagonal, occasionally prismatic, crystals ranging from 0.1 to 2.5 cm in size, which are disseminated throughout the calcite matrix (Fig. 6C). Pyrochlore forms dark-brown, glassy octahedral crystals as well as irregular masses (Fig. 6D). Typically, it is coarse-grained, ranging in size from some tenths of a millimetre to greater than 2 mm. In places the carbonatite is characterised by dark-greenish phlogopite (Mg-biotite) phenocrysts (Fig. 6F). No REE minerals were observed in the Epembe carbonatite samples, except for monazite in trace amounts.

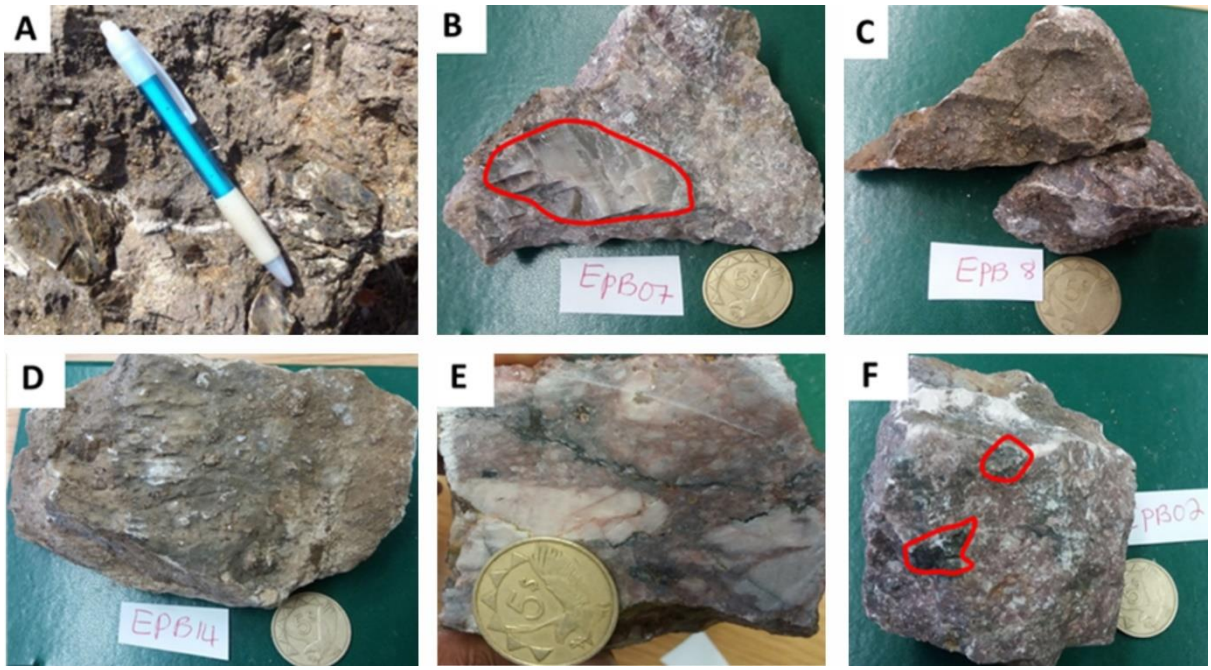

Figure 6. A) Biotite phenocrysts (up to 50 mm) in heavily weathered, feldspar-free carbonatite cross-cut by late hydrothermal calcite veins; B) Coarse-grained calcite crystals (circled in red) up to 5 mm in size; C) Carbonatite sample displaying equigranular, holocrystalline grains of sugary calcite - the pinkish to brownish colour is due to the presence of feldspar and darker minerals including pyrochlore and aegirine; D) Carbonatite sample with dark-brown pyrochlore crystals; E) Fresh carbonatite sample with calcite crystals and late-stage veins stained by iron oxides; F) Medium-grained, pinkish-brown carbonatite with dark-greenish phlogopite (Mg-biotite) phenocrysts (circles); pen = 15 cm, diameter of coin = 25 mm

Ten thin sections were studied with a polarising Carl Zeiss Axiolab microscope under plane- and cross-polarised light to identify main minerals, accessory phases and textures. Confirming field observation and XRD analysis, the most common mineral in the Epembe carbonatite was found to be calcite (~90%), of which two generations are present. In some samples calcite forms large euhedral grains with well-developed cleavages (Fig. 7A), while it is medium- to fine-grained in others (Fig. 7B), possibly reflecting divergent crystallisation histories.

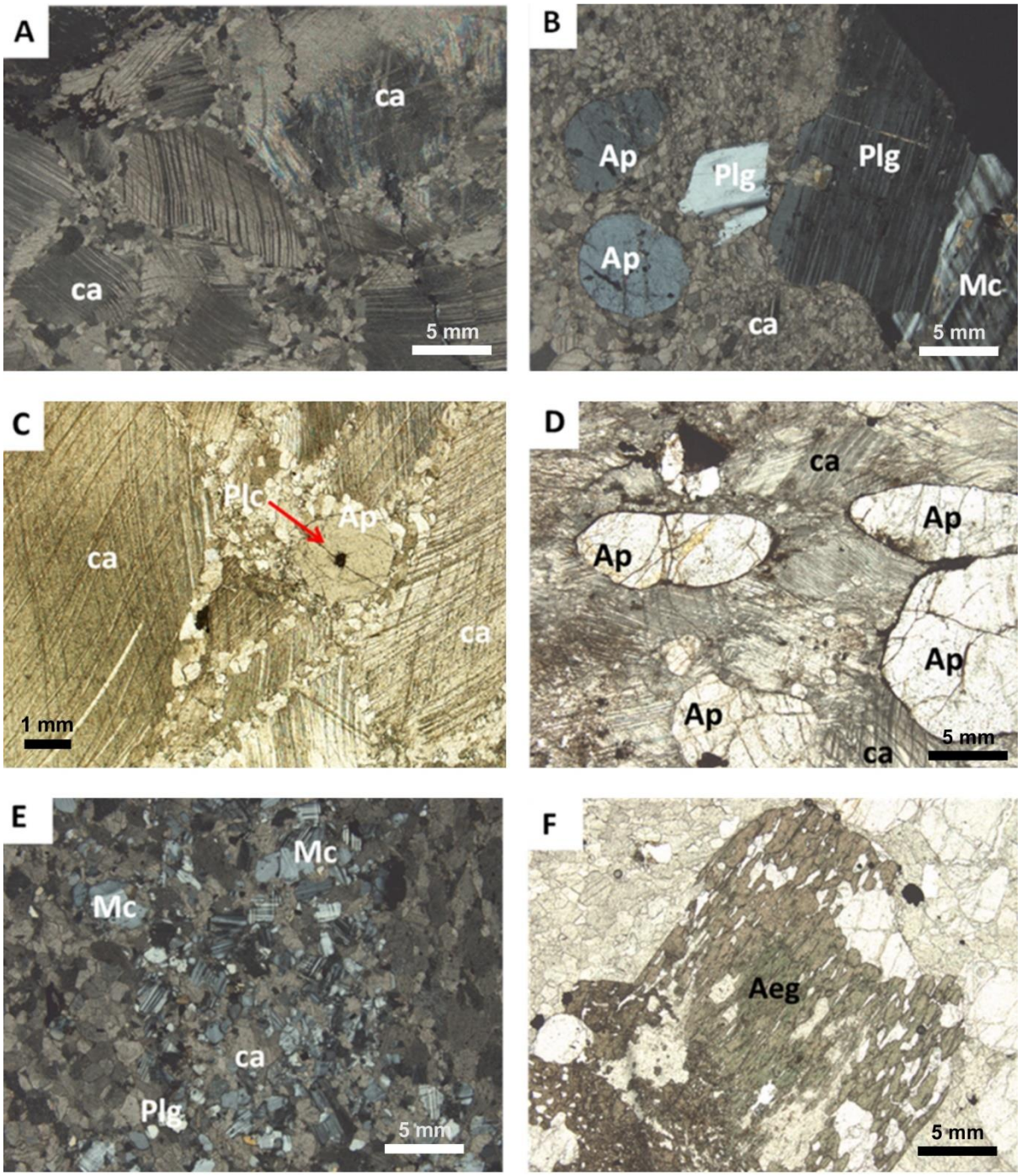

Figure 7. Photomicrographs of representative carbonatite samples in cross- (XPL) and plane-polarised light (PPL): A) EPB01 - coarse-grained calcite with mica filling cracks and fractures (XPL); B) EPB02 - ovoid apatite grains and feldspars embedded in calcite matrix (XPL); C) EPB03 - coarse-grained calcite and ovoid apatite grain enclosing a pyrochlore grain (arrow; PPL); D) EPB08 - elongated and aligned apatite and calcite grains (PPL); E) EPB13 - medium- to fine-grained granular groundmass of anhedral feldspar, interstitial calcite and minor quartz forming an equigranular texture (XPL) of unoriented grains; F) EPB13 - coarse-grained aegirine in calcite matrix (XPL). Abbreviations: Aegirine (Aeg), Apatite, (Ap), Calcite (ca), Microcline (Mc), Pyrochlore (Plc), Plagioclase (Plg)

The second most abundant mineral is apatite, which has been observed in all the studied carbonatite samples. Apatite grains are subrounded to oval and occur in association with pyrochlore, feldspar, calcite and aegirine (Figs 7C & D). Some apatite grains appear elongated and aligned.

Another principal accessory mineral is pyrochlore. The honey-brown to pale yellow mineral occurs as opaque fine- to medium-grained (1µm - 0.5 cm) crystals, especially in veins. Pyrochlore usually is found intricately intergrown with apatite and calcite. Some crystals exhibit zonation, which may indicate a long-lasting crystallisation process within the magma chamber (Wyllie and Biggar, 1966), restricted to late-stage carbonatite magmatism.

Knudsen (1989) describes the development of pyrochlore composition throughout magmatic evolution. During the initial stage of carbonatite magmatism, Ta and Nb are possibly transported as fluoride and phosphate complexes, which explains the common association of apatite with pyrochlore. In places, pyrochlore forms inclusions (Fig. 7C) within apatite crystals showing that pyrochlore formed before apatite.

Micas (mainly biotite and phlogopite) and feldspars (plagioclase – albite, microcline) are found in affiliation with magnetite, hematite and chlorite within the groundmass (Fig.7E) of the carbonatite. They primarily occur in clusters of discrete grains; in places they coat the margins of minerals such as pyrochlore, which identifies them as late-stage crystallisation products. Aegirine forms coarse grains (up to 1 cm) in the calcite matrix (Fig. 7F), and dolomite occurs in minor amounts as fine-grained crystals in veinlets, or as replacement of calcite. Occasionally dolomite coats the grain boundaries of pyrochlore and apatite. Optical characteristics of the observed mineral phases are summarised in Table 2.

Minerals	**Texture and Characteristics**
Calcite	Coarse-grained calcite is the dominant mineral (~90%). It shows well-developed cleavages (multiple twinning) with high birefringence.
Apatite	Apatite forms white or light-grey to colourless, spherical to subrounded crystals, up to 2.5 mm in size. It is scattered throughout the coarse-grained calcite matrix producing a porphyritic texture.
Pyrochlore	Pyrochlore forms reddish-brown euhedral to subhedral crystals, < 0.2 mm in size, which occur as isolated grains in the calcite matrix. It also occurs as inclusions within apatite.
Feldspar	Feldspar is one of the most common accessory minerals. Colourless plagioclase (albite?) is found in the fine-grained matrix, varying in size from fine-grained in veins to medium-grained.
	Holocrystalline K-feldspar (microcline) occurs within an equigranular groundmass of subhedral, medium- to coarse-grained alkali feldspar.
Mica	Biotite (phlogopite?) forms pale to deep brown or greenish-brown tabular crystals filling interstices between aggregates of other minerals.
Hematite / Magnetite	Rectangular, opaque and cubic grains of iron minerals are observed either in interstices between coarse calcite grains or in the fine-grained matrix.
Aegirine	Where present, aegirine is typically brownish-green in colour, appearing as large (up to 4 mm), aligned phenocrysts either disseminated throughout the matrix or as cumulate concentrations.
Quartz	Quartz occurs rarely either as inclusions within other minerals or as part of the groundmass in association with Fe-bearing minerals and mica.
Chlorite	Where present, chlorite is found in clusters or exploiting fractures.
Dolomite	Dolomite coexists with calcite and is dominant along the margins of opaque minerals.

Table 2. Optical characteristics of minerals identified in the Epembe carbonatite

Geochemistry

Sixteen representative samples of the Epembe carbonatite and adjacent rocks were analysed for major and trace elements including rare earth elements. Major elements were analysed by X-Ray Fluorescence (XRF) and trace elements by inductively coupled plasma mass spectrometry (ICP-MS; see also chapter "Methodology").

Major elements

Major element compositions show high calcium (CaO: 38.01 to 55.31 wt. %), variable iron (FeO: 0.87 to 9.29 wt.% / Fe_2O_3: 0.97 to 10.33 wt%) and low magnesium concentrations (MgO: 0.19 to 1.33 wt. %), which classifies the Epembe samples as calcio-carbonatites and subordinate ferro-carbonatites, on an MgO – CaO – FeO_t (+MnO) ternary diagram (Woolley and Kempe, 1989; Fig. 8). Compared with the global average for calcio-carbonatites (Woolley and Kempe, 1989; Table 3), average Epembe carbonatite shows elevated SiO_2 (4.07 wt. %), and FeO / Fe_2O_3, (2.77 / 3.08 wt. %) concentrations, while MgO (0.40 wt. %) is significantly below average; other elements, including calcium fall within the same range as global averages. Apart from calcite, the Epembe carbonatite contains dolomite [(Ca, Mg $(CO_3)_2$], where randomly substituted magnesium is present in a disordered calcite lattice. Chromium (Cr_2O_3) occurs in trace amounts (<0.025 wt. %; Table 3), and phosphorus is enriched in some of the samples while being depleted in others (compared to the global average; Table 3).

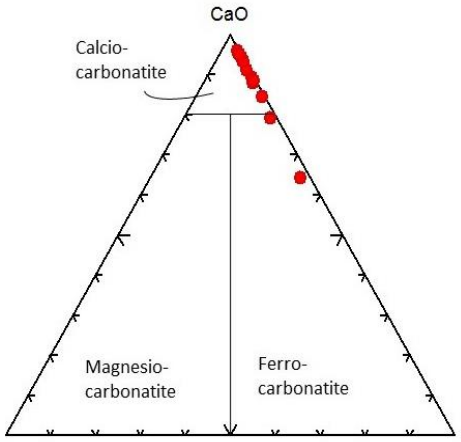

Figure 8. Ternary MgO-CaO-FeOt diagram for carbonatites (after Woolley and Kempe, 1989)

The high proportion of volatiles as evidenced by the high loss on ignition of the Epembe carbonatites (LOI: 28.18 to 41.56 wt. %) is similar to that of average calcio-carbonatites (37.4 wt. %; Table 3). In comparison, fenite and syenite samples only show an LOI of 0.67 wt. % and 3.03 wt. %, respectively. The high LOI in the analysed carbonatite is ascribed to a loss of carbon dioxide (CO_2) during heating.

Sample No	Lithology	SiO_2	Al_2O3	Fe_2O_3	(FeO)	MnO	MgO	CaO	Na_2O	K_2O	TiO_2	P_2O_5	Cr_2O_3	LOI	Total
EPB01	Carbonatite	5.28	1.28	4.41	(3.97)	0.28	0.35	48.98	0.22	0.55	0.13	3.62	0.02	34.71	99.83
EPB02	Carbonatite	3.71	0.52	2.89	(2.60)	0.25	0.23	49.47	0.44	0.19	0.09	2.81	0.02	36.78	97.40
EPB03	Carbonatite	10.89	4.45	10.33	(9.29)	0.25	1.33	38.01	0.21	1.52	1.06	3.43	0.02	28.18	99.68
EPB04	Carbonatite	3.91	1.17	2.25	(2.02)	0.24	0.33	50.00	0.11	0.59	0.14	2.22	0.03	37.14	98.13
EPB05	Fenite	67.81	15.37	3.32	(2.99)	0.05	0.88	1.49	5.10	5.62	0.74	0.32	0.02	0.67	101.39
EPB06	Carbonatite	1.73	0.16	0.97	(0.87)	0.31	0.25	55.31	0.05	0.02	0.03	0.46	0.02	40.83	100.14
EPB07	Carbonatite	1.99	0.52	1.67	(1.50)	0.31	0.23	53.90	0.03	0.15	0.03	0.53	0.02	40.29	99.67
EPB08	Carbonatite	2.62	0.65	1.36	(1.22)	0.29	0.19	51.54	0.01	0.42	0.06	1.18	0.02	39.88	98.22
EPB09	Carbonatite	1.30	0.35	1.18	(1.06)	0.31	0.26	54.69	0.04	0.17	0.03	0.16	0.02	41.56	100.07
EPB10	Syenite	54.57	19.96	2.24	(2.02)	0.07	0.34	4.48	7.01	6.65	0.25	0.37	0.02	4.79	100.75
EPB11	Carbonatite	6.26	1.61	5.83	(5.25)	0.25	0.76	46.18	0.19	0.91	0.33	0.75	0.02	36.08	99.17
EPB12	Carbonatite	2.41	0.79	3.29	(2.96)	0.38	0.59	52.33	0.03	0.36	0.14	2.30	0.03	37.53	100.18
EPB13	Carbonatite	3.42	0.63	3.10	(2.79)	0.29	0.27	49.41	0.34	0.28	0.05	1.50	0.03	38.11	97.43
EPB14	Carbonatite	7.90	2.27	1.55	(1.39)	0.34	0.20	48.83	0.26	1.44	0.03	1.66	0.02	34.41	98.91
EPB15	Carbonatite	1.51	0.50	1.22	(1.10)	0.26	0.19	54.45	0.01	0.15	0.05	0.34	0.02	41.04	99.74
EPB16	Syenite	55.64	20.21	5.73	(5.16)	0.09	1.44	2.73	9.64	1.77	0.62	0.23	0.02	3.03	101.15
Epembe carbonatite	**Average**	**4.07**	**1.15**	**3.08**	**(2.77)**	**0.29**	**0.40**	**50.24**	**0.15**	**0.52**	**0.17**	**1.61**	**0.02**	**37.43**	
Calcio-carbonatite	**Global average**	**2.72**	**1.06**	**2.25**	**1.01**	**0.52**	**1.80**	**49.12**	**0.29**	**0.26**	**0.15**	**2.10**	**N/A**	**37.40**	

Table 3. Whole rock major element oxides (wt. %) of Epembe rocks and average calcio-carbonatite composition (after Woolley and Kempe, 1989); as major element analyses obtained by XRF cannot provide both Fe_2O_3 and FeO, FeO is taken as Fe_2O_3 x 0.8998 (stoichiometric calculations after Gaillard *et al*., 2003)

Sample No	EPB01	EPB02	EPB03	EPB05	EPB04	EPB06	EPB07	EPB08	EPB09	EPB10	EPB11	EPB12	EPB13	EPB14	EPB15	EPB16	Epembe carbonatite	Epembe carbonatite	Global Calcio-carbonatite
Lithology	Carbon-atite	Carbon-atite	Carbon-atite	Fenite	Carbon-atite	Carbon-atite	Carbon-atite	Carbon-atite	Carbon-atite	Syenite	Carbon-atite	Carbon-atite	Carbon-atite	Carbon-atite	Carbon-atite	Syenite	Range	Average	Average
Li	1.86	0.49	4.53	6.40	1.37	0.49	1.21	0.75	0.34	8.15	2.01	1.71	0.51	0.77	0.73	46.18	0.3-4.5	1.29	0.1
P	18076.91	11637.61	12778.69	1158.75	8314.23	2024.97	2546.25	5109.31	751.43	1314.42	3516.50	11330.12	7512.34	7694.05	1491.79	1110.54	751.4-18076.9	7137.25	N/A
Sc	4.38	7.03	3.96	4.29	3.66	1.19	0.78	1.77	0.45	0.16	1.86	2.36	6.38	1.51	1.07	1.61	0.45-7.0	2.80	7
Ti	674.36	381.25	5122.76	4018.86	644.72	43.60	137.70	217.33	69.00	863.49	1535.99	600.21	184.22	113.75	144.34	3749.91	43.6-5122.8	759.17	N/A
V	161.81	89.28	116.55	51.45	33.90	2.72	8.25	17.29	5.45	12.07	47.35	28.60	148.95	3.72	19.43	58.22	2.7-161.8	52.56	80
Cr	12.13	9.57	8.32	84.73	6.05	4.62	13.25	3.82	3.96	48.70	8.62	8.45	23.91	10.36	5.34	67.25	3.8-23.9	9.11	13
Co	7.55	3.25	11.47	5.92	4.39	2.64	2.20	4.06	2.19	2.17	7.92	10.62	5.67	4.27	3.44	8.96	2.2-11.5	5.36	11
Ni	19.65	17.75	11.88	7.32	17.32	19.84	21.22	16.59	19.30	3.71	24.07	31.68	21.52	27.21	30.22	11.91	11.9-31.7	21.40	18
Cu	9.27	7.89	7.43	32.45	4.55	9.73	6.29	9.38	3.51	4.24	17.73	19.23	6.88	5.98	4.49	9.82	3.5-19.2	8.64	24
Zn	13.75	12.87	99.36	42.48	15.10	6.71	6.37	518.03	10.57	25.55	59.37	27.73	8.97	54.41	5.99	93.41	6.0-518.0	64.55	188
Ga	12.47	7.06	16.12	22.93	8.22	3.29	3.71	4.66	4.97	28.30	15.18	8.22	6.33	6.63	3.79	27.56	3.3-16.1	7.74	<5
Rb	17.99	6.35	20.90	223.12	20.86	0.99	3.41	7.24	9.58	56.34	77.38	13.53	7.19	21.39	3.72	124.77	1.0-77.4	16.19	14
Sr	4232.20	12315.44	7544.46	444.70	8641.79	5108.84	4538.52	8954.93	5381.32	782.81	8282.47	3354.48	9446.24	7502.44	4832.95	1074.92	3354.5-12315.4	6933.54	N/A
Zr	125.73	99.53	114.13	461.50	94.08	2.61	2.45	116.13	3.07	199.56	224.42	34.96	72.88	6.87	7.64	292.52	2.45-224.4	69.58	189
Nb	1532.57	1090.02	2022.64	20.90	159.58	7.69	40.05	280.70	45.17	26.22	150.53	225.13	64.15	51.78	24.80	141.54	7.7-2022.6	438.06	1204
Ba	96.63	134.62	205.81	2637.84	142.23	53.78	516.21	135.76	110.28	669.35	182.43	saturated	141.36	247.50	98.64	633.98	53.8->LD	172.10	N/A
Sn	18.09	17.93	11.40	2.69	4.23	0.24	1.70	3.68	0.97	0.21	4.62	1.04	16.98	1.44	1.05	3.20	0.2-18.1	6.41	N/A
Cs	0.63	0.24	1.35	3.98	0.71	0.02	0.20	0.07	1.88	1.38	2.95	0.96	0.15	0.12	0.12	5.20	0.02-2.95	0.72	20
Hf	5.04	5.68	3.05	10.62	2.10	0.12	0.13	2.09	0.19	3.56	3.95	0.84	3.59	0.19	0.29	4.96	0.1-5.7	2.10	N/A
Ta	76.50	187.42	367.28	1.15	33.41	0.49	10.76	54.01	8.36	1.13	12.84	48.35	8.42	2.16	3.02	6.43	0.5-367.3	62.54	5
W	0.65	0.12	0.27	0.40	0.19	0.14	0.23	0.12	0.24	0.16	0.37	0.27	0.10	0.22	0.15	0.51	0.1-0.65	0.23	N/A
Pb	5.81	6.74	6.21	27.35	5.02	6.50	2.99	143.84	6.99	2.87	4.76	19.16	7.04	23.24	1.74	11.60	1.7-143.8	18.46	56
Th	21.90	6.37	8.06	72.78	2.08	0.40	0.34	3.22	3.28	0.94	3.05	2.26	0.41	0.76	0.96	4.44	0.3-21.9	4.08	52
U	26.74	331.90	480.06	7.43	25.15	2.18	6.19	67.62	10.67	2.33	6.00	50.28	9.09	1.92	2.10	4.10	1.9-480.1	78.45	8.7

Table 4. Trace element composition (ppm) of Epembe rocks and average calcio-carbonatite (after Woolley and Kempe, 1989; 'calcio-carbonatite' represents samples with CaO/(CaO+MgO+FeOt+MnO) > 80%; N/A= data not available)

Sample No	EPB01	EPB02	EPB03	EPB04	EPB05	EPB06	EPB07	EPB08	EPB09	EPB10	EPB11	EPB12	EPB13	EPB14	EPB15	EPB16	Epembe carbonatite	Epembe carbonatite	Global calcio-carbonatite
Lithology	Carbon-atite	Carbon-atite	Carbon-atite	Carbon-atite	Fenite	Carbon-atite	Carbon-atite	Carbon-atite	Carbon-atite	Syenite	Carbon-atite	Carbon-atite	Carbon-atite	Carbon-atite	Carbon-atite	Syenite	Range	Average	Average
La	176.88	159.36	151.28	166.47	157.42	131.63	123.83	109.64	163.84	13.11	167.19	172.03	133.58	76.81	141.43	26.98	**76.8-176.9**	144.15	608
Ce	347.77	296.86	267.93	307.59	290.66	260.13	241.30	210.87	341.54	32.61	290.23	saturated	257.33	168.92	254.80	53.40	**168.9->LD**	270.44	1687
Pr	39.42	32.69	30.41	33.87	28.65	26.03	26.52	23.07	35.45	2.49	31.95	40.21	29.80	21.57	28.56	6.68	**23.1-40.2**	30.74	219
Nd	159.16	132.66	136.07	136.48	102.65	100.02	112.51	94.82	149.78	10.58	130.90	saturated	128.71	82.44	103.42	27.59	**82.4->LD**	122.25	883
Sm	28.77	23.41	20.86	22.54	15.60	16.18	18.17	17.69	25.30	2.00	20.78	28.64	21.63	17.87	17.80	5.36	**16.2-28.8**	21.51	130
Eu	8.59	6.93	6.14	6.69	3.24	4.51	5.25	5.33	6.90	0.72	6.19	8.59	6.43	5.46	5.00	1.50	**4.5-8.6**	6.31	39
Gd	29.34	24.16	20.80	23.70	12.80	17.95	19.32	19.32	26.83	1.79	21.87	30.04	22.34	18.46	18.21	4.41	**17.6-30.1**	22.49	105
Tb	3.49	2.75	2.28	2.70	1.10	2.20	2.27	2.32	3.04	0.18	2.43	3.52	2.63	2.36	2.07	0.53	**2.1-3.5**	2.62	9
Dy	18.10	14.24	11.17	13.91	4.68	12.35	12.36	13.15	16.08	0.93	12.61	18.10	14.03	12.61	10.50	2.78	**10.5-18.1**	13.78	34
Ho	2.98	2.43	1.82	2.36	0.67	2.29	2.19	2.33	2.80	0.15	2.14	3.10	2.40	2.28	1.86	0.47	**1.8-3.1**	2.38	6
Er	6.78	5.72	4.33	5.70	1.75	5.96	5.49	5.53	6.82	0.37	5.36	7.43	5.76	5.38	4.68	1.22	**4.3-7.4**	5.76	4
Tm	0.93	0.80	0.58	0.79	0.20	0.95	0.85	0.82	0.95	0.05	0.75	1.04	0.83	0.81	0.68	0.19	**0.6-1.0**	0.83	1
Yb	5.66	5.11	3.61	5.07	1.28	6.49	5.63	5.21	6.09	0.30	4.78	6.51	5.16	5.12	4.37	1.26	**3.6-6.5**	5.29	5
Lu	0.77	0.70	0.50	0.72	0.17	0.97	0.81	0.74	0.86	0.04	0.68	0.91	0.74	0.73	0.64	0.19	**0.5-1.0**	0.75	1
Y	83.48	75.31	54.56	72.66	19.44	76.14	70.69	74.33	91.07	3.43	69.77	86.18	67.44	63.28	52.53	10.57	**52.5-91.1**	72.11	119
Total REE + Y	**912.11**	**783.12**	**712.34**	**801.25**	**640.30**	**663.79**	**647.17**	**585.15**	**877.33**	**68.75**	**767.63**	**320.13**	**698.80**	**484.11**	**646.551**	**143.14**		721.41	3850

Table 5: Rare Earth element composition (ppm) of Epembe rocks and average calcio-carbonatite (after Woolley and Kempe, 1989)

Trace and REE elements

Trace and rare earth element results are presented in Tables 4 and 5, respectively. In comparison to fenite and syenite, the analysed carbonatite samples show high concentrations of phosphorus (up to 18076 ppm; EPB01), titanium (up to 5122 ppm; EPB03), strontium (up to 12315 ppm; EPB02) and niobium (up to 2022 ppm; EPB03) (Table 4), while barium exceeds the detection limits of ICP-MS in sample EPB12. Cesium and tungsten are low in the carbonatite samples, with concentrations of < 3 ppm and < 1 ppm, respectively, while other trace elements show moderate concentrations. The high content of phosphorus in sample EPB01 is indicative of the presence of apatite ($Ca_5[PO_4]_3[F, OH]$), while high Ta and Nb concentrations imply an abundance of pyrochlore ($[Na, Ca, Sr, Pb, U]_2 (Nb, Ta, Ti)_2 O_6 (OH, F)$ in samples EPB02 and EPB03.

REE contents of the Epembe carbonatites are high relative to fenite and syenite, though low compared to the global average (Table 5); Ce and Nd in sample EPB12 are above the detection limit of ICP-MS. At the same time, sample EPB12 records the lowest total rare earth (REE_t + Y) concentration of only 406 ppm, while the maximum concentration of 912 ppm occurs in sample EPB01. The total REE content of fenite (640.30 ppm, EPB05) is somewhat lower than that of carbonatites, but significantly higher than in syenite (68.75 ppm in EPB10 and 143.14 ppm in EPB16). The elevated REE content of fenites relative to syenites (Fig. 9, Table 5) is attributed to metasomatic processes, whereby REE constituents were introduced through carbonatitic hydrothermal fluids. Analytical results for REE were normalised to chondrite values (Rock, 1987). Normalised REE values are presented in Table 6 and REE patterns are illustrated in Fig. 9.

REE distribution throughout the Epembe carbonatite dyke exhibits considerable differences, as shown by total REE contents (Tables 5, 6) and chondrite-normalised REE patterns (Fig. 9). The general trend displays a distinct negative (downward) slope from LREE to HREE, demonstrating a strong enrichment of light rare earth elements (LaN/YbN = 10.19 to 28.49) compared to heavy rare earth elements (GdN/YbN = 2.24 to 4.66; Table 6). This is a feature common to most carbonatites, because of the favourable environment they present for the formation of LREE minerals, such as monazite, which has been observed in the Epembe carbonatite, even though only in trace amounts. All samples are characterised by a slight negative Eu anomaly and a positive Gd anomaly.

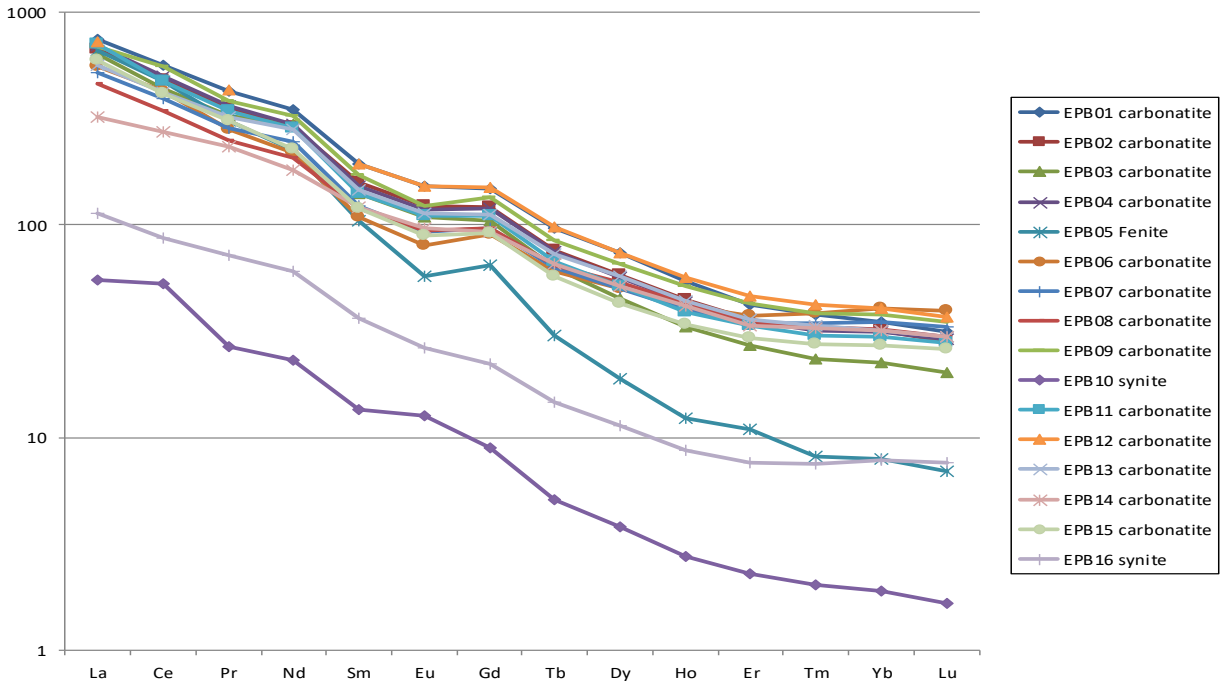

Figure 9. REE patterns for carbonatite, fenite and syenite samples from the Epembe carbonatite dyke and surrounding rocks (chondrite-normalised REE values after McDonough and Sun, 1995)

Sample No	**EPB01**	**EPB02**	**EPB03**	**EPB04**	**EPB05**	**EPB06**	**EPB07**	**EPB08**	**EPB09**	**EPB10**	**EPB11**	**EPB12**	**EPB13**	**EPB14**	**EPB15**	EPB16	Chondrite normalising factors
Lithology	Carbon-atite	Carbon-atite	Carbon-atite	Carbon-atite	Fenite	Carbon-atite	Carbon-atite	Carbon-atite	Carbon-atite	Syenite	Carbon-atite	Carbon-atite	Carbon-atite	Carbon-atite	Carbon-atite	Syenite	
La	746.32	672.41	638.33	702.41	664.20	555.41	522.48	462.63	691.29	55.32	705.46	725.86	563.63	324.10	596.76	113.85	0.237
Ce	567.33	484.27	437.09	501.78	474.15	424.36	393.64	343.99	557.16	53.19	473.46		419.79	275.56	415.65	87.11	0.613
Pr	424.82	352.23	327.74	364.96	308.73	280.52	285.82	248.59	381.95	26.85	344.25	433.32	321.14	232.44	307.79	72.00	0.093
Nd	348.26	290.29	297.74	298.64	224.63	218.85	246.19	207.47	327.75	23.15	286.44		281.65	180.39	226.30	60.37	0.457
Sm	194.36	158.20	140.92	152.32	105.43	109.30	122.76	119.52	170.93	13.50	140.39	193.52	146.16	120.74	120.24	36.23	0.148
Eu	152.52	123.07	109.11	118.81	57.57	80.11	93.20	94.58	122.49	12.70	109.93	152.63	114.14	96.96	88.85	26.55	0.056
Gd	147.44	121.40	104.50	119.12	64.30	90.22	97.08	97.08	134.81	8.97	109.89	150.97	112.24	92.75	91.51	22.17	0.199
Tb	96.65	76.23	63.27	74.65	30.36	60.91	62.74	64.32	84.29	5.07	67.37	97.42	72.96	65.40	57.34	14.76	0.036
Dy	73.56	57.87	45.39	56.55	19.03	50.18	50.25	53.46	65.35	3.79	51.28	73.56	57.02	51.27	42.68	11.32	0.246
Ho	54.56	44.45	33.32	43.26	12.27	41.90	40.02	42.67	51.25	2.77	39.18	56.79	44.03	41.83	34.05	8.66	0.055
Er	42.38	35.75	27.09	35.64	10.91	37.26	34.30	34.56	42.61	2.29	33.47	46.43	36.01	33.64	29.24	7.63	0.160
Tm	37.69	32.43	23.56	32.02	8.14	38.38	34.29	33.24	38.46	2.02	30.16	42.19	33.48	32.71	27.61	7.49	0.025
Yb	35.18	31.74	22.40	31.49	7.93	40.31	34.96	32.33	37.83	1.89	29.68	40.43	32.04	31.81	27.14	7.83	0.161
Lu	31.26	28.33	20.12	29.11	6.95	39.31	33.01	29.88	34.96	1.67	27.80	37.15	29.88	29.80	26.18	7.60	0.025
Total REE	**2952.33**	**2508.66**	**2290.57**	**2560.76**	**1994.59**	**2067.03**	**2050.75**	**1864.34**	**2741.12**	**213.18**	**2448.74**	**2050.28**	**2264.17**	**1609.42**	**2091.34**	**483.58**	**2.510**
Chondrite-normalised ratios																	
Eu/Eu*	0.06	0.05	0.05	0.05	0.04	0.05	0.05	0.05	0.05	0.07	0.05	0.05	0.05	0.05	0.05	0.05	
Ce/Ce*	0.62	0.61	0.58	0.61	0.64	0.66	0.62	0.62	0.66	0.85	0.59		0.60	0.62	0.59	0.59	
LaN/YbN	21.21	21.19	28.49	22.31	83.74	13.78	14.94	14.31	18.28	29.30	23.77	17.95	17.59	10.19	21.99	14.55	
LaN/SmN	3.84	4.25	4.53	4.61	6.30	5.08	4.26	3.87	4.04	4.10	5.03	3.75	3.86	2.68	4.96	3.14	
GdN/YbN	4.19	3.82	4.66	3.78	8.11	2.24	2.78	3.00	3.56	4.75	3.70	3.73	3.50	2.92	3.37	2.83	
LaN/LuN	23.87	23.73	31.72	24.13	95.55	14.13	15.83	15.48	19.77	33.19	25.37	19.54	18.86	10.88	22.80	14.98	

Table 6. REE chondrite-normalised data for sixteen samples of carbonatite, fenite and syenite from the Epembe Subsuite (chondrite values after McDonough and Sun (1995). Chondrite-normalised ratios: Eu/Eu* represents the amplitude of the Eu anomaly [(Eu*=Eu/√(SmN x GdN)], with all carbonatite samples having ratios < 0.07, while Ce/Ce* gives the amplitude of the Ce anomaly [Ce*=Ce/√(LaN x PrN)], with nine samples (including one fenite and one syenite sample) having ratios > 0.6 and the remainder ratios below but close to 0.6; LaN/YbN (=La normalised to chondrite/Yb normalised to chondrite) gives the general steepness of the REE pattern (carbonatite: 10.19 to 28.49; fenite: 83.74); LaN/SmN represents the steepness of LREE (carbonatite: 2.68 to 5.08) and GdN/YbN the steepness of HREE (carbonatite: 2.24 to 4.66).

Discussion and Conclusions

Field relationships indicate that the Epembe carbonatite dyke intruded nepheline syenite of the Epembe Subsuite (Epembe–Swartbooisdrift Alkaline Suite). Contacts between the country rocks and the carbonatite show a very high degree of fenitisation, and blocks of veined, brecciated fenite occur as xenoliths in the carbonatite (Fig. 10). It is assumed that the high temperature of the carbonatite melt caused a mineralogical change in the surrounding country rocks, forming a prominent thermal aureole. Radiogenic age determinations confirm the observed field relationships. While an emplacement age of 1184 ± 10 Ma (U-Pb single zircon; Simon, 2017) was determined for the carbonatite, the nepheline syenites were dated at 1216 ± 2.4 Ma and 1213 ± 2.5 Ma (U-Pb single zircon; Seth *et al*. 2003) and are thus clearly the older.

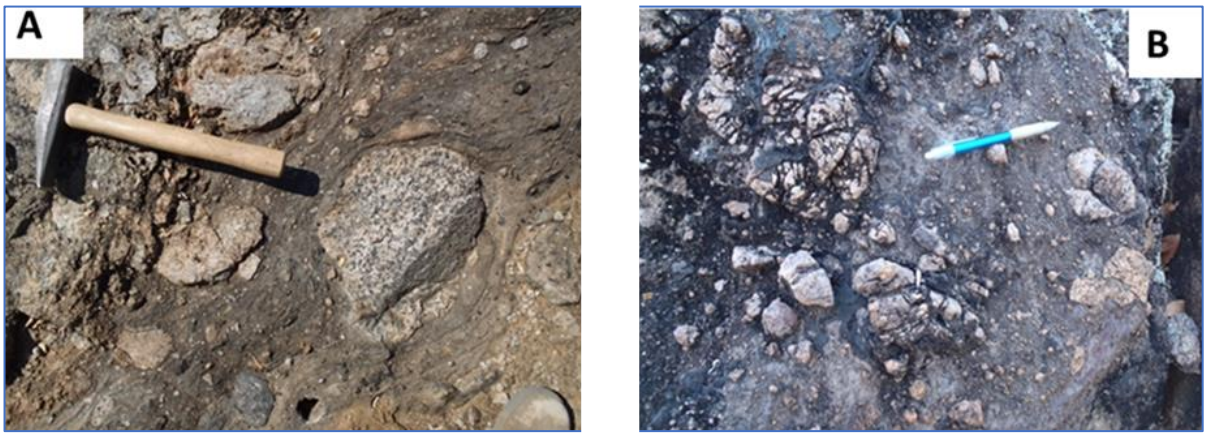

Figure 10. Xenoliths of syenite within the Epembe carbonatite: A) Syenite xenoliths with NW-SE oriented flow-banding; B) Carbonatite with xenoliths of syenite and aegirine-rich fenite (hammer = 35 cm, pen =15 cm)

Major and trace element geochemistry

The geochemistry of the Epembe carbonatites is consistent with established normal values for carbonatite. Based on the classification system of Gittins and Harmer (1997), which uses the dominant carbonate mineral to categorise carbonatites, the Epembe rocks classify as calcio-carbonatites. Similarly, the chemical classification system of Woolley and Kempe (1989) indicates that the Epembe carbonatites are calcio- or calcite-carbonatites.

The Epembe carbonatites have CaO/ (CaO + MgO + Fe_2O_3 + MnO) ratios of 50.24/ (50.24 + 0.4 + 3.08 + 0.29) = 0.93 on average, which is in agreement with typical calcio-carbonatite with CaO / (CaO + MgO + FeO + Fe_2O_3 + MnO) ratios > 0.8 This classification is supported by petrological studies which show the samples to consist of more than 80% calcite, in accordance with the definition of carbonatite as a rock composed of more than 50% carbonate (Shelley, 1993; Streckeisen, 1979).

Although displaying a certain degree of variation, the whole rock major and trace element composition of the Epembe carbonatites is comparable with the global average for calcio-carbonatites (Woolley and Kempe, 1989; Table 3). While the Epembe carbonatite is characterised by lower-than-average MnO, MgO, Na_2O, V, Cr, Co, Cu, Zn, Y, Zr, Cs and Th (Table 4), the values are still within the global ranges reported for these elements in the literature (e. g. Woolley and Kempe, 1989; Woolley and Church, 2005). Conversely, the Epembe carbonatite shows elevated contents of Li, Ti, Ta, U and Nb in relation to other trace elements (Table 4). Higher than average phosphorus values in some of the samples (Tables 3, 4) are attributed to the local abundance of apatite. Similarly, the high concentrations of tantalum, uranium and, locally, of niobium (EPB01 – 03) indicate the presence of phosphate minerals (pyrochlore and apatite), where uranium can substitute for niobium or tantalum in the mineral structure of pyrochlore, while in the crystal lattice of apatite it substitutes for calcium or phosphate ions. This agrees with exploration results by Kunene Resources, who found the economically inter-

esting rare metals tantalum and niobium contained abundantly in pyrochlore, thus identifying the Epembe carbonatite dyke as a potential Ta-Nb-U deposit (Mariano and Mariano, 2013).

The slightly higher values of CaO and Al_2O_3 in the Epembe carbonatite compared to global average is attributed to the copious presence of calcite, feldspar (microcline) and micas (biotite, phlogopite), respectively, while elevated Fe_2O_3 is due to the occurrence of hematite and magnetite. Finally, low concentrations of K_2O and Na_2O are typical of carbonatites in general.

The new geochemical data show a marked enrichment in critical metals such as niobium and tantalum in the Epembe carbonatite. While these two elements are commonly found together and are chemically similar, they have a very different genesis due to subtle variations in their chemical affinities and the specific conditions under which they form. Both elements are enriched in highly differentiated igneous rocks such as granites, alkali granites, rare metal pegmatites, syenites and carbonatites (Chakhmouradian, 2006). It is concluded that some of the Epembe carbonatites are more fractionated compared to average calcio-carbonatites (Woolley and Kempe, 1989). Elevated silica contents in the Epembe carbonatite (av. ~4 wt% *vs* 2.72 wt. %; Table 3) are related to contamination by the silica-rich, syenitic country rocks, which also occur as xenoliths in the carbonatite.

REE Geochemistry

Total REE concentrations in the Epembe carbonatite range from 406 to 912 ppm (Table 5). REE patterns of Epembe carbonatites resemble each other closely, with a steady decrease from LREE to HREE (Figs 9 and 12), a feature common to most carbonatites (e. g. Jones *et al*., 2013). The Epembe carbonatites, nepheline syenites and fenites display a general enrichment of incompatible over compatible elements, which is reflected by elevated contents of LREE (La-Gd). LREE are more incompatible than HREE and tend to remain in the melt to be incorporated into late-stage (more fractionated) minerals. These may accumulate during the genesis of the carbonatitic melt and subsequent fractional crystallisation (Unger *et al*., 2018). Accordingly, it is assumed that EPB01 is the most fractionated sample, characterised by the highest LREE content (789 ppm), and EPB12 the least fractionated ($LREE_t$ 308 ppm), thus indicating a decrease in fractionation from NW to SE. This is supported by compositional characteristics: while EPB01 displays an intergranular texture of low-temperature minerals such as alkali feldspar and abundant apatite, EPB12 contains more calcite and less feldspar and apatite.

According to Jones and Wyllie (1986), REE, except for Ce and Eu, have a 3^+ valence in most cases. However, in some geological environments, Ce and Eu can have valences of 4^+ and 2^+, respectively, which may lead to anomalous behaviour of these elements relative to other REE. Rollinson (1993) states that europium anomalies are mostly controlled by feldspar in contrast to the trivalent state REE, which are incompatible. The observed negative europium (Eu) anomaly in the Epembe carbonatite indicates the removal of Eu from the magma, with Eu^{2+} substituting for Ca^{2+} in minerals such as plagioclase (both having the same charge and similar radii of 99 vs 107 pm) during fractional crystallisation. While feldspar is retained in the solid residue, a negative Eu anomaly is induced in the melt from which the carbonatite crystallises. A negative europium anomaly is therefore characteristic of REE patterns of late-magmatic carbonatite with Eu^{2+} replacing Ca^{2+} in the crystal lattice of plagioclase, which is stable at temperatures of ≤1000ºC and pressures of < 1 GPa (equalling a depth of less than 30 km; e. g. Wyllie, 1995).

High (La/Yb)N ratios (13 - 29) also show that the Epembe carbonatite is enriched in LREE, which is a general aspect of carbonatites and often related to Sr and Ba enrichment (e. g. Tucker *et al*., 2012). The chondrite-normalised REE pattern of the Epembe carbonatites is comparatively flat in relation to average calcio-carbonatite (Fig. 11). The low absolute and average (721 ppm) REE content of the Epembe carbonatites as compared to the global average for calcio-carbonatites (3850 ppm; Table 5) is attributed to the absence of REE minerals, except rare monazite ([Ce, La, Y, Th] PO_4), in the former.

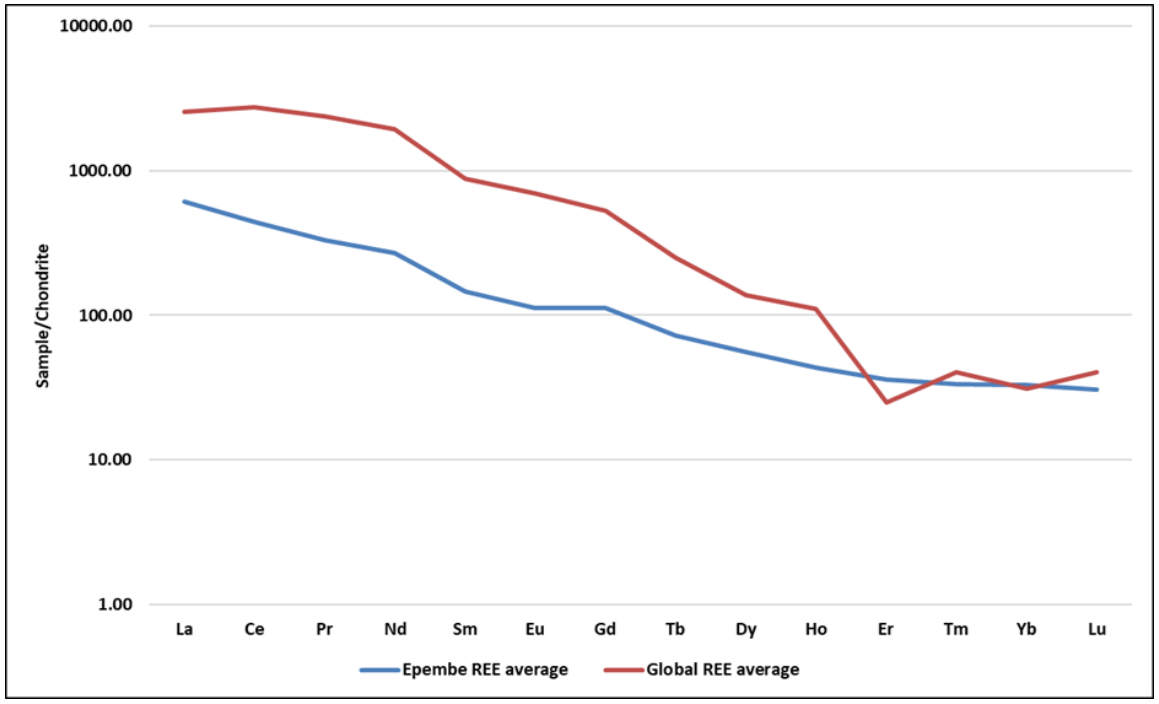

Figure 11. Chondrite- normalised rare earth element (REE) composition of the Epembe carbonatite as compared to global average calcio-carbonatite (after Woolley and Kempe, 1989; chondrite-normalising data from Sun and McDonough, 1995).

REE distribution in Epembe carbonatite

Of all igneous rocks carbonatite has the highest REE content, but their affiliation with specific minerals is less well understood (Kjarsgaard, 1998). Earlier studies of REE distribution (e. g. Kapustin, 1966; Viladkar and Pawaskar, 1989) have established that REE can be strongly enriched in both whole rock and most primary minerals (e. g. calcite, dolomite, pyrochlore, apatite, Ca-silicates). Al Ani *et al*. (2011) state that REE reside mostly in Ca-bearing phases such as apatite ($Ca_5[PO_4]_3[F,OH]$), pyrochlore ($[Na,Ca]_2Nb_2O_6[OH,F]$) and carbonates (e. g. calcite ($CaCO_3$) and ankerite ($Ca\ [Fe,Mg,Mn]\ [CO_3]_2$)), where Ca^{2+} can be replaced by REE cations and / or Sr^{2+}. As no significant REE minerals were found in the Epembe carbonatite, it is assumed that the occurrence and distribution of REE is due to chemical substitution of Ca^{2+} by divalent REE of similar ionic radii.

In carbonatites, REE are mainly concentrated by fractional crystallisation (Chakhmouradian *et al*., 2017; Orris and Grauch, 2002; Williams-Jones *et al*., 2012). At Epembe, the main REE-bearing phases appear to be phosphates and silicates, which are common accessories throughout. REE may also be present in gangue minerals, such as zircon and organic ligands (carbonates), where they can be easily complexed, with trivalent REE acting as electron pair acceptors and ligands donating electron pairs to form coordinate bonds (Edahbi *et al*., 2018).

Whole rock geochemical results are in general agreement with published analyses of apatite and pyrochlore from the Epembe carbonatite-syenite subsuite (Simon *et al*., 2017; Mariano and Mariano, 2013; Unger *et al*., 2018), who concluded that REE are mainly associated with apatite and other phosphates, while Nb and Ta are hosted in pyrochlore.

Acknowledgments

Acknowledgments are due to Kunene Resources (Pty) and the Gecko Exploration team, especially Dr R. Ellmies, for granting permission to work on their EPL, as well as for access to literature and data related to this research project. In addition, I would like to thank Mr Abner Nghoongholoka (GSN) and Mr Iyambo Nekwaya (Gecko Exploration) for their assistance and pleasing company during field work.

References

Al Ani, T., Heikura, P. and Sarapää, O. 2011. *REE-mineralogy and geochemistry of selected drill cores from the southern side of of the Sokli Carbonatite Complex, NE-Finland*. Report of the Geological Survey of Finland, Espoo, Finland, 28 pp.

Beetz, P. F. W. 1933. Geology of South West Angola between Kunene and Lunda Axis. *Transactions of The Geological Society of South Africa*, **36**, 137–176.

Brandt, S. 2003. *Metamorphic evolution of Ultrahigh–temperature granulite facies and upper amphibolite facies rocks of the Epupa Complex, NW Namibia*. PhD Thesis, University of Würzburg, Germany, 285 pp.

Brandt, S., Klemd, R. and Okrusch, M. 1999. Metamorphic evolution of the pre-Pan-African Epupa Complex, Namibia, 23. *Abstracts 31th International Geological Congress*, Rio de Janeiro, Brazil.

Brandt, S., Klemd, R. and Okrusch, M. 2000. Evidence for Ultrahigh – temperature metamorphism in the Pre – Pan-African Epupa Complex, NW Namibia. *Abstracts Geoluanda 2000*, Luanda, Angola, 33-34.

Brandt, S., Will, T. M. and Klemd, R. 2007. Ultrahigh-temperature metamorphism and anticlockwise PT-paths of sapphire-bearing orthopyroxene-sillimanite gneisses from the Proterozoic Epupa Complex, NW Namibia. *Precambrian Research*, **153**, 143-178.

Bybee, G. M., Hayes, H. Owen-Smith, T. M., Lehmann, J., Ashwal, L. D., Brower A. M., Hill, C. M., Corfu, F. and Manga, M. 2019. Proterozoic massif-type anorthosites as the archetypes of long-lived (≥ 100 Myr) Magmatic systems—new evidence from the Kunene Anorthosite Complex (Angola). *Precambrian Research*, **332**, https://doi.org/10.1016/j.precamres.2019.105393.

Chakhmouradian, A. R. 2006. High-field-strength elements in carbonatitic rocks: geochemistry, crystal chemistry and significance for constraining the sources of carbonatites. *Chemical Geology*, **235**, 138–160.

Chakhmouradian, A. R., Reguir, E. P., Zaitsev, A. N., Couëslan, C., Xu, C., Kynický, J., Mumin, A. H. and Yang, P. 2017. Apatite in carbonatitic rocks: Compositional variation, zoning, element partitioning and petrogenetic significance. *Lithos*, **274**, 188–213.

Drüppel, K. 1999. *Petrologie und Geochemie von Anorthositen des Kunene-Intrusiv-Komplexes, NW Namibia*. Diplom Thesis, University of Würzburg, Germany, 224 pp.

Drüppel, K. 2003. *Petrogenesis of the Mesoproterozoic anorthosite, syenite and carbonatite suites of NW Namibia and their contribution to the metasomatic formation of the Swartbooisdrif sodalite deposits*. PhD thesis, University of Würzburg, Germany, 345+199 pp.

Drüppel, K., Littmann, S., Romer, R. and Okrusch, M. 2001. Fenitizing Processes Induced by Ferrocarbonatite Magmatism at Swartbooisdrif, NW Namibia. *Journal of Petrology*, **46**, 377–406.

Drüppel, K., Littmann, S., Romer, R. L. and Okrusch, M. 2007. Petrology and isotope geochemistry of the Mesoproterozoic anorthosite and related rocks of the Kunene Intrusive Complex, NW Namibia. *Precambrian Research*, **156**, 1-36.

Edahbi, M., Plante, B., Benzaazoua, M., Kormos, l. and Pelletier, M. 2018. Rare Earth Elements (La, Ce, Pr, Nd, and Sm) from a Carbonatite Deposit: Mineralogical Characterization and Geochemical Behavior. *Minerals*, **8(2)**, 55, https://doi.org/10.3390/min8020055.

European Commission. 2014. *Report on critical raw materials for the EU*. http://ec.europa.eu/enterprise/policies/raw-materials/files/docs/crm-report-on-critical-raw-materials_en.pdf.

Falshaw, S. 2012. *The Geology and Rare Metal Metallogenesis of the Epembe Carbonatite dyke, North West Namibia*. MSc. Thesis, University of Exeter, Camborne School of Mines, Penryn, UK, 126 pp.

Gaillard, F., Pichavant, M. and Scaillet B. 2003. Experimental determination of activities of FeO and Fe_2O_3 components in hydrous silicic melts under oxidizing conditions. *Geochimica et Cosmochimica Acta*, **67**, 4389-4409.

Gittins, J. and Harmer R. E. 1997. What is ferrocarbonatite? A revised classification. *Journal of African Earth Sciences*, **25**, 159-168.

Jones, A. P. and Wyllie, P. J. 1986. Solubility of rare earth elements in carbonatite magma indicated by the liquidus surface in $CaCO_3Ca(OH)_2La(OH)_3$ at 1 kbar pressure. *Applied Geochemistry*, **1**, 95-102.

Jones, A. P., Genge, M. and Carmody, L. 2013. Carbonate Melts and Carbonatites. *Reviews in Mineralogy and Geochemistry*, **75**, 289-322.

Kapustin, Y. l. 1966. Geochemistry of Rare Earth Elements in carbonatites. *Geochemistry International*, **3**, 1054–1064.

Kanazawa, Y. and Kamitani, M. 2006. Rare earth minerals and resources in the world. *Journal of Alloys and Compounds*, **408**, 1339-1343.

Knudsen, C. 1989. Pyrochlore Group Minerals from the Qaqarssuk Carbonatite Complex. *In*: Möller, P., Černý, P., Saupé, F. (Eds) *Lanthanides, Tantalum and Niobium*. *Special Publication of the Society for Geology Applied to Mineral Deposits*, **7**, Springer, Berlin-Heidelberg, 80-99.

Kjarsgaard, B. A. 1998. Rare earth elements in sövitic carbonatites and their mineral phases. *Journal of Petrology*, **39**, 2105-2121.

Köstlin, E. C. 1967. *The geology of part of the Kunene basic complex, Kaokoveld, South-West Africa*. M. Sc. Thesis, University of Cape Town, South Africa, 92 pp.

Maier, W. D., Teigler, B. and Miller, R. McG. 2008. The Kunene Anorthosite Complex and its satellite intrusions. *In*: Miller, R. McG. (Ed.). *The Geology of Namibia*, **Vol. 1**, chapter 9, 18 pp. Geological Society of Namibia, Windhoek.

Mariano, A. N. and Mariano A. 2013. *A Preliminary mineralogical study of selected rocks from the Ta-rich carbonatite occurrences, Epembe complex, Namibia*. Confidential Report for Kunene Resources, 91 pp.

Mayer, A., Hofmann, A. W., Sinigoi, S. and Morais, E. 2004. Mesoproterozoic Sm-Nd and U-Pb ages for the Kunene Anorthosite Complex of SW Angola. *Precambrian Research*, **133**, 187-206.

Martin, H. 1965. The Precambrian geology of South West Africa and Namaqualand. *Bulletin of the Precambrian Research Unit*, **161**, University of Cape Town, South Africa, 159 pp.

McCourt, S., Armstrong, R. A., Jelsma, H. and Mapeo, R. B. M. 2013. New U–Pb SHRIMP ages from the the Lubango region, SW Angola: insights into the Palaeoproterozoic evolution of the Angolan Shield, southern Congo Craton, Africa. *Journal of the Geological Society, London*, **70**, 353–363.

McDonough, W. F. and Sun, S. S. 1995. The Composition of the Earth. *Chemical Geology*, **120**, 223-253.

Menge, G. F. W. 1986. Sodalite-carbonatite deposits of Swartbooisdrift, South West Africa/Namibia. *In*: Anhaeusser, C.R. and Maske, S. (Eds) *Mineral deposits of Southern Africa*, **Vol. 2**. Geological Society of South Africa, Johannesburg, 2261-2268.

Menge, G. F. W. 1996. The eastern portion of the Kunene complex, its satellite intrusions and the alkaline suite between Epembe and Swartbooisdrif, Kaokoland, South West Africa. Unpublished report, Geological Survey of Namibia, 128 pp.

Norrish, K. and Hutton, J. T. 1969. An accurate x-ray spectrographic method for the analysis of a wide range of geological samples. *Geochimica et Cosmochimica Acta*, **33**, 431–453.

Orris, G. J. and Grauch, R. I. 2002. Rare Earth Element Mines, Deposits and Occurrences. U.S. Geological Survey, *Open File Report*, 02-189, USA, 174 pp.

Rock, N. M. S. 1987. The need for standardization of normalized multi-element diagrams in geochemistry: a comment. *Geochemical Journal*, **21**, 75-84.

Rollinson, H. R. 1993. *Using geochemical data: Evaluation, presentation, interpretation*. Longman Scientific and Technical Press, Routledge, London, 384 pp.

Seth, B., Armstrong, R. A., Brandt, S., Villa, I. M. and Kramers, J. D. 2003. Mesoproterozoic U-Pb and Pb-Pb ages of granulites in NW Namibia: reconstructing a complex orogenic cycle. *Precambrian Research*, **126**, 147-168.

Shelley, D. 1993. *Igneous and Metamorphic rocks under the microscope. Classification, textures, microstructures and mineral preferred orientations*. Chapman and Hall, London, 445 pp.

Simon, S. J. 2017. The *Epembe Niobium-Tantalum Deposit, NW Namibia. U-Pb Age and Resource Estimation*. M. Sc. Thesis,

China University of Mining and Technology, Xuzhou, China, 96 pp.

Simon, S. J., Wei, C. T., Ellmies, R., Yang, H., and Soh Tamehe, L. 2017. New SIMS U-Pb age on zircon from the Epembe carbonatite dyke, NW Namibia: Implications for Mesoproterozoic evolution of carbonatites at the southern margin of the Congo Craton. *Journal of African Earth Sciences*, **135**, 108-114.

Streckeisen, A. L. 1979. Classification and nomenclature of volcanic rocks, lamprophyres, carbonatites, and melilitic rocks: Recommendations and suggestions of the IUGS subcommission on the systematics of igneous rocks. *Geology*, **7**, 331–335.

Tucker, R. D., Belkin, H. E., Schulz, K. J., Peters, S. G., Horton, F., Buttleman, K. and Scott, E. R. 2012. A major light rare earth element (LREE) resource in the Khanneshin Carbonatite Complex, southern Afghanistan. *Journal of Economic Geology*, **207**, 197-205.

Unger, G., Zimmermann, R. and Gloaguen, R. 2018. 3D-Modeling of the Epembe (Namibia) Nb-Ta-P-(LREE) Carbonatite Deposit: New Insights into Geometry Related to Rare Metal Enrichment. *Minerals*, **8(12)**, 600; https://doi.org/10.3390/ min8120600.

Viladkar, S. G. and Pawaskar, P. B. 1989. Rare earth element abundances in carbonatites and fenites of the Newania complex, Rajasthan, India. *Bulletin of the Geological Survey of Finland*, **61**, 113-122.

Wall, F. 2014. Rare earth elements. *In*: Gunn, G. (Ed.), *Critical Metals Handbook*. John Wiley and Sons, Hoboken, New Jersey, 312-339.

Williams-Jones, A. E., Migdisov, A. A. and Samson, I. M. 2012. Hydrothermal mobilisation of the rare earth elements: A Tale of "Ceria" and "Yttria". *Elements*, **8**, 355–360.

Woolley, A. R. and Kempe, D. R. C. 1989. Carbonatites: nomenclature, average chemical compositions, and element distribution. *In*: Bell, K. (Ed.) *Carbonatites - Genesis and Evolution*. Unwin Hyman, London, 1-14.

Woolley, A. R. and Church, A. A. 2005. Extrusive carbonatites: A brief review. *Litho*s, **85**, 1–14.

Wyllie, P. J. 1995. Experimental petrology of upper-mantle materials, processes and products. *Journal of Geodynamics*, **20**, 429–468.

Wyllie, P. J. and Biggar, G. M. 1966. Fractional crystallization in the "carbonatite systems" CaO-MgO-CO_2-H_2O and CaO-CaF_2-P_2O_5-CO_2-H_2O. *In*: *Papers and Proceedings of the 4th General Meeting, International Mineralogical Association*. I.M.A. Volume, Mineralogical Society of India, 92-105.

A giant glacial erratic of Cryogenian (end-Sturtian) age

Paul F. Hoffman[1,2*] and Adrian Tasistro-Hart[3]

1. School of Earth & Ocean Sciences, University of Victoria, Victoria, BC V8P 5C2, Canada
**Corresponding author <paulfhoffman@gmail.com>*
2. Department of Earth & Planetary Sciences, Harvard University, Cambridge, MA 02138, USA
3. Department of Earth Science, University of California, Santa Barbara, CA 93106, USA

Abstract :- Near the village of Duurwater Pos at the foot of the Fransfontein Ridge, north-western Namibia, an erratic megalith of basement monzogranite (Huab gneiss), 130 m long by 52 m wide, is perched on a pedestal of early Cryogenian (Sturtian) tillite. The pedestal had at least 134 m of palaeotopographic relief, plus the additional 41 m (tilt-corrected) height of the erratic itself. The tillite pedestal is inferred to be a hoodoo structure formed by differential erosion with shielding of the pedestal by the hard basement erratic. The erratic and its pedestal were preserved because of rapid marine inundation during Snowball Earth deglaciation, followed by onlap and burial by postglacial carbonate sediments of the middle Cryogenian Berg Aukas and Okonguarri Formations. As a glacial erratic, it is possibly the largest and oldest example known.

Keywords :- Glacial erratic, Cryogenian, Chuos glaciation, Snowball Earth, Fransfontein Ridge

To cite this paper :- Hoffman, P. F. and Tasistro-Hart, A. 2024. A giant glacial erratic of Cryogenian (end-Sturtian) age. *Communications of the Geological Survey of Namibia,* **27**, 40-46.

Introduction

Erratic boulders, lithologically incompatible with local bedrock, are among the most visible memorials to the power of vanished Quaternary ice sheets in Patagonia, New Zealand, Eurasia and North America (Sugden and John, 1976; Denton and Hughes, 1981; McCabe, 2008; Krüger, 2013; Evans *et al*., 2021). They are susceptible to erosion, however, and few if any such erratics have been described from pre-Quaternary ice ages. The largest Quaternary example is said to be Okotoks ('big rock' in the indigenous Blackfoot language), an erratic of Cambrian quartzite, derived from the Rocky Mountains and measuring 41 x 18 m where it lies (in two pieces) on the plains of southern Alberta in western Canada.

The purpose of this paper is to describe a larger and older erratic from the Sturtian (local Chuos) glaciation, the older of two Cryogenian (720 and 635 Ma) 'Snowball Earth' epochs. It measures 130 by 52 m in exposed diameter and is composed of weakly-foliated, porphyritic monzogranite derived from the Orosirian crystalline basement (1.86−1.83 Ga) of the Kamanjab Inlier (Burger *et al*., 1976; Kleinhanns *et al*., 2015). It is located near the village of Duurwater Pos (−20.203° S, 15.152° E) at the foot of the Fransfontein Ridge (Kunene Region, northern Namibia). Restoration of the enclosing Cryogenian strata, which are inclined ~52° towards the southwest, shows that the erratic is mounted atop a 134 m-high pedestal of glacial tillite (Chuos Formation). Corrected for tilt, the erratic itself was ≥41 m high from base to top, and was onlapped and buried by postglacial marine carbonate sediments of mid-Cryogenian age, following inundation by syn-deglacial sea-level rise. Its position atop a pedestal of tillite is most easily explained by differential subaerial erosion, the pedestal having been protected from erosion by the erratic itself. Rapid burial saved it from further erosion until its Recent exhumation. Hidden by *Acacia mellifera* trees, the erratic is no longer a wonder to the eye, but its restoration is wondrous for the imagination.

Location, palaeogeography and stratigraphic succession

The erratic is centered at longitude 15.14638° on the Fransfontein Ridge, a southwards-dipping monocline of carbonate-dominated Cryogenian and early Ediacaran strata (Otavi/Swakop Group) at the southern limit of the anticlinal Kamanjab basement inlier (Fig. 1). The sedimentary succession in the area of the erratic consists of four sequences, the youngest of which (Karibib Formation, Tkb) is Ediacaran in age. The early and late Cryogenian sequences, i. e. the Chuos (Ac) and Ghaub (Tg) Formations, respectively (Figs 2 and 3), represent the global Sturtian (717−662 Ma) and Marinoan (645±6−635 Ma) 'Snowball Earth' glaciations. The 11 to 23 Ma long middle Cryogenian ('inter-Snowball') sequence consists of the Berg Aukas (Aa), Okonguarri (Ao), Narachaams (An) and Frannis-aus (Af) Formations in ascending order.

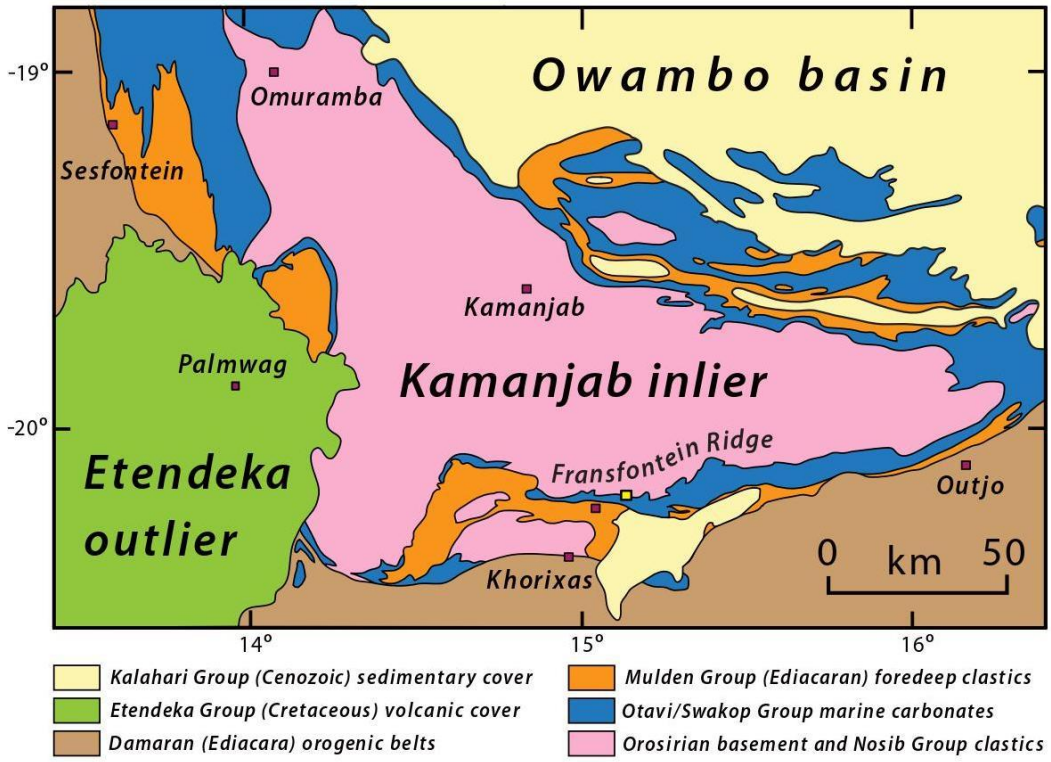

Figure 1. Bedrock geology around the Kamanjab Inlier exposing Orosirian basement rocks of the Congo Craton at the junction of the Ediacaran Central Kaoko Zone (upper left) and the Northern Damara Zone (lower right). The area shown in Fig. 2A is indicated by the tiny yellow box beneath the 'fo' in Fransfontein Ridge.

The erratic rests on Chuos Formation diamictite deposited in a small terrestrial rift-basin within a broad rift-shoulder uplift of exposed crystalline basement during the Sturtian glaciation. Middle Cryogenian crustal flexure, near the tip-line of a regional-scale south-dipping normal fault, transformed the area into the middle foreslope of a rapidly-subsiding Otavi Group carbonate shelf (Hoffman and Halverson, 2008; Hoffman, 2021a; Hoffman *et al*., 2021). The WNW−ESE trend of the Fransfontein Ridge in the area of the erratic (Fig. 2) was roughly parallel to the inferred slope contours. To the east, the strike of the Fransfontein Ridge changes to SW−NE and the outcrop section climbs obliquely across the upper foreslope and onto the outer shelf (Hoffman *et al*., 2021). Carbonate production ended when the area became part of a collisional foredeep during closure of the Northern Damara (Outjo) Sea at ca 600−590 Ma (Lehmann *et al*., 2015; Hoffman, 2021b).

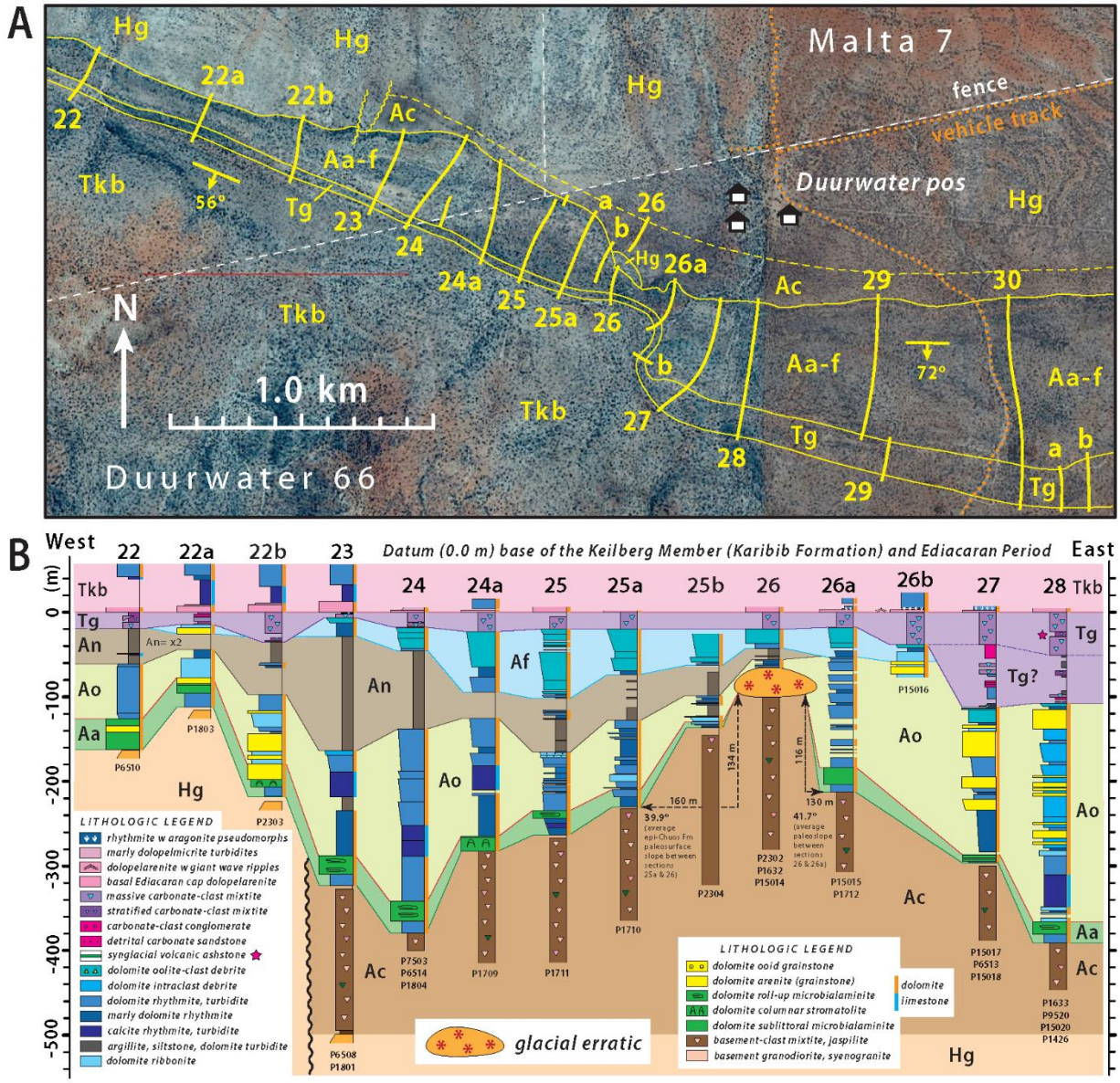

Figure 2. Bedrock geology of the Fransfontein Ridge in the area of Duurwater Pos: (**A**) Annotated satellite image showing farm boundary (white dashed line), vehicle tracks (orange dotted lines) and stratigraphic contacts (thin yellow lines) with units symbolised as in B and described in the text; strata dip 56–72° towards SSE. Heavy yellow lines are measured sections numbered 22 to 28 from west to east. Google Earth: Image © 2020 CNES/Airbus. (**B**) Fence diagram of columnar sections measured normal to stratification. Units: Hg, Huab Gneiss, Orosirian granitoids; Ac, Chuos Formation (Sturtian glaciation); Aa, Berg Aukas Formation; Ao, Okonguarri Formation; An, Narachaams Formation; Af, Frannis-aus Formation; Tg, Ghaub Formation (Marinoan glaciation); Tkb, Karibib Formation with basal Ediacaran 'cap' dolomite. Datum is the base of the Karibib Formation (base of the Ediacaran Period). Stratigraphic assignment of the interval labelled Tg? is tentative. It could alternatively be interpreted as Narachaams (±Frannis-aus) Formation. Average palaeosurface slopes (in magenta) are calculated from the horizontal distance (h) and difference in stratigraphic height (v), relative to the datum, of the top of the Chuos Formation between sections 25a and 26, and between 26 and 26a (tan α = v/h).

In the area of the erratic, the Chuos Formation (Ac, Fig. 2) exceeds 130 m in thickness and is composed of mainly massive, polymictic diamictite (tillite) in which rounded boulders of basement granodiorite are dispersed in a schistose siltwacke matrix. The diamictite is interspersed with thin layers of jaspilite and detrital dololutite. West of section 23 (Fig. 2), the Chuos Formation abuts against a high-angle rift-fault that is overstepped by the Berg Aukas Formation, the post-Sturtian 'cap' dolomite. The basement in the footwall of the rift fault is

a granodiorite gneiss (Hg, Fig. 2), in which subordinate mafic minerals (biotite and hornblende?) are replaced by retrograde chlorite.

The Berg Aukas Formation (Aa, Fig. 2B) sharply overlies the Chuos Formation and is generally a laterally continuous dark- to pale-grey dolomite, 20−40 m thick. It begins with flat-laminated rhythmite and shoals upwards into sublittoral microbialaminite, locally with columnar stromatolites, pillored thrombolites or microbial roll-up structures (Pruss *et al*., 2010). Its top is a subaqueous flooding surface (i. e. an abrupt increase in inferred water depth), but it lacks both the upper grainstone member that characterises the post-Sturtian Rasthof Formation on the western shelf area and the subaerial exposure surface at its top (Hoffman *et al*., 2021).

The Okonguarri Formation (Ao, Fig. 2B) is a polycyclic assemblage of limestone and dolomite rhythmites and ribbonites (flat and wavy-bedded, respectively). It passes eastwards (upslope) into dolomite grainstone, in part oolitic and stromatolitic, resembling the Gauss Formation of the Otavi Mountainland but lacking the plethora of tepeed subaerial exposure surfaces that characterise the Gruis Formation on the western Otavi Group shelf area (Hoffman *et al*., 2021). Westwards, the Okonguarri Formation is dominated by carbonate turbidites and rhythmite (e. g. in the Soutput subbasin on farm Toekoms 508 west of Khorixas (Hoffman *et al*., 2021).

The recessive Narachaams Formation (An, Fig. 2B), much favoured by thorn bushes, is composed of argillite with thin beds of buff-coloured dolomite turbidite. It is sharply overlain by the Frannis-aus Formation (Af, Fig. 2B), an upward-coarsening sequence of dolomite rhythmite, turbidite and intraclast debrite, interpreted as a glacio-eustatic falling-stand wedge related to extratropical ice-sheet growth in advance of the Ghaub glaciation on the Otavi Group palaeo-platform.

The Ghaub Formation (Tg, Fig. 2) represents the Marinoan Snowball Earth. In the area of the erratic, it disconformably overlies the Frannis-aus, Narachaams or Okonguarri (?) Formation, depending on the depth of sub-Ghaub erosion (Fig. 2). Its dominant lithology is massive, polymictic, carbonate diamictite, with subordinate stratified diamictite, carbonate-clast rudite (conglomerate) and arenite, all of glaciomarine origin (Domack and Hoffman, 2011; Hoffman *et al*., 2021). The Ghaub Formation in section 28 (Fig. 2) contains a volcanic tuff yielding zircon grains with a published U−Pb CA-ID-TIMS age of 639.29 ± 0.26 Ma (Prave *et al*., 2016). The stratigraphic assignment of the lower Ghaub Formation (Tg?, Fig. 2) in sections 27−28 is tentative. This interval could alternatively be Narachaams ± Frannis-aus Formation. Thin diamictites within this interval could be debrites, which occur low in the Narachaams Formation in other areas.

The Ghaub Formation is conformably overlain by the Karibib Formation (Tkb, Fig. 2), at the base of which is a post-Marinoan 'cap' dolomite correlative with the Keilberg Member (basal Maieberg Formation) of the Otavi Group (Tk, Fig. 3). Its base marks the start of the Ediacaran Period (Knoll *et al.* 2006; Narbonne *et al.* 2012). The cap dolomite consists of laminated, pale buff to pinkish, peloidal dolarenite, that thins eastwards from an average of 11.0 m in sections 22a to 23, to 5.9 m in section 26 (above the erratic) and 3.0 m in sections 26a to 27 (Fig. 2). It passes upwards gradationally into marly limestone or dolomite of the maximum post-glacial flooding stage, with pseudomorphosed crystal fans of benthic aragonite cement in the transition zone of sections 26a to 27 (Fig. 2). The remainder of the Karibib Formation consists of dolomite rhythmite, turbidite, debrite and cherty dolarenite, hundreds of metres thick in aggregate. The Karibib Formation is correlative with the entire Tsumeb Subgroup on the Otavi Group palaeo-platfom (Halverson *et al*., 2005) and is disconformably overlain by synorogenic foredeep siliciclastic deposits of the Kuiseb Formation and Mulden Group (Hoffman, 2021b; Hoffman *et al*., 2021).

Palaeorestoration of the Duurwater Pos erratic and its source

The datum for the stratigraphic 'fence' diagram (Fig. 2B) is the base of the Karibib Formation. The top of the Chuos Formation beneath the erratic in section 26 is closer to the datum than in any other section. This suggests that the erratic was perched on a palaeotopographic high on the final surface of Chuos diamictite. This is supported by evident onlap of middle Cryogenian strata. The Berg Aukas Formation is absent over the erratic and must

pinch-out against the inferred 39.9° (tan α=134/160 m) and 41.7° (tan α=116/130 m) average palaeosurface slopes (relative to the datum) to the west (sections 25a to 26) and east (26 to 26a) of the erratic, respectively (Fig. 2B). The calculated average palaeoslope west of the erratic would steepen if the Narachaams Formation argillite were decompacted. The Okonguarri Formation thins dramatically from 147.4 m (section 25a) and 131.4 m (section 26a) to only 9.9 m above the erratic (section 26). Thinning of the Narachaams and Frannis-aus Formations is much less (Fig. 2), consistent with burial of the erratic by the end of Okonguarri deposition and partial compaction of Narachaams argillite before the end of Frannis-aus accumulation. Taken together, these stratigraphic relations imply that the erratic, before burial, was mounted on a pedestal of unlithified glacial till (Chuos Formation) with at least 116−134 m of palaeotopographic relief. Corrected for tilt, the erratic itself would have added ~41 m (52 m times sin 52°; Fig. 3) to the height of the hoodoo.

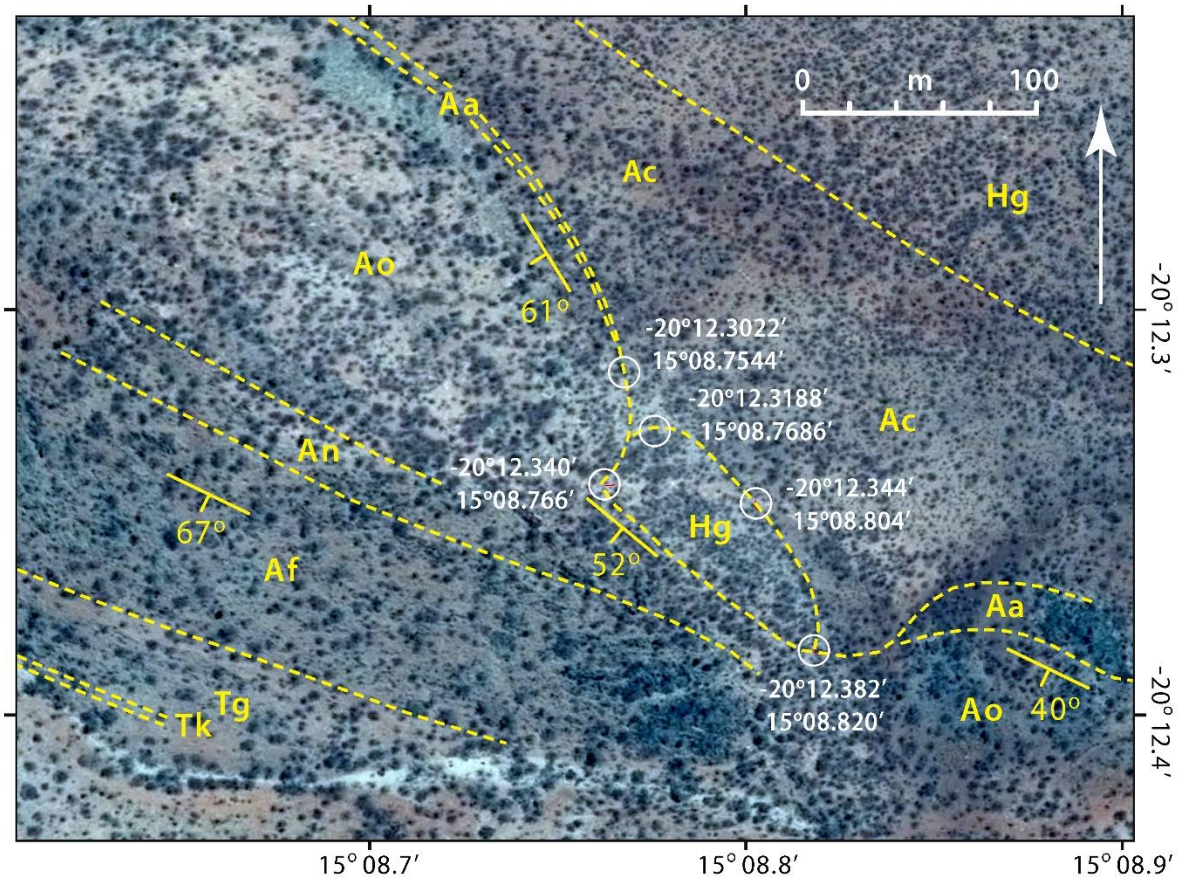

Figure 3. Annotated satellite image of the glacial erratic (Hg, centre right), located 650 southwest of Duurwater Pos. Coordinates are for circled locations that define its dimensions. The west to east drainage between circled locations provides the best-exposed section of the erratic and its relations with the enclosing strata (Fig. 2B), which dip 60−67° towards the southwest (Google Earth: Image © 2024 Airbus)

Assuming that the erratic was carried by a glacier, did the till pedestal exist when the erratic was placed there by glacial meltdown? This cannot be ruled out, but a more consanguineous explanation is that the till pedestal is a product of differential erosion, during which the general till surface was lowered but the pedestal was protected by the presence of the relatively hard monzogranite erratic. American geomorphologists describe such landforms as 'hoodoos,' a term apparently co-opted from African mythology (Jackson, 1997). Subaerial erosion predicts that boulder lags would have formed in axial channels on the till surface, but none were encountered.

From where was the erratic derived? One possible source is the synglacial rift fault between sections 22b and 23 (Fig. 2), which is only 1.03 km distant in the line of the sections. The erratic (porphyritic monzogranite) is not a

perfect lithologic match for the basement granodiorite exposed on both sides of the fault. Tilt correcting the ESE-dipping strata (Fig. 2A) would have little effect on the strike of the fault plane, which projects north of the erratic. But there is no independent constraint on the flow direction of Chuos glacial ice.

Conclusions

Near the village of Duurwater Pos at the foot of the Fransfontein Ridge, an outcrop of basement monzogranite, 130 m long and ≤52 m wide, is sandwiched between early Cryogenian tillite (Chuos Formation) and post-Sturtian middle Cryogenian marine carbonate (Fig. 3). Stratigraphic restoration reveals that the monzogranite erratic was mounted on a pedestal of tillite with ≥134 m of palaeotopographic relief, to which was added the ≥41 m height of the erratic itself (Fig. 2B). The pedestal is interpreted as a palaeo-hoodoo, formed by differential erosion and shielding of the pedestal by the erratic itself. If correctly interpreted, this palaeo-erratic is perhaps the largest and oldest glacial erratic on record. What is extraordinary about the Duurwater Pos erratic is less about its formation than about its preservation. Preservation may be related to the magnitude and speed of sea-level rise that accompanied the meltdown of a Snowball Earth, as well as the high rate of carbonate production in its torrid aftermath.

Acknowledgments

The authors are grateful to the owners of farm Malta 7 for access and the residents of Duurwater Pos for hospitality. Field work in 2016, when the erratic was discovered was assisted by students Kelsey Lamothe (McGill University) and Sam Lobianco (Harvard University). Joneel Zinto (UC Santa Barbara) and Mbweti Costa (University of Namibia) assisted during field work in 2022 and 2023, respectively.

References

Burger, A. J., Clifford, T.N. and Miller, R. McG. 1976. Zircon U−Pb ages of the Fransfontein granitic suite, northern SW Africa. *Precambrian Research*, **3**, 415−431.

Denton, G. H. and Hughes, T.J. (Eds) 1981. *The Last Great Ice Sheets.* John Wiley and Sons, New York, 484 pp. and 21 maps and charts

Domack, E. W. and Hoffman, P. F. 2011. An ice grounding-line wedge from the Ghaub glaciation (635 Ma) on the distal foreslope of the Otavi carbonate platform, and its bearing on the Snowball Earth hypothesis. *Geological Society of America Bulletin*, **123**, 1448−1477.

Evans, D. J. A., Phillips, E. R. and Atkinson N. 2021. Glacitectonic rafts and their role in the generation of Quaternary subglacial bedforms and deposits. *Quaternary Research*, **104**, 101−135.

Halverson, G. P., Hoffman, P. F., Schrag, D. P., Maloof, A. C. and Rice, A. H. N. 2005. Toward a Neoproterozoic composite carbon-isotope record. *Geological Society of America Bulletin*, **117**, 1181−1207.

Hoffman, P. F. 2021a. On the kinematics and timing of Rodinia breakup: a possible rift-transform junction of Cryogenian age at the southwest cape of Congo Craton (northwest Namibia). *South African Journal of Geology*, **124(2)**, 401−420.

Hoffman, P. F. 2021b. Cusp tectonics: an Ediacaran megakarst landscape and bidirectional mass slides in a Pan-African syntaxis, NW Namibia. *In:* Murphy, J.B., Strachan, R.A. and Quesada C (Eds) *Pannotia to Pangaea: Neoproterozoic and Palaeozoic Orogenic Cycles in the Circom-Atlantic Region.* Geological Socity, London, Special Publications, **503**, 105−142.

Hoffman, P. F. and Halverson, G. P. 2008. Otavi Group of the western Northern Platform, the Eastern Kaoko Zone and the western Northern Margin Zone. *In*: Miller, R.McG. (Ed.). *The Geology of Namibia*, Vol. **2**, chapter 13, 69-136. Geological Society of Namibia, Windhoek.

Hoffman, P. F., Halverson, G. P., Schrag, D. P., Higgins J. A., Domack, E. W., Macdonald,

F. A., Pruss, S. B., Blättler, C. L., Crockford, P. W., Hodgin, E. B., Bellefroid, E. J., Johnson, B. W., Hodgskiss, M. S. W., Lamothe, K. G., LoBianco, S. L. C., Busch, J. F., Howes, B. J., Greenman, J. W. and Nelson, L. L. 2021. Snowballs in Africa: sectioning a long-lived Neoproterozoic carbonate platform and its bathyal foreslope (NW Namibia). *Earth-Science Reviews*, **219**, 1−231.

Jackson, J. A. (Ed.) 1997. *Glossary of Geology, (4th Edition).* American Geological Institute, Alexandria, VA, p. 303 of 769.

Kleinhanns, I. C., Füllgraf, T., Wilsky, F., Nolte, N., Fliegel, D., Klemd, R. and Hansen, B. T. 2015. U−Pb zircon ages and (isotope) geochemical signatures of the Kamanjab Inlier (NW Namibia): constraints on Palaeoproterozoic crustal evolution along the southern Congo Craton. *In:* Roberts, N. M. W., van Kranendonk, M., Parman, S., Shirey, S. and Clift, P. D. (Eds) Continent Formation Through Time. *Geological Society London Special Publications*, **389**, 165−195.

Knoll, A. H., Walter, M. R., Narbonne, G. M. and Christie-Blick, N. 2006. The Ediacaran Period: a new edition to the geologic time scale. *Lethaia*, **39**, 13−30.

Krüger, T. 2013. *Discovering the Ice Ages.* Brill, Leiden, The Netherlands, 534 pp.

Lehmann, J., Saalmann, K., Naydenov, K. V., Milani, L. Belyanin, G. A., Zwingmann, H., Charlesworth, G. and Kinnaird, J. A. 2016. Structural and geochonological constraints on the Pan-African tectonic evolution of the northern Damara Belt, Namibia. *Tectonics*, **35**, 103−135.

McCabe, M. 2008. *Glacial Geology and Geomorphology: The Landscapes of Ireland.* Dunedin, Edinburgh, 274 pp.

Narbonne, G. M., Xiao, S. H. and Shields, G. A. 2012. The Ediacaran Period. *In:* Gradstein, F. M., Ogg, J. G., Schmitz, M. D. and Ogg, G. M. (Eds) *The Geologic Time Scale 2012.* Elsevier, Amsterdam, 413−435.

Prave, A. R., Condon D. J., Hoffmann, K.-H., Tapster, S. and Fallick, A. F. 2016. Duration and nature of the end-Cryogenian (Marinoan) glaciation. *Geology*, **44**, 631−634.

Pruss, S. B., Bosak, T., Macdonald, F. A., McLane, M. and Hoffman, P. F. 2010. Microbial facies in a Sturtian cap carbonate, the Rasthof Formation, Otavi Group, northern Namibia. *Precambrian Research*, **181**, 187−198.

Sugden, D. E. and John, B. S. 1976. *Glaciers and Landscape: A Geomorphological Approach.* Edward Arnold, London, 376 pp.

Bat-eared fox (Canidae, *Otocyon*) from the Pleistocene of northern Namibia

Martin Pickford[1], Jorge Morales[2], Helke Mocke[3], Dominique Gommery[4] and Brigitte Senut[5]

1. CR2P (MNHN, CNRS, SU), 8, rue Buffon, 75005, Paris, France <martin.pickford@mnhn.fr>
2. Departamento de Paleobiología, Museo Nacional de Ciencias Naturales-CSIC - C/José Gutiérrez Abascal 2, 28006, Madrid, Spain <jorge.morales@mncn.csic.es>
3. Geological Survey of Namibia, Aviation Road, Windhoek, Namibia <helke.mocke@mme.gov.na>
4. CR2P (MNHN, CNRS, SU), Campus Pierre et Marie Curie, T.46-56, E.5, 4, Place Jussieu, 75005, Paris, France <dominique.gommery@sorbonne-universite.fr>
5. CR2P (MNHN, CNRS, SU), 8, rue Buffon, 75005, Paris, France <brigitte.senut@mnhn.fr>

Abstract :- Fossils of the bat-eared fox, *Otocyon*, have been found at various localities in Southern and Eastern Africa, often in archaeological contexts. In Namibia the genus has previously only been recorded from four Holocene localities. We herein describe a specimen from Kombat, Otavi Mountains, which is likely to be of Pleistocene age. The origin of the bat-eared fox lineage is still poorly understood. One scenario in the literature, which has been contested, is that it originated in Eurasia (or ultimately North America) and then spread to Africa before going extinct in Eurasia. Our preferred interpretation is that the earliest phases of the evolution of bat-eared foxes as a distinct lineage from other canids occurred in Africa during the Early Pliocene, because, by the mid-Pliocene a species is known from the Upper Laetoli Beds (3.85-3.6 Ma) Tanzania, and an Early Pleistocene species (*Prototocyon recki*) is known from Olduvai Bed I, Tanzania (ca 2.0-1.8 Ma) and the lineage is quite common in southern African Late Pliocene, Pleistocene and Holocene localities.

Keywords :- Canidae, Otavi Mountainland, Holocene, Plio-Pleistocene, Evolution

To cite this paper :- Pickford, M., Morales, J., Mocke, H., Gommery, D. and Senut, B. 2024. Bat-eared fox (Canidae, *Otocyon*) from the Pleistocene of northern Namibia. *Communications of the Geological Survey of Namibia*, **27**, 47-65.

Introduction

The Namibia Palaeontology Expedition, a collaborative project between the Geological Survey of Namibia, Windhoek, and the Centre de Recherche en Paléontologie, Paris (CR2P), has been carrying out palaeontological research in the country since 1991. Screening of unconsolidated sediments in the 'A' fissure at Kombat E-900 (Fig. 1, 3, 4) has yielded abundant fossils including the first remains of equids and canids recorded from the deposits.

This paper describes and interprets the canid fossil from the site and discusses the origin of the bat-eared foxes. It is hypothesised that they may well have originated in southern Africa during the Early Pliocene, evolving from a species of Canidae that had dispersed to Africa (from North America via Eurasia) in the Latest Miocene or Early Pliocene.

The main evolutionary tendencies of the bat-eared fox group include a slight reduction in body size, the acquisition of accessory molars and the development of an «insectivorous» morphology of the molar crowns (Kieser, 1995), a thick pelage, and large ears (hence the common name of the species).

Clark (2005) postulated that the large ears of *Otocyon megalotis* might play a role in thermo-regulation, an adaptation to the arid environment it lives in. However, field observations indicate that its large ears are used to locate underground insects, such as harvester termites (*Hodotermes mossambicus*) that comprise one of its main sources of food and other cryptic insects such as beetles (Stuart *et al*., 2003). In support of the latter idea the authors wrote that "*the distribution of harvester termites …. and bat-eared fox …. in southern Africa, when superimposed on a map, show a 95% overlap.*"

After bat-eared foxes had evolved in southern Africa, it is inferred that they then spread northwards to East Africa during the middle of the Pliocene, but did not disperse as far as the Tropic of Cancer nor to Eurasia.

Previous Work

The fossiliferous fissure fillings at Kombat, Otavi Mountains were first described by Pickford and Senut (2010) who estimated that the deposits in the 'A' fissure at E-900 were Holocene, but, following recent collections from the infillings, it is more likely that they are of Late Pleistocene age. A sedimentary infilling in the nearby 'C' fissure contains similar unconsolidated deposits and a variety of lithic implements and waste flakes of Middle Stone Age aspect.

Fossil remains of bat-eared foxes have been recorded from a number of localities in Southern and Eastern Africa (Avery, 2019; Savage, 1978; Werdelin and Peigné, 2010) (Fig. 1, 2; Table 1). Most of the records (13 from Pleistocene deposits, 10 of Holocene age) are simple mentions in faunal lists. An exception is the genus and species, *Prototocyon recki* Pohle, 1928, from the Early Pleistocene of Tanzania, which is known from cranial elements (Pohle, 1928) and an almost complete mandible (Petter, 1973) (Fig. 7).

Because of the general lack of descriptions and illustrations of the fossils attributed to *Otocyon*, we herein describe and illustrate the specimen from the Kombat 'A' fissure. Even though the representation of bat-eared foxes at the site is currently based on a single fossil, the Kombat specimen prompts enquiries about the origins of the lineage, mainly because the specimen is substantially larger than any of the extant material available for study, and it is slightly larger than the extinct species *Prototocyon recki* (Fig. 8). The possibility thus exists that extant bat-eared foxes are smaller than their Pleistocene and Pliocene ancestors.

Figure 1. Distribution of fossil localities that have yielded remains of *Otocyon* and *Prototocyon*. Pleistocene sites are named; for locations and names of Holocene sites see Fig. 2. The white dotted outlines depict the distribution of extant *Otocyon megalotis*.

Country	Locality	Latitude	Longitude	Pleisto-cene	Holo-cene	References
Kenya	Lainyamok	01°49'S	36°10'E	x	o	Potts and Deino, 1995
Namibia	Kombat E-900 Fissure 'A'	19°42'S	17°44'	x	o	This paper
South Africa	Boegoeberg	28°46'S	16°34'E	x	o	Klein *et al*., 1999
South Africa	Cave of Hearths	24°10'S	29°11'E	x	o	Savage, 1978
South Africa	Lincoln Cave (Sterkfontein)	26°01'S	27°44'E	x	o	Reynolds *et al*., 2003, 2007; Wadley, 2015
South Africa	Pinnacle Point	34°11'S	22°05'E	x	o	Armstrong, 2016; Marean *et al*., 2004; McGrath *et al*., 2015; Rector and Reed, 2010; Wadley, 2015
South Africa	Plovers Lake	25°59'S	27°47'E	x	o	Brophy *et al*., 2006, 2014; De Ruiter *et al*., 2008; McKee *et al*., 1995; Reynolds, 2010; Thackeray and Watson, 1994; Wadley, 2015
South Africa	Sterkfontein	26°01'S	27°44'E	x	o	Ewer, 1958; McKee *et al*., 1995; O'Regan, 2007; Reynolds, 2010; Reynolds and Kibii, 2011; Reynolds *et al*., 2003, 2007; Turner, 1987
South Africa	Swartkrans	26°02'S	27°43'E	x	o	Ewer, 1958; McKee *et al*., 1995; Reynolds, 2010; Turner, 1993; Watson, 1993
South Africa	Tobias Cave (Taung)	27°37'S	24°37'E	x	o	McKee, 1994
Tanzania	Laetoli	03°13'S	35°11'E	x	o	Dehghani, 2008; Werdelin and Dehghani, 2011
Tanzania	Olduvai Gorge	02°59'S	35°21'E	x	o	Petter, 1973; Pohle, 1928
Botswana	White Paintings Rock Shelter	18°25'S	21°30'E	x	x	Robbins, 1990; Robbins *et al*., 2000
South Africa	Equus Cave	27°37'S	24°38'E	x	x	Klein *et al*., 1991; Kuhn *et al*., 2016; McKee *et al*., 1995
Botswana	Caecae	19°47'S	21°04'E	o	x	Wilmsen, 1989
Botswana	Divuyu	18°45'S	21°44'E	o	x	Denbow, 2011; Turner, 1987
Botswana	Matlapaneng	19°S	23°E	o	x	Turner, 1987
Botswana	Nqoma	18°45'S	21°45'E	o	x	Turner, 1988
Namibia	Big Elephant Shelter	21°42'S	15°40'E	o	x	Wadley, 1979
Namibia	Bremen	25°S	17°E	o	x	Cruz-Uribe and Klein, 1981–1983
Namibia	Maguans Andalusia	25°S	16°E	o	x	Cruz-Uribe and Klein, 1981–1983
Namibia	Striped Giraffe Shelter	21°48'S	15°42'E	o	x	Plug, 1979
South Africa	Abbot's Cave	31°27'S	24°39'E	o	x	Plug, 1993b, 1993c; Plug and Sampson, 1996
South Africa	Doornfontein	28°12'S	23°02'E	o	x	Beaumont and Boshier, 1974; Klein, 1979; Thackeray *et al*., 1983
South Africa	KN6-3C	30°13'S	17°14'E	o	x	Dewar, 2007
South Africa	Schroda	22°11'S	29°25'E	o	x	Plug, 2000; Voigt, 1980
South Africa	Spoeg River	30°18'S	17°16'E	o	x	Webley, 2001a, 2001b
Tanzania	67 km W of Itigi and WNW of Kilimatinde	05°41'S	33°53'E	o	x	Reck and Pohle, 1922

Table 1. Localities having yielded fossil remains of *Otocyon* and other bat-eared foxes (x - present; o - no record)

Geological and Palaeontological Contexts

The bedrock in the Kombat E-900 area consists of Proterozoic dolostones and phyllite/ shales that were subsequently mineralised with diverse sulphides during the Proterozoic (Deane, 1995; Nghoongoloka *et al*., 2020).

Figure 2. Southern African Holocene localities having yielded remains of *Otocyon megalotis*; image of bat-eared fox from Skinner and Smithers (1990)

During the Cenozoic Era, near-surface fissures and caves developed in the dolostone of the Upper Hüttenberg Formation, and as a result the E-900 zone at Kombat is characterised by narrow fissures and small caves that have acted as receptacles for sediments of diverse kinds (Pickford and Senut, 2010; Fig. 3, 4). The latter authors estimated the age of the fissure fillings as Recent, but subsequent surveys suggest that the 'A' fissure filling, which is unconsolidated, is more likely to be Late Pleistocene in age. The nearby 'C' fissure at E-900 yields lithic implements of Middle Stone Age aspect, and there are older well-indurated fissure fillings near the vehicle adit of the mine. The Asis Ost cave breccia, which is close by, is of Late Pleistocene to Recent age on the basis of the faunal remains that it has yielded.

The sedimentary infilling of the 'A' fissure at E-900 consists of unconsolidated dark brown, sandy to clayey sediment rich in small euhedral quartz crystals and small angular clasts of bedrock (dolostone and phyllite/schist) derived from the subjacent Proterozoic bedrock. Fossils are scattered randomly in the sediment, many of them being broken into fragments. The fossils are generally dark brown to black, but many have turquoise or green colouration due to copper minerals that have impregnated the bone or enamel and dentine of the teeth.

A comprehensive list of localities that have yielded fossil remains of bat-eared foxes is given in Table 1. The fauna currently known from fissure 'A' is listed in Table 2.

Figure 3. Kombat E-900 open pit showing the positions of fissures 'A', 'B' and 'C' in dolostones of the Upper Hüttenberg Formation; fissure 'B' is poorly fossiliferous and the 'C' fissure contains abundant Middle Stone Age lithic implements and waste flakes.

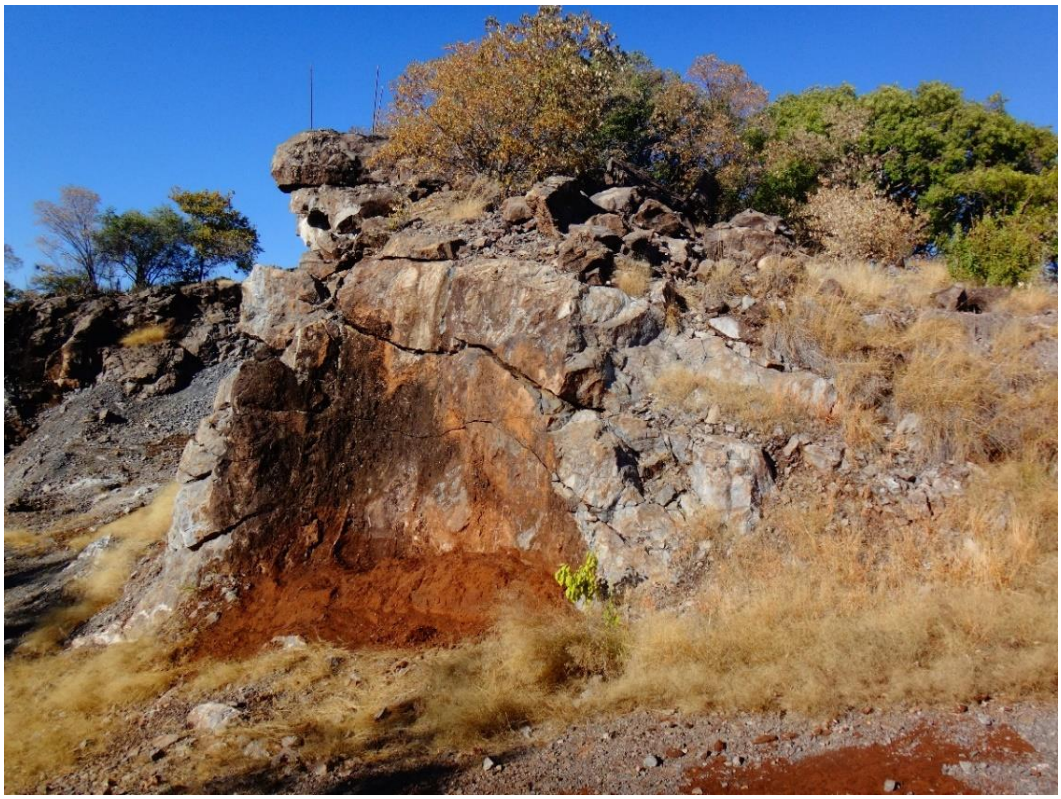

Figure 4. The 'A' fissure at Kombat E-900 with its infilling of fossiliferous dark brown sediment (image taken in May, 2024)

Amphibia
Ophidea
Lacertidae
Aves
Chiroptera
Erinaceidae
Carnivora
- Felidae (Leopard?)
- Canidae
  - *Otocyon* cf *megalotis*

Rodentia
- Otomyinae
- *Steatomys*
- *Aethomys*
- *Pedetes*
- *Petromyscus*
- *Petromus*
- Others

Lagomorpha
- *Pronolagus* sp.

Chrysochloridae
Hyracoidea
- *Procavia capensis*

Macroscelidea
- ?*Petrodromus*?

Perissodactyla
- Equidae
  - *Equus* sp.

Artiodactyla
- Bovidae
  - *Antidorcas* sp.
  - 2 other spp.

Table 2. Faunal List - Kombat E-900 'A' fissure

Material and Methods

GSN KOM 80'24 is an isolated lower molar from the 'A' fissure at the Kombat E-900 pit, Otavi Mountainland, northern Namibia (Fig. 5). It is coloured turquoise and black due to impregnation of copper, iron and manganese into the enamel.

The specimen was compared with material of extant *Otocyon megalotis* (Fig. 6) and with a cast of the extinct species *Prototocyon recki* from Olduvai Gorge, Bed I, Tanzania (Fig. 7), housed at the Palaeontology Collection, Muséum National d'Histoire Naturelle, Paris (Petter, 1973). Reference was also made to the literature (Koyasu, 1993; Kieser, 1995), which deals with the dentition of *Otocyon megalotis*.

Measurements of teeth were taken with sliding calipers to the nearest tenth of a millimetre (Table 3). Photographs were captured with a Sony Cybershot digital camera, and treated with Photoshop Elements 15 to increase contrast and to remove unwanted background.

Systematic Palaeontology

Order Carnivora Bowdich, 1821

Family Canidae Fischer von Waldheim, 1817

Genus *Otocyon* Müller, 1836

Species *Otocyon* cf *megalotis* Desmarest, 1822

Material. KOM 80'24, left m/2 (Fig. 5).

Locality and Age. Kombat E-900, 'A' Fissure (19°42'35''S : 17°43'55''E), Late Pleistocene (Fig. 3, 4).

Description

The crown of KOM 80'24 is ovoid in occlusal view, with the anterior part slightly broader than the posterior part. The protoconid and metaconid are well developed both in volume and in height, with the metaconid being the taller of the two cusps. The mesial valley is narrow, bordered buccally by a mesial cristid that extends towards the low, vestigial paraconid positioned in the centreline of the tooth. The basal cingulum on the protoconid is well developed. The talonid is shorter and narrower than the trigonid, and is dominated by a large hypoconid that is almost as tall as the protoconid. The entoconid is smaller than the hypoconid and is slightly compressed transversely and is positioned obliquely with respect to the transverse axis of the tooth. Between the two cusps of the talonid there is a small, low, cuspid. There is a weak pre-entoconid cristid and distally the hypoconulid closes the talonid valley, which is deep.

The crown is 7.0 mm in mesio-distal diameter, the mesial lophid is 5.0 mm broad, and the distal lophid is 4.5 mm broad.

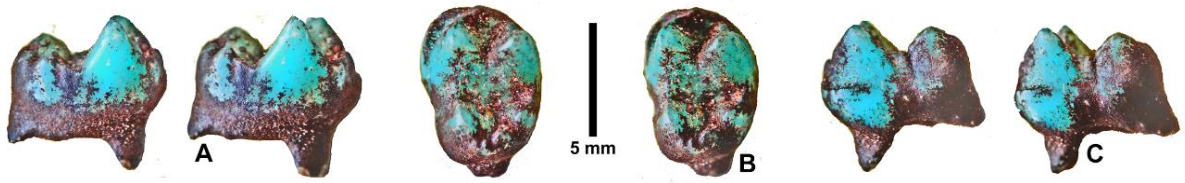

Figure 5. Stereo images of GSN KOM 80'24, left m/2 of *Otocyon* sp. From Kombat E-900 (fissure 'A'), Otavi Mountainland, Namibia. A – lingual view, B – occlusal view, C – buccal view

Discussion

The strong development and height of the trigonid cusps (protoconid-metaconid) and the talonid (hypoconid-entoconid) of the Kombat molar are characters that occur in posterior lower molars of *Otocyon megalotis*, being features that distance it from molars of other extant canids such as *Vulpes*, *Lupulella* and *Nyctereutes* and their fossil species. In addition, the latter forms tend to have relatively elongated, narrower, m/2s with low talonid cusps. On this basis, even though the Kombat fossil seems rather large for *Otocyon megalotis* (ca 20% greater than the mean of m/2 : Table 3; Fig. 8) its morphology agrees closely with the corresponding teeth of this species.

Catalogue	Number	Locality	Tooth	Mesio-distal length	Bucco-lingual breadth
MNHN	2007-19	Cap de Bonne Espérance	m/2 lt	5.5	4.4
MNHN	1973-135	Ethiopia	m/2 lt	5.4	4.0
MNHN	1973-136	Ethiopia	m/2 lt	4.9	3.5
MNHN	1972-392	Ethiopia	m/2 lt	6.0	4.2
MNHN	1933-2794	Ethiopia	m/2 lt	5.7	4.2
MNHN	1933-115	Ethiopia	m/2 lt	5.6	3.8
MNHN	1969-481	Ethiopia	m/2 lt	5.6	4.2
MNHN	1977-19	Somalia	m/2 rt	5.3	4.0
MNHN	1965-205	Ménagerie	m/2 rt	5.4	4.4
MNHN	2007-19	Cap de Bonne Espérance	m/3 lt	4.9	4.2
MNHN	1973-135	Ethiopia	m/3 lt	5.0	4.0
MNHN	1973-136	Ethiopia	m/3 lt	4.8	3.9
MNHN	1972-392	Ethiopia	m/3 lt	5.2	4.0
MNHN	1933-2794	Ethiopia	m/3 lt	5.0	4.2
MNHN	1933-115	Ethiopia	m/3 lt	4.7	3.5
MNHN	1969-481	Ethiopia	m/3 lt	5.2	3.9
MNHN	1977-19	Somalia	m/3 rt	5.5	4.0
MNHN	1965-205	Ménagerie	m/3 rt	5.1	4.0

Table 3. Measurements (in mm) of posterior lower molars of *Otocyon megalotis* housed in the Collection of Comparative Anatomy, Muséum National d'Histoire Naturelle (MNHN), Paris (lt – left; rt – right)

In *Otocyon megalotis* the m/2 tends to be somewhat larger than the m/3 but in the bivariate plots there is overlap of the measurements of these teeth (Fig. 8). In addition the talonid of the m/2 is usually only slightly narrower than the trigonid, whereas in the m/3 the talonid is in general noticeably narrower than the trigonid. The molar from Kombat has a relatively narrow talonid which resembles the proportions seen in m/3s of *Otocyon megalotis*, but its overall cuspal morphology indicates that it it more likely to be an m/2.

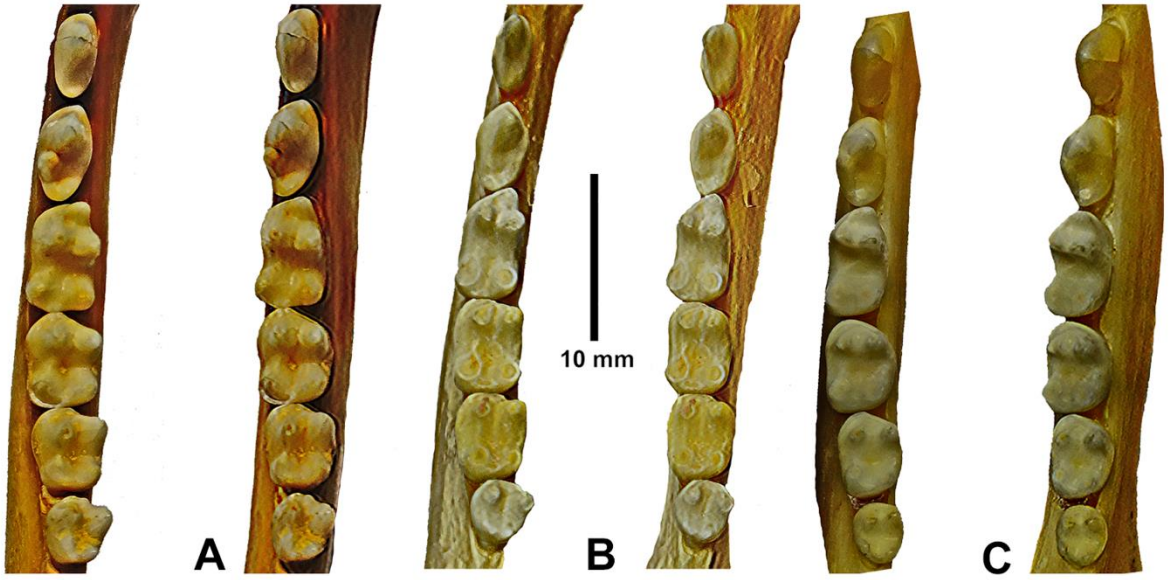

Figure 6. Stereo occlusal views of lower cheek teeth (p/3-m/4) of extant *Otocyon megalotis*. A – MNHN 1965-205 (right teeth reversed), B – MNHN 1973-135 (right teeth reversed), C – MNHN 1969-481 (left teeth).

Figure 7. FLK N1 761, left mandible of *Prototocyon recki* from Olduvai Bed I, Tanzania (cast in MNHN, Paris); A – lingual view, B – buccal view, C – stereo occlusal view of p/3-m/2 and alveolus of m/3 (enlarged)

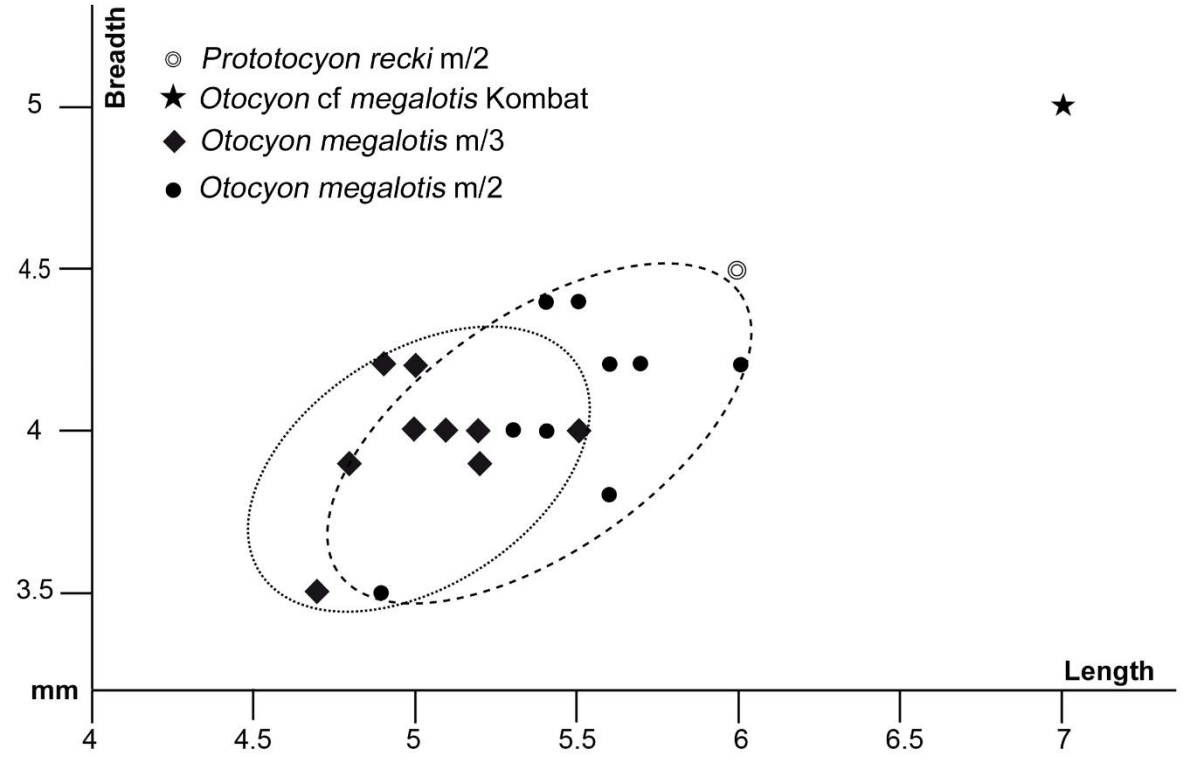

Figure 8. Bivariate (length-breadth) plots of posterior lower molars (m/2 and m/3) of extant *Otocyon megalotis* (MNHN collection) and the Kombat fossil. Measurements of *Prototocyon recki* are from Petter (1964). Our measurements of the m/2 in a cast of *Prototocyon recki* in the MNHN are 5.6 x 5.1 mm.

General Discussion

The presence of accessory molars in the small African canid, *Otocyon megalotis*, has intrigued zoologists for well over a century (Huxley, 1880; Lydekker, 1884; Winge, 1895; Carlsson, 1905; Matthew, 1924; Pilgrim, 1932; Petter, 1964, 1973; Ewer, 1965; Clutton-Brock *et al*., 1976; Koyasu, 1993; Kieser, 1995; Nel and Maas, 2004).

Whilst it has been almost universal for zoologists to classify the genus *Otocyon* in the

family Canidae, there has been little consensus regarding the question of its relationships to other genera of canids (Tedford *et al*., 1995). Is it a member of a separate subfamily - Otocyoninae - distinct from other dogs - Caninae (Clutton-Brock *et al*., 1976) - or is it a form derived from a *Vulpes*-like ancestor, and thus a Caninae? (Carlsson, 1905). Both views are available in the literature.

Much of the debate revolves around the presence of accessory molars in *Otocyon* (Lydekker, 1884; Koyasu, 1993) and the observation that the molars show morphology derived towards an insectivorous diet (Petter, 1964, 1973; Kieser, 1995). These factors have been interpreted in contrasting ways, the accessory molars and molar morphology being cited either as primitive retentions (plesiomorphies; Huxley, 1880) or as derived characters (apomorphies) (Winge, 1895; Carlsson, 1905). Skinner and Smithers (1990) summarised the situation succinctly when they commented that « *The ancestors of the wild dog and the bat-eared fox are unknown and there are no clues to the links between Miocene and Pleistocene canids* ».

Although not explicitly stated in the literature, there seems to have been an underlying assumption on the part of most authors who have written about the origin of bat-eared foxes, that the canid lineage from which they descended was already of small dimensions. However, the fossils from the Pleistocene of Tanzania (Petter, 1973) and now from Kombat, suggest that the ancestral lineage may have been somewhat larger (10-20% greater) than the extant *Otocyon megalotis*, a possibility that opens up new avenues of interpretation of hitherto doubtfully identified fossil post-cranial bones, for example, some of the specimens from Swartkrans, South Africa, identified as Canidae indet. by Watson (1993).

When commenting on the small Pleistocene canid described by Bose (1880) from the Pinjor-Markanda area, Siwalik Hills, India, Lydekker (1884) wrote « *The most probable interpretation of the genetic affinity of* Canis curvipalatus *is that it is a form derived from the primitive ancestral stock of* Otocyon … ». The supposedly primitive nature of *Otocyon* inferred by Lydekker (1884) was based on the presence of additional molars when compared to other canids. In his logic, Lydekker (1884) was adhering to Huxley's (1880) view that *Otocyon* is a primitive form, the presence of M4/ being interpreted by him as a survival of the dentition of ancestors of the Canidae and carnivorous marsupials (see Pilgrim, 1932). This interpretation was vigorously challenged by Winge (1895) and, even though Carlsson (1905) supported the systematic viewpoint of Lydekker (1884) she considered that the presence of extra molars in *Otocyon* was a derived condition, and not the retention of a primitive feature.

In tune with Lydekker's (1884) view, Pohle (1928) wrote that the small canid from the Pleistocene of Pinjor, India, could represent the base of the *Otocyon* lineage. He proposed that it was most probably a descendant of *Nothocyon curvipalatus* (Bose) via *Prototocyon recki* Pohle to *Otocyon megalotis* (Desmarest). Under this interpretation, the base of the *Otocyon* lineage would be a genus that originated in North America (*Nothocyon* Wortman and Matthew, 1899). However, Wang and Tedford (1992) transferred this genus to the Arctoidea and some of the species included in it were transferred to *Leptocyon* (a primitive canid) (Tedford *et al*., 2009).

Pilgrim (1932) discussed the issue of *Canis curvipalatus* in detail, and even though he wrote that « *Pohle's (1928) view that the three species form a genetic group seems to be justified* » ... he concluded that *« it appears better that the Indian fossil species should be distinguished by a generic name of its own, and for this I propose that of* Sivacyon ». By doing so, Pilgrim (1932) effectively excluded the possibility that the *Otocyon* lineage descended directly from a North American genus. Geraads *et al*. (2015) in contrast, considered that *Sivacyon* was closely related to *Vulpes* (*sensu stricto*) and concluded that there was « *no reason to connect it to* Otocyon *as has sometimes been done* ».

Of historical interest is the phylogeny of Thenius and Hofer (1960) that positioned *Otocyon* close to *Nyctereutes*, *Speothos*, *Dusicyon* and *Chrysocyon*, but with a question mark at the base of its lineage. In their phylogeny, the ultimate ancestral canid from which *Otocyon* was thought to derive was *Cynodesmus*, a North American Miocene genus according to the authors. The *Vulpes* and *Fennecus* group was positioned further off from *Otocyon* than the *Nyctereutes-Dusicyon* group (Fig. 9).

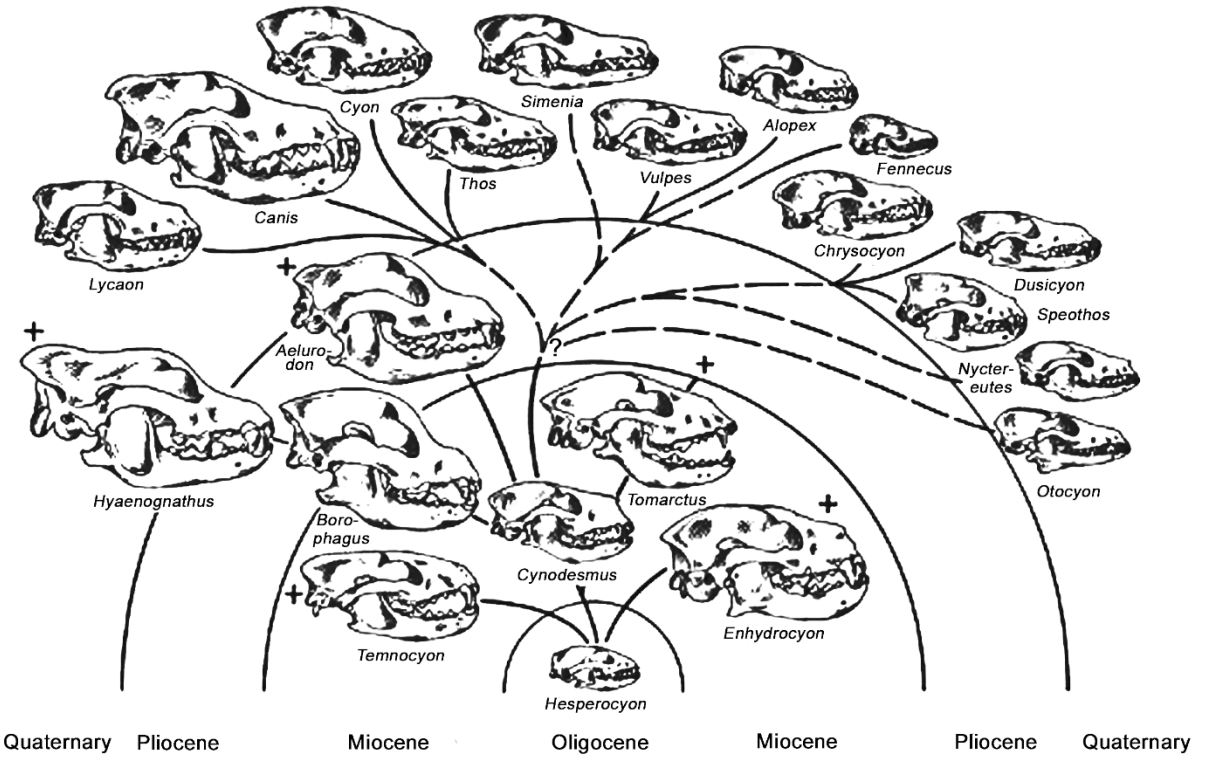

Figure 9. Phylogeny of the Canidae based on Thenius and Hofer (1960). Note the question mark at the base of the *Otocyon* lineage. « **+** » signifies the extinction of a lineage.

On the basis of observations on fossils from Olduvai Gorge, Tanzania, discovered after the work of Pohle (1928), Petter (1964) discussed the origin of the bat-eared fox lineage. She concluded that Pohle's genus and species *Prototocyon recki* was indeed distinct from *Otocyon*.

Unlike Pohle (1928) and Petter (1964) however, Ewer (1965) considered that the Olduvai bat-eared fox belonged to the same genus as the extant *Otocyon megalotis*, as the combination *Otocyon recki*. In her interpretation, the differences in cranial and dental features between the fossils and extant specimens represented interspecific variations rather than higher level distinctions. In response, Petter (1973) who had examined additional fossils from Olduvai Gorge, including a mandible, considered that *Prototocyon recki* was indeed distinct at the genus level from *Otocyon*. Its dentition is somewhat more primitive than that of *Otocyon megalotis* as noted by Pohle (1928), but overall, she concluded that the species *P. recki* was a typical bat-eared fox, but with one molar fewer in the upper and lower jaws than *Otocyon megalotis*, among other features such as differences in the length of the symphysis and the relative development of the subangular process.

Citing the publications of Wayne *et al*. (1987) and Wayne and O'Brien (1987), Tedford *et al*. (1995) pointed out that in the Canidae, different data sources led to different phylogenies. As concerns the bat-eared fox, they wrote « *Problem taxa include the foxes* Urocyon *and* Otocyon, *considered sister taxa and members of the Vulpini clade osteologically, but either as members of the Canini clade (with* Fennecus*) on chromosome morphology or in a basal unresolved multichotomy with other canines on allozyme evidence* ».

Werdelin and Peigné (2010) wrote that « *The Canidae are exclusive to North America until the late Miocene, after which* Eucyon- *and* Vulpes-*like taxa appear in Western Europe, Asia, and Africa ….. Recently, Morales* et al. *(2005) described from Lukeino (ca. 6 Ma) what was then the oldest canid of Africa,* Eucyon intrepidus. *Even more recently, however, a foxlike canid has been discovered from older sediments in Chad (Toros-Menalla, ca. 7 Ma; Bonis* et al., *2007). The family reaches southern Africa in the early Pliocene and northwestern Africa in the mid-Pliocene. The final radiation of the Canidae (Caninae) in the Pleistocene is seen mainly in eastern Africa, but also in South Africa and*

Algeria ». However, the dating of the Chad material is not secure, the assemblage of fossils from Toros Menalla consisting of surface finds ranging in age from 10 Ma to 4 Ma (Pickford, 2008a). It is thus insecure to consider that *Vulpes*-like canids existed in Africa during the Late Miocene, even though other canids (*Eucyon*) are well represented in the continent, in Kenya at Lukeino (Morales *et al*., 2005) and Lemudong'o (Howell *et al*., 2007).

The earliest plausibly well-dated occurrences of *Vulpes* in Africa are from the Pliocene of the Mursi Formation, Ethiopia (ca 4 Ma, Geraads *et al*., 2015), Makapansgat (Ewer, 1957) and Matjihabeng (De Ruiter *et al*., 2010) South Africa, and possibly Ahl Al Oughlam, Morocco (Geraads, 1997, 2008) with younger material known from various sites in northern, eastern and southern Africa (Avery, 2019; Werdelin and Peigné, 2010).

Several recently published phylogenetic scenarios, including some based on molecular biology, appear to place *Otocyon* as the most primitive member of the family in its own clade (Clutton-Brock *et al*., 1976) but others (Zrzavý and Řičánková 2004) classify it close to *Vulpes*, *Nurocyon* and *Nyctereutes*, but in varying positions depending upon the data analysed.

On the basis of cranial and dental characters, and using numerical analysis, Clutton-Brock *et al*. (1976) generated a centroid linkage dendrogram (Fig. 10) in which *Otocyon* was positioned at the base of the canid radiation, far removed from *Vulpes*, *Urocyon* and *Nyctereutes*, but closer to *Cuon*, *Speothos*, *Lycaon*, *Dusicyon* and *Canis*.

On the basis of chromosomal data Wayne *et al*. (1987) positioned *Otocyon* close to *Urocyon* and *Fennecus*, but far from *Nyctereutes* and *Vulpes*, whereas Wayne and O'Brien (1987) on the basis of allozyme data positioned *Otocyon* close to *Urocyon* and *Nyctereutes*, far from *Vulpes* and *Fennecus*, and well removed from *Speothos* and *Lycaon*.

In contrast, basing their cladogram on morphological data, Tedford *et al*. (1995, figs 8 and 9) positioned *Otocyon* and *Urocyon* close together, with *Nyctereutes* close to *Speothos*, but far from *Fennecus* and *Vulpes*. In their figure 2, however, Tedford *et al*. (1995) positioned *Otocyon* close to *Urocyon* and *Vulpes*, but distanced it from *Nyctereutes* and *Speothos*, with *Cuon* and *Lycaon* even further removed from it (Fig. 10).

Tedford *et al*. (2009) positioned *Otocyon* and *Prototocyon* far from Canini, but closer to *Urocyon* and slightly further from *Vulpes*.

Westbury (2018) placed *Otocyon* close to *Nyctereutes* and *Vulpes*, with *Urocyon* further off, and with *Cuon*, *Speothos*, *Lycaon* and *Canis* even further off (Fig. 10).

On the basis of all unweighted characters analysed, Zrzavý *et al*. (2018) positioned *Otocyon* close to *Nyctereutes* and *Nurocyon* and to some, but not all, species of *Vulpes*, with *Cuon*, *Canis* and *Speothos* far removed from it. Using nHC and molecular characters (Fig. 10), the same authors proposed that *Otocyon* was close to *Nurocyon*, *Nyctereutes* and *Vulpes*, with *Urocyon* some way off, followed by *Canis*, *Cuon*, *Lycaon* and *Speothos*, along with a diversity of other canid taxa.

On the basis of mitochondrial DNA analyses, Geffen *et al*. (1992) wrote that « *The grey fox,* Urocyon cinereoargenteus, *and the bat-eared fox,* Otocyon megalotis, *are not closely related to each other or to any of the sampled fox taxa* » (*Fennecus*, *Vulpes*). Thus, in their view, *Otocyon* is an outlier in canid phylogeny, not closely related to other fox-like taxa.

In contrast, Bardeleben *et al*. (2005) hypothesised that *Otocyon* was close to *Nyctereutes*. They wrote « *Differences between trees derived from the nuclear data and those from the mitochondrial data include the grouping of the bush dog and maned wolf into a clade with the South American foxes, the grouping of the side-striped jackal* (Canis adustus) *and black-backed jackal* (Canis mesomelas) *and the grouping of the bat-eared fox* (Otocyon megalotis) *with the raccoon dog* (Nyctereutes procyonoides) ».

After analysing morphological and molecular datasets, Zrzavý and Řičánková (2004) wrote that « Otocyon *and* Nyctereutes *are the most problematic canid genera, causing an unresolved branching pattern of* Otocyon, Vulpes, Nyctereutes *and DC (dog-like canid) clades* » whereas, on the combined basis of morphology, behaviour, genes and fossils, Zrzavý *et al.* (2018) concluded that « Otocyon, Nyctereutes *and* Nurocyon *form a clade* ». This proposal is interesting because *Nurocyon* Sotnikova, 2006, is a large canid first described from Chono-Kariakh in Transbaikalia, Mongolia (Pliocene, MN 14) (Rook, 2009).

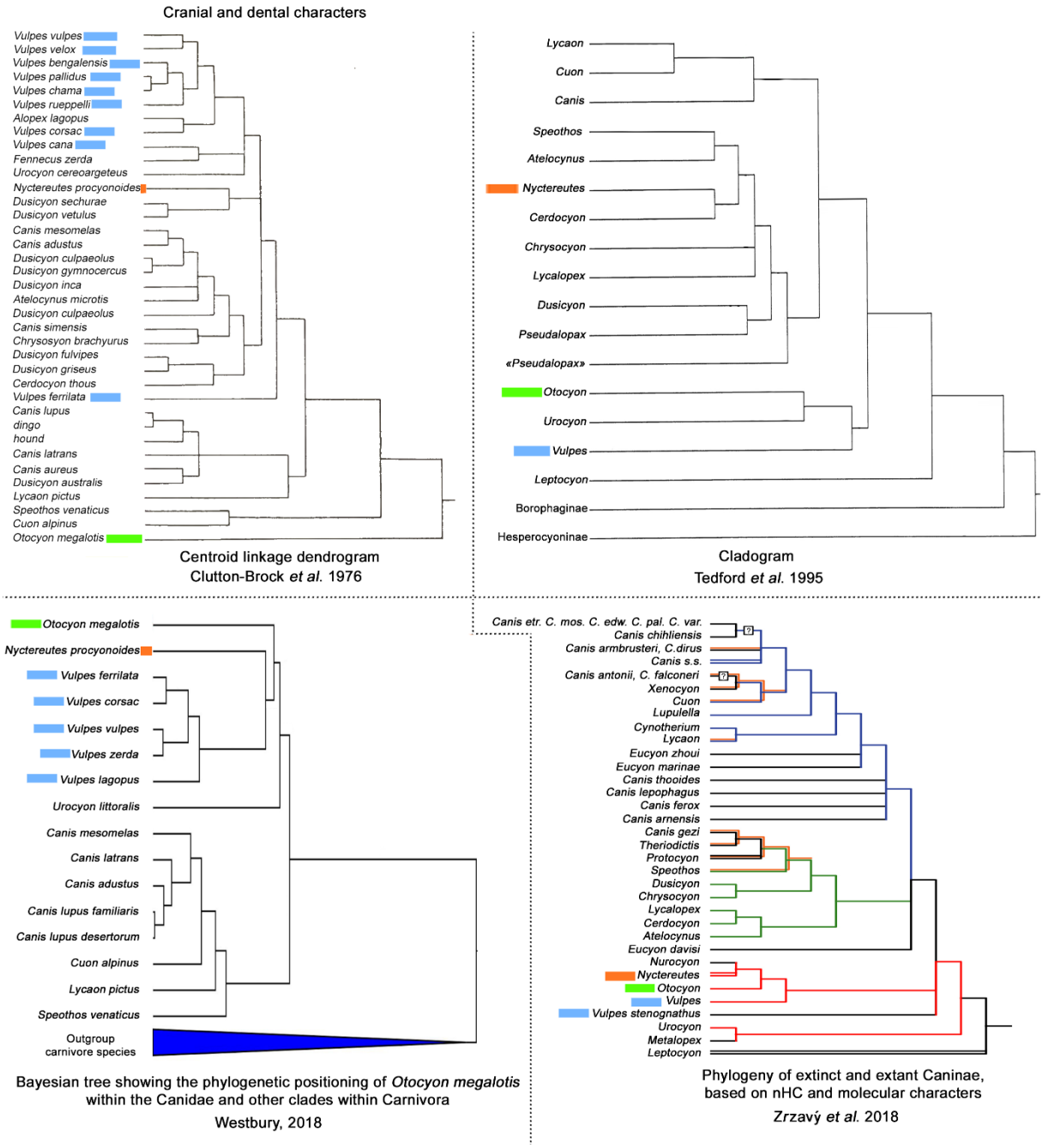

Figure 10. Four 'phylogenies' of Canidae containing *Otocyon*. For ease of reading, *Otocyon*, *Vulpes* and *Nyctereutes* have been highlighted in green, blue and brown respectively.

Thus the debate about the affinities of *Otocyon* within the Canidae remains unresolved, even though diverse approaches to phylogeny reconstruction have been attempted including classic comparative anatomy (Huxley, 1880; Thenius and Hofer, 1960; Tedford *et al.*, 1995), numerical methods (Clutton-Brock *et al.*, 1976), and molecular biology (Bardeleben *et al.*, 2005; Westbury, 2018; Zrzavý *et al.*, 2018).

The uncertainty about the phylogenetic position of *Otocyon* reflects that concerning the uncertainty of the position of jackals in general, and, above all, that of the hunting dog, *Lycaon*.

In our opinion, *Otocyon* is most likely to be a Vulpini. But we note that *Fennecus zerda* presents certain similarities to *Otocyon megalotis* (and to *Prototocyon recki*) in the morphology of the m/1 and m/2 (large broad talonid in the m/1; m/2 with the metaconid hypertrophied). However, the similarities between the

upper dentition of *Otocyon* and *Fennecus* are weaker.

The role of biogeography in the origin of *Otocyon* has been less frequently evoked in the literature, but historically early scenarios tended to look towards Asia (Lydekker, 1884) or Asia and North America (Pohle, 1928) as the region where the lineage originated. It is widely accepted that the Family Canidae (including Canini and Vulpini) is of North American origin (Tedford *et al*., 1995; Werdelin and Peigné, 2010) and that it dispersed to Eurasia and eventually to Africa during the latter part of the Miocene, reaching Kenya by ca 6 Ma (*Eucyon intrepidus*, described by Morales *et al*., 2005 and Rook, 2009). In this sense, the ancestors of *Otocyon* were ultimately of North American origin, but when the peculiarities of the dentition and mandible, along with the enlarged ears, dense furry pelage and relatively small body dimensions are taken into account, the most likely region in which the genus became distinct from other lineages of canids, was in Sub-Saharan Africa, in particular Southern Africa. Such a possibility has not previously been clearly articulated.

In support of a southern origin of the bat-eared fox lineage is the observation that *Otocyon* moults its fur on an annual basis. Such an adaptation is common in taxa that survive in higher latitudes where seasonal climatic changes are dominated by a winter/summer cycle, but is less common in tropically adapted species in which the alternations are more of a wet season/dry season nature. The bat-eared fox grows thick fur during the cooler months of the southern winter and moults it at the onset of the warmer months (Skinner and Smithers, 1990).

If the above biogeographic and developmental scenarios are valid, then *Otocyon* would be an exclusively African lineage and has remained so ever since its origin. It possibly descended from a form such as *Eucyon* Tedford and Qiu (1996) which was one of the earliest members of the family Canidae to disperse to the African continent, the oldest securely dated specimen being aged ca 6 Ma (*Eucyon intrepidus*, Lukeino Formation, Kenya; Morales *et al*., 2005). This scenario would imply a moderate reduction in body dimensions, modifications of dental morphology and the acquisition of extra molars and other featuressuch as the length of the mandibular symphysis (Petter, 1973).

Alternatively, the possibility exists that a currently unknown *Vulpes*-like form may have dispersed from North America to Africa via Eurasia during the Early Pliocene. The earliest *Vulpes*-like canids in North America date from ca 7 Ma, and genera such as *Metalopex* and *Urocyon* are known in that continent from the Latest Miocene and Pliocene respectively (Tedford *et al*., 2009). In Africa (discounting the Chad fossil, the age of which is poorly constrained), Vulpini are known from the mid-Pliocene of Mursi, Ethiopia (Geraads *et al*., 2015), and Makapansgat, South Africa (Ewer, 1957), and younger sites (Avery, 2019).

The supposed Late Miocene dating of the Toros-Menalla (Chad) specimens (Bonis *et al*., 2007) is doubtful. If correct, however, then it would imply an exceptionally rapid dispersal of *Vulpes* to Africa after the origin of the lineage in North America.

Whatever the case, the evolution of *Prototocyon* and *Otocyon* implies the development of additional molars, the modification of molar cuspal morphology and the proportions of the posterior teeth towards a more insectivorous diet, modification of the subangular process of the mandible where the digastric muscle inserts (Tedford *et al*., 1995; Skinner and Smithers, 1990; Clark, 2005), elongation of the mandibular symphysis (Petter, 1973), and very probably the enlargement of the ears, as well as the evolution of a more dense pelage and bushier tail. Because bat-eared foxes live and breed in underground dens their limbs are relatively short when compared with those of other foxes and jackals, but the metatarsals are long (personal observations) suggesting that the ancestor probably had longer femur and tibia than the extant form.

If the Pliocene and Pleistocene bat-eared foxes were somewhat larger (10-20%) than the extant forms, as indicated by the Olduvai and Kombat specimens, then some of the canid post-cranial fossils previously excluded from the group, because they were larger than those of *Otocyon megalotis*, could belong to it. Among the many fossils from the South African cave sites such as Swartkrans, that have been listed as « canid indet. » (Watson, 1993) because they were slightly too big to match their counterparts in *Otocyon megalotis*, there could be some that represent ancient bat-eared foxes.

At present, *Otocyon* occurs in two disjunct regions of Sub-Saharan Africa (Fig. 1) separated by more than 1000 km (Skinner and Smithers, 1990). The greatest area of distribution is Southern Africa, but the species is also widespread in the drier parts of Eastern Africa.

All fossils attributed to *Otocyon* and *Prototocyon* have been found within the same zones as the living species. The currently available fossil record, when combined with the apparent absence of fossils of bat-eared foxes from Northern Africa, the Middle East and Eurasia, suggests that the lineage evolved in Southern Africa, and then, like several other mammals (Pickford, 2008b) spread northwards to the more arid parts of East Africa, but did not disperse any further. This scenario accords with other biogeographic evidence which suggests that Southern Africa was an important centre of evolution (Pickford, 2004, 2008b) and not an evolutionary cul-de-sac as some people have thought.

From a palaeoenvironmental perspective the presence of *Otocyon* at Kombat E-900 accords with the other faunal elements (Table 2) suggesting that the climate and vegetation was comparable to what it is today - semi-arid woodland-savannah with summer rainfall.

Conclusions

The sedimentary infilling of the 'A' fissure at Kombat E-900, Otavi Mountainland, Namibia, has yielded a rich and diverse assemblage of fossil vertebrates which, taken together, indicate a Late Pleistocene age. The nearby 'C' fissure with a similar sedimentary infilling contains lithic implements and waste flakes that suggest a broad correlation to the Middle Stone Age. The 'B' filling is poorly fossiliferous, but the few specimens that it has yielded are similar to material in the 'A' fissure.

Among the fossils from the 'A' fissure, there is a lower molar attributed to a bat-eared fox on the basis of the close morphological similarities that it shares with posterior lower molars of the extant species *Otocyon megalotis*. However, the Kombat tooth is appreciably larger (ca 20%) than the mean of the corresponding element in the extant species. Given the restricted nature of the sample, however, we refrain from naming a new species, and attribute the specimen to *Otocyon* cf *megalotis*.

The observation that some fossils of Pleistocene bat-eared foxes (*Prototocyon recki* and the Kombat fossil) are somewhat larger than the corresponding parts of the extant species suggests that there has probably been a reduction in body size in this lineage through geological time.

Finally, following the dispersal of the family Canidae from North America to Africa (via Asia) at the end of the Miocene (with forms such as *Eucyon* and of vulpines during the Pliocene), it is plausible that *Otocyon* evolved exclusively within Africa (more likely Southern Africa than East Africa) and did not subsequently disperse to other continents, nor even to parts of Africa north of the Tropic of Cancer.

A holistic approach to the origin of the bat-eared fox lineage, taking into account its skeletal and dental morphology, molecular biology, behaviour, body dimensions, physiology (including seasonal adaptations such as moulting), as well as its admittedly relatively sparce fossil record, indicates that it most probably evolved in Southern Africa from a lineage of canids that dispersed to Africa during the latest Miocene, probably ultimately from North America via Eurasia.

For a period of over two centuries, scenarios based on only one or two of the data sources have failed to resolve the issues concerning canid phylogenetics and systematics.

Acknowledgements

For administrative help, the NPE thanks the French Embassy in Namibia (Sébastien Minot, Marion Christmann, Silvia Ricoveri), the Centre de Recherche en Paléontologie, Paris (CR2P) (Dr Sylvie Crasquin, Dr Silvain Charbonnier, Angelina Bastos and Suzy Colas).

Funding was provided by the ATM project PalPrim Namibie (Paléo-biodiversité des Primates du Néogène et du Quaternaire en Namibie) (MNHN) and the Prix Del Duca of the Académie des Sciences.

Access to the osteology collections at the MNHN was facilitated by Christine Lefèvre and Géraldine Veron.

In Windhoek, Ms Gloria Simubali and Ms Anna Nguno of the Geological Survey of Namibia provided help and encouragement. We thank Jane Eiseb and Anna Williams for their cooperation. Especial thanks to Ute Schreiber for her editorial commitment.

Thanks to Erica Ndalikokule, Lucia Namushinga and Edith Stanley of the Namibian National Heritage Council for arranging authorisation to carry out research in Namibia. Thanks to Gernot Piepmeyer and Junias Shangala of the National Commission on Research, Science and Technology of Namibia for authorisation to carry out reseach in the country.

Finally, thanks to Fanie Muller and Sydney Garoeb (Kombat Mines) for help in accessing the Kombat E-900 deposits.

References

Armstrong, A. 2016. Small mammal utilization by Middle Stone Age humans at Die Kelders Cave 1 and Pinnacle Point Site 5-6, Western Cape Province, South Africa. *Journal of Human Evolution*, **101**, 17-44.

Avery, D. M. 2019. *A Fossil History of Southern African Land Mammals*. Cambridge University Press, 315 pp.

Bardeleben, C., Moore, R. L. and Wayne, R. K. 2005. A molecular phylogeny of the Canidae based on six nuclear loci. *Molecular Phylogenetics and Evolution*, **37**(**3**), 815-831.

Beaumont, P. B. and Boshier, A. K. 1974. Report on test excavations in a prehistoric pigment mine near Postmasburg, northern Cape. *South African Archaeological Bulle*tin, **29**, 41-59.

Bonis, L. de, Peigné, S., Likius, A., Mackaye, H. T., Vignaud, P. and Brunet. M. 2007. The oldest African fox (*Vulpes riffautae* n. sp., Canidae, Carnivora) recovered in late Miocene deposits of the Djurab desert, Chad. *Naturwissenschaften*, **94**, 575-580.

Bose, P. N. 1880. On undescribed fossil Carnivora from the Sivalik Hills. *Quarterly Journal of the Geological Society, London*, **36**, 119-136.

Bowdich, T. E. 1821. *An Analysis of the Natural Classifications of the Mammalia, for the Use of Students and Travellers*. Paris, J. Smith, 180 pp.

Brophy, J. K., De Ruiter, D. J., Athreya, S. and De Witt, T.J. 2014. Quantitative morphological analysis of bovid teeth and implications for paleoenvironmental reconstruction of Plovers Lake, Gauteng Province, South Africa. *Journal of Archaeological Science*, **41**, 376-388.

Brophy, J. K., De Ruiter, D. J., Lewis, P. J., Churchill, S. E. and Berger, L. R. 2006. Preliminary investigation of the new Middle Stone Age site of Plovers Lake, South Africa. *Current Research in the Pleistocene*, **23**, 41-43.

Carlsson, A. 1905. Ist *Otocyon caffer* die Ausgangsform des Hundegeschlechts oder nicht? *Zoologische Jahrbücher, Abteilung für Systematik, Geographie und Biologie der Tiere.* **XXII**, 717-754.

Clark, H. O. 2005. *Otocyon megalotis*. *Mammalian Species*, *American Society of Mammalogists*, **766**, 1-5.

Clutton-Brock, J., Corbet, G. B. and Hills, M. 1976. A Review of the Family Canidae, with a Classification by Numerical Methods. *Bulletin of the British Museum (Natural History) Zoology*, **29**(**3**), 117-119.

Cruz-Uribe, K. 1991. Distinguishing hyena from hominid bone accumulations. *Journal of Field Archaeology*, **18**, 467-486.

Cruz-Uribe, K. and Klein, R. G. 1981–1983. Faunal remains from some Middle and Later Stone Age sites in South West Africa. *Journal of the South West Africa Scientific Society*, **36-37**, 91-114.

De Ruiter, D. J., Brophy, J. K., Lewis, P. J., Churchill, S. E. and Berger, L. R. 2008. Faunal assemblage composition and paleo-environment of Plovers Lake, a Middle Stone Age locality in Gauteng Province, South Africa. *Journal of Human Evolution*, **55**, 1102-1117.

De Ruiter, D. J., Brophy, J. K., Lewis, P. J., Kennedy, A. M., Stidham, T. A., Carlson, K. B. and Hancox, P. J. 2010. Preliminary investigation of Matjhabeng, a Pliocene fossil locality in the Free State of South Africa. *Palaeontologia Africana*, **45**, 11-22.

Deane, J. G. 1995. The structural evolution of the Kombat deposits, Otavi Mountainland, Namibia. *Communications of the Geological Survey of Namibia*, **10**, 99-107.

Dehghani, R. 2008. *Aspects of Carnivoran Evolution in Africa*. PhD Thesis Summary, University of Stockholm, Sweden, 31 pp.

Desmarest, A. G. 1822. Mammalogie ou description des espèces de mammifères. Seconde partie, contenant les ordres de Rongeurs des Edentes, des Pachydermes, des ruminans et des Cetacés, **7**, 277-555. *In*: *Encyclopédie méthodique*, 196 vols, Veuve Agasse, Paris, France.

Denbow, J. 2011. Excavations at Divuyu, Tsodilo Hills. *Botswana Notes and Records*, **43**, 76-94.

Dewar, G. I. 2007. *The Archaeology of the Coastal Desert of Namaqualand, South Africa: a Regional Synthesis*. Unpublished PhD Thesis, University of Cape Town, 320 pp.

Ewer, R. F. 1957. Some fossil carnivores from the Makapansgat Valley. *Palaeontologia Africana*, **4**, 57-67.

Ewer, R. F. 1958. Appendix A: faunal lists for the sites of Sterkfontein, Swartkrans, Kromdraai A and Makapansgat Limeworks. *In*: Brain, C. K. (Ed.) The Transvaal Ape-man Bearing Cave Deposits. *Transvaal Museum Memoir*, **11**, 128-130.

Ewer, R. F. 1965. Large Carnivora. *In*: Leakey, L. S. B. *Olduvai Gorge, 1951*, Cambridge University Press, Vol. 1, 19-22.

Fischer von Waldheim, G. 1817. Adversaria zoologica. *Mémoires de la Société impériale des naturalistes de Moscou*, **5**, 357-472.

Geffen, E., Mercure, A., Girman, D. J., Macdonald, D. W. and Wayne, R. K. 1992. Phylogenetic relationships of the fox-like canids : mitochondrial DNA restriction fragment, site and cytochrome *b* sequence analysis. *Journal of Zoology*. https://doi.org/10.1111/j.1469-7998.1992.tb 04430.x

Geraads, D. 1997. Carnivores du Pliocène terminal de Ahl al Oughlam (Casablanca, Maroc). *Géobios*, **30**, 127-164.

Geraads, D. 2008. Plio-Pleistocene Carnivora of northwestern Africa: a short review. *Comptes Rendus Palévol*, **7**, 591-599.

Geraads, D., Drapeau, M. S. M., Bobe, R. and Fleagle, J. G. 2015. *Vulpes mathisoni*, sp. nov., a new fox from the Pliocene Mursi Formation of Southern Ethiopia and its Contribution to the Origin of African Foxes *Journal of Vertebrate Paleontology*, **35(4)** e943765 (7 pages).

Howell, F. C. and García, N. 2007. Carnivora (Mammalia) from Lemudong'o (Late Miocene, Narok District, Kenya). *Kirtlandia*, **56**, 121-139.

Huxley T. H. 1880. On the cranial and dental characters of the Canidae. *Proceedings of the Zoological Society of London*, 238-288, 16 text figs.

Kieser, J. A. 1995. Gnathomandibular morphology and character displacement in the bat-eared Fox. *Journal of Mammalogy*, **76(2)**, 542-550.

Klein, R. G. 1979. Palaeoenvironmental and cultural implications of late Holocene archaeological faunas from the Orange Free State and north-central Cape Province, South Africa. *South African Archaeological Bulletin*, **34**, 34-49.

Klein, R. G., Cruz-Uribe, K. and Beaumont, P. B. 1991. Environmental, ecological and paleo-anthropological implications of the Late Pleistocene mammalian fauna from Equus Cave, northern Cape Province, South Africa. *Quaternary Research*, **36**, 94-119.

Klein, R. G., Cruz-Uribe, K., Halkett, D., Hart, T. and Parkington, J. E. 1999. Paleoenvironmental and human behavioral implications of the Boegoeberg 1 Late Pleistocene hyena den, Northern Cape Province, South Africa. *Quaternary Research*, **52**, 393-403.

Koyasu, K., 1993. Variability of dentition in the bat-eared fox, *Otocyon megalotis*. *Aichi Gakuin Journal of Dental Science*, **31(1)**, 63-104.

Kuhn, B. F., Herries, A. I. R., Price, G. J., Baker, S. E., Hopley, P., Menter, C. and Caruana, M. V. 2016. Renewed investigations at Taung: 90 years after the discovery of *Australopithecus africanus*. *Palaeontologia Africana*, **51**, 10-26.

Lydekker, R. 1884. Indian Tertiary and Post-Tertiary Vertebrata. *Palaeontologica Indica*, **(10) II**, i-xv + 1-363, 45 plates.

Marean, C. W., Nilssen, P. J., Brown, K. S., Jerardino, A. and Stynder, D. D. 2004. Palaeo-anthropological investigations of Middle Stone Age sites at Pinnacle Point, Mossel Bay, South Africa: archaeology and hominid remains from the 2000 field season. *Paleoanthropology*, **1**, 14-83.

Matthew, W. D. 1924. Third contribution to the Snake Creek Fauna. *Bulletin of the American Museum of Natural History*, **50**, 59-210, 63 text figs.

McGrath, J. R., Cleghorn, N., Gennari, B., Henderson, S., Kyriacou, K., Nelson-Viljoen, C., Nilssen, P., Richardson, L., Shelton, C., Wilkins, J. and Marean, C. 2015. The Pinnacle Point shell midden complex: a Mid- to Late Holocene record of Later Stone Age coastal foraging along the southern Cape coast of South Africa. *South African Archae-ological Bulletin*, **70**, 209-219.

McKee, J. K. 1994. Catalogue of fossil sites at the Buxton Limeworks, Taung. *Palaeontologia Africana*, **31**, 73-81.

McKee, J. K., Thackeray, J. F. and Berger, L. R. 1995. Faunal assemblage seriation of southern African Pliocene and Pleistocene fossil deposits. *American Journal of Physical Anthropology*, **96**, 235-250.

Morales, J., Pickford, M. and Soria, D. 2005. Carnivores from the Late Miocene and basal Pliocene of the Tugen Hills, Kenya. *Revista de la Sociedad Geológica de España*, **18**, 39-61.

Müller, S. 1836. Jahresbericht über die Fortschritte der anatomisch-physiologischen Wissenschaften im Jahre 1834. *Archiv für Anatomie und Physiologie*, **1835**, 1-151, 225-243.

Nghoongoloka, A., Bowell, R., Kamona, F. and Mocke, H. 2020. Re-evaluation of Kombat-style mineralization and implications for exploration in the Otavi Mountainland, Namibia. *Open Journal of Geology*, **10**, 1119-1152.

O'Regan, H. J. 2007. A revision of the Carnivora from Member 5, Sterkfontein, South Africa, based on a reassessment of published material and site stratigraphy. *Annals of the Transvaal Museum*, **44**, 209-214.

Nel, J. A. J. and Maas, B. 2004. Bat-eared Fox *Otocyon megalotis* (Desmarest, 1822) *In*: Sillero-Zubiri, C, Hoffmann, M. and Macdonald, D. W. (Eds) *Canids : Foxes, Wolves, Jackals and Dogs. Status Survey and Conservation Action Plan*, 183-189. IUCN, Gland.

Petter, G. 1964. Origine du genre *Otocyon* (Canidae africain de la sous-famille des Otocyoninae). *Mammalia*, **28**(**2**), 529-538.

Petter, G. 1973. Carnivores pléistocènes du ravin d'Olduvai Tanzanie. *In*: Leakey, L. S. B., Savage, R. J. G. and Coryndon, S. C. (Eds) *Fossil Vertebrates of Africa*, Vol. **3**, 43-100. Academic Press, London.

Pickford, M. 2004. Southern Africa: a cradle of evolution. *South African Journal of Sci*ence, **100**, 205-214.

Pickford, M. 2008a. *Libycosaurus petrocchii* Bonarelli, 1947, and *Libycosaurus anisae* (Black, 1972) (Anthracotheriidae, Mammalia): nomenclatural and geochronological implications. *Annales de Paléontologie*, **94**, 39-55.

Pickford, M. 2008b. Southern Africa: a cradle of evolution. *Memoir of the Geological Survey of Namibia*, **20**, 539-554.

Pickford, M. and Senut, B. 2010. Karst Geology and Palaeobiology of Northern Namibia. *Memoir of the Geological Survey of Namibia*, **21**, 1-74.

Pilgrim, G. E. 1932. The fossil Carnivora of India. *Palaeontologica Indica, New Series*, **18**, 1-232, 10 plates.

Plug, I. 1993a. KwaThwaleyakhe Shelter: the faunal remains from a Holocene site in the Thukela Basin, Natal. *Natal Journal of Humanities*, **5**, 37-45.

Plug, I. 1993b. The faunal remains from Nanda, an Early Iron Age site in Natal. *Natal Journal of Humanities*, **5**, 99-107.

Plug, I. 1979. Appendix: Striped Giraffe Shelter faunal report. *In*: Wadley L. (Ed.) Big Elephant Shelter and its role in the prehistory of central South West Africa. *Cimbebasia* Series B, **3**, 71-72.

Plug, I. 2000. Overview of Iron Age fauna from the Limpopo Valley. *South African Archaeological Society Goodwin Series*, **8**, 117-126.

Plug, I. and Sampson, C. G. 1996. European and Bushman impacts on Karoo fauna in the nineteenth century: an archaeological perspective. *South African Archaeological Bulletin*, **51**, 26-31.

Pohle, H. 1928. Die Raubtiere von Oldoway. *Wissenschaftliche Ergebnisse der Oldoway-Expedition. 1913*, Neue Folge, **3**, 45-54.

Potts, R. and Deino, A. 1995. Mid-Pleistocene change in large mammal faunas of eastern Africa. *Quaternary Research*, **43**, 106-113.

Reck, H. and Pohle, H. 1922. Über einen vermutlich diluvialen Säugetierrest von der Mittellandbahn in Deutsch-Ostafrika. *Centralblatt für Mineralogie, Geologie und Paläontologie*, Stuttgart, **1922**, 546-557.

Rector, A. L. and Reed, K. E. 2010. Middle and Late Pleistocene faunas of Pinnacle Point and their paleoecological implications. *Journal of Human Evolution*, **59**, 340-357.

Reynolds, S. C. 2010. Where the wild things were: spatial and temporal distribution of carnivores in the Cradle of Humankind Gauteng, South Africa, in relation to the accumulation of mammalian and hominin assemblages. *Journal of Taphonomy*, **8**, 233-257.

Reynolds, S. C. and Kibii, J. M. 2011. Sterkfontein at 75: review of palaeoenvironments, fauna and archaeology from the hominin site of Sterkfontein Gauteng Province, South Africa. *Palaeontologia Africana*, **46**, 59-88.

Reynolds, S. C., Clarke, R. J. and Kuman, K. 2007. The view from the Lincoln Cave: mid- to late Pleistocene fossil deposits from Sterkfontein hominid site, South Africa. *Journal of Human Evolution*, **53**, 160-271.

Reynolds, S. C., Vogel, J. C., Clarke, R. J. and Kuman, K. 2003. Preliminary results of excavations at Lincoln Cave, Sterkfontein, South Africa. *South African Journal of Science*, **99**, 286-288.

Robbins, L. H. 1990. Excavation at the White Paintings Rock-Shelter Tsodilo Hills. *Nyame Akuma*, **34**, 2-4.

Robbins, L. H., Murphy, M. L., Brook, G. A., Ivester, G. H., Campbell, A. C., Klein, R. G., Milo, R. G., Stewart, K. M., Downey, W. S. and Stevens, N. J. 2000. Archaeology, palaeo-environment and chronology of the Tsodilo Hills White Paintings Rock Shelter, northwest Kalahari Desert, Botswana. *Journal of Archaeological Science*, **27**, 1085-1113.

Rook, L. 2009. The wide ranging genus *Eucyon* Tedford and Qiu, 1996 (Mammalia, Carnivora, Canidae, Canini) in the Mio-Pliocene of the Old World. *Geodiversitas*, **31**(**4**), 723-741.

Savage, R. J. G. 1978. Carnivora. *In*: Maglio, V. J. and Cooke, H. B. S. (Eds) *Evolution of African Mammals*. Harvard University Press, Cambridge, Massachusetts, 249-267.

Skinner, J. D. and Smithers, R. H. N. 1990. *The Mammals of the Southern African Subregion*. University of Pretoria, South Africa, 771 pp.

Sotnikova, M. V. 2006. A new canid *Nurocyon chonokhariensis* gen. et sp. nov. (Canini, Canidae, Mammalia) from the Pliocene of Mongolia. *Courier Forschungsinstitut Senckenberg*, **256**, 11-21.

Stuart, C. T., Stuart, T. and Pereboom, V. 2003. Diet of the bat-eared fox (*Otocyon megalotis*), based on scat analysis, on the Western Escarpment, South Africa. *Canid News*, **6**(**2**), 1-5.

Tedford, R. H. and Qiu, Z. 1996. A new canid genus from the Pliocene of Yushe, Shanxi Province. *Vertebrata PalAsiatica*, **34**, 27-40.

Tedford, R. H., Taylor, B. E. and Wang, X.-M. 1995. Phylogeny of the Caninae (Carnivora: Canidae) the Living Taxa. *American Museum Novitates*, **3146**, 1-37.

Tedford, R. H., Wang, X.-M. and Taylor, B. E. 2009. Phylogenetic Systematics of the North American Fossil Canidae (Carnivora : Canidae). *Bulletin of the American Museum of Natural History*, **325**, 1-218.

Thackeray, A. I., Thackeray, J. F. and Beaumont, P. B. 1983. Excavations at the Blinkklipkop specularite mine near Postmasburg, northern Cape. *South African Archaeological Bulletin*, **38**, 17-25.

Thackeray, J. F. and Watson, V. 1994. A preliminary account of faunal remains from Plovers Lake. *South African Journal of Science*, **90**, 231-233.

Thenius, E. and Hofer, H. 1960. *Stammesgeschichte der Säugetiere*. Springer Verlag, Berlin, Göttingen, Heidelberg, 312 pp.

Turner, A. 1987. New fossil carnivore remains from the Sterkfontein hominid site Mammalia: Carnivora. *Annals of the Transvaal Museum*, **34**, 319-347.

Turner, A. 1993. New fossil carnivore remains from Swartkrans. *In*: Brain, C. K. (Ed.) Swartkrans: A Cave's Chronicle of Early Man. *Transvaal Museum Monograph*, **8**, 151-165.

Turner, G. 1987a. Early Iron Age herders in northwestern Botswana: the faunal evidence. *Botswana Notes and Records*, **19**, 7-23.

Turner, G. 1987b. Hunters and herders of the Okavango Delta, Botswana. *Botswana Notes and Records*, **19**, 25-40.

Voigt, E. A. 1980. Appendix. The faunal sample from Msuluzi Confluence. *In*: Maggs, T., Msuluzi Confluence: a seventh century Early Iron Age site on the Tugela River. *Annals of the Natal Museum*, **24**, 140-145.

Wadley, L. 1979. Big Elephant Shelter and its role in the Holocene prehistory of central South West Africa. *Cimbebasia* B, **3**, 1-76.

Wadley, L. 2015. Those marvellous millennia: the Middle Stone Age of Southern Africa. *Azania*, **50**, 155-226.

Wang, X.-M. and Tedford, R. H. 1992. The status of genus *Nothocyon* Matthew, 1899, (Carnivora): an arctoid not a canid. *Journal of Vertebrate Paleontology*, **12**, 223-229.

Watson, V. 1993. Composition of the Swartkrans bone accumulations, in terms of skeletal parts and animals represented. *In*: Brain, C. K. (Ed.) Swartkrans: A Cave's Chronicle of Early Man. *Transvaal Museum Monograph*, **8**, 35-73.

Wayne, R. K. and O'Brien, S. J. 1987. Allozyme divergence within the Canidae. *Systematic Zoology*, **36**, 339-355.

Wayne, R. K., Nash, W. G. and O'Brien, S. J. 1987. Chromosomal evolution of the Canidae, II. Divergence from the primitive carnivore karyotype. *Cytogenetics and Cell Genetics*, **44**, 134-141.

Webley, L. 2001a. Excavations at /hei-/khomas Vaalhoek in the Richtersveld, Northern Cape. *Southern African Field Archaeology*, **10**, 46-74.

Webley, L. 2001b. The re-excavation of Spoegrivier Cave on the West Coast of South Africa. *Annals of the Eastern Cape Museums*, **2**, 19-49.

Werdelin, L. and Dehghani. R. 2011. Carnivora. *In*: Harrison, T. (Ed.) *Paleontology and Geology of Laetoli, Tanzania: Human Evolution in Context*. Vertebrate Paleobiology and Paleoanthropology Series. Springer, New York, 189-232.

Werdelin, L. and Peigné, S. 2010. Carnivora. *In*: Werdelin, L. and Sanders, W. (Eds) *Cenozoic Mammals of Africa*. University of California Press, Berkeley, Los Angeles, Chapter **32**, 603-657.

Westbury, M. V. 2018. *Unraveling Evolution through Next Generation Sequencing*. PhD Thesis, University of Potsdam, Germay, 129 pp.

Wilmsen, E. N. 1989. The antecedents of contemporary pastoralism in western Ngamiland. *Botswana Notes and Records*, **20**, 29-39.

Winge, H. 1895. Jordfundne og nulevende Rovdyr (Carnivora) fra Lagoa Santa Minas Geraes, Brasilien. *Museo Lundii Afhandlinger, Copenhagen*, **II**(**4**) 3-104, pls i-viii.

Wortmann, J. L. and Matthew, W. D. 1899. The ancestry of certain members of the Canidae, the Viverridae, and Procyonidae. *Bulletin of the American Museum of Natural History*, **XII**, 109-138, PIs vi, 10 text figs.

Zrzavý, J. and Řičánková, V. P. 2004. Phylogeny of Recent Canidae (Mammalia, Carnivora) ; relative reliability and utility of morphol-ogical and molecular datasets. *Zoologica Scripta*, **33**(**4**), 311-333.

Zrzavý, J., Duda, P., Robovský, J., Okřinová, I., and Řičánková, V. P. 2018. Phylogeny of the Caninae (Carnivora): Combining morphology, behaviour, genes and fossils. *Zoologica Scripta*, https://doi.org/10.1111/zsc.12293

Taxonomic revision of the extinct avian oospecies *Diamantornis karingarabensis* (Senut *et al*., 1998) from the Latest Miocene of Namibia

Martin Pickford

CR2P (MNHN, CNRS, SU), 8, rue Buffon, 75005, Paris, France
<martin.pickford@mnhn.fr>

Abstract :- Restudy of the fossil eggshells originally identified as *Struthio karingarabensis* indicates that they are more likely to belong to the extinct oogenus *Diamantornis* than to *Struthio*. Re-measurement of the entire sample of eggshell fragments from the type locality reveals that the range of variation in thickness is slightly different from previously published estimates. In particular the holotype is thinner than originally reported.

Keywords :- Struthionidae, Eggshells, Late Miocene, Systematics, Ootaxa

To cite this paper :- Pickford, M. 2024. Taxonomic revision of the extinct avian oospecies *Diamantornis karingarabensis* (Senut *et al*., 1998) from the Latest Miocene of Namibia. *Communications of the Geological Survey of Namibia*, **27**, 66-71.

Introduction

Fossil eggshells of struthious birds have proven to be useful for biostratigraphy in Afro-Arabia (Pickford and Dauphin, 1993; Senut and Pickford, 1995; Senut *et al*., 1998; Senut, 2000; Harris and Leakey, 2003; Stidham, 2004, 2008; Harrison and Msuya, 2005; Bibi *et al*., 2006; Stewart and Beech, 2006; Pickford, 2014; Louchart *et al*., 2022; Pickford *et al*., 2023).

New discoveries of fossil eggs in Oman (Pickford *et al*., 2023) prompted a restudy of the previously described material from Namibia, during which it was noticed that some of the published measurements are erroneous.

The aim of this paper is to amend the description of the relatively poorly known oospecies *Struthio karingarabensis*, in particular to provide illustrations of the available sample from the type locality, and to provide more accurate measurements of the thickness of the eggshells.

Previous Work

The extinct avian oospecies *Struthio karingarabensis* was erected by Senut *et al*. (1998) and the oxygen and carbon isotopes of the eggshells were analysed by Ségalen *et al*. (2002). Further mention of the species was made by Pickford (2014).

The species is known from its type locality in the middle section of the Karingarab aeolianite succession and from the Awasib Cliffs in the Namib-Naukluft Park (Senut *et al*., 1998). The age of the deposits has been estimated to be Latest Miocene.

Material and Methods

GSN KG 26’95, 25 eggshell fragments from the middle section of the Karingarab aeolianite succession, Namibia. The holotype and paratype are labelled ‘A’ and ‘B’ respectively (Fig. 1), and the remainder of the fragments are numbered from 1 to 23 (Fig. 2). The fossils are curated at the National Earth Science Museum, Geological Survey of Namibia, Windhoek.

Measurements were taken with sliding calipers to the nearest tenth of a mm. Images were captured with a Sony Cybershot Camera and treated with Photoshop Elements 15 to remove unwanted background and to enhance the contrast. The holotype and paratype were each measured at three points along the edges of the fragments (Fig. 3), while the other fragments were measured at one point only.

Systematic Palaeontology

Order Struthioniformes Latham, 1790

Family Struthionidae Vigors, 1825

Genus *Diamantornis* Pickford and Dauphin, 1993

Diagnosis (translated from French). Avian oogenus with large eggs (16 x 13.3 cm) with the external surface ornamented with large circular pore complexes (megapores) ranging in diameter from 2 to 8 mm. Each pore complex contains multiple smaller pores. In section the pore canals are ramified.

Species *Diamantornis karingarabensis* (Senut *et al*., 1998)

Original diagnosis (translated from French). Pore structure – the outer surface ornamented with pore complexes ranging in diameter from 2.4 to 2.7 mm, forming shallow depressions with an irregular outline; thickness – ranging from 2.95 to 3.2 mm (measured on a single fragment); description of the microstructure – in transverse section, the limit of the internal mammillary layer is generally unclear, not only in naturally fractured sections but also in polished section, due to diagenetic effects; in effect, the cleavage of the calcite tends to obscure the divergent fibres, this cleavage is also present in the columnar and spongy layers; the disposition in columns is visible, but the edges of the columns have become unclear; the complex, ramified structure of the pores, as well as their overall funnel-like shape are preserved; the spherolites on the internal surface are usually eroded.

Emended diagnosis. As above except that the thickness of the shells, measured on 25 fragments from the type locality, ranges from 2.0 to 2.9 mm (Table 1; Fig. 3).

Holotype and Paratype. GSN KG 26’95 ‘A’ and GSN KG 26’95 ‘B’ respectively (Fig. 1).

Other material. GSN KG 26’95, 1-23, eggshell fragments from the same locality as the holotype (Fig. 2).

Locality and Age. Karingarab (28°12'16.2"S : 16°21'34.7"E), middle section of the aeoliantes, Latest Miocene.

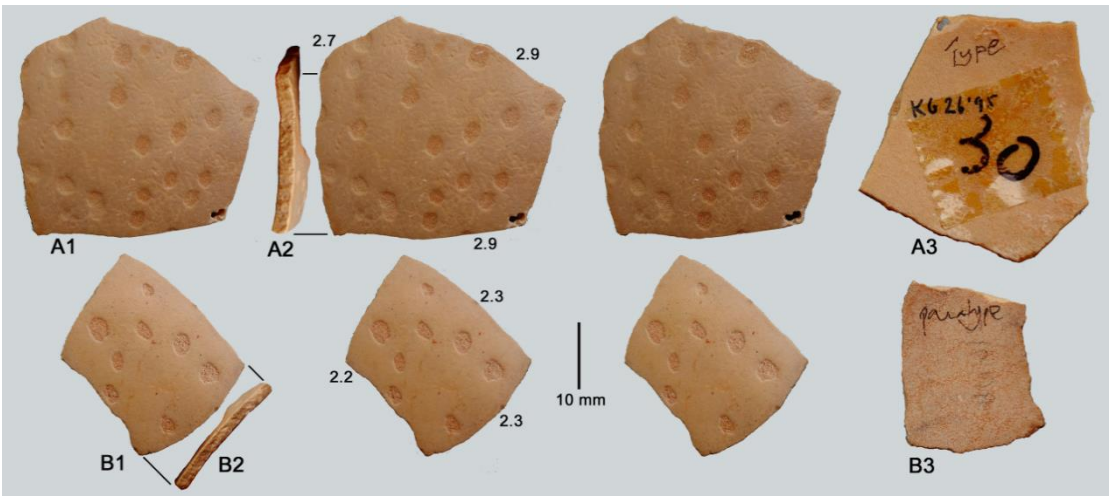

Figure 1. GSN KG 26’95, images of the holotype ‘A’ and paratype ‘B’ of *Diamantornis karingarabensis* from Namibia. 1 – stereo views of external surface, 2 – view of naturally broken section, 3 – internal surface. The measurements are of the thickness of the shells

Description

The eggshell fragments attributed to *Diamantornis karingarabensis* range in thickness from 2.0 to 2.9 mm. The external surface of the shells is patterned with abundant shallow ovoid depressions in which the pores are concentrated, the shell between the depressions being smooth and devoid of pores. The depressions range in diameter from 2.4 to 2.7 mm and are randomly distributed over the surface of the shells.

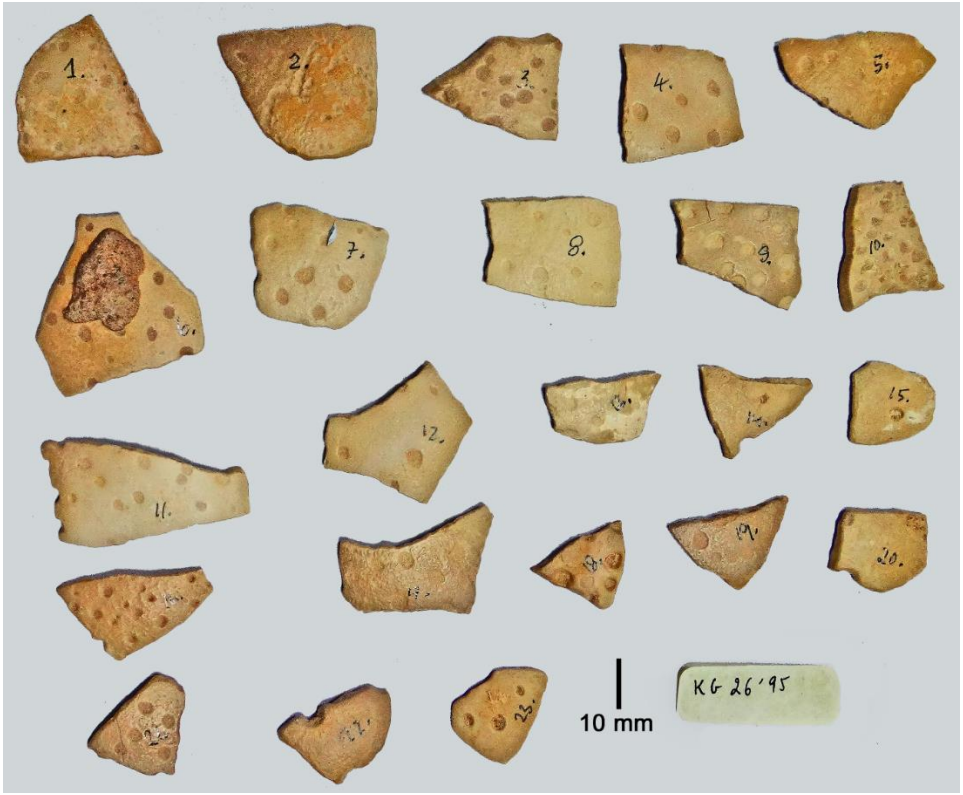

Figure 2. GSN KG 26'95, images of the external surfaces of 23 eggshell fragments of *Diamantornis karingarabensis* from the type locality of the species

Catalogue GSN	Thickness	Comment	Catalogue GSN	Thickness	Comment
KG 26'95 'A'	2.7	Holotype	KG 26'95 '10'	2.5	
KG 26'95 'A'	2.9	Holotype	KG 26'95 '11'	2.5	
KG 26'95 'A'	2.9	Holotype	KG 26'95 '12'	2.7	
KG 26'95 'B'	2.2	Paratype	KG 26'95 '13'	2.9	
KG 26'95 'B'	2.3	Paratype	KG 26'95 '14'	2.4	
KG 26'95 'B'	2.3	Paratype	KG 26'95 '15'	2.2	
KG 26'95 '01'	2.6		KG 26'95 '16'	2.0	
KG 26'95 '02'	2.5		KG 26'95 '17'	2.5	
KG 26'95 '03'	2.8		KG 26'95 '18'	2.2	
KG 26'95 '04'	2.6	Fig'd Pickford 2014	KG 26'95 '19'	2.6	
KG 26'95 '05'	2.6		KG 26'95 '20'	2.4	
KG 26'95 '06'	2.5		KG 26'95 '21'	2.3	
KG 26'95 '07'	2.5		KG 26'95 '22'	2.7	
KG 26'95 '08'	2.6		KG 26'95 '23'	1.8	Damaged
KG 26'95 '09'	2.8				

Table 1. Measurements (in mm) of the thickness of eggshell fragments of *Diamantornis karingarabensis* from Karingarab, Latest Miocene, Namibia

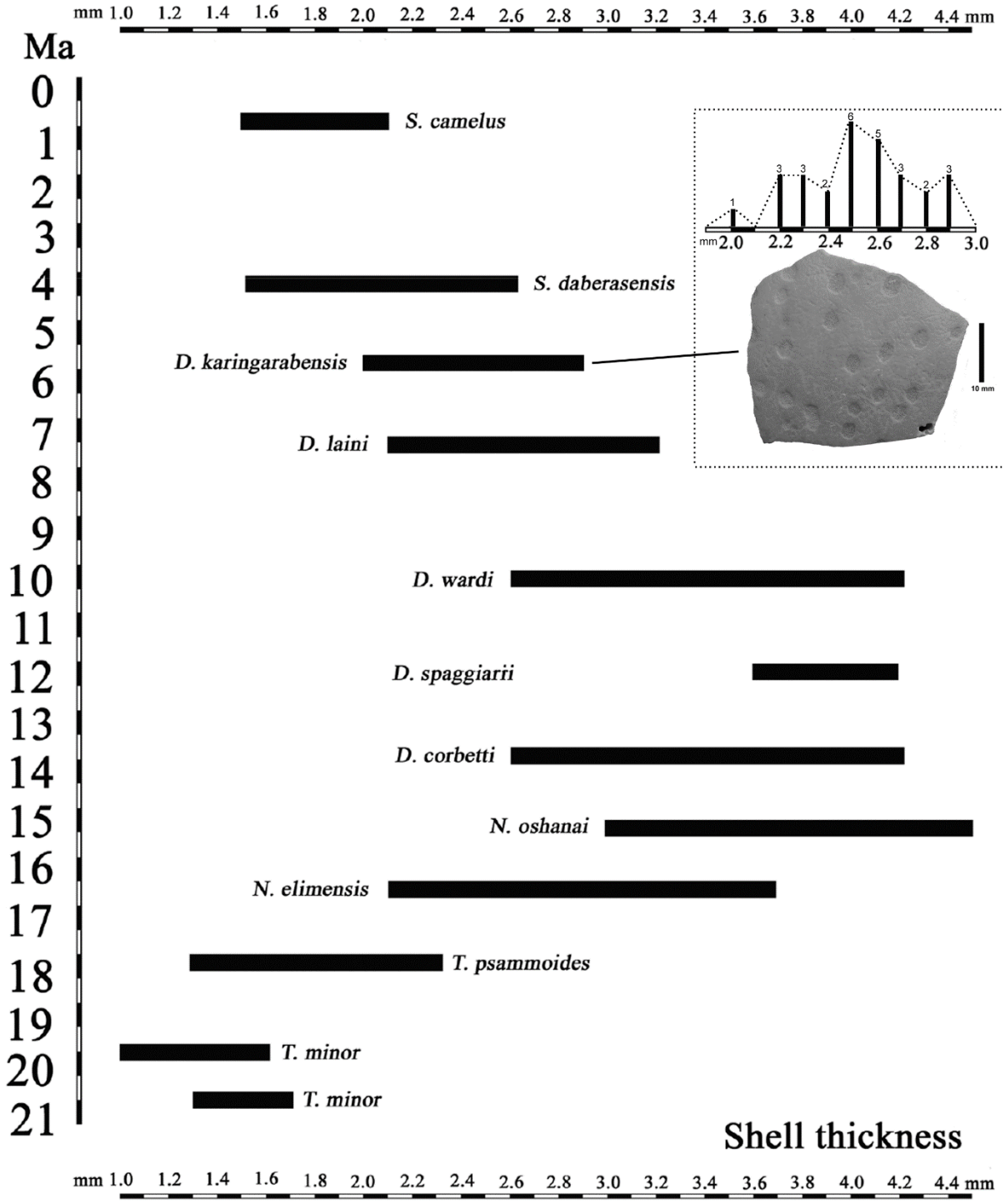

Figure 3. Ranges of thicknesses of fossil struthious eggshells from Namibia (Early Miocene to Recent), highlighting the new intrepretation of *Diamantornis karingarabensis*. The illustrated eggshell fragment is the holotype of the species (GSN KG 26'95 'A') and the inset is a frequency histogram of the thicknesses of eggshells from the same locality – mode 2.5 mm. (*T - Tsondabornis, N - Namornis, D - Diamantornis, S - Struthio*). Figure modified from Pickford (2014)

Discussion

Restudy of the entire sample of eggshell frragments from the type locality of *Struthio karingarabensis* (25 fragments) reveals that their thickness is somewhat less than previously reported, ranging in thickness from 2.0 to 2.9 mm (mode 2.5 mm) (Fig. 3). Furthermore,

the pore complexes are morphologically similar to those that occur in species of *Diamantornis*, even though they are of smaller diameter than them and are more irregular in outline, as originally reported by Senut *et al*. (1998). The pores are clustered close together in the depths of shallow depressions with well-marked margins, as in *Diamantornis corbetti*, *Diamantornis spaggiarii*, *Diamantornis wardi* and *Diamantornis laini*, and the shell between the pore complexes is smooth and devoid of pores, also as in these species. In species of *Struthio*, in contrast, the pores are generally scattered over the surface of the eggshell, not forming clusters of many closely-packed pores in clearly defined shallow ovoid depressions but forming groups of a few pores in shallow linear or curved grooves. It is therefore logical to transfer the Karingarab species to *Diamantornis* as the combination *Diamantornis karingarabensis*.

Previous attribution of the Karingarab eggshells to the genus *Struthio* reflected the rather irregular outlines of the pore complexes as well as their relatively diminutive dimensions when compared with those present in *Diamantornis wardi* which are larger and more circular in outline (Pickford and Dauphin, 1993; Pickford, 2014). As such the form of pore complexes of the eggshells of *D. karingarabensis* is intermediate between those of *D. wardi* and *Struthio camelus*. The specimens are also intermediate in thickness and age between *D. wardi* and *S. camelus* (Fig. 3) so it is plausible that *D. karingarabensis* eventually gave rise to *Struthio*. However, on the basis of the morphology of the pore complexes and the thickness of the shells, it is considered that the Karingarab fossils are better classified in *Diamantornis* than in *Struthio*.

The pores in eggshells are channels via which gases are exchanged between the developing chick inside the egg and the surrounding atmosphere, with carbon dioxide and water vapour being ‘exhaled’, and oxygen ‘inhaled’.

By concentrating the pores in shallow depressions in the external surface of the eggshell, species of *Diamantornis* effectively reduce the distance between the inner surface of the eggshell and the atmosphere, while maintaining an overall thick shell related to the greater dimensions of the egg. Eggs of *Struthio*, in contrast, are thinner and smaller than those of *Diamantornis*, so even though the pores penetrate similar thicknesses of shell as they do in the latter genus, they are not concentrated into depressions in the outer surface of the eggs, but are scattered liberally all over the egg, often in shallow grooves.

In view of the usefulness that fossil struthious eggshells have shown for Afro-Arabian Neogene biochronology, it is deemed necessary to refine the data base concerning the dimensions of the eggshells in *Diamantornis karingarabensis*, because previous reports on their thickness (Senut *et al*., 1998; Pickford, 2014) differ slightly from the new measurements (Table 1; Fig. 3).

Conclusion

Re-examination of the sample of eggshell fragments from the type locality of *Struthio karingarabensis* Senut *et al*. (1998) reveals that the specimens are morphologically closer to those of the oogenus *Diamantornis* rather than to those of *Struthio*. For this reason they are herein classified as the combination *Diamantornis karingarabensis*.

A few published measurements of the material, in particular of the holotype, overestimated the upper end of the range of variation of eggshell thickness, so a revised compilation of measurements of the entire sample of eggshell fragments from the type locality is provided.

Acknowledgements

For administrative help, the NPE thanks the French Embassy in Namibia (Sébastien Minot, Marion Christmann, Silvia Ricoveri), the Centre de Recherche en Paléontologie, Paris (CR2P) (Dr Sylvie Crasquin, Dr Silvain Charbonnier, Angelina Bastos and Suzy Colas). Funding was provided by the ATM project PalPrim Namibie (Paléo-biodiversité des Primates du Néogène et du Quaternaire en Namibie) (MNHN) and the Prix Del Duca.

In Windhoek, Ms Gloria Simubali and Ms Anna Nguno of the Geological Survey of

Namibia provided help and encouragement as did Helke Mocke. Thanks also to Jane Eiseb and Anna Williams for their cooperation.

Erica Ndalikokule, Lucia Namushinga and Edith Stanley of the Namibian National Heritage Council arranged for authorisation to collect fossils in Namibia. Thanks to Gernot Piepmeyer and Junias Shangala of the National Commission on Research, Science and Technology of Namibia for authorisation to carry out reseach in the country.

Finally, Namdeb staff in Lüderitz and Oranjemund (Jürgen Jacob, Gottfried Grobbelaar, Hugh-Reese Boer and Renee Strauss) are thanked for providing logistic and administrative help for the surveys in the Sperrgebiet. Thanks also to Claudine Losper (Sperrgebiet Diamonds).

References

Bibi, F., Shabel, A., Kraatz, B. and Stidham, T. 2006. New fossil ratite (Aves: Palaeognathae) eggshell discoveries from the Late Miocene Baynunah Formation of the United Arab Emirates, Arabian Peninsula. *Palaeontologica electronica*, **9**(**1**) **2A**, 1-13.

Harris, J. M. and Leakey, M. G. 2003. Lothagam birds. *In*: Leakey, M. G. and Harris, J. M. (Eds) *Lothagam: The Dawn of Humanity in Eastern Africa*. Columbia University Press, New York, 161-166.

Harrison, T. and Msuya, C. 2005. Fossil struthionid eggshells from Laetoli, Tanzania: Taxonomic and biostratigraphic significance. *Journal of Human Evolution*, **41**, 303-315.

Latham, J. 1790. Index Ornithologicus, Sive Systema Ornithologiae: Complectens Avium Divisionem. *In: Classes, Ordines, Genera, Species, Ipsarumque Varietates* (2 Volumes). Leigh and Sotheby, London, UK.

Louchart, A., Bibi, F. and Stewart, J. R. 2022. Birds from the Baynunah Formation. *In*: Bibi, F., Kraatz, B., Beech, M. J. and Hill, A. (Eds) *Sands of Time: Ancient Life in the Late Miocene of Abu Dhabi, United Arab Emirates*. Springer, 125-139.

Pickford, M. and Dauphin, Y. 1993. *Diamantornis wardi*, nov. gen., nov. sp., giant extinct bird from Roilepel, lower Miocene, Namibia. *Comptes Rendus de l'Académie des Sciences, Paris*, **316**, 1643-1650.

Pickford, M., Al-Kindi, M., Rajhi, M., Al Marjibi, T. and Al Rawahi, F. 2023. Correlation of the Marsawdad Formation, Oman, Late Miocene (Turolian-Ventian), based on fossil avian eggshells. *Estudios Geológicos*, **79** (**2**): e153. https://doi.org/10.3989/egeol.44974.631.

Pickford, M., Senut, B. and Dauphin, Y. 1995. Biostratigraphy of the Tsondab Sandstone (Namibia) based on gigantic avian eggshells. *Geobios*, **28**(**1**), 85-98.

Ségalen, L., Renard, M., Pickford, M., Senut, B., Cojan, I., Le Callonec, L. and Rognon, P. 2002. Environmental and climatic evolution of the Namib Desert since the Middle Miocene: the contribution of carbon isotope ratios in ratite eggshells. *Comptes Rendus Geoscience*, **334**, 917-924.

Senut, B. 2000. Fossil ratite eggshells: a useful tool for Cainozoic biostratigraphy in Namibia. *Communications of the Geological Survey of Namibia*, **12**, 367-373.

Senut, B., Dauphin, Y. and Pickford, M. 1998. Nouveaux restes aviens du Néogène de la Sperrgebiet (Namibie): complément à la biostratigraphie avienne des éolianites du désert de Namib. *Comptes Rendus de l'Académie des Sciences, Paris*, **327**, 639- 644.

Senut, B. and Pickford, M. 1995. Fossil eggs and Cenozoic continental biostratigraphy of Namibia. *Palaeontologia Africana*, **32**, 33-37.

Stewart, J. R. and Beech, M. J. 2006. The Miocene birds of Abu Dhabi (United Arab Emirates) with a discussion of the age of modern species and genera. *Historical Biology*, **18**(**2**), 103-113.

Stidham, T. 2004. Extinct ostrich eggshell (Aves; Struthionidae) from the Pliocene Chiwondo Beds, Malawi: implications for the potential biostratigraphic correlation of African Neogene deposits. *Journal of Human Evolution*, **46**, 489-496.

Stidham, T. A. 2008. The importance of *Diamantornis* eggshell (Aves, Struthio-nidae) in the age and correlation of the Prospect Hill Formation, South Africa. *South African Journal of Geology*, **111**, 459-461.

Vigors, N. A. 1825. Sketches in ornithology; or, observations on the leading affinities of some of the more extensive groups of birds. Arrangement of genera of birds. *Zoological Journal*, **2**, 368-405.

Soil characterisation for suitability for construction work: A Case Study of Rehoboth and Acacia (Windhoek), Namibia

Sam P. Shuuya

Geological Survey of Namibia, 6 Aviation Road, Windhoek
<Sam.Shuuya@mme.gov.na>

Abstract :- The populations of Windhoek and Rehoboth, located some 90 km south of the capital, are growing rapidly, leading to major construction to meet people's needs. Due to this rapid increase of the urban population and the resulting demand for housing and facilities in the limited space available, adequate groundwork, necessary for the safety and stability of the planned development, is often lacking. At three sites where construction for residential use was taking place, i. e. Rehoboth South, Rehoboth North and the suburb of Acacia in Windhoek, pertinent soil characteristics were investigated. Soil samples were tested for moisture content, grain size distribution and gradation as these factors, among others, determine the suitability of a building site and the foundation type to be adopted. Failure to ascertain carrying capacity and other essential aspects of the proposed site prior to construction start can have a significant impact on stability and – subsequently – on cost for later modifications. This study, carried out as a B. Sc. (Hons) project at the University of Namibia, provides basic information for construction work, emphasising the need of adequate building ground investigation both for reasons of safety and economy. It presents the findings from the investigation of three construction sites, which encompassed general site reconnaissance and geotechnical field and laboratory tests.

Keywords :- Soil characteristics, Foundation type, Moisture content, Bearing capacity, Gradation analysis, Trace elements

To cite this paper :- Shuuya, S. P. 2024. Soil characterisation for suitability for construction work: A Case Study of Rehoboth and Acacia (Windhoek), Namibia. *Communications of the Geological Survey of Namibia*, **27**, 72-96.

Introduction

Soil is one of the most important yet the most frequently overlooked factor in construction projects, such as housing, roads, bridges and dams. Soil is the natural foundation that supports all structures and infrastructure investment. Although a thorough soil investigation averages less than one percent of the total construction cost, it is often neglected during the conceptual project phase, and its importance underestimated (Kunkolienkar, 2016). Some contractors base their design on an assumed bearing capacity and rate of settlement (Fame, 2013). However, as the physical and chemical characteristics of soil can vary even within the limits of a proposed construction site, such assumptions cannot substitute for a thorough on-site investigation. Also, climatic influences, site management and a host of other natural and anthropogenic factors can affect the bearing capacity of soil, and, consequently, require foundations designed in accordance with local conditions and the proposed usage to avoid failure of the structure (Arya and Agarwal, 2007). To forestall uncontrolled development of urban areas, with deleterious effects on the environment in the long and short term, obtaining accurate information about the physical properties of the soil underlying a proposed construction site must form the basis for planning, designing and, eventually, building.

To establish the suitability of a particular soil as foundation material, various physical, chemical and mechanical tests are employed (Das, 1990):

a) Atterberg Limits Test to determine plasticity of the soil (includes tests for liquid limit, plastic limit and shrinkage limit);
b) Sieve analysis to determine grain size distribution, which affects soil strength and stability;
c) Proctor Compaction Test to determine the maximum dry density and optimum moisture content of the soil, which affects its ability to resist deformation and support loads;

d) California Bearing Ratio (CBR) test to determine load-bearing capacity;
e) pH test to determine acidity or alkalinity, and the potential for chemical reactions, which may affect strength and stability;
f) Organic Matter Content test to determine the proportion of organic material in the soil, which also may affect strength and stability;
g) Shear Strength test to determine ability of the soil to withstand stress and strain;
h) Cone Penetration test (CPT) to determine the bearing capacity of granular soils (sand, gravel) and estimate the strength of cohesive soils (clay, silt);
i) Natural Moisture Content test to determine the amount of water present in the soil, which affects stability.

The objectives of this site investigation were (a) to define the type, grading and nature of the soil at the proposed building sites in Rehoboth and Windhoek (Figs 1, 2, 3), (b) to determine the bearing capacity of the soil and identify potential problems, and (c) to select the type and depth of foundation required for the planned construction work of single-storey buildings for residential use. For the three sites, geotechnical tests b), h) and i) above were chosen as they encompass the essential soil properties that are crucial for this type of development. Other work carried out in the course of the investigation was soil profiling - a visual assessment of the soil layers - at each location, X-ray fluorescence analyses to determine elemental composition and X-ray diffraction analyses for mineralogical composition.

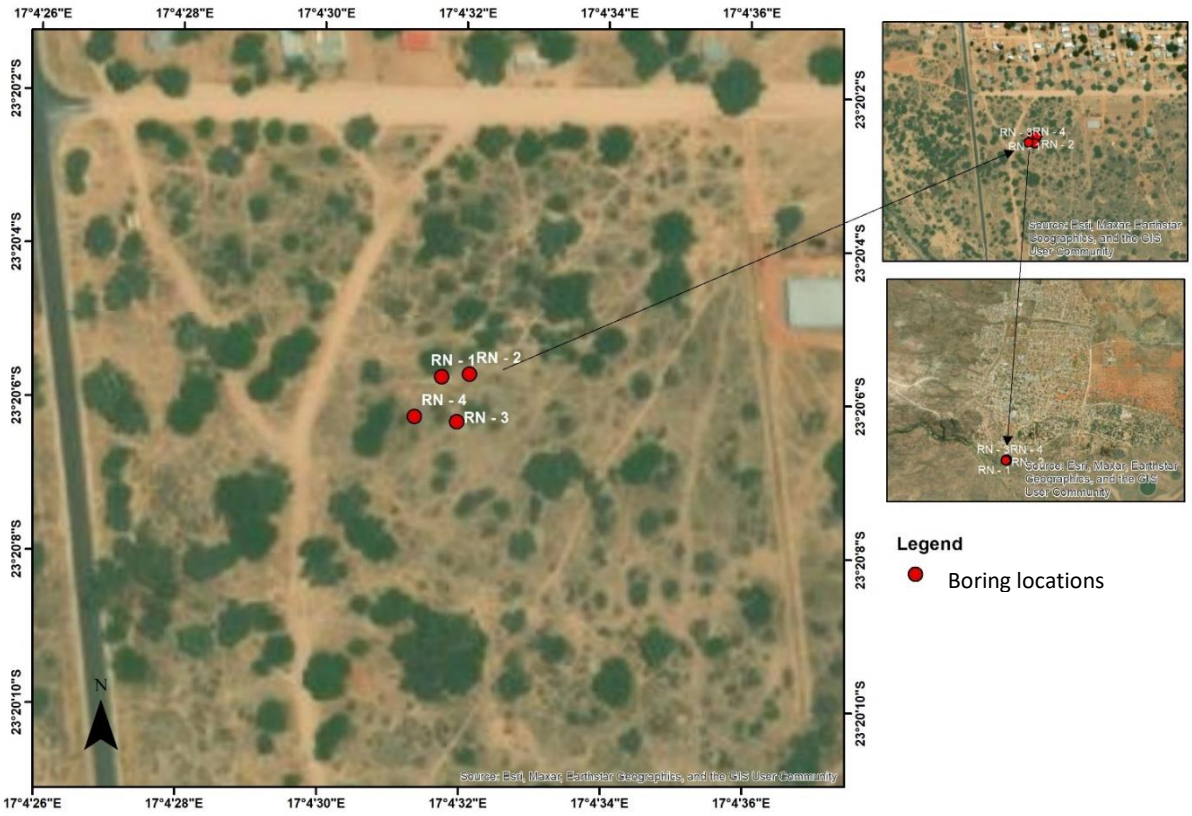

Figure 1. Satellite image (Google Earth) showing construction site at Rehoboth North and boring locations

Due to rapid increase of the urban population during the last 12 years (Windhoek: 33 %; Rehoboth: 29.3 %; NSA, 2024) - pressure is put on development projects, which often leads to adequate site investigation prior to construction start being neglected. To make matters worse, the high demand for building ground, allied to the local topography, has resulted in the allocation of land in sloping areas, which are prone to landslides, erosion and soil movement, for construction. In order to prevent or minimise damage to buildings and their foundations from these causes, full geotechnical investigations and drainage control are especially important.

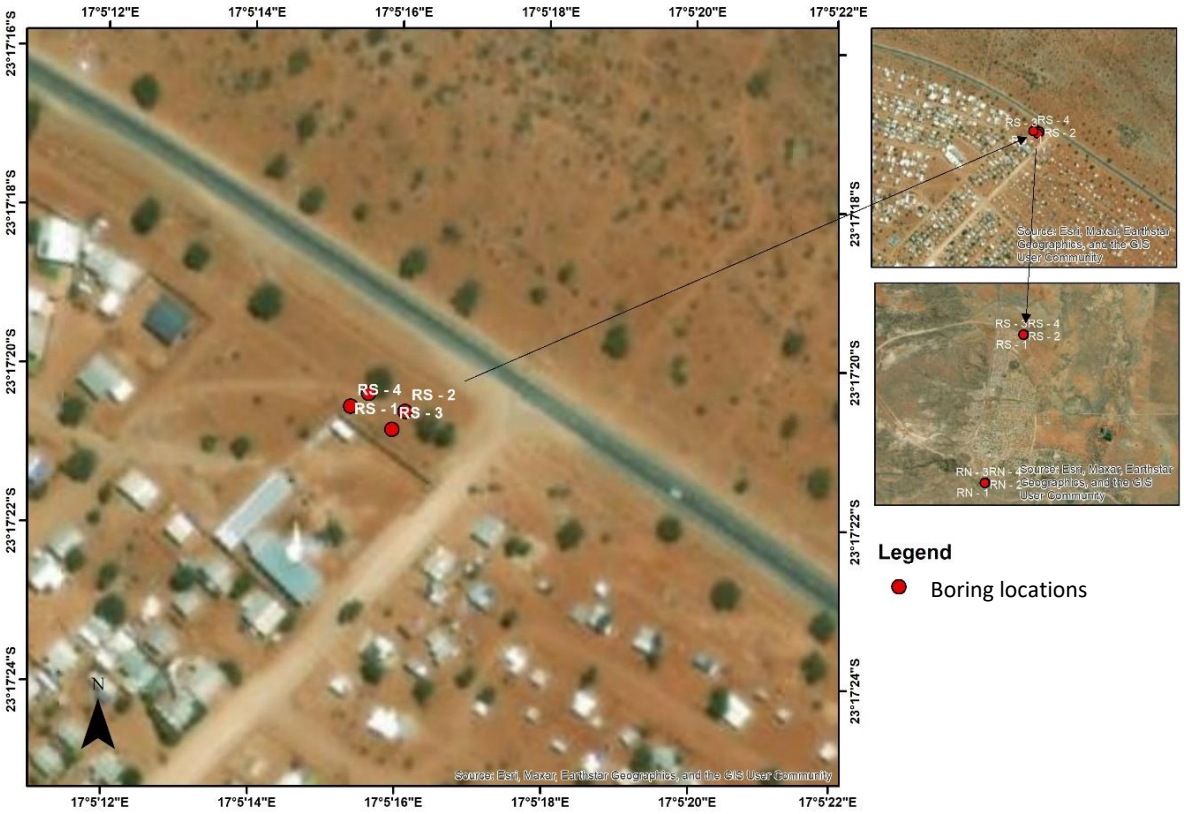

Figure 2. Satellite image (Google Earth) showing construction site at Rehoboth South and boring locations

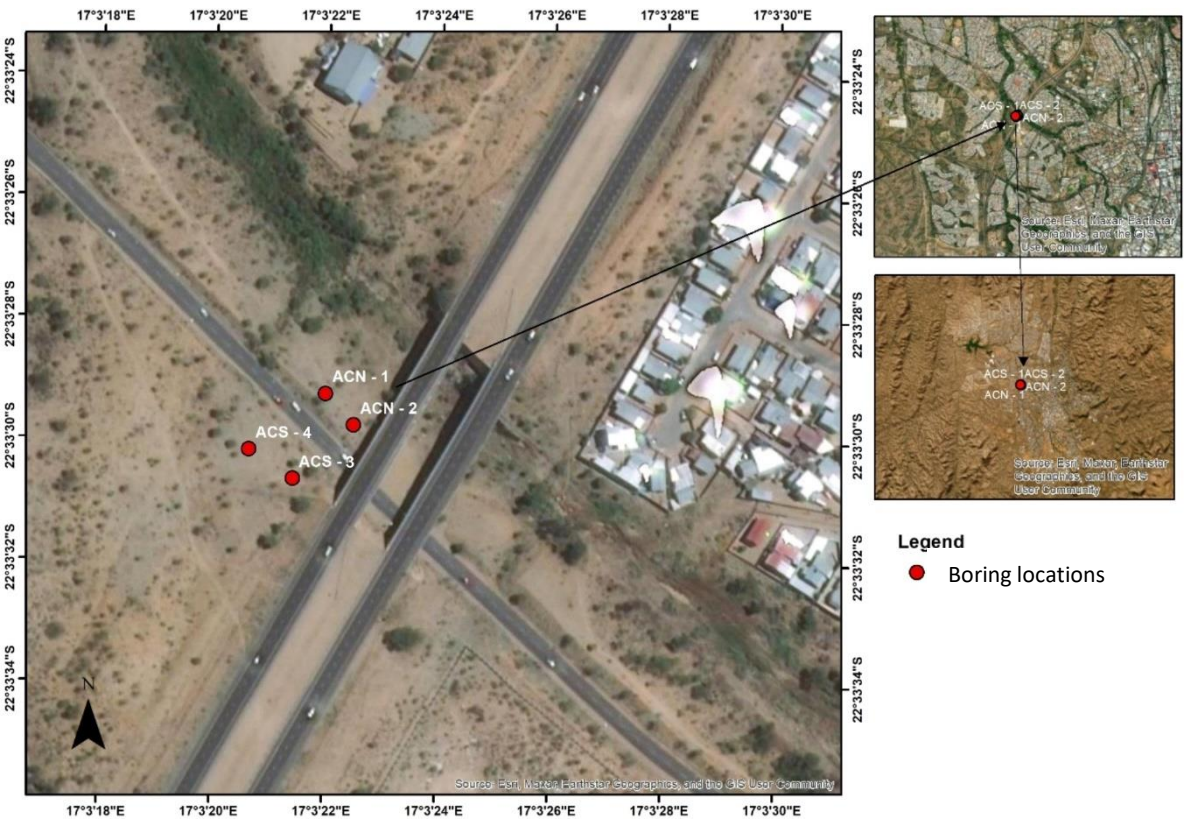

Figure 3. Satellite image (Google Earth) showing construction site at Acacia (Windhoek) and boring locations

Location of the study area

The soil investigations for this study were carried out at three construction sites in Rehoboth, some 93 km south of Windhoek, and Acacia, a suburb of Windhoek between Dorado Park and Dorado Valley (Figs 1, 2, and 3) during the dry season of 2016 (June to September). The soils at each site were observed and tested to determine the soil profile and to decide its suitability for the planned construction work (Fig. 4). The two Rehoboth sites are underlain by sandy soil, while at Acacia the proposed building ground consists of mica schist and quartz gravel, with hardly any soil development.

Figure 4. Site images: (a) Boring at Rehoboth North; (b) Acacia sampling site; (c) Location of housing construction at Rehoboth South; (d) Boring location in Acacia underlain by mica schist and quartz

Regional geology of the investigated sites

The area of interest around Rehoboth North and South is underlain by rocks of Mesoproterozoic age (Fig. 5). Cross-bedded orthoquartzite of the Billstein Formation, with a maximum thickness of approximately 100 m, rests unconformably on Palaeoproterozoic basement gneisses (Kangas Metamorphic Complex). A transitional contact exists between the quartzite and overlying intercalated, locally sericitic, schist and conglomerate, which have a combined thickness of at least 2000 m. Conglomerate clasts consist of granite, vein quartz and quartzite. The Billstein rocks are overlain by the mostly rhyolitic Langberg Formation along a sheared contact; this unit starts with a polymict, ill-sorted, clast-supported conglom-

erate, followed by a succession of felsic volcanic rocks several hundred metres thick. Basal ignimbrite layers, up to 20 m thick, are intercalated with crystal-rich tuff beds, while reddish quartzite and schist form the top of the succession. The uppermost Opdam Formation rests unconformably upon the Langberg Formation or transgresses the Billstein Formation. It is composed of amygdaloidal basaltic lavas with flow-top breccias, interbedded with polymict conglomerate, slate, phyllite and greyish quartzite. Minor pillow structures have been observed within the basaltic flows. Locally the Mesoproterozoic rocks are covered by the calcrete-cemented Weissrand conglomerate of Palaeogene age. To the east exposures are scarce, with most of the bedrock buried under unconsolidated sediments (sand, gravel, scree and calcrete) of the Kalahari Group. Alluvial sediments occur along river courses.

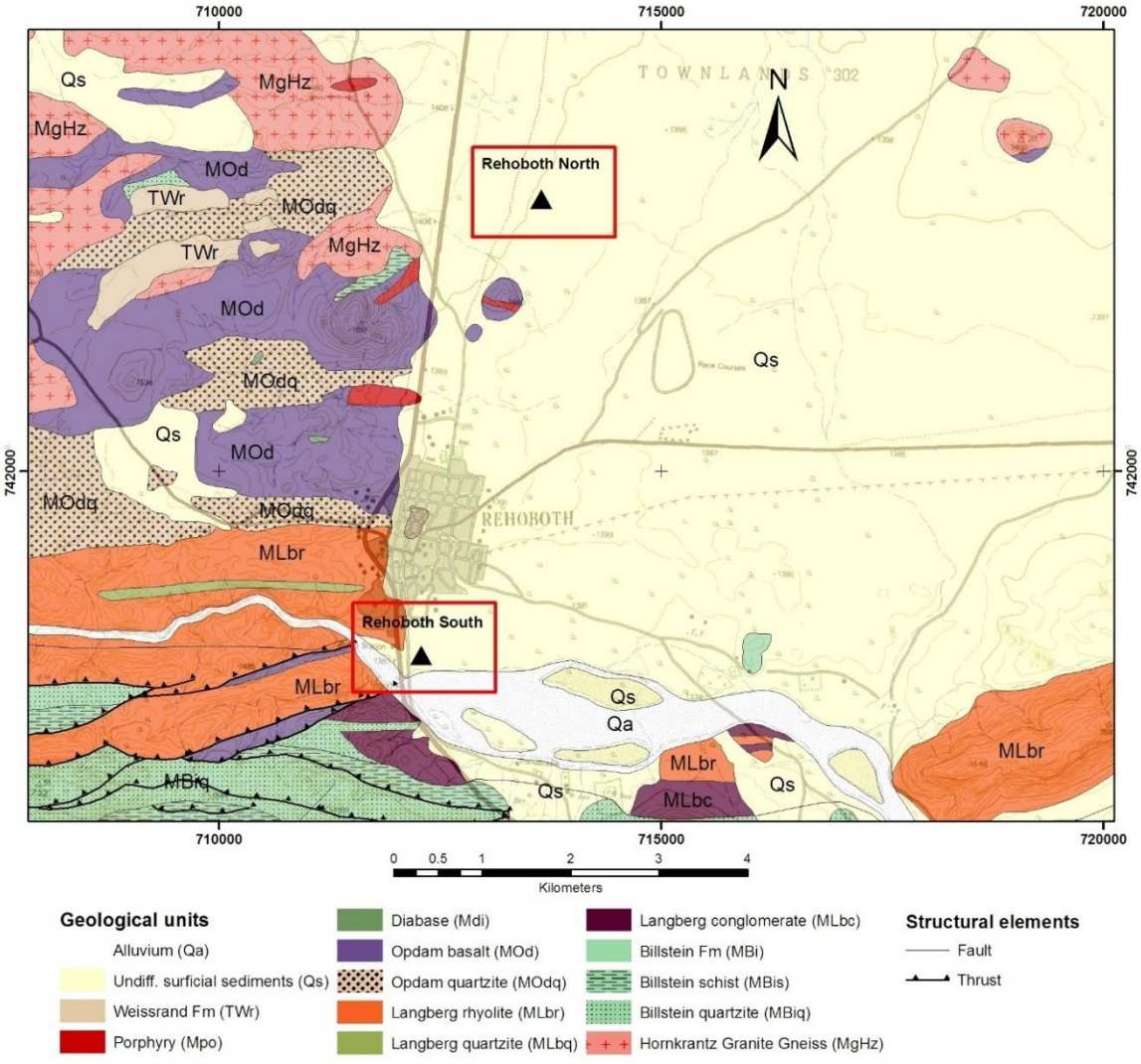

Figure 5. Regional geology of Rehoboth and environs indicating the investigated sites (after Schalk *et al*., 2006)

The regional geology of Windhoek and surroundings (Fig. 6) is characterised by Neoproterozoic metamorphic rocks of the Khomas Complex, consisting of mica schists of the Kuiseb Formation intercalated with Kleine Kuppe quartzites. Also interlayered with the schists are the mafic metavolcanic rocks (amphibolites) of the Matchless Suite, which are both in tectonic and intrusive contact with the Kuiseb schists. Parts of the area are covered by alluvium, sand, gravel or scree.

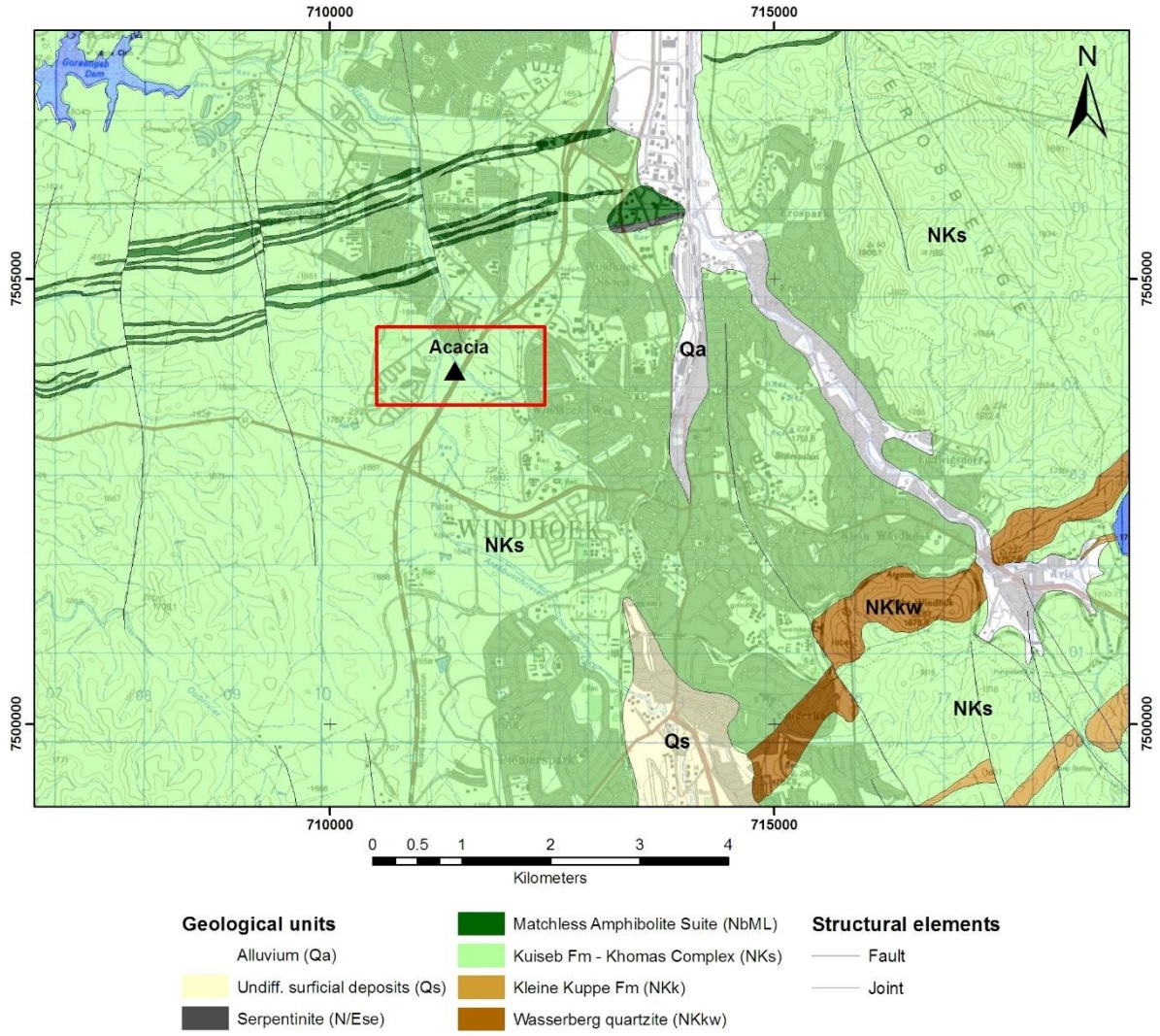

Figure 6. Regional Geology of Windhoek and environs indicating location of investigated site (after Hälbich *et al*., 2006)

Methodology

A total of twelve holes were dug to a depth of ca 50 cm, and the soil profiles described. Seventy-two soil samples, collected from the three construction sites, underwent various laboratory tests, including grain size distribution analysis and determination of elemental and mineralogical composition. A cone penetrometer was used to establish the bearing capacity of the soils; note was taken also of local topography, geological features, vegetation cover, and other relevant environmental data at the three sites.

Field investigation and sampling

Digging and sampling at Rehoboth (North and South) consisted of eight soil borings labelled RN-1 to 4 and RS-1 to 4, respectively, while in Windhoek (Acacia) four soil borings labelled ACN-1 & 2 and ACS-3 & 4 were dug (Table 1). All borings extended to a depth of approximately 50 cm below the surface. This depth was chosen as the soil profile in the investigated areas is relatively consistent, with similar soil properties throughout, and because the planned light construction work does not require deeper penetration. Boring locations at the proposed sites were selected based on accessibility. At each boring locality cone penetration tests (CPT) were carried out to determine the strength, i. e. resistance to penetration, of the soil using a hand-pushed (portable) penetrometer with a cone base area of 2 cm^2.

Area Name	Boring No	Easting (m)	Northing (m)	UTM Zone
Rehoboth North	RN - 1	712200	7417882	WGS84_33S
Rehoboth North	RN - 2	712211	7417883	WGS84_33S
Rehoboth North	RN - 3	712206	7417864	WGS84_33S
Rehoboth North	RN - 4	712189	7417866	WGS84_33S
Rehoboth South	RS - 1	713519	7422951	WGS84_33S
Rehoboth South	RS - 2	713533	7422944	WGS84_33S
Rehoboth South	RS - 3	713528	7422937	WGS84_33S
Rehoboth South	RS - 4	713512	7422946	WGS84_33S
Acacia North	ACN - 1	711420	7503939	WGS84_33S
Acacia North	ACN - 2	711434	7503923	WGS84_33S
Acacia South	ACS - 3	711403	7503896	WGS84_33S
Acacia South	ACS - 4	711381	7503911	WGS84_33S

Table 1. Boring locations of the investigated construction sites

Relatively disturbed soil samples were collected at each boring from surface (0 cm) to 25 cm depth, from 25 to 35 cm depth and from 35 to 50 cm depth to establish soil type, gradation, classification, consistency, density and stratification. At each depth two samples were taken, one for sieve analysis and one for X-ray fluorescence (XRF) and X-ray diffraction (XRD) analysis. Samples are considered "disturbed" as the sampling process itself modifies their natural structure (Munfakh *et al*., 1997). A total of seventy-two samples were obtained in the course of field investigations from the three sites.

American Society of Testing and Materials (ASTM) Standard References	
Soil Properties	**Specification**
Classification	ASTM D 2487 - 17: Standard Practice for Classification of Soils for Engineering Purposes (Unified Soil Classification System)
Particle-Size Analysis of Soils (Sieve Analysis)	ASTM D 422 - 63: Standard Test Method for Particle-Size Analysis of Soils
Water (Moisture) Content of Soil	ASTM D 2216 - 19: Standard Test Method for Laboratory Determination of Water (Moisture) Content of Soil, Rock, and Soil-Aggregate Mixtures
Soil Strength (Penetration Test)	ASTM D 3441 - 16: Standard Test Method for Mechanical Cone Penetration Tests of Soil

Table 2. Standard laboratory tests for the determination of soil properties in geotechnical engineering (ASTM)

Laboratory Testing

After an on-site description of the soil samples, their physical and mechanical properties were determined at the laboratories of the Geological Survey of Namibia and the UNAM (University of Namibia) Geology Department. Tests included grain size analysis, determination of water content, X-Ray Fluorescence and X-Ray Diffraction analysis. A total of thirty-six soil samples was prepared for grain size (sieve) analysis and water content determination in accordance with the requirements of the American Society of Testing and Materials (ASTM; Table 2). Twelve samples were submitted for examination by XRF (Niton Portable XRF XL3t GOLDD+950) to determine the elemental

composition of the soil, and five for XRD analysis (D8 Advance XRD Instrument C79249-A3054-A21) to establish its mineral components. XRF analysis was performed on pressed powder pellets of the dried, pulverised and homogenised soil samples; for XRD analysis coarser particles of the dried soil sample were selected. To determine grain size distribution in the investigated soils, the dried samples were passed through a stack of sieves of diminishing aperture (Fig. 7).

Figure 7. Sieve analysis at the University of Namibia's Geology Laboratory: (a) Weighing unsieved samples from different depths; (b) and (c) Sieves stacked according to diminishing aperture; (d) Weighing each size fraction for classification of the soil

Results

Results of the above tests and analyses are presented as:

- Soil profiles with soil descriptions (Tables 3, 4)
- Water content determination (Table 5)
- Cone Penetration Test (CPT) results from various depths relating to the strength of the tested soils and their bearing capacity for foundations (Tables 6 to 11; Figs 8, 9, 10).
- Geochemical compositions as determined by portable X-ray fluorescence spectrometer (Table 13)
- Mineralogical composition as determined by X-ray diffraction (Table 14; Figs 11 to 15)
- Sieve analysis results (Tables 4, 15; Figs 17, 18, 19)

Soil profiling

Table 3 shows the soil profiles, i. e. the overall soil types present at various depths, at the three investigated sites. Detailed soil descriptions for each boring depth are given in Table 4. Grain size distribution curves of selected representative soil samples from different depths (from surface to 50 cm) are presented in figures 17, 18 and 19. Parameters defining the grain size distribution curves for each soil sample are listed in Table 4.

Water Content

During the site investigation the soil samples were collected without any interruption in the sampling process; most of the soil samples appeared to be quite dry. Table 5 shows the measured water content of all soil samples, which was determined by the Oven Dry Method (ASTM D 422 - 63) at a temperature of 105 to 110 degrees Celsius. The low percentages of water found in the soils from the three sites (on average < 1 wt %) confirmed field observations; only one sample from Acacia showed a significant water content (ACN-2; 20.2 wt %). The generally low water content of the examined samples is attributed to the absorption of moisture by underlying porous and/or fractured rocks, such as sandstones and schists, which allow the water to drain away, combined with evaporation occasioned by dry weather.

C**one Penetration Test**

Cone Penetration Tests (CPT) offer a valuable tool for discovering the nature of the ground beneath our feet. At the three sites, CPTs were conducted to establish soil strength and its variation with depth, as well as overall bearing capacity. The process involved taking manometer readings, which represent the force needed to push a cone-shaped penetrometer steadily downward into the soil. These readings, expressed in Newtons (N; Tables 6, 7 and 8), are transformed into cone resistance (qc) values through division by the cone's base area (2 cm^2); results are expressed in Megapascals (MPa; Tables 9, 10 and 11). Based on cone resistance, the Begemann Penetration Resistance (BPR; Libric *et al*., 2017) soil strength classification divides soils into six categories with distinct behavioural properties (Table 12). Relationships between cone resistance (MPa) and depth (cm) are displayed by the curves plotted in figures 8, 9 and 10.

Site Name	Depth (cm)	Soil Description
Rehoboth South	0-25	Dry, light brown, loose, granular sandy soil with dead plant roots
	25-35	Dry, light brown, firm, massive sandy soil
	35-50	Dry to moderately moist, light brown, firm, massive sandy soil with plant roots
Rehoboth North	0-25	Dry, reddish-brown, loose, massive sandy soil
	25-35	Dry, reddish-brown, firm, massive sandy soil with plant roots
	35-50	Dry, reddish, firm, massive sandy soil with plant roots
Acacia, Windhoek	0-25	Dry, brown-greyish, loose, granular sandy gravel soil with plant roots and rock fragments approximately 5 cm in diameter
	25-35	Dry, brown-greyish, hard, granular gravel sandy soil with pebbles
	35-50	Dry, brown-greyish, hard, granular gravel sandy soil with pebbles

Table 3. On-site description of the soil profiles at Rehoboth South, Rehoboth North and Acacia

Sample	Depth (cm)	Soil Description	% Gravel	% Sand	% Fines	D_{10}	D_{25}	D_{30}	D_{50}	D_{60}	D_{75}	C_C	C_U	S_0
RN-1	0 - 25	Dry, reddish-brown, loose, massive sandy soil	1.46	94.41	4.13	0.09	0.18	0.21	0.28	0.30	0.34	1.63	3.33	1.37
RN-1	25 - 35	Dry, reddish-brown, firm, massive sandy soil with plant roots	1.34	95.15	3.51	0.08	0.14	0.16	0.23	0.28	0.34	1.14	3.50	1.56
RN-1	35 - 50	Dry, reddish, firm, massive sandy soil with plant roots	1.36	94.18	4.46	0.08	0.14	0.15	0.23	0.27	0.33	1.04	3.38	1.54
RN-2	0 - 25	Dry, reddish-brown, loose, massive sandy soil	2.35	93.10	4.55	0.09	0.16	0.19	0.28	0.30	0.39	1.34	3.33	1.56
RN-2	25 - 35	Dry, reddish-brown, firm, massive sandy soil with plant roots	1.88	94.87	3.25	0.16	0.23	0.25	0.30	0.33	0.40	1.18	2.06	1.32
RN-2	35 - 50	Dry, reddish-brown, firm, massive sandy soil with plant roots	1.71	94.27	4.02	0.13	0.22	0.24	0.30	0.32	0.40	1.38	2.46	1.35
RN-3	0 - 25	Dry, reddish-brown, loose, massive sandy soil	1.54	95.47	2.99	0.10	0.19	0.21	0.28	0.31	0.38	1.42	3.10	1.41
RN-3	25 - 35	Dry, reddish, firm, massive sandy soil with plant roots	1.56	95.24	3.20	0.15	0.18	0.21	0.30	0.32	0.39	0.92	2.13	1.47
RN-3	35 - 50	Dry, reddish, firm, massive sandy soil with plant roots	2.83	92.11	5.06	0.08	0.16	0.18	0.27	0.30	0.37	1.35	3.75	1.52
RN-4	0 - 25	Dry, reddish-brown, loose, massive sandy soil	2.55	94.14	3.31	0.13	0.21	0.23	0.30	0.31	0.39	1.31	2.38	1.36
RN-4	25 - 35	Dry, reddish-brown, firm, massive sandy soil with plant roots	3.64	92.67	3.69	0.09	0.16	0.18	0.28	0.30	0.38	1.20	3.33	1.54
RN-4	35 - 50	Dry, reddish-brown, firm, massive sandy soil with plant roots	2.40	93.09	4.51	0.08	0.15	0.16	0.27	0.30	0.40	1.07	3.75	1.63
RS-1	0 - 25	Dry, light brown, loose, granular sandy soil with dead plant roots	3.34	94.33	2.33	0.16	0.24	0.26	0.32	0.36	0.60	1.17	2.25	1.58
RS-1	25 - 35	Dry, light brown, firm, massive sandy soil	3.77	94.18	2.05	0.15	0.18	0.26	0.32	0.39	0.70	1.16	2.60	1.97
RS-1	35 - 50	Dry to moderately moist, light brown, firm, massive sandy soil with plant roots	5.05	92.88	2.07	0.12	0.21	0.24	0.30	0.35	0.80	1.37	2.92	1.95
RS-2	0 - 25	Dry, light brown, loose, sandy soil with dead plant roots	4.53	93.19	2.28	0.12	0.21	0.25	0.34	0.40	0.70	1.30	3.33	1.83
RS-2	25 - 35	Dry, light brown, firm, massive sandy soil	4.50	93.31	2.19	0.10	0.20	0.23	0.32	0.39	0.65	1.36	3.90	1.80
RS-2	35 - 50	Dry to moderately moist, light brown, firm, massive sandy soil with plant roots	5.16	92.47	2.37	0.14	0.25	0.27	0.36	0.42	0.80	1.24	3.00	1.79
RS-3	0 - 25	Dry, light brown, loose, granular sandy soil with dead plant roots	3.70	94.80	1.50	0.16	0.25	0.27	0.32	0.38	0.60	1.20	2.38	1.55
RS-3	25 - 35	Dry, light brown, firm, massive sandy soil	2.78	95.43	1.79	0.13	0.22	0.24	0.31	0.37	0.58	1.20	2.85	1.62
RS-3	35 - 50	Dry, light brown, firm, massive sandy soil	3.19	94.77	2.04	0.10	0.20	0.23	0.31	0.38	0.60	1.39	3.80	1.73
RS-4	0 - 25	Dry, light brown, loose, granular sandy soil with dead plant roots	3.55	95.46	0.99	0.15	0.25	0.27	0.31	0.38	0.60	1.28	2.53	1.55
RS-4	25 - 35	Dry, light brown, firm, massive sandy soil	4.12	94.21	1.67	0.15	0.24	0.26	0.32	0.39	0.62	1.16	2.60	1.61
RS-4	35 - 50	Dry to moderately moist, light brown, firm, massive sandy soil with plant roots	4.97	92.78	2.25	0.13	0.23	0.25	0.34	0.40	0.70	1.20	3.08	1.74
ACN-1	0 - 25	Dry, brown-greyish, loose, granular sandy gravel soil with plant roots and rock fragments	18.16	76.82	5.02	0.09	0.22	0.25	0.35	0.60	1.60	1.16	6.67	2.70
ACN-1	25 - 35	Dry, brown-greyish, hard, granular gravel sandy soil with rock pebbles	15.98	79.09	4.93	0.10	0.22	0.25	0.35	0.44	1.40	1.42	4.40	2.52
ACN-1	35 - 50	Dry, brown-greyish, hard, granular gravel sandy soil with rock pebbles	22.40	72.55	5.05	0.08	0.14	0.15	0.30	0.70	1.80	0.40	8.75	3.59
ACN-2	0 - 25	Dry, brown-greyish, loose, granular sandy gravel soil with plant roots and rock fragments approximately >5 cm in diameter	21.38	73.29	5.33	0.08	0.09	0.11	0.30	0.60	1.60	0.25	7.50	4.22
ACN-2	25 - 35	Dry, brown-greyish, hard, granular gravel sandy soil with rock pebbles	20.84	73.86	5.30	0.08	0.13	0.15	0.28	0.42	1.60	0.67	5.25	3.51
ACN-2	35 - 50	Dry, brown-greyish, hard, granular gravel sandy soil with rock pebbles	17.38	77.70	4.92	0.08	0.14	0.16	0.29	0.36	1.30	0.89	4.50	3.05
ACS-3	0 - 25	Dry, brown-greyish, loose, granular sandy gravel soil with plant roots and rock fragments approximately 5 cm in diameter	19.06	75.60	5.34	0.08	0.13	0.15	0.25	0.32	1.20	0.88	4.00	3.04
ACS-3	25 - 35	Dry, brown-greyish, hard, granular gravel sandy soil with rock pebbles	16.44	79.56	4.00	0.09	0.19	0.21	0.30	0.35	0.90	1.40	3.89	2.18
ACS-3	35 - 50	Dry, brown-greyish, hard, granular gravel sandy soil with rock pebbles	16.69	79.16	4.15	0.15	0.23	0.25	0.32	0.37	0.90	1.13	2.47	1.98
ACS-4	0 - 25	Dry, brown-greyish, loose, granular sandy gravel soil with plant roots and rock fragments approximately ~5 cm in diameter	19.04	79.13	1.83	0.10	0.20	0.23	0.32	0.40	1.50	1.32	4.00	2.74
ACS-4	25 - 35	Dry, brown-greyish, hard, granular gravel sandy soil with rock pebbles	18.49	79.55	1.96	0.09	0.16	0.20	0.32	0.40	1.50	1.11	4.44	3.06
ACS-4	35 - 50	Dry, brown-greyish, hard, granular gravel sandy soil with rock pebbles	21.41	77.19	1.40	0.13	0.23	0.25	0.34	0.60	1.80	0.80	4.62	2.80

Table 4. Soil types at different depths; parameters of Grain Distribution Curves for Rehoboth North (RN), Rehoboth South (RS) and Acacia (ACN, ACS) shown in Figs 17, 18 and 19; D_{10} = Effective size (10% finer); D_{25} = 25% finer; D30 = 30% finer; D_{50} = Median grain size; D_{60} = 60% finer; D_{75} = 75% finer; $C_u = D_{60}/D_{10}$; $C_c = (D_{30})^2/(D_{60}D_{10})$; $S_0 = \sqrt{D_{75}/D_{25}}$

Sample Name	Weight of container M_c (g)	Weight of container + wet soil M_{CMS} (g)	Weight of container + dry soil M_{CDS} (g)	Mass of soil solids M_s (g)	Mass of pore water M_w (g)	Water Content w (%)
RS1 0-25	6.7	292.3	290.9	284.2	1.4	0.5
RS1 25-35	6.7	317.7	314.6	307.9	3.1	1.0
RS1 35-50	6.5	313.5	310.0	303.5	3.5	1.2
RS2 0-25	6.7	289.3	286.0	279.3	3.3	1.2
RS2 25-35	6.6	268.4	267.0	260.4	1.4	0.5
RS2 35-50	6.7	259.9	256.9	250.2	3.0	1.2
RS3 0-25	6.6	283.9	282.7	276.1	1.2	0.4
RS3 25-35	6.8	217.3	215.2	208.4	2.1	1.0
RS3 35-50	6.6	241.0	238.4	231.8	2.6	1.1
RS4 0-25	6.8	294.0	292.6	285.8	1.4	0.5
RS4 25-35	6.8	287.4	284.5	277.7	2.9	1.0
RS4 35-50	6.6	237.4	233.8	227.2	3.6	1.6
RN1 0-25	6.8	223.1	222.6	215.8	0.5	0.2
RN1 25-35	6.7	239.7	239.2	232.5	0.5	0.2
RN1 35-50	6.8	221.6	221.2	214.4	0.4	0.2
RN2 0-25	6.7	191.1	190.6	183.9	0.5	0.3
RN2 25-35	6.7	272.6	272.0	265.3	0.6	0.2
RN2 35-50	6.9	241.0	240.5	233.6	0.5	0.2
RN3 0-25	6.7	304.3	303.8	297.1	0.5	0.2
RN3 25-35	6.6	300.8	300.4	293.8	0.4	0.1
RN3 35-50	7.0	207.2	206.8	199.8	0.4	0.2
RN4 0-25	6.7	260.1	259.7	253.0	0.4	0.2
RN4 25-35	6.7	220.2	219.8	213.1	0.4	0.2
RN4 35-50	6.8	205.2	205.0	198.2	0.2	0.1
ACN1 0-25	6.7	277.7	276.4	269.7	1.3	0.5
ACN1 25-35	6.6	276.2	274.4	267.8	1.8	0.7
ACN1 35-50	6.8	219.1	218.0	211.2	1.1	0.5
ACN2 0-25	6.8	228.2	227.1	220.3	1.1	0.5
ACN2 25-35	6.8	227.4	190.3	183.5	37.1	20.2
ACN2 35-50	7.0	251.4	249.9	242.9	1.5	0.6
ACS3 0-25	7.0	227.9	227.4	220.4	0.5	0.2
ACS3 25-35	7.1	246.4	245.8	238.7	0.6	0.3
ACS3 35-50	7.1	237.1	236.4	229.3	0.7	0.3
ACS4 0-25	6.9	269.0	268.1	261.2	0.9	0.3
ACS4 25-35	6.8	259.1	258.5	251.7	0.6	0.2
ACS4 35-50	6.9	355.0	353.2	346.3	1.8	0.5

Table 5. Water content of samples from Rehoboth North (RN), Rehoboth South (RS) and Acacia (ACN, ACS)

Depth (cm)	RN-1 (N)	RN-2 (N)	RN-3 (N)	RN-4 (N)
5	300	400	300	390
10	380	380	340	440
25	420	475	375	490
35	420	500	520	550
45	580	460	505	500

Table 6. Manometer readings for borings at Rehoboth North

Depth (cm)	RS-1 (N)	RS-2 (N)	RS-3 (N)	RS-4 (N)
5	-	490	510	440
10	425	495	500	510
20	420	560	560	570
30	460	530	600	540
40	525	540	480	700

Table 7. Manometer readings for borings at Rehoboth South

Depth (cm)	ACN-1 (N)	ACN-2 (N)	ACS-3 (N)	ACS-4 (N)
5	440	400	410	230
10	470	460	430	390
20	420	520	430	450
30	470	500	480	470
40	530	540	470	500
50	-	680	-	-

Table 8. Manometer readings for borings at Acacia (Windhoek)

N (Newton) equals force exacted upon cone pushed into the soil

Depth (cm)	RN-1 (MPa)	RN-2 (MPa)	RN-3 (MPa)	RN-4 (MPa)
5	1.5	2	1.5	1.95
10	1.9	1.9	1.7	2.2
25	2.1	2.375	1.875	2.45
35	2.1	2.5	2.6	2.75
45	2.9	2.3	2.525	2.5

Table 9. Cone resistances at varying depths for borings at Rehoboth North

Depth (cm)	RS-1 (MPa)	RS-2 (MPa)	RS-3 (MPa)	RS-4 (MPa)
5	-	2.45	2.55	2.2
10	2.125	2.475	2.5	2.55
20	2.1	2.8	2.8	2.85
30	2.3	2.65	3	2.7
40	2.625	2.7	2.4	3.5

Table 10. Cone resistances at varying depths for borings at Rehoboth South

Depth (cm)	ACN-1 (MPa)	ACN-2 (MPa)	ACS-3 (MPa)	ACS-4 (MPa)
5	2.2	2	2.05	1.15
10	2.35	2.3	2.15	1.95
20	2.1	2.6	2.15	2.25
30	2.35	2.5	2.4	2.35
40	2.65	2.7	2.35	2.5
50	-	3.4	-	-

Table 11. Cone resistances at varying depths for borings at Acacia (Windhoek)

MPa (Megapascal) =
N/cm^2 (cone base area) * 0.01
equals soil resistance to penetration

Category	Cone Resistance (qc) Range (MPa)	Soil Description
I	qc > 8.0	Very stiff to hard clays, dense sands, and gravels
II	3.0 - 8.0	Stiff clays, medium-dense sands, and gravels
III	1.5 - 3.0	Firm clays, loose to medium-dense sands and gravels
IV	0.5 - 1.5	Soft clays, silty clays, loose sands
V	0.2 - 0.5	Very soft clays, organic soils
VI	< 0.2	Water or fluidized soils

Table 12: Six categories of classifying soil using the Begemann Penetration Resistance (BPR) system (Libric *et al.*, 2017)

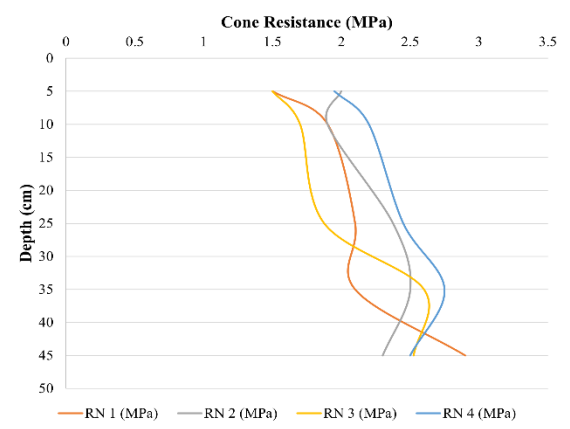

Figure 8. Strength analysis curves for borings at Rehoboth North up to a depth of 45 cm

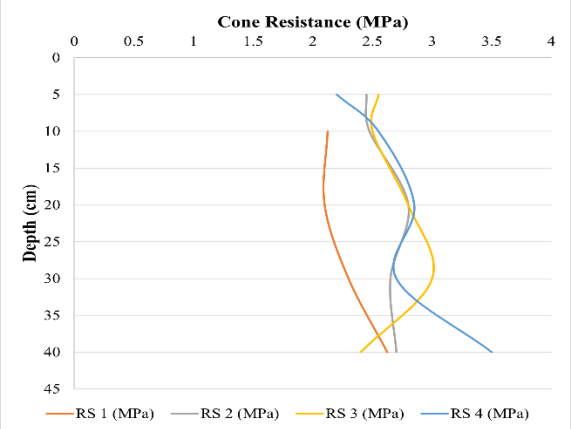

Figure 9. Strength analysis curves for borings at Rehoboth South up to a depth of 40 cm

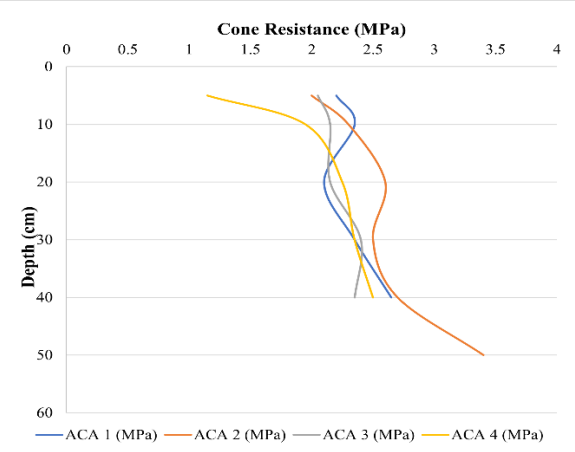

Figure 10. Strength analysis curves for borings at Acacia to depths of 40 cm and 50 cm, respectively

Remarks:

Compaction/cone resistance (qc) of the tested soils increases with depth (as is common), except in borings RN-2, RN-3, RN-4, RS-3, and ACS-3 where it decreases indicating less compacted soil at depth. According to the BPR system (Table 12), the overall cone resistance (qc) of soils at the three sites falls into category III (1.5 – 3 MPa) excluding ACN-2 (with qc > 3 MPa down depth falling into Category II). These resistances are typical for firm clays, and loose to medium-dense sands and gravels, which implies conditional suitability for (light) construction.

X-ray Fluorescence (XRF) and X-ray Diffraction (XRD) analysis of soil samples

Table 13 shows the major and trace element composition of the soil samples from the three investigated sites as determined by portable XRF. Apart from quartz and albite, which are present at all three investigated sites, X-ray diffraction peaks of composite soil samples from borings RN-1 (Fig. 11), RN-3 (Fig. 12), RS-1 (Fig. 13), ACN-2 (Fig. 14) and ACS-4 (Fig. 15) in addition show ferroan magnesio-hornblende at Rehoboth North and microcline at Rehoboth South. Associated clay minerals are koninckite (Rehoboth South), polylithionite and dickite (Acacia; Table 14). These findings suggest that the clay fraction of the soil is dominated by non-expansive clays (koninckite and dickite), with polylithionite the only expansive clay mineral observed. As non-expansive clays tend to be more stable when wet, with less potential for shrinkage or cracking during dry periods, this increases overall soil strength as well as shear strength and reduces the soil's propensity for erosion.

SAMPLE NO	Si %	Al %	Fe %	K %	Mg %	Ca %	Ti %	P %	S %	Ba %	Mn ppm	Cr ppm	Zr ppm	Sr ppm	Rb ppm	Zn ppm	Cu ppm	Ni ppm
ACN-1	22.04	29.16	4.88	4.76	3.74	0.86	0.59	0.15	0.02	0.04	687	153	238	86	110	81	31	53
ACN-2	23.15	29.96	5.17	4.59	3.68	0.74	0.6	0.13	0.03	0.04	704	174	235	97	113	84	28	49
ACS-3	26.1	24.75	3.36	3.53	2.78	0.49	0.54	0.11	0.02	0.02	678	172	196	60	69	39	26	40
ACS-4	26.04	24.6	4.22	3.91	3.19	0.68	0.56	0.11	0.02	0.03	747	204	272	94	95	62	29	32
RN-1	25.02	19.68	3.69	3.34	2.22	1.12	0.54	0.12	0.02	0.05	611	108	124	82	85	31	44	50
RN-2	27.19	19.93	3.59	3.43	2.37	1.19	0.55	0.13	0.02	0.05	497	131	142	80	88	26	44	66
RN-3	26.48	19.71	3.66	3.39	1.91	1.22	0.61	0.12	0.02	0.05	550	138	207	79	83	27	44	51
RN-4	26.32	19.95	3.81	3.73	1.29	1.12	0.52	0.1	0.01	0.05	587	128	219	79	85	30	43	66
RS-1	32.19	14	1.89	2.33	1.17	0.52	0.35	0.1	0.03	0.02	324	150	199	62	45	13	15	23
RS-2	30.88	15.85	2.14	2.58	1.69	0.57	0.45	0.13	0.03	0.02	332	144	156	64	53	20	17	32
RS-3	30.78	15.26	2.01	2.41	1.88	0.57	0.42	0.16	0.03	0.02	337	139	227	61	52	25	44	35
RS-4	26.04	11.07	2.11	2.3	1.01	0.56	0.41	0.13	0.02	0.02	326	127	131	57	49	22	< LOD	< LOD

Remarks: 1% = 10 000, 1ppm = 0.0001%

Table 13. X-ray Fluorescence results showing geochemical composition of the soils at Rehoboth (North and South) and Acacia (Windhoek)

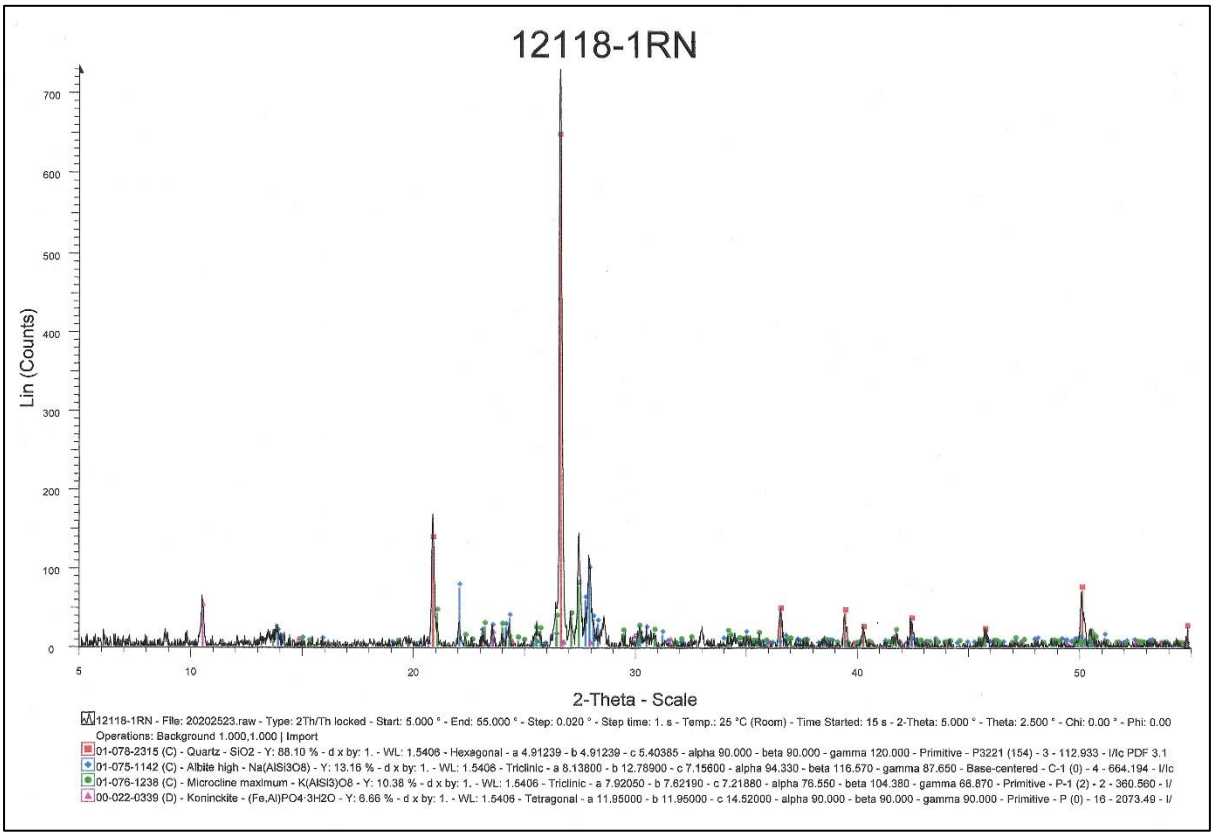

Figure 11: XRD graph for combined samples from boring RN-1 (Rehoboth North) indicating the presence of quartz, albite, microcline and koninckite

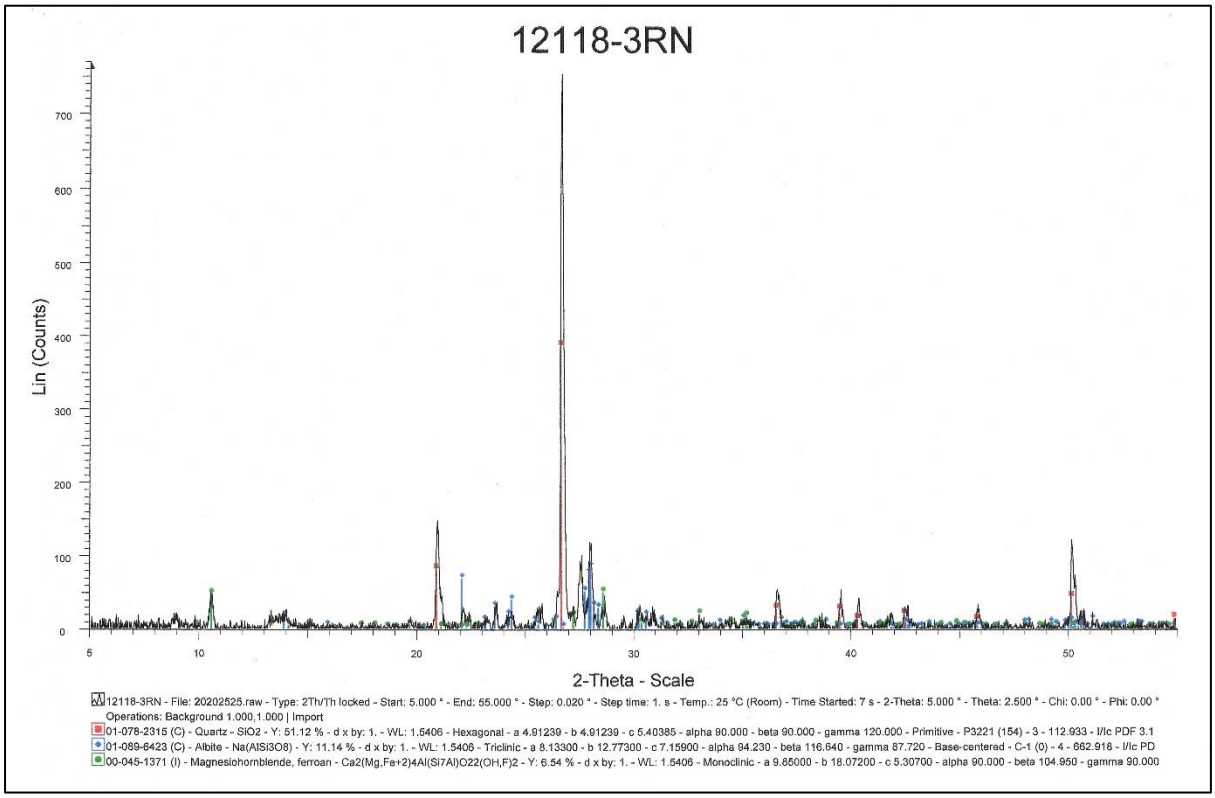

Figure 12: XRD graph for combined samples from boring RN-3 (Rehoboth North) indicating the presence of quartz, albite and magnesio-hornblende

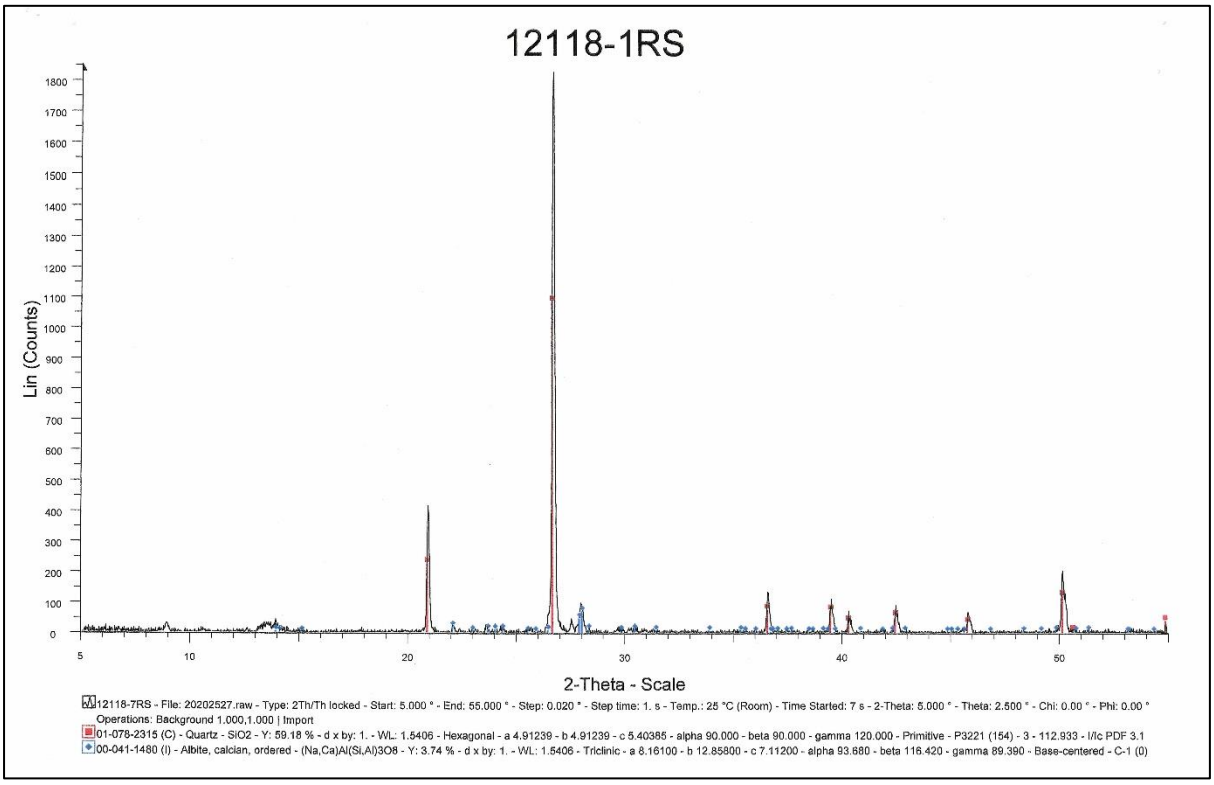

Figure 13: XRD graph for combined samples from boring RS-1 (Rehoboth South) indicating the presence of quartz and calcian albite

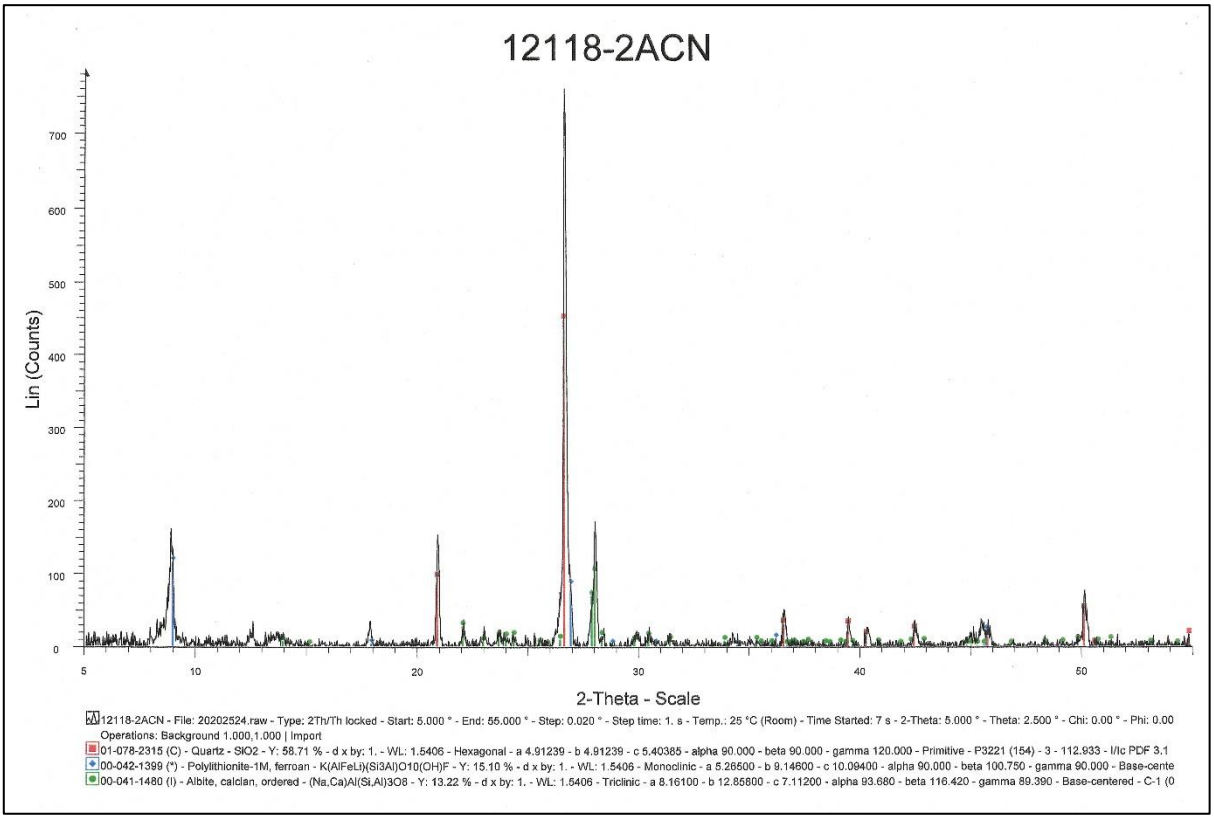

Figure 14. XRD graph for combined samples from boring ACN-2 (Acacia) indicating the presence of quartz, polylithionite and calcian albite

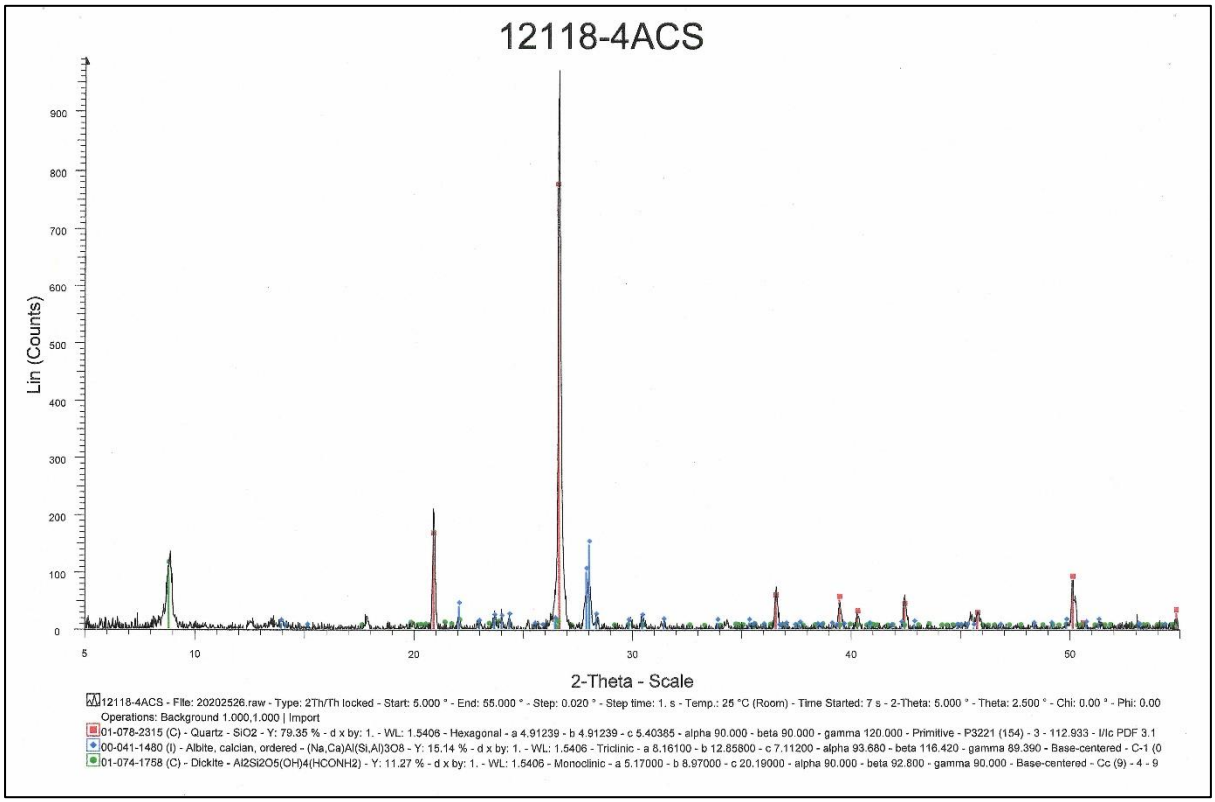

Figure 15: XRD graph for combined samples from boring ACS-4 (Acacia) indicating the presence of quartz, calcian albite and dickite

Sample No	Location	Minerals
12118-3RN	Rehoboth North	Quartz (SiO_2); albite ($Na[AlSi_3O_8]$); ferroan magnesio-hornblende ($Ca_2[Mg,Fe^{*2}]_4Al[Si_7Al]O_{22}[OH,F]_2$
12118-1RN	Rehoboth North	Quartz (SiO_2); albite ($Na[AlSi_3O_8]$); microcline ($K[AlSi_3O_8]$); koninckite ($[Fe,Al]PO_4*3H_2O$)
12118-1RS	Rehoboth South	Quartz (SiO_2); calcian albite ($[Na,Ca]Al[Si,Al]_3O_8$)
12118-2ACN	Acacia	Quartz (SiO_2); polylithionite $K(Al,Fe,Li)(Si_3Al)O_{10}(OH),F$; calcian albite ($[Na,Ca]Al[Si,Al]_3O_8$)
12118-4ACS	Acacia	Quartz (SiO_2); albite ($Na[AlSi_3O_8]$); dickite ($Al_2Si_2O_5[OH]_4[HCONH_2]$

Table 14. Mineralogical composition of composite samples from the three investigates sites

Sieve analysis and soil gradation

Results of average sieve analyses for soils from the three investigated locations are presented in Table 15. It is of note that the soil at the Acacia site contains considerably less sandy material and more gravel than the soil at the two locations in Rehoboth, with Rehoboth North soil containing the smallest proportion of gravel; the percentage of fines is more or less even at all sites.

Acacia:	Sand 77%	Gravel 19%	Fines (clay and silt) 4%
Rehoboth North:	Sand 94.1%	Gravel 2.0%	Fines (clay and silt) 3.9%
Rehoboth South:	Sand 94%	Gravel 4.0%	Fines (clay and silt) 2%

Table 15. Sieve analysis for the three sites

In general, well-graded soils with a balanced mix of different particle sizes are more suitable for construction than poorly graded soils (composed, for instance, predominantly of fines), as they are more stable and capable of supporting greater loads (Das, 2022). They are also more permeable, which allows water to drain away from the foundations. In the classification of soils, logarithmic intervals (decades) and grain size curvature (S_0) are used to describe grain size distribution (Tables 4 and 16).

S_0 provides insight into the distribution of particle sizes between the quartiles D_{75} and D_{25}. While S_0 values close to 1 indicate a relatively uniform distribution of particle sizes between D_{75} and D_{25}, values significantly higher or lower than 1 suggest a more curved distribution, where particles are concentrated towards either the coarser (D_{75}) or finer (D_{25}) end of the range. Other important parameters to describe soil gradation are the Uniformity Coefficient (C_u) and the Coefficient of Curvature (C_c; Table 4). C_u measures the range of particle sizes present in the soil on the grain size distribution curve, while C_c compares the proportion of fine and coarse particles relative to medium-sized particles. Figure 16 visualises the main gradation types.

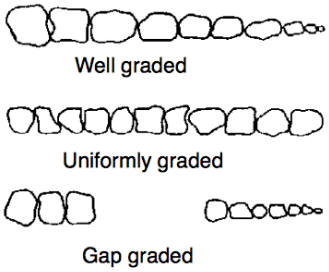

Figure 16. Soil gradation classification

Decade	Description	Particle Size (mm)	Logarithmic Size Interval	Example Particles
-1 - 0	Very fine silt and clay	0.01 – 0.1	10^{-2} - 10^{-1}	Fines (very fine silt and clay)
0 - 1	Very fine sand and silt	0.1 - 1	10^{-1} - 10^{0}	Clay, silt, very fine sand
1 - 2	Fine and medium sand	1 - 10	10^{0} - 10^{1}	Fine sand, medium sand
2 - 3	Coarse and very coarse sand	10 - 100	10^{1} - 10^{2}	Coarse sand, very coarse sand, small gravel

Table 16. Grain size classification according to Unified Soil Classification System (USCS)

A number of soil classification systems (Table 17) are used because they offer different levels of detail and specification. ASTM and USCS (Unified Soil Classification System) provide a broad classification based on C_u and C_c, while standards developed by the American Association of State Highway and Transportation Officials (AASHTO) or the American Concrete Institute (ACI) delve deeper into specific applications or materials (e. g. permeability for road construction or concrete mix design).

Representative grain size distribution curves for the three sites are shown in figures 17, 18 and 19; detailed sieve analysis results are given in Appendix A and Shuuya (2016). Comparison between figures 17, 18 and to 19 (based on decades) and Table 17 (based on C_c and C_u), with reference to suitability of the investigated sites for construction, shows the soil at Rehoboth North as poorly graded over three decades (Fig. 18), but well-graded according to USCS standards (C_c = 1.25 and C_u = 3.04; Table 17). The Rehoboth South site classifies as poorly graded both over three decades (Fig. 17) and by C_c (1.25) and C_u (2.93; after ASTM), while the soil at Acacia is poorly graded over three decades (Fig. 19), and gap-graded with C_c = 0.95 and C_u = 5.04 according to ACI standards (Table 17). Based on these classifications, the investigated sites are considered suitable for the planned light construction of single storey housing development, with Rehoboth North possessing the best gradation of the three.

Cu Range	Cc Range	Grading	Suitability	Reference
< 3	Any	Poorly graded	Light construction only	ASTM D2487-17
3 - 6	1 - 3	Well-graded	Most construction, good load-bearing capacity	USCS
3 -6	< 1 or > 3	Gap-graded	May be suitable for specific applications, requires further testing	ACI 318-19
> 6	Any	Poorly graded	Not recommended for most construction	AASHTO T88-22

Table 17. Suitability of soils for construction based on uniformity coefficient (*Cu*) and curvature coefficient (*Cc*)

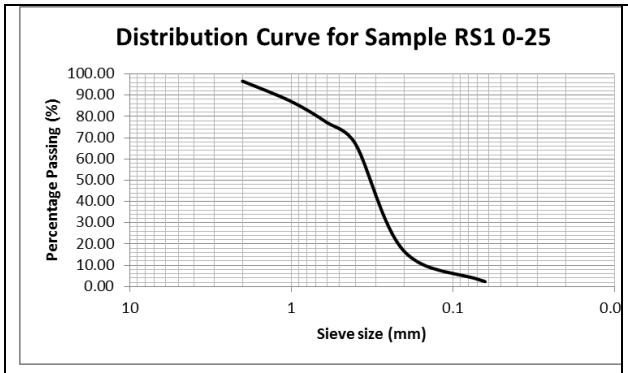

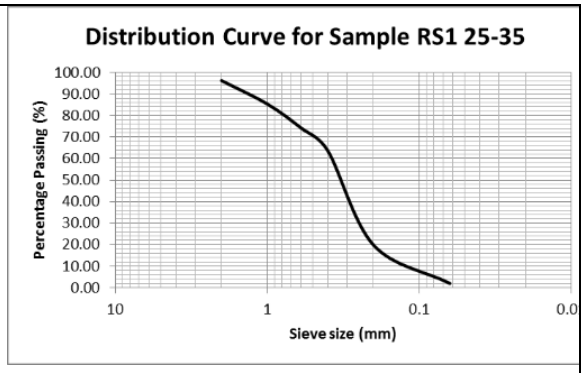

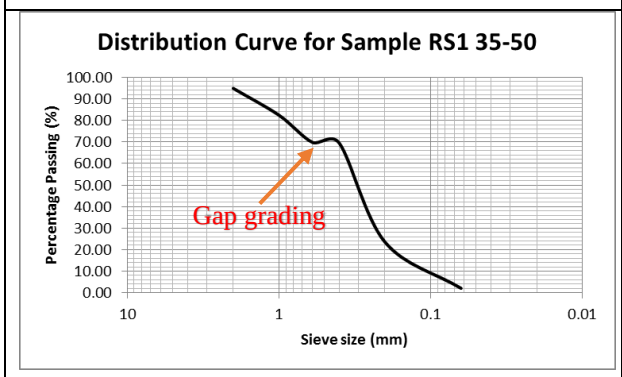

Summary of grain size analysis:
The soil from this boring lacks a good representation of continuous particle sizes from fine to coarse, causing gaps in the distribution curve. It is poorly graded over three decades for all three samples. The sample from 35 to 50 cm depth shows gap grading (missing particle sizes) for the grain sizes 0.4 to 0.6 mm. Therefore, this soil is classed as poorly / uniformly graded, silty, very fine- to medium-grained sand, with low carrying capacity for foundations.

Figure 17. Representative grain size distribution curves for Rehoboth South taken from boring RS-1 at varying depths from surface to 50 cm

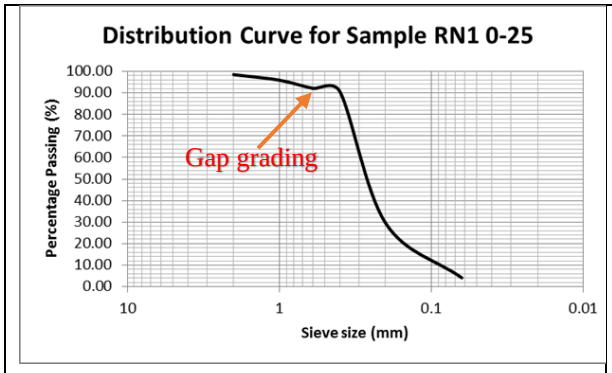

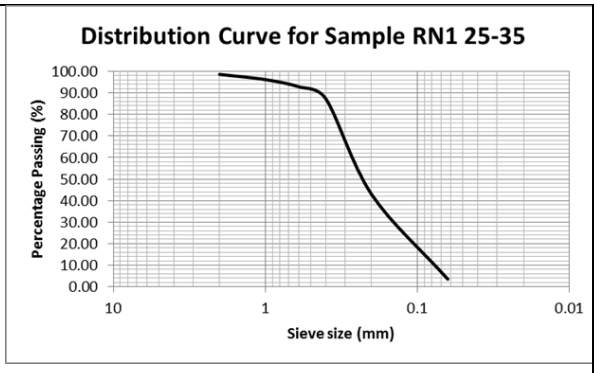

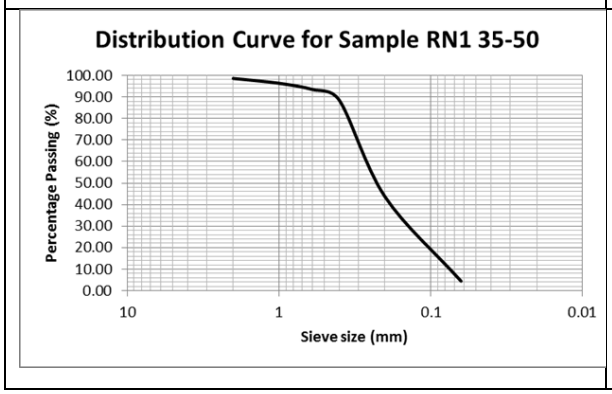

Summary of grain size analysis:
The soil from this boring lacks a good representation of continuous particle sizes from fine to coarse. It is poorly graded over three decades at all depths. The sample from 0 to 25 cm depth shows gap-grading for the grain sizes of 0.6 mm to 0.7 mm. This soil is classified as poorly / uniformly graded, silty, very fine- to medium-grained sand, with low carrying capacity for foundations.

Figure 18. Representative grain size distribution curves for Rehoboth North taken from boring RN1 at varying depths from surface to 50 cm

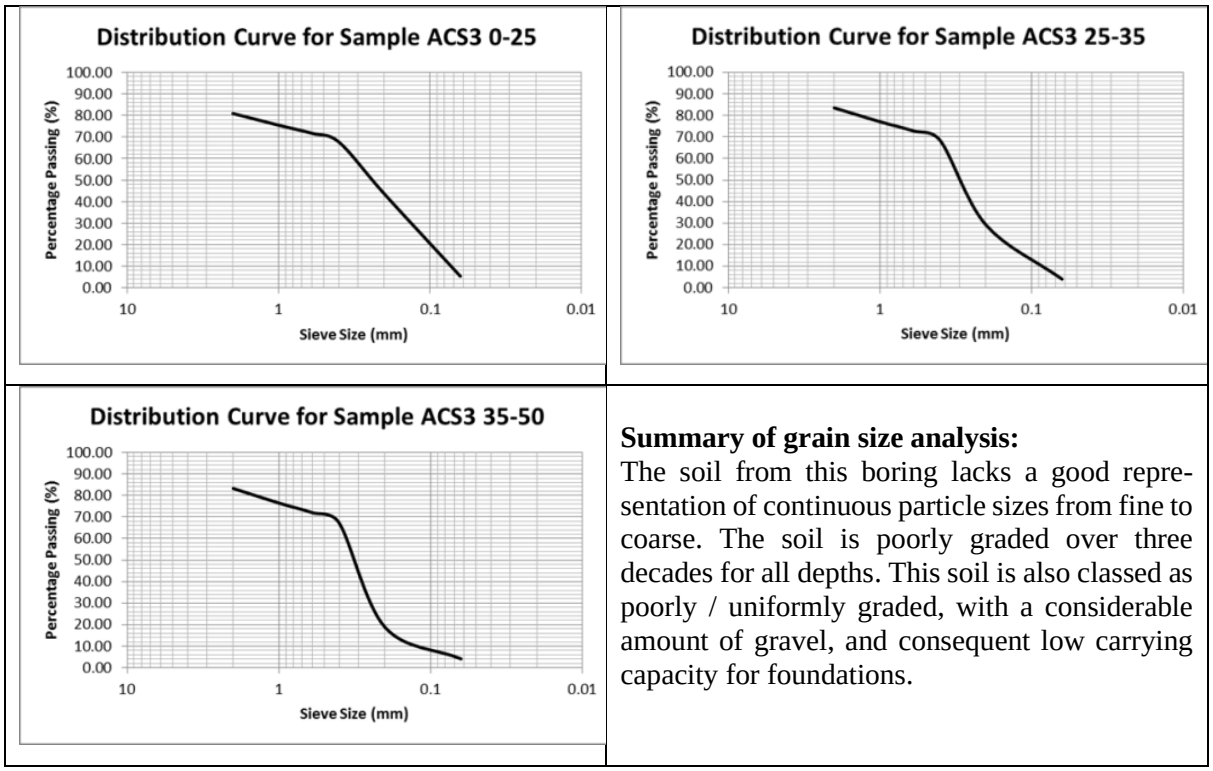

Figure 19. Representative grain size distribution curves for Acacia (Windhoek) taken from boring ACS-3 at varying depths from surface to 50 cm

Discussion

The study of soil properties, the most critical of which are summarised and discussed below, is essential in foundation design in order to avoid failure or damage to structures with resulting high costs and/or loss.

Water Content

Soil samples for this study were collected during the dry season at three sites vegetated by tree-and-shrub savannah, which is the typical vegetation of the central Namibian Khomas Highlands. Water content, expressed as a percentage of the dry weight of the soil, is an important factor to consider when choosing foundation types and depths. In general, soils with high water content are more likely to swell and shrink, which can cause damage to foundations; consequently, foundations in soils with high water content should be deep enough to reach stable ground. Other factors influencing foundation depth are soil type, water table fluctuations, expected loads, as well as local building codes and regulations. Foundations should be placed below the anticipated maximum water table level to minimise buoyancy and potential uplift. Table 5 shows the water content of soil samples taken at different depths in Acacia and Rehoboth. At Rehoboth South, the water content of the soil increases with depth, which is normal as water tends to drain downwards, leaving the topsoil drier than the bottom. The presence of vegetation can influence water content by siphoning off water from the soil or by shading the surface and thus reducing evaporation. At Rehoboth North, the water content in the soil is very constant at 0.2%, with a variation of 0.1%, indicating a uniformly dry soil due to a high proportion of sand; in such soils water can drain quickly through the pore space between grains, preventing significant moisture retention. In contrast, at Acacia a high variation in water content was observed, owing to the variable composition of the soil. At this site, it contains significant proportions of gravel, sand, silt and clay (Table 15), which have different water-retaining capacities; because of its greater particle size and porosity, sand has a lower capacity to hold water than clay and will consequently be drier. Generally, the water content at the three sites varies between 0.1% and 1.6%, except in boring ACN-2. Here, at a depth of 25-35 cm, the soil was found to contain

20.2% water due to an accumulation of clay minerals, with a high capacity to retain water, due to their low porosity and high surface area.

Penetration

Cone penetration tests (CPT) were conducted on twelve soil borings. The strength analysis curves for Rehoboth North, Rehoboth South and Acacia show the relationship of cone resistance to depth (Figs 8, 9 and 10). At Rehoboth North, the cone resistance of the soil increases to a depth of 45 cm, which is typical of a normally compacted soil. In Rehoboth South, the situation is similar, with the difference that in boring RS-3 a layer of weak soil with lower cone resistance was encountered at a depth of approximately 30 cm. Due to their larger grain size and higher porosity sand and gravel compact more easily than clay or silt, requiring less force to penetrate. CPT results show (in accordance with Table 17) the soil in Rehoboth South to be poorly graded, with most soil samples having $C_u < 3$ and $C_c > 1$, except for four samples from borings RS-2 (0-25, 25-35 and 35-50 cm) and RS-3 (35-50 cm); in these cases, $C_u > 3$ and C_c between 1 and 3 indicate a well-graded soil, suitable for most construction projects. At the Acacia sites layer(s) of weak soil, composed of mixed clays, sands and gravels, occur at depths > 40 cm in all four borings, including the waterlogged layer in ACN-2.

In general, soils with high cone resistance are capable of carrying considerable loads, while soils with low to medium cone resistance, as encountered at the three investigated sites, require treatment - such as compaction or stabilisation - before they can bear structures with safety. However, other parameters, such as moisture content, grain size, chemical and mineralogical composition, all of which are interlinked, need to be taken into consideration.

Geochemical composition

Elemental composition of the soil samples was determined with a portable X-ray Fluorescence Analyser. Results show that the soils at the three investigated sites are composed primarily of silica, aluminium, iron and potassium (Table 13), which are the most common constituents of all rocks and soils. Concomitant with the decrease in silica is an increase of most other major and trace elements (Table 18); titanium, phosphorus, sulphur and barium show very little variation in all the samples.

	Si %	Al %	Fe %	K %	Mg %	Ca %	Mn ppm
Rehoboth South	29.97	14.05	2.04	2.41	1.44	0.56	330
Rehoboth North	26.25	19.82	3.69	3.47	1.95	1.16	561
Acacia	24.33	27.12	4.41	4.20	3.35	0.69	704
	Cr ppm	Zr ppm	Sr ppm	Rb ppm	Zn ppm	Cu ppm	Ni ppm
Rehoboth South	140	178	61	50	20	21	25
Rehoboth North	126	173	80	85	28.5	44	58
Acacia	176	235	84	97	66.5	28.5	43.5

Table 18. Summary of XRF results showing average element concentrations from the three sites

Mineral composition

The mineral composition of the investigated soils was determined by X-Ray diffraction. It was found to be similar at all three sites, consisting mainly of quartz and albite, with subordinate hornblende, microcline and various clay minerals (Table 14), which suggests relatively slow to moderate decomposition and erosion of the parent rocks. Expansive clays, which can pose a serious threat to the stability of foundations by recurrent shrinking and swelling during the dry and wet seasons, were observed only at the Acacia site (polylithionite), while other minerals harmful to the stability of foundations, such as sulphates and pyrite, are absent. As the latter react with water to form corrosive acids, they can damage concrete and thus cause foundation failure.

Recommendations and Limitations

Table 19 summarises the test results of the three construction sites in Rehoboth and Windhoek. Based on particle size distribution, water content, compaction, geochemical and

mineralogical composition, it is concluded that the soils at the three investigated sites are conditionally suitable for light construction, i. e. after appropriate treatment to improve bearing capacity and/or with the design of adequate foundations to mitigate inherent deficiencies. Two types of soil were observed, i. e. (reddish) sandy soil (Rehoboth) and gravelly sandy soil with pebbles (Acacia). All soils are poorly graded over three decades but well-graded over one decade, which makes them unsuitable as foundation material for double-storey structures. It is recommended that the foundation ground in Rehoboth (both North and South) be replaced with a compactable soil allowing easy water drainage; alternatively, foundations could be placed in solid rock (after the removal of the soil cover), in which case the integrity of the bedrock needs to be examined. Grain size variation in the gravelly soil at Acacia ensures adequate drainage even when closely packed.

Site	Test results			Suitability for planned construction
	Grain size composition/Grading (Sieve analysis)	Water content	Compaction (Cone Penetration Test)	
Acacia	Poorly graded/Gap-graded	Low	Moderate	Suitable for light construction
Rehoboth North	Poorly graded to well graded	Low	Moderate	Suitable for light construction
Rehoboth South	Poorly graded	Low	Moderate	Conditionally suitable for light construction

Table 19: Overall soil testing results from the three investigated sites

Foundations

The type of foundation to be laid depends on subsoil conditions and the structure to be erected. The parameters for the design of an appropriate foundation system encompass foundation type, depth, bearing capacity of the soil and the type of structure to be erected (Gopi, 2009). In accordance with the test results obtained, two types of foundations are recommended for the three sites, i. e. raft and strip foundations, both of which are shallow foundation types. French (1999) defined raft foundations as continuous concrete slabs covering the entire footprint of the building, thus distributing the weight evenly. This type of foundation is suitable for soft or loose soils with low bearing capacity (as encountered at Rehoboth South and North), for buildings with large or concentrated loads and for structures in areas with high seismic activity. Strip foundations are defined as continuous concrete strips laid under the walls of a building, transferring the load directly to the soil (Sivakugan, 2021). Strip foundations are thus preferred for soils with good to moderate grading (e. g. gravelly soil at Acacia), for smaller buildings with evenly distributed loads and in areas with low seismic activity.

According to the field investigations, laboratory tests and engineering analyses carried out for this study, the following recommendations are made:

Acacia:

- **Foundation type**: Strip foundations, potentially with pre-treatment such as physically altering the soil structure to improve its properties
- **Foundation depth**: Deeper than 40 cm to avoid weak layers
- **Limitations:** Variable water content, which can lead to differential settlement, necessitating drainage solutions and foundation monitoring

Rehoboth (North and South):

- **Foundation Type**:

a) without soil replacement: raft foundations

b) with soil replacement: after replacement with a compactable soil of higher bearing capacity, e. g. soil with dominant sand (~60%) and significant silt (~20%), strip foundations may be considered, subject to a thorough geotechnical investigation and engineering analysis to confirm their stability in the new soil conditions.

- **Depth**: Deeper than 30 cm to avoid the weak layer
- **Limitations**: Poorly graded soil can lead to settlement in the long term. Monitoring of foundation performance and soil improvement techniques (e. g. mechanical and chemical stabilisation, geosynthetics and soil replacement) are advisable.

References

Arya, A. S. and Agarwal, A. 2007. Condition Assessment of Buildings for Repair and Upgrading. Gol-UNDP *Disaster, Risk Management Programme*. National Disaster Management Division, Government of India, New Delhi, 16 pp. https://nidm.gov.in /PDF/ safety/earthquake/link13.pdf

ASTM. 2007. D422 - 63, "Standard Test Method for Particle-Size Analysis of Soils." https://www.astm.org/

ASTM. 2016. D3441 - 16, "Standard Test Method for Mechanical Cone Penetration Tests of Soils." https:// www.astm.org/

ASTM. 2017. D2487 - 17, "Standard Practice for Classification of Soils for Engineering Purposes (Unified Soil Classification System)." https://www.astm. org/

ASTM. 2019. D2216 - 19, "Standard Test Method for Laboratory Determination of Water (Moisture) Content of Soil, Rock, and Soil-Aggregate Mixtures." https:// www. astm.org/

Das, B. M. 1990. Principles of Foundation Engineering (5th Ed.). PWS-KENT Series in Civil Engineering, Univ. Michigan, USA, 731 pp.

Das, B. M. 2022. Principles of geotechnical engineering (10th ed.). Cengage Learning, Boston, USA. https://www.cengage.com/c/ principles-of-geotechnical-engineering-10e-das/9780357420478PF/

Fame, P. 2013. "Why Soil Investigation Is Necessary for Your Building Project". NAIRALAND. http://www. nairaland.com/ 1364248/why-soil-investigation-necessary-building

French, S. 1999. Settlement of Foundations on a Soil Mass. *In*: *Design of Shallow Foundations*, chapter 7, 181-206. ASCE (American Society of Civil Engineers) Press, USA. https://doi.org/10.1061/9780784403716

Gopi, S. 2009. Foundation. *In*: *Basic Civil Engineering*, chapter 13, 82-90. Pearson Education, India.

Hälbich, I., Hoffmann, K.-H. and Schalk, K. E. L. 2006. Geological Map of Area 2217 C Windhoek. Geological Survey of Namibia, Windhoek.

Kunkolienkar, A. 2016. "Soil Investigation-What is it and why is it important?". TRIDENTIA. https://www.tridentia.in/buying-a-home/soil-investigation-what-is-it-and-why-is-it-important/

Libric, L., Jurić-Kaćunić, D. and Kovacevic, MS. 2017. Application of cone penetration test (CPT) results for soil classification. *Graðevinar*, **69(1)**, 11-20. https://doi.org/ 10.14256/ JCE.1574.2016

Munfakh, G., Arman, A., Samtani, N. and Castelli, R. 1997. Training Course in Geotechnical and Foundation Engineering, NHI Course No. 13231 - Module 1. Subsurface Investigations. Participants Manual. Federal Highway Administration, U.S. Department of Transportation, 318 pp. https://highways. dot.gov/research/publications/infrastructure /FHWA-HI-97-021

Namibia Statistics Agency (NSA). 2024. *2023 Population & Housing Census – Preliminary Report*. https://nsa.org.na/

Schalk, K. E. L., De Waal, S. A., Munch, H. G. and Schulze-Hulbe, A. 2006. Geological Map of Area 2317 A Rehoboth. Geological Survey of Namibia, Windhoek.

Shuuya, S. P. 2016. *Characterisation of soils to determine their suitability as foundation material for construction at Rehoboth and Acacia (Windhoek), Namibia*. B. Sc. (hons) Thesis, University of Namibia, Windhoek.

Sivakugan, N. 2021. Soil Mechanics and Foundation Engineering: Fundamentals and Applications. McGraw Hill, New York. Retrieved from https://www.access engineeringlibrary.com/content/book/9781260468489

Appendix A: Sieve analysis results for grain size distribution curves shown in figures 17, 18 and 19

	Sieve - Aperture Ø (mm)	Mass of empty sieve/pan (g)	Mass of sieve/pan + soil retained (g)	Soil retained (g)	Percentage retained (%)	Percentage passing (%)
Sample RS-1: 0-25 cm	2	368.70	378.30	9.60	3.34	96.66
	1	310.30	337.80	27.50	9.58	87.08
	0.6	289.50	318.00	28.50	9.92	77.16
	0.4	299.70	328.50	28.80	10.03	67.13
	0.2	254.30	399.30	145.00	50.49	16.64
	0.0063	238.60	279.70	41.10	14.31	2.33
Pan		893.80	900.50	6.70	2.33	0.00
		Total weight of sample (g):		287.20	100.00	

	Sieve - Aperture Ø (mm)	Mass of empty sieve/pan (g)	Mass of sieve/pan + soil retained (g)	Soil retained (g)	Percentage retained (%)	Percentage passing (%)
Sample RN-1: 0-25 cm	2	368.70	371.80	3.10	1.46	98.54
	1	310.30	315.80	5.50	2.58	95.96
	0.6	289.50	297.60	8.10	3.80	92.16
	0.4	299.70	302.80	3.10	1.46	90.70
	0.2	254.30	384.50	130.20	61.16	29.54
	0.0063	238.60	292.70	54.10	25.41	4.13
Pan		893.80	902.60	8.80	4.13	0.00
		Total weight of sample (g):		212.90	100.00	

	Sieve - Aperture Ø (mm)	Mass of empty sieve/pan (g)	Mass of sieve/pan + soil retained (g)	Soil retained (g)	Percentage retained (%)	Percentage passing (%)
Sample RS-1: 25-35 cm	2	368.70	380.50	11.80	3.77	96.23
	1	310.30	344.30	34.00	10.88	85.35
	0.6	289.50	324.30	34.80	11.13	74.22
	0.4	299.70	332.80	33.10	10.59	63.63
	0.2	254.30	391.30	137.00	43.83	19.80
	0.0063	238.60	294.10	55.50	17.75	2.05
Pan		893.80	900.20	6.40	2.05	0.00
		Total weight of sample (g):		312.60	100.00	

	Sieve - Aperture Ø (mm)	Mass of empty sieve/pan (g)	Mass of sieve/pan + soil retained (g)	Soil retained (g)	Percentage retained (%)	Percentage passing (%)
Sample RN-1: 25-35 cm	2	368.70	371.90	3.20	1.34	98.66
	1	310.30	316.10	5.80	2.42	96.24
	0.6	289.50	297.60	8.10	3.38	92.86
	0.4	299.70	313.00	13.30	5.56	87.30
	0.2	254.30	360.60	106.30	44.40	42.90
	0.0063	238.60	332.90	94.30	39.39	3.51
Pan		893.80	902.20	8.40	3.51	0.00
		Total weight of sample (g):		239.40	100.00	

	Sieve - Aperture Ø (mm)	Mass of empty sieve/pan (g)	Mass of sieve/pan + soil retained (g)	Soil retained (g)	Percentage retained (%)	Percentage passing (%)
Sample RS-1: 35-50cm	2	368.70	382.60	13.90	5.05	94.95
	1	310.30	344.60	34.30	12.45	82.50
	0.6	289.50	324.40	34.90	12.67	69.84
	0.4	299.70	300.60	0.90	0.33	69.50
	0.2	254.30	381.00	126.70	45.99	23.51
	0.0063	238.60	297.70	59.10	21.45	2.06
Pan		893.80	899.50	5.70	2.07	-0.01
		Total weight of sample (g):		275.50	100.01	

	Sieve - Aperture Ø (mm)	Mass of empty sieve/pan (g)	Mass of sieve/pan + soil retained (g)	Soil retained (g)	Percentage retained (%)	Percentage passing (%)
Sample RN-1: 35-50cm	2	368.70	371.60	2.90	1.36	98.64
	1	310.30	315.10	4.80	2.25	96.39
	0.6	289.50	295.70	6.20	2.91	93.48
	0.4	299.70	310.30	10.60	4.97	88.51
	0.2	254.30	349.80	95.50	44.81	43.70
	0.0063	238.60	322.20	83.60	39.23	4.47
Pan		893.80	903.30	9.50	4.46	0.01
		Total weight of sample (g):		213.10	99.99	

	Sieve - Aperture Ø (mm)	Mass of empty sieve/pan (g)	Mass of sieve/pan + soil retained (g)	Soil retained (g)	Percentage retained (%)	Percentage passing (%)
Sample ACS-3: 0-25 cm	2	368.70	400.80	32.10	19.06	80.94
	1	310.30	319.40	9.10	5.40	75.53
	0.6	289.50	295.90	6.40	3.80	71.74
	0.4	299.70	306.40	6.70	3.98	67.76
	0.2	254.30	295.00	40.70	24.17	43.59
	0.0063	238.60	303.00	64.40	38.24	5.35
Pan		893.80	902.80	9.00	5.34	0.01
		Total weight of sample (g):		168.40	99.99	

	Sieve - Aperture Ø (mm)	Mass of empty sieve/pan (g)	Mass of sieve/pan + soil retained (g)	Soil retained (g)	Percentage retained (%)	Percentage passing (%)
Sample ACS-3: 25-35 cm	2	368.70	399.50	30.80	16.44	83.56
	1	310.30	322.30	12.00	6.41	77.15
	0.6	289.50	297.60	8.10	4.32	72.83
	0.4	299.70	308.10	8.40	4.48	68.35
	0.2	254.30	327.70	73.40	39.19	29.16
	0.0063	238.60	285.70	47.10	25.15	4.01
Pan		893.80	901.30	7.50	4.00	0.00
		Total weight of sample (g):		187.30	99.99	0.01

	Sieve - Aperture Ø (mm)	Mass of empty sieve/pan (g)	Mass of sieve/pan + soil retained (g)	Soil retained (g)	Percentage retained (%)	Percentage passing (%)
Sample ACS-3: 35-50 cm	2	368.70	400.90	32.20	16.69	83.31
	1	310.30	323.40	13.10	6.79	76.52
	0.6	289.50	298.20	8.70	4.51	72.01
	0.4	299.70	309.00	9.30	4.82	67.19
	0.2	254.30	347.60	93.30	48.37	18.82
	0.0063	238.60	266.90	28.30	14.67	4.15
Pan		893.80	901.80	8.00	4.15	0.00
		Total weight of sample (g):		192.90	100.00	

The Southern Namibian Mapping Programme (SNMP) 2013 to 2022 – a decade of research collaboration and detailed mapping

Anna Nguno[1] and Paul Macey[2,3]

1. Geological Survey of Namibia, 6 Aviation Road, Windhoek <Anna.Nguno@mme.gov.na>
2. Council for Geoscience, Western Cape Regional Office, 3 Oos Street, Bellville 7530, South Africa
3. Department of Geological Sciences, University of Cape Town, Rondebosch 7701, South Africa <macerock72@gmail.com>

Abstract :- Geological mapping and research has been carried out in Namibia since the early 1900s, resulting in a rather heterogenous information coverage. Also, in the 1990s and early 2000s stagnation of field mapping led to little new data being generated by the Geological Survey, although archival data were captured electronically and made available in digital and hardcopy format. In 2013, a co-operation/contract project between the Geological Survey of Namibia and the Council for Geoscience (South Africa) was initiated to remap the Meso- and Palaeoproterozoic rocks of the Warmbad area, //Karas Region (southern Namibia) - a programme which combined the acquisition of more detailed geological maps and geoscientific research with training and capacity building at both the Namibian and South African geological surveys. Its initial contract fulfilled, the project's activities expanded to other parts of the highly prospective //Karas Region, and over the following decade produced ninety-five 1:50 000 scale geological maps, with accompanying reports and associated geochemical, geochronological and structural data, plus a number of research publications, conference abstracts and post-graduate theses.

Keywords :- Mapping, Research collaboration, Capacity building, Geoscience outreach

To cite this report :- Nguno, A. and Macey, P. 2024. The Southern Namibian Mapping Programme 2013 to 2022 – a decade of research collaboration and detailed mapping. *Communications of the Geological Survey of Namibia*, **27**, 97-109.

Background

Geological maps and associated research products provide base information for a wide range of applications, most notably minerals exploration, but also for finding groundwater resources, infrastructure development and environmental investigations (including climate change and geohazards), as well as for promoting geotourism and geoheritage-related activities. Regional geological mapping at various scales has been carried out by the Geological Survey of Namibia (GSN), and its predecessors, for more than a century, complemented by the work of local and international research institutions and mining / mineral exploration companies. A highly heterogeneous geological map coverage and information base for the country resulted, with some areas surveyed in great detail, others mapped only at reconnaissance level, and the Cenozoic generally receiving little attention. With the advent of GIS, these archival geological data were compiled into 1:250 000 and 1:100 000 scale digital maps covering some two thirds of the country, excepting only the largely sand-covered northeast (Fig. 1).

However, understaffing and a lack of experienced personnel at GSN caused new geological mapping of the country to lag since the 1990s. Therefore, in 2013 GSN embarked on a new, systematic and higher detail 1:50 000 scale regional geological mapping programme combining contract mapping by experienced senior geologists of the Council for Geoscience (CGS) and training of GSN staff in modern mapping and map production techniques. The //Karas Region of southern Namibia was selected as the first focal area, because the geologically complex Precambrian Namaqua and Gariep rocks are highly prospective for a wide range of mineralisation types and commodities. Furthermore, previous mapping of the area was completed at 1:100 000 to 1:250 000 scale more than 40 years earlier and therefore due for revision applying modern research and mapping techniques, and scientific insights. Developing a unified stratigraphy across the Orange River was another important objective of the project.

Project Implementation

The Southern Namibia Mapping Programme (SNMP) was carried out by a team of mapping geologists from GSN and CGS, supported by Namibian and South African university students and academics. Annual activities followed a standard mapping workflow starting with database construction and remote sensing. Comprehensive ArcGIS geospatial databases of archival and published geological maps, as well as data from research publications and theses were overlaid with satellite and airborne geophysical and multi- / hyperspectral imagery for the compilation of base maps for field mapping. Lithological and structural mapping (>30 000 structural readings) and sample collection campaigns were carried out by both senior and junior geologists from mobile tented base camps. Field observations and measurements were captured into new geospatial databases and many thousands of digital photographs linked to waypoint locations. Analytical work included petrography, whole rock major, trace and REE geochemistry (~950 samples), stable (O, C) and radiogenic (Sm, Rb, Hf) isotope geochemistry (>500 analyses), P-T pseudo-section studies and U-Pb zircon, monazite and titanite geochronology (236 samples; Table 1). Thin section preparation, whole rock geochemical analyses and zircon separation were done at the CGS laboratory (Pretoria), while isotope analyses, metamorphic studies and U-Pb dating were carried out at the Universities of Cape Town and Stellenbosch (South Africa) and Curtin University (Australia), respectively. Field and laboratory data were integrated into 1:50 000 scale geological maps and explanatory reports. Map compilation by the CGS Spatial Data Management Unit involved training of GSN staff in modern cartographic techniques, with the last maps being produced at GSN. The project received assistance from the Ministry of Environment, Forestry and Tourism, local farmers and mineral licences holders, who facilitated access to the land; in addition, NAMDEB provided in-kind support during work in the Tsau //Khaeb (Sperrgebiet) National Park.

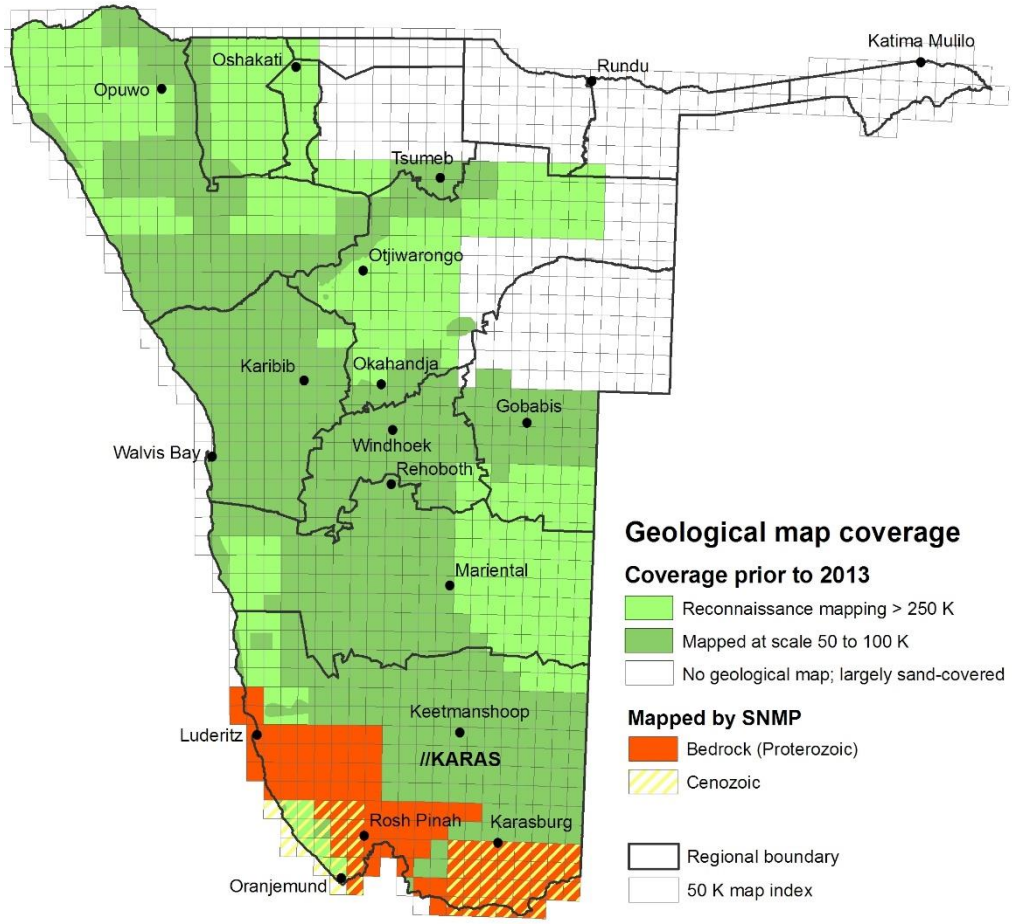

Figure 1. Geological map coverage prior to 2013 and areas mapped by the SNMP

Progressive phases of the SNMP:

- 1:50 000 scale geological mapping of the Palaeo- and Mesoproterozoic Namaqua Metamorphic Province in the areas of
  - ✓ Warmbad, Ariamsvlei and Haib (2013-2015)
  - ✓ East of Rosh Pinah (Namuskluft), central Sperrgebiet (Aurus Mountains) and Grünau (2015)
  - ✓ Lower Fish River and Konkiep canyons, Ai-Ais and Huns Mountains (2015-2017)
  - ✓ Aussenkjer (2019; including the Cambrian Kuboos-Bremen line of intrusives)
  - ✓ Lüderitz and Aus (including Aukam valley (2019-2021)
  - ✓ Hottentot Bay north of Lüderitz (2021)
- 1:50 000 scale geological mapping of the Neoproterozoic Port Nolloth Group (Port Nolloth Zone, Gariep Belt) in the
  - ✓ Rosh Pinah, Namuskluft and Witputs areas (2016-2017)
  - ✓ Northern Sperrgebiet (2019-2021)
- 1:250 000 scale reconnaissance mapping of the Cenozoic geology of the
  - ✓ 2818 Warmbad map sheet
  - ✓ southern Sperrgebiet north of Oranjemund
- Training and supervision of GSN staff in modern mapping and research techniques by gradually transferring responsibility:
  - ✓ Mapping by CGS geologists accompanied by GSN staff
  - ✓ Mapping by CGS geologists in tandem with GSN colleagues
  - ✓ Mapping by GSN geologists under limited supervision from CGS staff

Area	Mapped by (GSN : CGS)	Period	Samples collected	Thin sections	U-Pb Geochronology	XRF+ICPMS major/trace/RE elements	Sr	Nd	Structural measurements	C, O Stable isotopes
Warmbad	30% : 70%	2013-15	1700	678	86	512	54	54	11612	0
Ariamsvlei	10% : 90%	2015	41	*no info*	0	0	0	0	672	0
Haib	90% : 10%	2015	81	*no info*	1	8	0	0	720	0
Namuskluft	0% : 100%	2015	117	*no info*	14	31	0	0	1383	0
Sperrgebiet	0% : 100%	2015	121	*no info*	15	56	0	0	1121	0
Grünau	20% : 80%	2015	105	*no info*	7	19	0	4	251	0
Lower Fish River Canyon/Ai-Ais	25% : 75%	2015	315	*no info*	20	65	14	19	758	0
Upper Fish River Canyon/Konkiep	35% : 65%	2016	264	82	21	54	0	7	2697	0
Gariep	25% : 75%	2016-17	238	57	8	11	0	0	2653	252
Huns Mountains	25% : 75%	2017	0		3	0	0	0	252	0
Aussenkjer	30% : 70%	2019	146	23	2	13	0	0	549	0
Lüderitz & N Sperrgebiet, Aus area	45% : 55%	2019-21	307	211	47	165	7	7	8373	112
Hottentot Bay	20% : 80%	2021	74	38	12	23	1	1	394	0
Total	**30% : 70%**	**2013-22**	**3509**	**1089**	**236**	**957**	**76**	**92**	**31435**	**364**

Table 1. Areas mapped and data generated by the SNMP during the period 2013-2022

Maps and Associated Products

In the ten years of collaboration and cooperation between CGS and GSN ninety-five full and partial 1 : 50 000 scale geological maps were produced, with the actually mapped terrain covering some 45 000 km^2 or ~5.5 % of the country's surface area (Figs 1, 2). All maps are fully digital and include point (structure, lithology, geochronology), line (lithology, structure) and polygon (lithology) data, with each coded feature having queryable attributes including information on tectonostratigraphy, lithostratigraphy, age, me-tamorphic grade and rock type. Several of the areas, such as the environs of Lüderitz, Hottentot Bay to the north of that town and the Aurus Mountains of the central Sperrgebiet (Fig. 3) were mapped for the first time in any kind of detail, requiring the introduction of a whole new set of stratigraphic units and names.

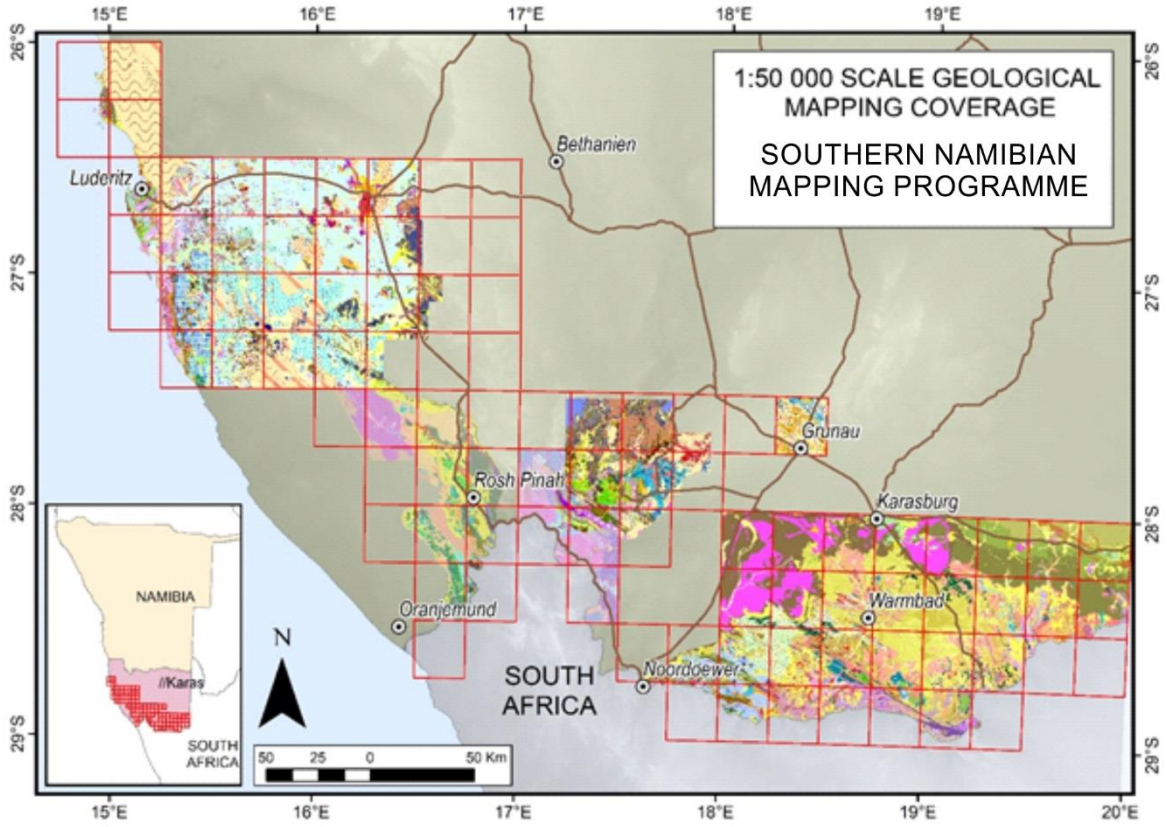

Figure 2. Areas mapped in detail by the SNMP between 2013 and 2022

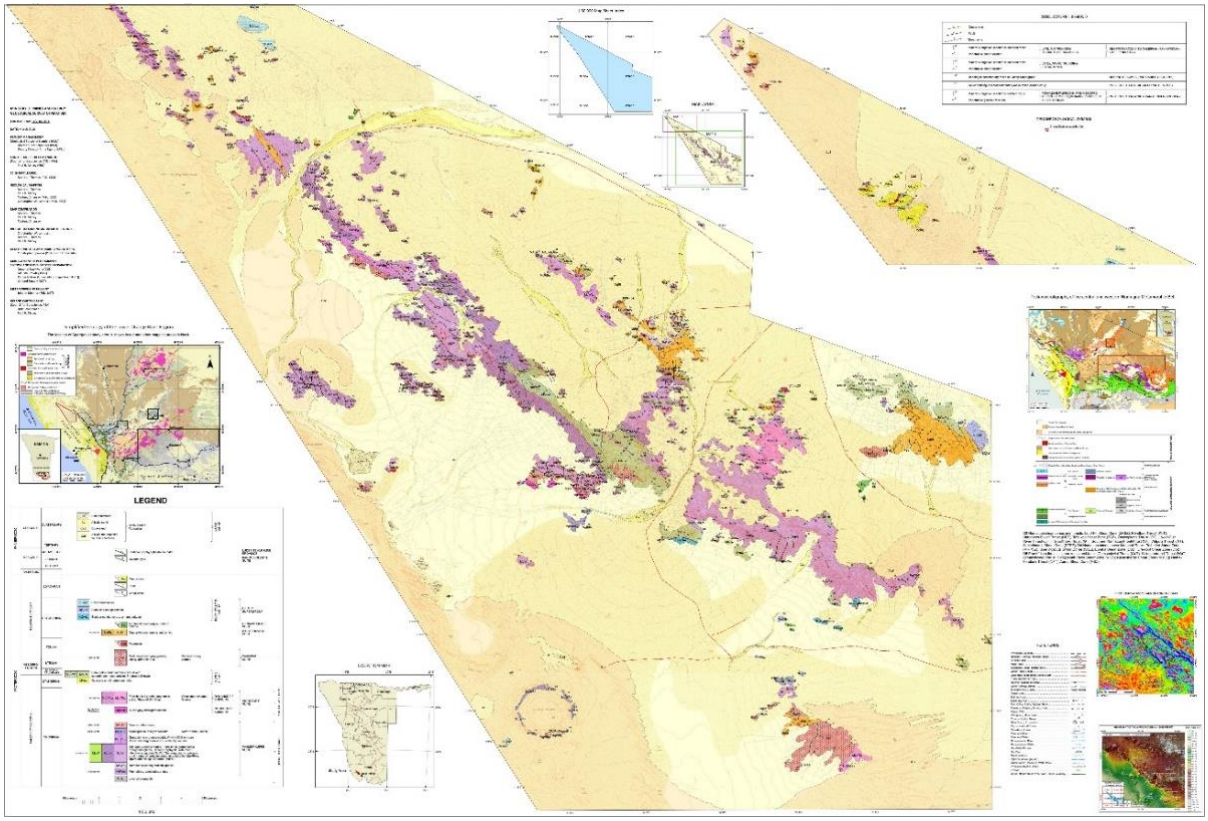

Figure 3. New 1: 50 000 scale geological map of the Aurus Mountains, central Sperrgebiet

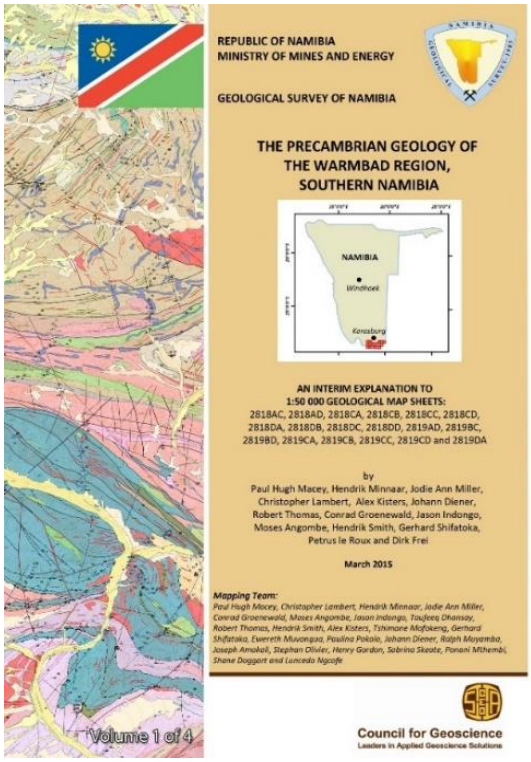

Figure 4. Map sheet explanations and mapping report compiled by the SNMP

Maps are accompanied by comprehensive reports (e. g. Macey *et al*., 2015, 2020, 2022; Thomas *et al*., 2016; Gresse *et al*., 2016, 2018), Shifotoka and Indongo, 2017) describing the main rock types and geological structures of the area within the context of new tectonic and stratigraphic subdivisions and geological models based on observed field relationships and new analytical data (Fig. 4). In addition to 1:50 000 scale "hard rock" maps, two 1:250 000 scale maps with explanations featuring the Cenozoic geology of the Warmbad area (Gresse and Mhopjeni, 2015) and the southern Sperrgebiet (Gresse and Nduutepo, 2020), respectively, were compiled. Incorporating the new map data, so far three 1:250 000 scale geological maps (2818 Warmbad, 2816 Oranjemund and 2716 Ai-Ais) have been updated. And lastly, a 1:40 000 scale hiking and geological map of the Fish River Canyon, one of the country's best-known geological landmarks and tourist attractions was produced in cooperation with Slingsby Maps, South Africa (Fig. 5).

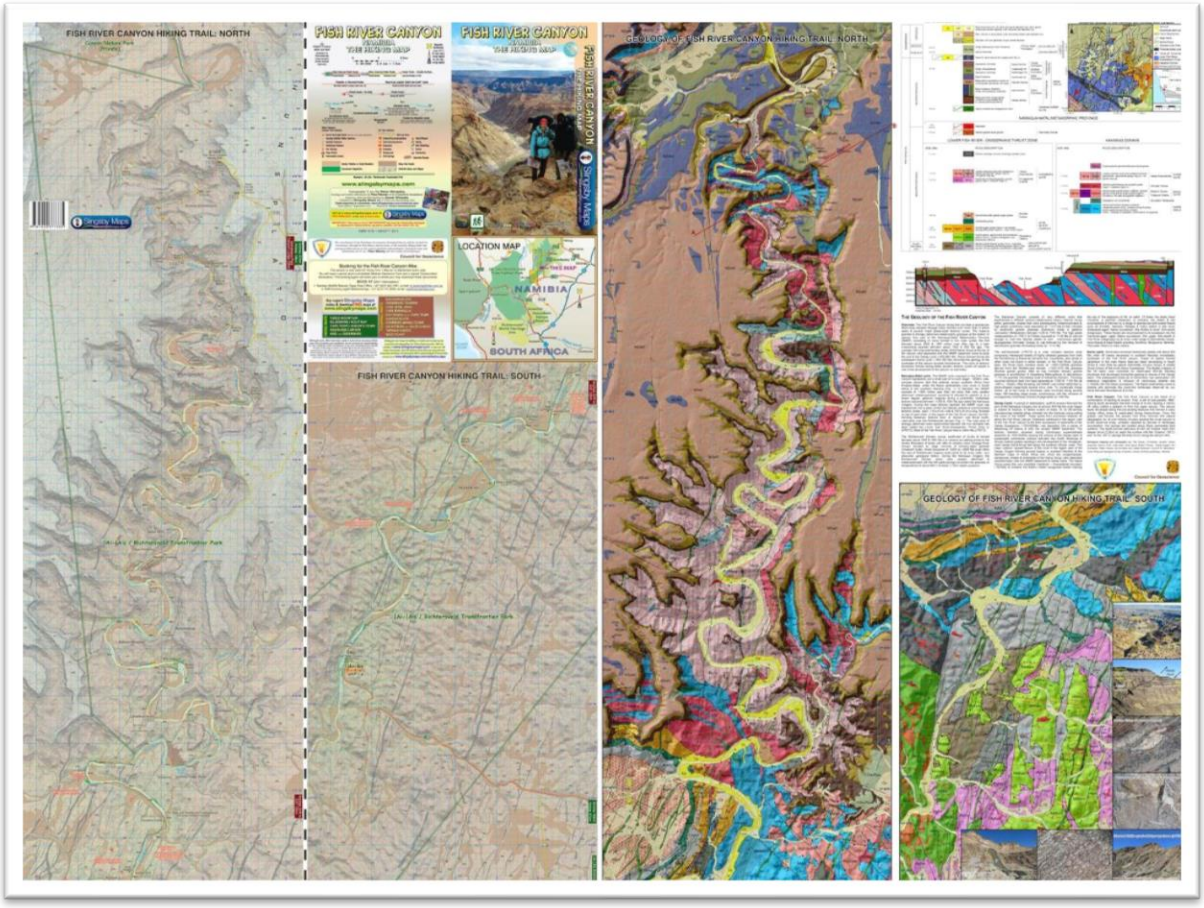

Figure 5. Hiking and Geological Map of the Fish River Canyon

Scientific Achievements

Regional mapping formed the basis for collaboration with university researchers and post-graduate students, which resulted in seventeen publications in international journals (Appendix A) and 41 conference abstracts (Appendix B). Eighteen post-graduate research projects (Appendix C) were completed as part of the SNMP, including twelve BSc (Hons) and five MSc theses from the University of Stellenbosch (South Africa), Cape Town (South Africa), Western Cape (South Africa), the University of Namibia and McGill University (Canada), as well as one PhD from McGill University.

Among the scientific achievements of the SNMP is the proposal of an alternative theory for the amalgamation of the southern African portion of the Rodinia supercontinent during the Mesoproterozoic, which favours a model of crustal reworking (Macey *et al*., 2015) over the traditional accretion of crustal terranes (e. g. Hartnady *et al*., 1985; Joubert, 1986; Colliston and Schoch, 2013). This hypothesis in turn led to a redefinition of crustal segments within the Namibian part of the Namaqua – Natal Metamorphic Province, which are from north to south the Konkiep Domain, the Kakamas Domain, the Aus Domain and the Richtersveld Magmatic Arc (Fig. 6). Structural mapping recognised significant late-Namaqua (~1100 Ma) deformation (Eureka and Sperlingsputs Shear Zones - Angombe, 2016; Indongo, 2017), while U-Pb zircon dating identified a new intrusive suite (Orange Falls Suite) younger by some 650 Ma than the Vioolsdrif granitoids with which it was previously grouped, as well as the first Archaean-derived rocks within the Namaqua Metamorphic Province of Namibia, i. e. the Bankwasser Migmatite Complex west of Warmbad and the Blue Mountain Group metapelites of the Hottentot Bay area (Doggart *et al*., 2023). In the Port Nolloth Zone of the Gariep Orogenic Belt detailed mapping also produced a new subdivision into a number of depositional and structural subzones, with special emphasis being placed on the correlation of the various diamictite deposits (Gresse *et al*., 2018), denoting global glaciation events ("Snowball earth"; Table 2).

BASINAL ZONE (WEST)				THRUST ZONE				RIFT ZONE				PLATFORM ZONE (EAST)			Glaciation/ Deglacation Sequence
Subgroup	Formation	Member	Igneous Complex/ Suite	Sub-group	Formation	Member	Igneous Complex/ Suite	Subgroup	Formation	Member	Igneous Complex/ Suite	Subgroup	Formation	Member	
Holgat	Daberas			Holgat	Daberas	Dreigratberg		Holgat	Daberas	Dreigratberg		Holgat	Uguchab	Dreigratberg	Cap carbonate 3
						Namuskluft				Namuskluft				Namuskluft	Marinoan (635 Ma)
		Bloeddrif				Bloeddrif				Bloeddrif				Bloeddrif	Cap carbonate 2
	Numees	Jakkalsberg			Numees	Jakkalsberg			Numees				Numees		Sturtian (720 Ma)
Hilda	Dabie River			Hilda	Dabie River			Hilda	Dabie River			Hilda	Dabie River		
	Wallekraal		Koivib		Wallekraal				Wallekraal				Wallekraal		
	Pickelhaube	Pickelhaube Peak	Spitskop/ Koivib		Pickelhaube	Pickelhaube Peak			Pickelhaube	Pickelhaube Peak			Pickelhaube	Pickelhaube Peak	
		Skorpion			Rosh Pinah	Gergarub	Spitskop/ Koivib		Rosh Pinah		Spitskop		Rosh Pinah		
	Rosh Pinah	Obib	Koivib			Een Oog				Een Oog				Een Oog	
	Kaigas								Kaigas	Trekpoort			Kaigas	Trekpoort	Cap carbonate 1
															Kaigas (>760 Ma)
Stinkfontein	Gumchavib		Koivib					Stinkfontein	Vredefontein			Stinkfontein	Vredefontein		

Table 2. Stratigraphy of the Port Nolloth Group, Gariep Supergroup, as refined by new detail mapping

Community Outreach in the //Karas Region

Objectives, achievements and expectations of the SNMP were presented to dignitaries of the //Karas Region and stakeholders during a two-day outreach event in August 2018 at the Ai-Ais Hot Spring Resort. Main aim of the occasion was the launch of the new detailed 1:50 000 scale maps and related research products (Fig. 7), to generate a better understanding of the many benefits of reliable geological information among officials and the public, and to emphasise the significance of cross-border collaboration in the field of geoscience.

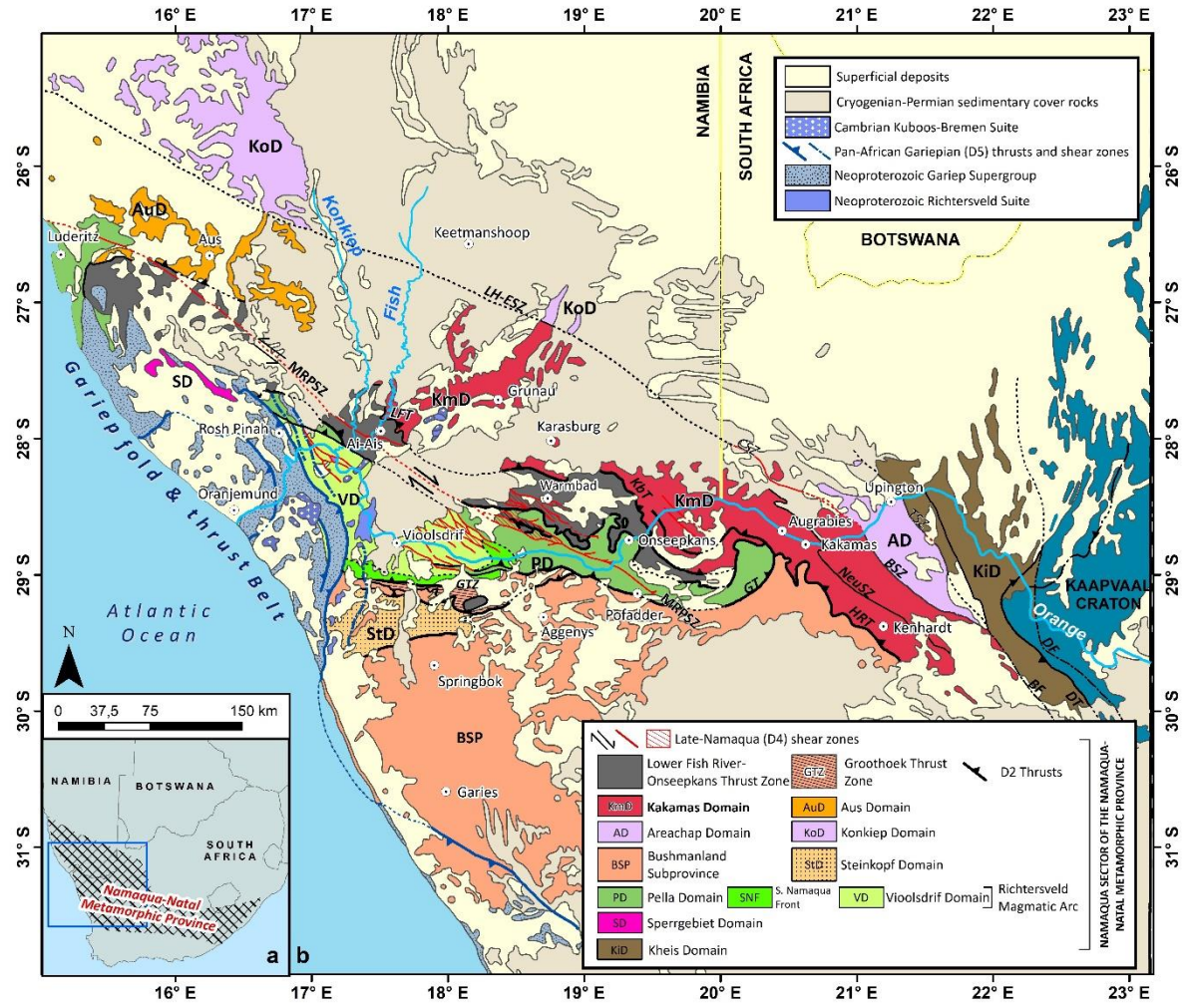

Figure 6. New tectonostratigraphic subdivision of the western Namaqua–Natal Belt (Macey *et al*., 2022)

Presentations focused on the applications of geological data, such as the search for water, mineral exploration, land-use planning and infrastructure development. Hosted by Minister of Mines and Energy, Tom Alweendo, the meeting was attended by the Governor of the //Karas Region, Lucia Basson, officials from local authorities and various Ministries, representatives of Namdeb Diamond Corporation, Epangelo Mining, Namibian Wildlife Resorts, the Council for Geoscience, University of Namibia, Nama Traditional Leaders Association, Namibia Agricultural Union, members of the small-scale mining community, local farmers and the media. The workshop ended with a visit to the Fish River Canyon introducing attendees to the geological field work entailed in the production of geological maps and reports (Fig. 8).

Figure 7. Official launch of the Fish River Canyon Hiking and Geological Map

Figure 8. Field visit to the lower Fish River Canyon

In the ten years of SNMP activities, a number of challenges were encountered not the least of which was the COVID-19 pandemic, which delayed both field and laboratory work with repeated lockdowns and travel restrictions. Apart from *force majeure,* the tight time frame and financial constraints occasionally required some ingenuity to make ends meet and extract the maximum benefit from the available resources.

On the technical side, some difficulty arose from the failure to set up strict symbology codes and data base attributes for the new data. To enable the smooth integration of newly mapped areas into an existing geological map coverage and data base, it is essential to stipulate certain guidelines, especially with regard to naming and symbolisation of newly identified geological units, at the outset of any major project of this kind. Rectification of ambiguities created by the absence of such norms, involving the renaming of units, changing of codes and colours, editing of reports and revision of map layouts and data base attributes, is a time-consuming and exacting task, which can be avoided by adherence to specified standards.

Conclusions

During the past decade the Southern Namibian Mapping Programme has contributed significantly to the long-term national geoscience objective of acquiring detailed (1:50 000 scale) geological map coverage for the entire country. Despite temporary setbacks and some stumbling blocks, the fact that the SNMP - initially tasked only with remapping the Palaeo- to Mesoproterozoic geology of the Warmbad area over a period of three years - continued for an entire decade, moving in scope far beyond its original boundaries, alone is indication of its success. Many of the Project's findings and conclusions featured at a special session during the 29th Colloquium of African Geology, which took place in Windhoek in September 2023, covering aspects of mineralisation, structure, metamorphism and stratigraphy, as well as GIS – related problems, the application of remote sensing in mapping and matters of project management. If the theories evolved from the new data may not all be uncontended, the data and maps themselves provide a solid footing on which to build mineralisation models for exploration, new hypotheses for geotectonic evolution, as well as development plans for infrastructure and land use. As shown by the close co-operation between the contract partners, major mapping programmes, such as SNMP, provide a platform for government and research institutions to collaborate on common objectives, share data and exchange expertise, with enhanced capacity and know-how not the least of many benefits.

References

Angombe, M. 2016. *The lithostratigraphy and structural components of the Eureka Shear Zone, southern Namibia*. M. Sc. thesis, University of Stellenbosch, 105 pp.

Colliston, W. P. and Schoch, A. E. 2013. Wrench-shearing during the Namaqua Orogenesis Mesoproterozoic late-stage deformation effects during Rodinia assembly. *Precambrian Research*, **232**, 44–58.

Doggart, S., Thomas, R., Macey, P., Smith, H., Shifotoka, G., Groenewald, C., Twala, M. and Frei, D. 2023. The oldest rocks in Namibia: Archaean crustal fragments in the 1.9 Ga Richtersveld Magmatic Arc, NW Namaqua-Natal Metamorphic Province. *Abstr. 29th Colloquium of African Geology*, 26-29 Sept., Windhoek, Namibia, 89.

Gresse, P. G. and Mhopjeni, K. K. 2015. *An Explanation of the Cenozoic and Kimberlite Geology of the 1:250 000 scale 2818 Warmbad map sheet*. Unpublished Report, Geological Survey of Namibia/Council for Geoscience (South Africa), 133 pp.

Gresse, P. G. and Nduutepo, A. 2020. *Introductory Report to the Cenozoic Geology of the Southern Sperrgebiet, //Karas Region, Southern Namibia*. Unpublished Report, Geological Survey of Namibia/Council for Geoscience (South Africa), 122 pp.

Gresse, P. G., Macey, P. H., Smith, H., Hartnady, M. I. and Frei, D. 2016. *The Pre-Gariep Geology East of Rosh Pinah, //Karas Region, Southern Namibia*. Unpublished Report, Geological Survey of Namibia/ Council for Geoscience (South Africa), 200 pp.

Gresse, P. G., Smith, H. P., Thomas, R. J., Macey, P. H., Hoffmann, K.-H., Lambert, C.W., Angombe, M., Shitotoka, G. and Bracciali, L. 2018. *Geology of the Port Nolloth Group and the Grootderm Formation, Gariep Supergroup, in the Rosh Pinah area, //Karas Region, Southern Namibia*. Unpublished Report, Vols I & II. Geological Survey of Namibia/Council for Geoscience (South Africa), 250 pp.

Hartnady, C. J. H., Joubert, P. and Stowe, C. W. 1985. Proterozoic crustal evolution in southwestern Africa. *Episodes*, **8**, 236 - 244.

Indongo, J. 2017. *The Lithological and Structural Characterisation of the Sperlingputs Shear Zone in Southern Namibia*. M. Sc. thesis, University of Stellenbosch, 119 pp.

Joubert, P. 1986. The Namaqualand Metamorphic Complex - A summary. *In*: C.R. Anhaeusser & S. Maske (Eds) *Mineral Deposits of South Africa*, Vols I & II, Geological Society of South Africa, Johannesburg, 1395-1420.

Macey, P. H., Minnaar, H., Miller, J.A., Lambert, C.W., Groenewald, C., Indongo, J., Angombe, M. T., Hendrik, S., Shifotoka, G., Diener, J., Le Roux, P. and Frei, D. 2015. *The Precambrian Geology of the Region South of Warmbad from Haib to Velloorsdrif, Southern Namibia*. Unpublished Report, Geological Survey of Namibia/Council for Geoscience (South Africa).

Macey, P. H. and Slingsby, P. 2018. *A hiking and geology map of the Fish River Canyon* (Poster). Geocongress, 18-20 July, Johannesburg, South Africa.

Macey, P., Shifotoka, G., Angombe, M., Smith, H., Indongo, J., Groenewald, C., Muvangua, E., Doggart, S., Mutongolume, C., Utoni, E., Gresse, P., Nguno, A., Ncume, M., Diene, J., Frei, D., Le Roux, P., Musekiwa, C., Radzuma, T., Phikiso. Z., Tiguely, X., Sarila, E., Grobbelaar, D. and Bracciali, L. 2020. *The Geology of the NW Namaqua Metamorphic Province in the Sperrgebiet and Adjacent Regions Between Lüderitz, Aus, Witputs and Bogenfels, Southern Namibia*. Unpublished Report, Geological Survey of Namibia/Council for Geoscience (South Africa), 181 pp.

Macey, P., Groenewald, C., Doggart, S., Thomas., R., Shifotoka, G., Smith, H., Gresse, P. G., Nguno, A., Frei, D., Musekiwa, C., Radzuma, T., Phikiso, Z., Grobbelaar, D., Twala, M., Jonk, L. and Coetzer, L. 2022. *The Geology of the NW Namaqua Metamorphic Province around Hottentot Bay North of Lüderitz, Southern Namibia*. Unpublished Report, Geological Survey of Namibia/Council for Geoscience (South Africa), 147 pp.

Shifotoka, G. and Indongo, J. L. 2017. *The Precambrian Geology of the Haib Área, Southern Namibia*. Unpublished Report, Geological Survey of Namibia/Council for Geoscience (South Africa), 57 pp.

Slingsby Maps. 2017. *Fish River Canyon. The Hiking Map*. ISBN 978-1-920377-33-5, www.slingsbymaps.com

Thomas, R. J., Macey, P. H., Dhansay, T., Spencer, C., Diener, J. and Lambert, C. W. 2016. *The Precambrian Geology of the Aurus Mountains, Sperrgebiet, SW Namibia*. Unpublished Report, Geological Survey of Namibia/Council for Geoscience (South Africa), 178 pp.

Appendix A. Peer-reviewed publications in international journals (in chronological order)

Melosh, B.L. Rowe, C.D., Smit, L., Groenewald, C., Lambert, C.W. and Macey, P. 2014. Snap, Crackle, Pop: Dilational fault breccias record seismic slip below the brittle-plastic transition. *Earth and Planetary Science Letters*, **403**, 432-445.
Thomas, R.J., Macey, P.H., Spencer, C., Dhansay, T., Diener, J.F.A., Lambert, C.W. and Nguno, A. 2016. The Sperrgebiet Domain, Aurus Mountains, SW Namibia: a ~2020 to 850 Ma window within the Pan-African Gariep Orogen. *Precambrian Research*, **286**, 35-58.
Macey, P.H., Thomas, R.J., Minnaar, H.M., Gresse, P.G., Lambert, C.W., Groenewald, C.A., Miller, J.A., Indongo, J.I., Angombe, M., Shifotoka, G., Frei, D., Diener, J.F.A., Kisters, A.F.M., Dhansay, T., Smith, H., Doggart, S., le Roux, P., Hartnady, M.I. and Tinguely, C. 2017. Origin and evolution of the ~1.9 Ga Richtersveld Magmatic Arc, SW Africa. *Precambrian Research*. **292**, 417–451.
Diener, J.F.A., Thomas, R.J. and Macey, P.H. 2017. Pan-African accretionary metamorphism in the Sperrgebiet Domain, Gariep Belt, SW Namibia. *Precambrian Research*, **292**, 152-162.
Melosh, B.L. Rowe, C.D., Gerbi, C., Smit, L., Groenewald, C., Lambert, C.W. and Macey, P.H. Seismic cycle feedbacks in a mid-crustal shear zone. 2018. *Journal of Structural Geology*, **112**, 95-11.
Macey, P.H., Abrahams, Y. and Miller, J.A. 2018. Lithostratigraphy of the Mesoproterozoic Stolzenfels Granite. *South African Journal of Geology*, **121**, 217-226.
Abrahams, Y. and Macey, P.H. 2020. Lithostratigraphy of the Mesoproterozoic Donkieboud Granodiorite Granite. *South African Journal of Geology*, **123**, 421-430.
Groenewald, C.A. and Macey, P.H. 2020. Lithostratigraphy of the Mesoproterozoic Yas-Schuitdrift Batholith. *South African Journal of Geology*, **123**, 431-440.
Martin, E.L., Spencer, C. J., Collins, W. J., Thomas, R. J., Macey, P. H., and Roberts, N. M. W. 2020. The core of Rodinia formed by the juxtaposition of opposed retreating and advancing accretionary orogens. *Earth-Science Reviews*, **211**.
Doggart, S., Macey, P.H. and Frei, D. 2021. Lithostratigraphy of the Mesoproterozoic Twakputs Gneiss. *South African Journal of Geology*, **124**, 783-794.
P.H. Macey, P.H., Smith, H.P., Thomas, R.J., Frei, D. and le Roux, P. 2021. Lithostratigraphy of the Naros Granite (Komsberg Suite), South Africa and Namibia. *South African Journal of Geology*, **124**, 795-804.
Cavosie, A.J., Spencer, C. Evans, N., Rankenburg, K. Thomas, R.J. and Macey, P. H. 2022. Granular titanite from the Roter Kamm crater in Namibia: Product of regional metamorphism, not meteorite impact. *Geoscience Frontiers*, **13**.
Johansson, A., Bingen, B., Huhma, H, Waight, T., Vestergaard, R., Soesoo, A., Skridlaite, G., Ewa Krzeminska, E., Shumlyanskyy, L., Holland, M.E., Holm-Denoma, C., Teixeira, W., Faleiros, F.M., Ribeiro, B., Jacobs, J., Wang, C., Thomas, R.J., Macey, P.H., Kirkland, C.L., Hartnady, M.I.H., Eglington, B.M., Puetz, S.J. and Condie, K.C. 2022. A geochronological review of magmatism along the external margin of Columbia and in the Grenville-age orogens forming the core of Rodinia. *Precambrian Research*, **371**.
Macey, P.H., Thomas, R.T., Kisters, A.F.M., Diener, J.F.A., Angombe, M., Doggart, S., Groenewald, C.A., Lambert, C.W., Miller, J.A., Minnaar, H., Smith, H., Moen, G., Muvuangua, E., Nguno, A., Shifotoka, G., Indongo, J., Frei, D., Spencer, C., le Roux, P., Armstrong, R.A. and Tinguely, C. 2022. A continental back-arc setting for the Namaqua belt: evidence from the Kakamas Domain. *Geoscience Frontiers*, **13**.
Walter. B.F., Giebel, R.J., Siegfried, P., Coetser, C., Doggart, S., Macey, P.H., Schiebel, D. and Kolb, J. 2023. The genesis of hydrothermal veins in the Aukam valley SW Namibia– a far field consequence of Pangean rifting? *Journal of Geochemical Exploration*, **250**.
Muir, R.A., Whitehead, B., New, T., Stevens, V., Macey, P.H., Groenewald, C., Salomon, G., Kahle, B., Hollingsworth, J., and Sloan, R.A. 2023. Exceptional Scarp Preservation in SW Namibia Reveals Geological Controls on Large Magnitude Intraplate Seismicity in Southern Africa. *Tectonics*, **42**.
Diener, J.F.A. and Macey, P.H. 2023 (in press). Pervasive and uniform low-pressure granulite facies conditions in the Grünau–Kakamas Domain, Namaqua–Natal Province, Namibia: A manifestation of thermal buffering during partial melting? *Journal of Metamorphic Geology*.

Appendix B. Conference abstracts produced by the SNMP (in chronological order)

Lambert, C., Groenewald, C., Macey, P.H., Kisters, A. and Frei, D. 2013. Melt migration along transcurrent shea zones: Case Study of the Pofadder Shear Zone and the Skimmelberg Pegmatite Stockwork (Poster). *24th Colloquium of African Geology, 8-14 Jan.*, Addis Ababa, Ethiopia.

Lambert, C.W., Kisters, A. F.M., Macey, P. H., Frei, D., Buick, I.S. and Groenewald, C. 2013. Melt-shear zone relationships during the lifespan of a continental transcurrent shear zone. *GSA Annual Meeting, 27-30 Oct., Denver USA.*
Lambert, C.W., Macey, P.H., Kisters, A.F.M., Groenewald, C.A., Frei, D., Buick, I.S. and Angombe, M. 2014. The Marshall Rocks-Pofadder Shear Zone and other Late-Namaqua shear zones: 45 million years of progressive deformation in the western Namaqualand Metamorphic Province. *Roy Miller Symposium*, 18-30 Aug., Windhoek Namibia, 42.
Macey, P.H., Minnaar, H., Miller, J.A., Lambert, C., Groenewald, C., Diener, J., Dhansay, T., Mofokeng, T., Le Roux, P., Muvangua, E., Indongo, J., Angombe, M., Frei, D., Ngcofe, L., Smith, H., Olivier, S., Mbtembi, P., Pokolo P., Shifotoka, G., Muyamba, R. and Amakali, J. 2014. Tracing Tectonic Terranes in Southern Namibia (Poster). *Roy Miller Symposium*, 18-30 Aug., Windhoek, Namibia, 67.
Angombe, M., Macey, P.H. and Miller, J.A. 2014. The Eureka Shear Zone (Poster). *Roy Miller Symposium*, 18-30 Aug., Windhoek, Namibia, 59.
Indongo, J. 2014. The Lithostratigraphy, Structure and Age of the Southern Namaqua Front and its Country Rocks Southern Namibia (Poster). *Roy Miller Symposium*, 18-30 Aug., Windhoek, Namibia, 64.
Shifotoka, G. 2014. The Orange Falls Suite, a newly recognised syntectoinc granitoid suite (Poster). *Roy Miller Symposium*, 18-30 Aug., Windhoek, Namibia, 74.
Smith, H., Miller, J.A., Macey, P.H. and Olivier, S. 2014. The emplacement and evolution of the Keimasmund Complex, Warmbad, Southern Namibia (Poster). *Roy Miller Symposium*, 18-30 Aug., Windhoek, Namibia, 77.
Miller, J., Macey, P., Lambert, C., Le Roux, P., Shifotoka, G. and Frei, D. 2015. Cannibalisation of Palaeoproteozoic Arc Terranes during the Mesoproterozoic in the Namaqua Metamorphic Belt, Southern Africa. *25th Annual Goldschmidt Conference*, 16-21 Aug., Prague, Czech Republic.
Macey, P.H., Lambert, C.W., Kisters, A.F.M., Gresse, P.G., Thomas, R., Miller, J.A., Groenewald, C, Angombe, M., Indongo, J., Shifotoka, G., Minnaar, H., Smith H., Dhansay, T., Diener, J., Frei, D., Muvangua, E., Spencer, C., le Roux, P. and Doggart, S. 2016. Towards a new geodynamic model for the western Namaqua Province. *International Geological Congress 35*, 27 Aug. - 4 Sep., Cape Town, South Africa.
Thomas, R.J., Macey, P.H., Spencer, C, Dhansay, T. and Lambert, C. 2016. Geological evolution of the Aurus Mountains, Sperrgebiet Domain, Namibia. *International Geological Congress 35*, 27 Aug. - 4 Sep., Cape Town South Africa.
Lambert, C.W, Macey, P.H., Kisters, A.F.M., Groenewald, C.A., Frei, D., Buick, I.S. and Angombe, M. 2016. The Marshall Rocks-Pofadder Shear Zone and other late-Namaqua dextral shear zones between Ai-Ais and Pofadder in the western Namaqualand Metamorphic Province: Fabrics, timing and late stage melt controls. *International Geological Congress 35*, 27 Aug. - 4 Sep., Cape Town, South Africa.
Shifotoka, G., Haimbodi, M., Macey, P.H., Miller, J.A. and Thomas, R. 2016. The Regional Geological Setting of the Haib Porphyry-Copper Deposit, southern Namibia (Poster). *International Geological Congress 35*, 27 Aug. - 4 Sep., Cape Town, South Africa.
Miller, J.A., Macey, P.H., Lambert, C.W., Angombe, M., Shifotoka, G., Thomas, R.J., Frei, D. and Le Roux, P. 2016. Reassessment of Mesoproterozoic granitic rocks in southern Namibia and their context within the broader western Namaqua Province. *International Geological Congress 35*, 27 Aug. - 4 Sep., Cape Town, South Africa.
Miller, J.A., Macey, P.H., Lambert, C.W., Frei, D., Le Roux, P. and Muvangua, E. 2016. Distribution and characteristics of gabbros, gabbronorites and amphibolites across the western Namaqua Province and their role in constraining terrane boundaries. *International Geological Congress 35*, 27 Aug. - 4 Sep., Cape Town, South Africa.
Indongo, J., Macey, P.H., Miller, J.A. and Shifotoka, G. 2016. The late-Namaqua Sperlingsputs Shear Zone System Haib region, southern Namibia. *International Geological Congress 35*, 27 Aug. - 4 Sep., Cape Town, South Africa.
Angombe, M., Macey, P.H., Miller, J.A. and Lambert, C.W. 2016. The lithostratigraphy and structural components of the Eureka Shear Zone, southern Namibia. *International Geological Congress 35*, 27 Aug. - 4 Sep., Cape Town South Africa.
Smith, H.P., Macey, P.H., Miller, J.A., Rowe, C., Lambert, C.W., Diener, J. and Frei, D. 2016. The Lower Fish-River / Onseepkans Thrust Zone: Time constraints and insights into Namaquan thrust tectonics. *International Geological Congress 35*, 27 Aug. - 4 Sep., Cape Town, South Africa.
Doggart, S.W., Buick, I., Frei, D., Lana, C., Macey, P.H. and Lambert, C.W. 2017. Monazite U/Pb geochronology and Sm/Nd isotope geochemistry of the Orange River pegmatite belt; a late stage felsic melt emplacement in the Namaqua Metamorphic Complex. Igneous & Metamorphic Studies Group (ISMG) Conference, Johannesburg, South Africa.
Diener, J.F.A. and Macey, P.H. 2018. Pervasive and uniform Low-P Granulite facies conditions in the Grünau-Kakamas Domain: A Manifestation of thermal buffering during partial melting? Igneous & Metamorphic Studies Group (ISMG) Conference, University of the Western Cape (Bellville), South Africa.
Macey, P.H. and Slingsby, P. 2018. A hiking and geology map of the Fish River Canyon (Poster). Geocongress, 18-20 July, Johannesburg, South Africa.

Doggart, S.W., Buick, I., Macey, P.H., Lambert, C.W., Lana, C., Frei, D. and Angombe, M. 2019. A new perspectiv on the origins of the Orange River Pegmatite Belt. *Geological Society of Namibia 50th Anniversary Conference*, 1-4 Sep., Windhoek, Namibia, 63.

Macey, P.H., Lambert, C.W., Thomas, R.J., Miller, J.A., Angombe, M., Smith, H., Indongo, J., Shifotoka, G., Nguno A., Minnaar, H., Groenewald, C.A., Muvangua, E., Dhansay, T., Doggart, S., Diener, J.F.A., Kisters, A.F.M, Frei D., Spencer, C., Bracciali, L., Le Roux, P., Musekiwa, C., Pokolo, P., Muyamba, R., Amakali, J., Rowe, C., Melosh B., Hartnady, M. and Tinguely, C.. 2019. The Namaqua Metamorphic Province: New perspectives from southern Namibia. *Geological Society of Namibia 50th Anniversary Conference*, 1-4 Sep., Windhoek, Namibia, 67-68.

Smith, H.P., Macey, P.H., Miller, J.A., Angombe, M., Lambert, C.W. and Rowe, C. 2019. Timing and characterisation of the 1200 - 1100 Ma tectonism in the Namaqua Metamorphic Complex, southern Namibia *Geological Society of Namibia 50th Anniversary Conference*, 1-4 Sep., Windhoek, Namibia, 69-70.

Indongo, J. 2019. The lithological and structural characterisation of the Sperlingsputs Shear Zone in southern Namibia (Poster). *Geological Society of Namibia 50th Anniversary Conference*, 1-4 Sep., Windhoek, Namibia, 84.

Shifotoka, G., Macey, P.H., Haimbodi, M., Miller, J.A. and Thomas, R. 2019. The regional geological setting of the Haib porphyry-copper deposits, southern Namibia (Poster). *Geological Society of Namibia 50th Anniversary Conference*, 1-4 Sep., Windhoek, Namibia, 95-96.

Spencer, C., Cavosie, A.J., Evans, N., Rankenburg, K. Thomas, R.J. and Macey, P.H. 2021. Granular titanite from the Roter Kamm crater in Namibia: Product of regional metamorphism, not meteorite impact. 52nd Lunar and Planetary Science Conference, 15-19 Mar. (virtual).

Macey, P.H., Thomas, R.J., Kisters, A.F.M, Diener, J.F.A., Angombe, M., Doggart, S., Groenewald, C.A., Lambert C.W., Miller, J.A., Minnaar, H., Smith, H., Moen, H F.G., Muvangua, E., Nguno, A., Shifotoka, G., Indongo, J., Frei D., Spencer, C., Le Roux, P., Armstrong, R.A., and Tinguely, C.. 2023. A continental back-arc setting for the Namaqua Belt: Evidence from the Kakamas Domain. *29th Colloquium of African Geology*, 26-29 Sept., Windhoek Namibia, 92.

Muvangua, E., Indongo, J. and Mutongolume, C. 2023. Geology of the Aukam Valley, Namaqua Metamorphic Complex, Southwestern Namibia: Implications for Regional Tectonostratigraphy. *29th Colloquium of African Geology*, 26-29 Sept., Windhoek, Namibia, 95.

Shifotoka, G., Bailie, R. and Macey, P. 2023. The Lüderitz Domain of the Richtersveld Magmatic Arc, southern Namibia. *29th Colloquium of African Geology*, 26-29 Sept., Windhoek, Namibia, 98.

Indongo, J., Macey, P.H., Miller, J.A. and Shifotoka, G. 2023. The late-Namaqua Sperlingsputs Shear Zone System Haib region, southern Namibia. *29th Colloquium of African Geology*, 26-29 Sept., Windhoek, Namibia, 91.

Nguno, A., Macey, P. and Hoffmann, K.-H. 2023. Using major mapping programmes to develop capacity and drive research collaboration. *29th Colloquium of African Geology*, 26-29 Sept., Windhoek, Namibia, 96.

Pokolo, P. 2023. The need of Guidelines and Standardization in New Mapping Projects. *29th Colloquium of African Geology*, 26-29 Sept., Windhoek, Namibia, 97.

Sloan, R.A., Muir, R.A., Whitehead, B.A., Matsebula, A., New, T., Macey, P.H., Stevens, V., Groenewald, C. Salomon, G., Kahle, B., Hollingsworth, J. and Rieger, S. 2023. Mapping Neotectonic Fault Scarps in Southern Namibia. *29th Colloquium of African Geology*, 26-29 Sept., Windhoek, Namibia, 99.

Doggart, S., Harris, C. and Macey, P. 2023. Geochemical and isotopic zonation of the Orange River Pegmatite Belt in Southwestern Africa – links to magmatic-hydrothermal events during the late Stenian-Tonian Rodinian assembly of the Namaqua Metamorphic Province. *29th Colloquium of African Geology*, 26-29 Sept., Windhoek, Namibia, 87.

Doggart, S., Macey, P., Buick, I., Mayne, M., Smith, H., Lambert, C.W. and Groenewald, C. 2023. How geoscience mapping and research in the Orange River Pegmatite Belt provide valuable insights into critical metal mineralization within the pegmatites of the Namaqua-Natal Metamorphic Province. *29th Colloquium of African Geology*, 26-29 Sept., Windhoek, Namibia, 88.

Doggart, S., Thomas, R., Macey, P., Smith, H., Shifotoka, G., Groenewald, C., Twala, M. and Frei, D. 2023. The oldest rocks in Namibia: Archaean crustal fragments in the 1.9 Ga Richtersveld Magmatic Arc, NW Namaqua-Natal Metamorphic Province. *29th Colloquium of African Geology*, 26-29 Sept., Windhoek, Namibia, 89.

Groenewald, C.A., Lambert, C.W., Macey, P.H., Kisters, A.F.M., Angombe, M., Doggart, S., Smith, H., Rowe, C. and Indongo, J. 2023. The long-lived ductile to brittle evolution of the Marshall Rocks-Pofadder Shear Zone during the final stages of the 1.2-0.96 Ma Namaqua Orogeny, Namaqua Metamorphic Province, Namibia and South Africa *29th Colloquium of African Geology*, 26-29 Sept., Windhoek, Namibia, 90.

Walter, B., Siegfried, P.R., Schiebel, D., Giebel, R.J., Doggart, S, Macey, P. and Kolb, J.. 2023. The Aukam Valley - a window into far-field, Jurassic age (?) fluorite and Cambrian age graphite mineralisation. *29th Colloquium of African Geology*, 26-29 Sept., Windhoek, Namibia, 100.

Mutongolume, C. 2023. Geological mapping, petrological characterization and geochemistry of rocks in the Aus area, southern Namibia: Implications for potential copper mineralization (Poster). *29th Colloquium of African Geology*, 26-29 Sept., Windhoek, Namibia, 94.

Musekiwa, C., Doggart, S., Cole, J., Janse van Rensburg, G., Phikiso, Z., Cole, P., Dudumashe, N., Sogayise, S. Macey, P. and Grobbelaar, D. 2023. Multispectral and hyperspectral remote sensing for geology mapping Namaqualand region, South Africa. *29th Colloquium of African Geology*, 26-29 Sept., Windhoek, Namibia, 93.

Appendix C. Post-graduate research projects completed during the SNMP (in chronological order)

Lambert (2013)	MSc	Stellenbosch University	Granitic melt transport and emplacement along transcurrent shear zones: Case study of the Pofadder Shear Zone in South Africa and Namibia
Smith (2013)	BSc Hons	Stellenbosch University	Mapping and Structural Characterisation of a Metamorphic Terrane near Warmbad, Southern Namibia
Skeate (2014)	BSc Hons	Stellenbosch University	Characterisation of the Provenance of the Velloorsdrif Schist (Grünau Terrane)
Gordon (2014)	BSc Hons	Stellenbosch University	Characterisation of F_3 Fold Structures in the Grünau Terrane, Southern Namibia and Implications for Reworking of the D_2 Namaquan Orogeny
Bate (2014)	BSc Hons	McGill University	Development of quantitative measures of seismically-induced brittle fracture
Melosh (2015)	PhD	McGill University	Earthquake cycling in the brittle-plastic transition of a transform boundary: The Pofadder Shear Zone, Namibia and South Africa
Sehloho (2015)	BSc Hons	Stellenbosch University	Petrography and Structure of the Ai-Ais Igneous Suite Host Rocks, Southern Namibia
Muller (2015)	BSc Hons	Stellenbosch University	Petrographic, Geochemical and Geochronological Analysis of the Ai-Ais Complex, Southern Namibia
Bishop (2015)	BSc Hons	University of Cape Town	A snapshot of the early Cambrian mantle: petrogenesis and geochemical investigation of the Grünau intrusives, Southern Namibia
Angombe (2016)	MSc	Stellenbosch University	The lithostratigraphy and structural components of the Eureka Shear Zone, southern Namibia
Indongo (2017)	MSc	Stellenbosch University	The Lithological and Structural Characterisation of the Sperlingputs Shear Zone in Southern Namibia
Doggart (2018)	MSc	Stellenbosch University	Geochronology and Isotopic Characterisation of LCT Pegmatites from the Orange River Pegmatite Province
Iiyambo (2019)	BSc Hons	University of Namibia	Chemostratigraphic correlation of a Diamictite-Cap Carbonate Succession in the Port Nolloth Zone, northern Sperrgebiet, Southern Namibia
Joseph (2019)	BSc Hons	University of Namibia	Geological Mapping, Petrographic and Geochemical Study of the Tschaukaib Granitic Suite in Comparison to the Komsberg Suite, South West Namibia
Togarepi (2019)	BSc. Hons	University of Namibia	Geological mapping, geochemistry and petrographic characterization of metapelites of the Garub Group rocks, South-East of Lüderitz
Vaino (2019)	BSc. Hons	University of Namibia	The geochemical and petrological characterization of the Lüderitz meta-gabbro (1.9 Ga) in comparison with the Vuurdood gabbro in the Richtersveld Magmatic Arc, South West Namibia
Niemandt (2020)	BSc Hons	Stellenbosch University	Igneous Petrology of the Gannakouriep Dyke Swarm and its Metamorphic and Structural Overprint by the Gariep Orogeny
Shifotoka (2023)	MSc	University of the Western Cape	The Lüderitz Domain, Namaqua Natal Metamorphic Belt

Geoscience education in the classroom – a case study of the first Namibian Teachers' Workshop

Josephine Uushona* and Martin Hipangwa

Geological Survey of Namibia, Geoinformation Division, 6 Aviation Road, Windhoek
**Corresponding author: <Josephine.Uushona@mme.gov.na>*

Abstract :- Science teachers play a key role in developing future leaders in science and technology by fuelling the curiosity of students and encouraging further exploration into topics of interest. Thus, it is important that educators are equipped and supported with well-grounded strategies to develop and improve their teaching methods in science education. Multimodal literacy encompasses visual, auditory and tactile communication modes, allowing for multiple forms of representation to create meaning. In science education in particular, the use of different modes of teaching, such as the incorporation of scientific videos, posters, art work and field observations into the curriculum, generates interest and a broader outlook. To equip science teachers with the know-how of introducing multimodal literacy in their classrooms was the aim of a science teachers' workshop that took place from 3 to 4 October 2023 in Windhoek, hosted by the Geological Survey of Namibia.

Keywords :- Geoscience education, Multimodal literacy

To cite this report :- Uushona, J. and Hipangwa, M. 2024. Geoscience education in the classroom - a case study of the first Namibian Teachers' Workshop. *Communications of the Geological Survey of Namibia*, **27**, 110-114.

Introduction

Multimodal media convey meaning through an amalgam of visual, auditory and / or tactile elements to create understanding (Kress, 2010). For example, a poster conveys meaning through a combination of written language, images and spatial design. Each mode has its own specific function in the process of creating understanding, and on its own usually carries only part of the message (Kress, 2010). Thus, multimodal literacy refers to the ability to understand, interpret and create meaning through various communication modes, including but not limited to text, images, videos, sounds, as well as interactive components (University of Montevallo, 2023).

In education, particularly in the sciences, the concept of multimodal literacy takes into account that individuals process information in diverse ways, and that effective communication and teaching requires the employment of multiple modes to convey abstract ideas. Thus, empowering science teachers with multimodal literacy skills, that is the know-how to transfer knowledge in various innovative ways other than by means of the traditional textbook, is imperative for improving science education in Namibian classrooms. Diagrams, graphs, equations and tables are examples of representations that are crucial to the way meaning is created and communicated in science (Nielsen and Yeo, 2022). In addition, the introduction of practical activities and interactive elements, such as experiments and role plays, will enhance science teaching and learning.

Importance of Geoscience Education

Geoscience education centres on the study of the earth's physical characteristics, processes and systems, along with natural and human-induced events that influence them (King, 2008). This wide field encompasses disciplines such as geology, oceanography, meteorology, climatology, environmental science and more. As even young children naturally tend to exhibit curiosity about the physical world surrounding them, everyday occurrences like thunderstorms, as well as rarer events such as the occasional earth tremor,

serve as illustrations in practical earth science education.

The importance of geoscience education is multi-faceted, addressing critical societal challenges (e. g. environmental protection, climate change) and enhancing our understanding of the earth's processes expressed through natural phenomena such as for instance volcanic eruptions and earthquakes. It plays a vital role in promoting environmental consciousness, sustainable development and scientific literacy in general. Also, geoscience education in the classroom contributes to the training of future generations of geoscientists, policy makers, educators and informed citizens in general (King, 2008). Outreach programmes, science fairs, workshops and seminars, among others, are effective platforms to create a basis for understanding scientific concepts, and for developing critical thinking and problem-solving skills in the young generation, which extends beyond the mere acquisition of scientific knowledge.

Given the accelerating threats posed by climate change, environmental pollution and general ecological damage, there is a need to review mankind's role in the world of today. Not an easy task, this calls for a concerted effort from universities, research institutions, primary and secondary schools and all sectors of society to implement a new model of geoscience education, with a view towards promoting a harmonious coexistence with nature. Central to achieving this objective is the education of individuals from an early age, starting at home and continuing at school. Therefore, investing in the training of capable science teachers must be regarded as an obligation of high importance.

Geoscience Education in Namibia

The Namibian educational system embraces the use of multimodal literacy, with posters, graphs and diagrams displayed in classrooms, as part of existing lesson plans. From the outset, when Namibia gained its independence in 1990, its emphasis has been on assisting students to develop self-reliance and critical thinking (Kangumbu, 2005), including scientific thinking and practices, and to promote problem-solving capabilities (Vivante and Vedder-Weiss, 2022). Therefore, teachers' knowledge of scientific concepts and methods is crucial for students' learning and development (Vivante and Vedder-Weiss, 2022). As teachers are the key agents in implementing changes in the classroom - not only in geoscience education, it is imperative that they are enabled to engage in scientific debate at grassroot level in order to improve their professional competence and subsequently their teaching (Kangumbu, 2005).

Keeping in mind that earth science is not an explicit subject taught in Namibian schools or even part of teachers' training, the likelihood of introducing it formally in the school curriculum or in teachers' instruction in the near future is remote. However, there are other ways in which geoscience can be brought home to young learners through outreach programmes and public engagement activities. For more than a decade the Geo-Information Division of the Geological Survey of Namibia has engaged in science communication programmes to raise awareness of the importance of geoscience in schools and communities (Mocke and Mhopjeni, 2020) through hands-on-activities, posters, videos and presentations. In as much as diversity in learning practices adds interest to the school curriculum by nurturing pupils' natural curiosity, the Division also recognises the necessity of including teachers in its initiatives to further science education in the classroom.

Accordingly, the Geological Survey of Namibia recently embarked on a geoscience teachers' workshop programme by inviting teachers from around the country to learn about earth science and how to incorporate it into the existing curriculum. This initiative is a collaborative effort with the GEOBUS programme of the University of St Andrews, Scotland, and provides teachers with innovative ways of bringing earth science to their students, such as hands-on activities in the classroom.

2023 Geoscience Teachers' Workshop

This workshop marks a pioneering initiative, as the first in Namibia to focus exclusively on geoscience education - rather than a broader science perspective - for primary and secondary school teachers. The main objective of the two-day workshop was to enhance the teaching of earth science in schools by integrating geoscience principles into existing school curricula, and introducing educators to new communication modes with readily available resources (Table 1). Like many countries globally, Namibia does not have a stand-alone geoscience subject in its school syllabus; however, elements of geoscience are embedded within traditional subjects such as chemistry, geography, physical science and life science. Apart from explaining the theoretical background, the workshop aimed to present teachers with the practical tools and knowledge needed to creatively teach geoscience concepts within the existing framework. Geoscience-related subjects covered during the workshop encompassed chemistry, physics, environmental science, mathematics and agriculture (Fig. 1).

Figure 1. Theoretical and practical sessions during the Teachers' Geoscience Workshop held at the Geological Survey of Namibia, 3 – 4 October, 2023

The workshop concentrated on the science curriculum for grades 6 to 11 (age 12 – 17), addressing geoscience topics such as plate tectonics, volcanoes (forces, pressure and speed), earthquakes (forces, movement and plate tectonics), earth's structure (including magma flow), fluvial processes, mining (including mining economics) and the periodic table (highlighting the use of specific elements in communication technologies, i. e. smartphones). Each lesson also contained a practical component, allowing teachers to engage them-

selves in hands-on activities for a better understanding of the benefits of interactive teaching and learning practices, and the generation of new ideas to bring to their students.

No.	Materials used	Concepts explained
1	Cookies (e. g. chocolate chip cookies), paperclips, chopsticks, tweezers	Mining activities, including economic and environmental aspects
2	Effervescent tablet, water, glue, film canister, stopwatch	Volcanoes, pressure
3	Water, water bucket, food colourant	Plate tectonics
4	Baking flour, food colourant, water	Earthquakes, layering of soil and sediments
5	Boxes, elastic bands, spaghetti, chopsticks	Earthquakes, vibrational forces

Table 1. Experimental materials used in the workshop in explaining geoscientific concepts

Conclusions

The workshop's aims to promote geoscience education in Namibian primary and secondary schools were realised in so far as most of the twenty-three participating teachers went away inspired, motivated and eager to implement new teaching methods in their classrooms. The participants gained skills and insights on how to incorporate geoscientific concepts into the current curriculum and include interactive teaching modes in their lessons, in order to enhance both learning results and professional competency in educators. A survey was conducted after the workshop for the purpose of improving future similar exercises and gaining a better understanding of the limitations faced by Namibian school teachers (Figs 2, 3).

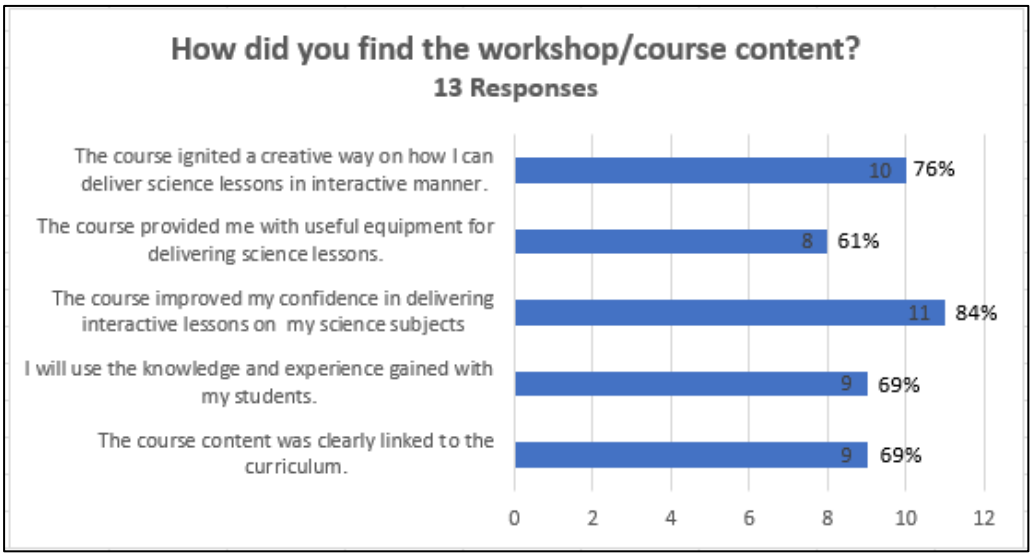

Figure 2. Teacher's response on workshop content

More than two thirds of the workshop participants found that the subjects covered were in line with the current curriculum and plan to incorporate the knowledge and experience acquired in their lessons, while nearly 85% stated that the workshop had heightened their confidence in teaching science subjects (Fig. 2). Still, despite special emphasis being placed on affordability in all experiments (Table 1), a considerable proportion professed their inability to obtain the required materials owing to lack of financial resources or standing of the school (Fig. 3).

Other comments and recommendations included the demand for this type of workshop being held on a regular basis to enable more teachers from around Namibia to discover the concept and benefits of multimodal literacy, the suggestion to extend the course to 3 or 4 days in order to cover a wider range of sub-

jects, and a request for greater emphasis being placed on environmental education. The overall success of the workshop can best be expressed by the acknowledgment of several of the participants that it succeeded in turning science from theory into practice, and making it more plausible to young students (and their teachers). Future plans include a proposal to take the workshop into all Namibian regions in turn, in order to reach more teachers and allow educators from remote rural areas to participate.

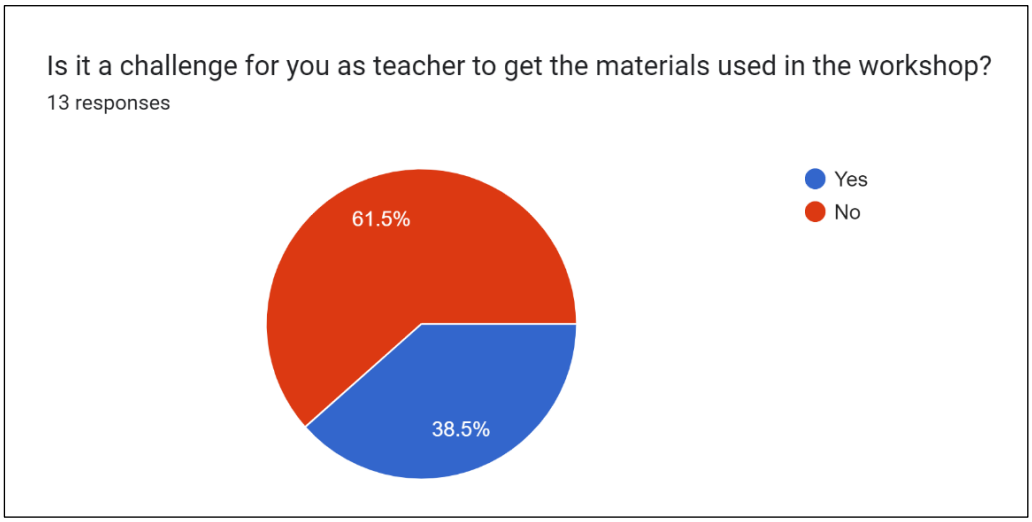

Figure 3. Teachers' response regarding the acquisition of materials used in the workshop

References

Kangumbu, M. 2005. Exploring Education Policy Transformation in Namibia in Terms of Democratic Change. Unpublished M.Sc. thesis, University of Namibia, Windhoek, 170 pp.

Kress, G. (2010). *Multimodality: a social semiotic approach to contemporary communication*. Routledge, London / New York. https://doi.org/10.4324/ 9780203970034

Mocke, H. and Mhopjeni, K., 2020. Twelve Years of Outreach at the Geological Survey of Namibia. *Communications of the Geological Survey of Namibia*, **22**, 116-134.

Nielsen, W. and Yeo, J. 2022. Introduction to the Special Issue: Multimodal Meaning-Making in Science. *Research and Science Education*, **52**, 751–754. https://link.springer.com/article/10.1007/s11165-022-10051-z

University of Montevallo. 2023. Keys to Communication: An Essential Guide to Communication in the Real World. *In*: *Communication in the Real World, An Introduction to Communication Studies*. https://pressbooks.pub/umcoms101/chapter/chapter-1-introduction-to-ommunication

Vivante, I. and Vedder-Weiss, D. 2023. Examining science teachers' engagement in professional development: A multimodal situated perspective. *Journal of Research in Science Teaching*, **60**, 1401–1430.

Namibia's IUGS Geological Heritage Sites

Ute Schreiber and Helke Mocke

Geological Survey of Namibia, 6 Aviation Road, Windhoek
<umschreiber@yahoo.com><helke.mocke@mme.gov.na>

Keywords :- Geoheritage

To cite this note :- Schreiber, U. and Mocke, H. 2024. Namibia's IUGS Geological Heritage Sites. *Communications of the Geological Survey of Namibia*, **27**, 115-119.

In 2021 the International Commission on Geoheritage of the International Union of Geological Sciences (IUGS) introduced a global programme for the nomination of Geological Heritage Sites (IGCP-731). According to IUGS, a Geological Heritage Site is a "key locality exhibiting geological elements and/or processes of international scientific relevance, used as a reference, and/or with a substantial contribution to the development of geological sciences through history" (https://iugs-geoheritage.org/selection-process). Under the slogan "The First 100" proposals were called for worldwide, requiring description, accurate location, geological significance and research history of the suggested sites, supported by suitable illustrations in the form of maps, sections, photographs or diagrams. Recognition as an IUGS Geological Heritage Site is expected to endorse its importance in demonstrating specific geological processes, ensure its preservation and protection in a changing - frequently endangered - environment, and promote geotourism through increasing its visibility in the public eye, with all attendant financial and environmental implications. The "First 100" were selected out of 181 entries from 56 countries by an international committee of geoscientists and announced on October 28, 2022, during the 60th Anniversary Meeting of the IUGS in Zumaia, Spain (Asrat *et al*., 2023). They are featured in a "coffee table" book entitled - predictably - "The First 100" (available here: www.iugsgeoheritage.org), which was designed to bring the wonders of geology and the forces that created them closer to an audience beyond the narrow circle of the geoscientific fraternity.

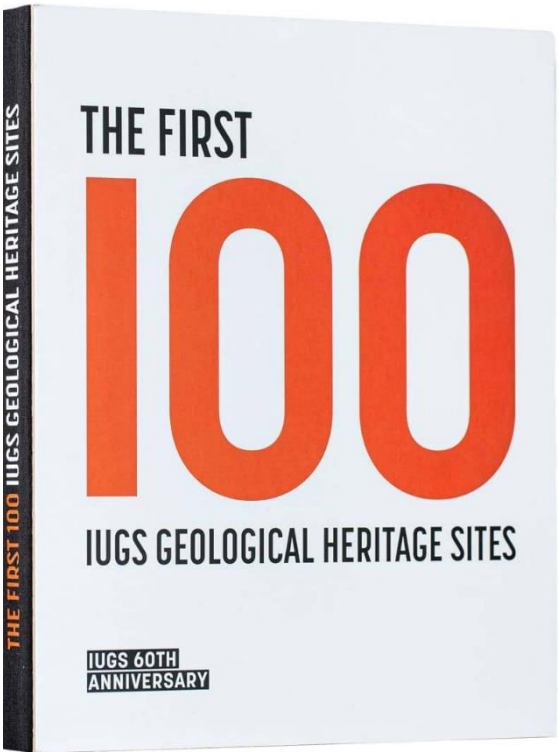

Namibia's "Top Three"

Among the Namibian sites considered for the "First 100" were such varied items as the unique Nama fossil assemblage belonging to the oldest metazoans on Earth, the well-preserved Marinoan glacial deposits of north-western Namibia, testifying to a global ice age during the mid-Neoproterozoic, the Fish River Canyon, as the second largest canyon of the world after the Grand Canyon of the Colorado, the world-renowned polymetallic Tsumeb ore deposit, the Namib Sand Sea, already distinguished as a UNESCO World Heritage Site since 2013, and the Spitzkoppen, a couple of distinct granitic inselbergs on the Namib Plains representing igneous activity during Gondwana break-up and the opening of the South Atlantic

Ocean. Coordinated by the Geological Survey of Namibia, four of them were eventually submitted to the IUGS selection committee.

When the results were known, Namibia had won three places amongst the "First 100", representing twenty percent of all selected sites from Africa - a notable achievement against tough competition from around the globe! The honours went to the Namib Sand Sea, the famous Tsumeb ore body and the glacial record of the Marinoan "snowball earth" (the order not reflecting on the relative importance or popularity of the selected sites).

With its many dune types, among them linear, transverse, star and barchan dunes, as well as rarer zibar and lace dunes (Miller, 2008), the Namib Sand Sea, extending between the Orange and Kuiseb River Deltas, well deserves the accolade of a "spectacular example for the geological and geomorphological development of a desert landscape". No less fascinating, at least to mineralogists and mineral collectors, is the now mined-out, polymetallic (lead, copper, zinc, silver, arsenic, antimony, cadmium, cobalt, germanium, gallium, iron, mercury, molybdenum, nickel, tin, tungsten and vanadium) Tsumeb ore body, a ~1800 m deep pipe-like palaeokarst feature filled with feldspathic sandstone within folded carbonate

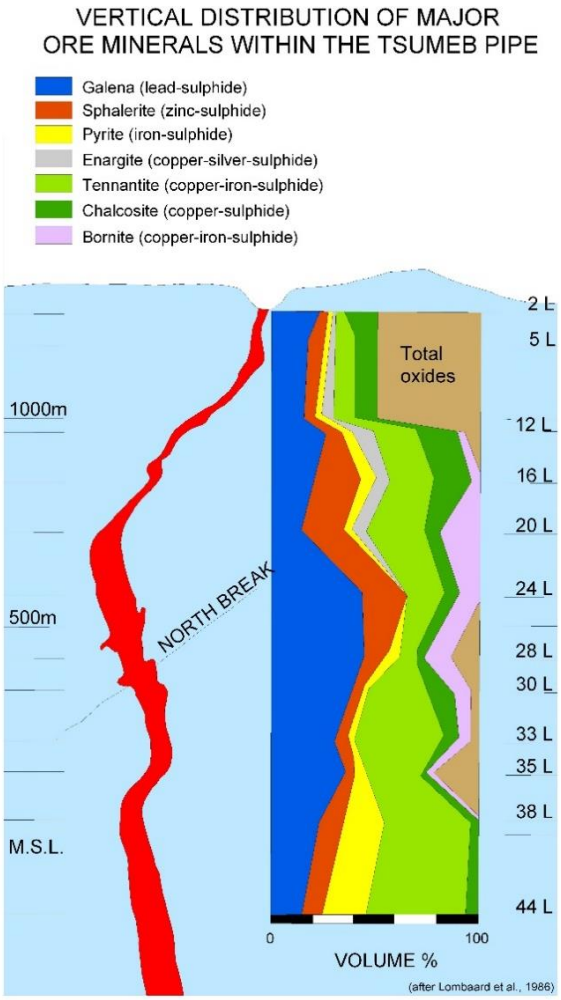

Look into the book: The Namib Sand Sea - Site 091 of "The First 100"

rocks of the Otavi Group (Lombaard *et al*., 1986). Well over 200 mineral types were recorded from Tsumeb over its hundred years or so of mine life, including several which have been found nowhere else. Indeed, minerals from Tsumeb grace many museum and private collections around the globe. Last but not least among Namibia's "Top Three" are the Marinoan glacial deposits of the Ghaub Formation (Otavi Group). The remarkable sedimentary features left by the ice bear witness to a worldwide ("snowball earth") glaciation around 635 million years ago, evidence of which can been found in the Neoproterozoic rock record throughout Namibia and around the world. Incidentally, this global ice age caused a dramatic sea-level fall of 400 m and an equal post-glacial rise (Hoffman and Halverson, 2008), which, projected into today's world, would gradually have inundated much more than just coastal cities and plains.

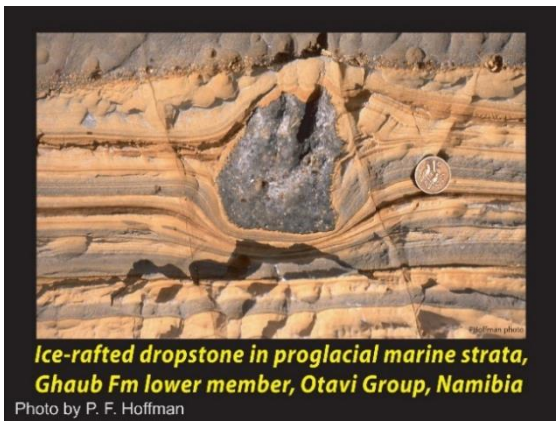

The Next Stage

Recognising that "The First 100" scarcely do justice to the geodiversity of Planet Earth, IUGS quickly followed up with a call for proposals for "The Second 100". By September 2023 there were 174 candidate sites from 64 countries - among them 23 "newcomers" - to be reviewed. The decision of the selection committee, composed of 89 international experts covering all geoscientific fields, will be announced in August 2024 during the 37th International Geological Congress in Busan, Republic of Korea. With luck, it may include Namibia's postponed candidate from the first round and / or a couple of new proposals (i. e. the singular Nama fossil assemblage, the impressive Fish River Canyon and the awe-inspiring Etosha Pan) – which, however, is not to say that they stand back behind the IUGS's choices for "The First 100" in either geological significance or natural grandeur!

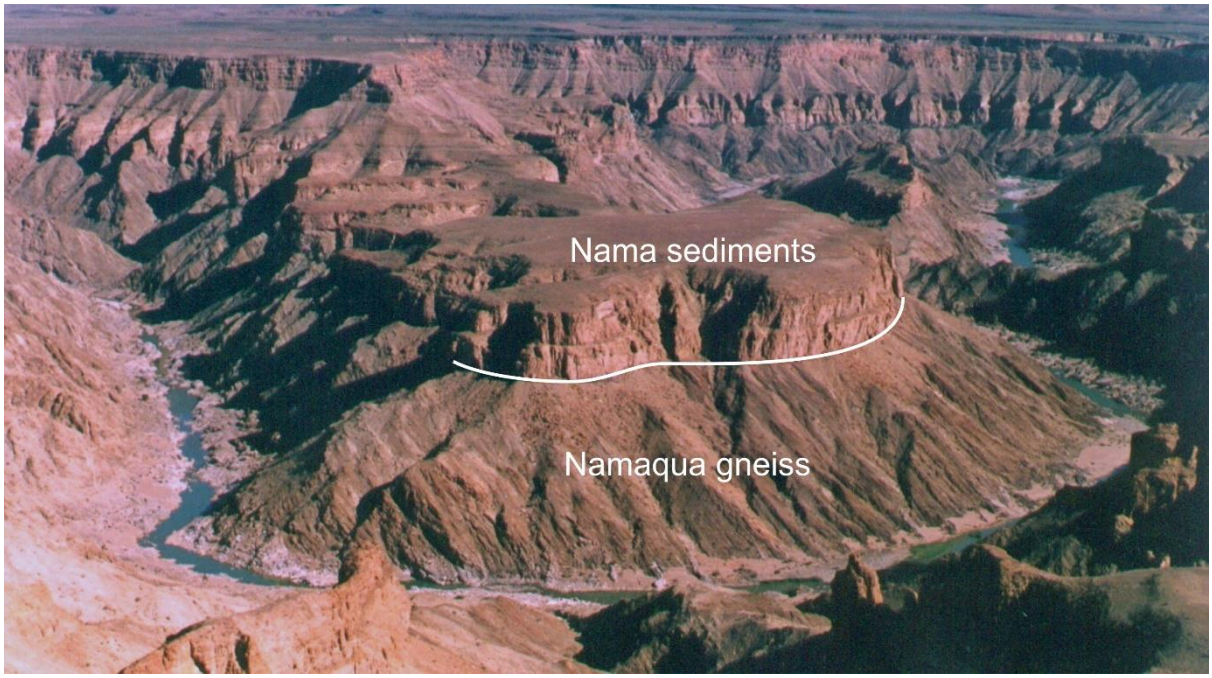

View of the Fish River Canyon from Hobas lookout point, southern Namibia

The 50 km long and 160 to 550 m deep Fish River Canyon, whose walls expose flat-lying late Precambrian Nama sediments unconformably overlying strongly deformed gneisses of the Mesoproterozoic Namaqua Metamorphic Complex, already is one of Namibia's top destinations not only for the geotourist, while the Nama fossils hold a unique place in the evolution of life. Considered older even than the South Australian Ediacara Fauna for which the terminal period of the Precambrian era was named, they encompass an exceptional suite of late Neoproterozoic fossil organisms including soft-bodied metazoans in sheet sandstones, calcified fossils in thrombolitic and stromatolitic reef complexes, distinctive Ediacaran trace fossils and a typical assemblage of terminal Proterozoic microfossils (Grotzinger and Miller, 2008). Last but not least among the new submissions is the ~4760 km^2 large Etosha Pan which - although it covers only a fraction of Pliocene "Lake Etosha" - is still one of the largest palaeolakes in the world, with a well-preserved and diverse fossil fauna from snails to mammoth tusks (Pickford *et al*., 2014).

There remains to be seen how this IUGS programme and its publications, which hope to bring the geological legacy bequeathed to mankind by its home planet to the notice – and appreciation - of a wider public, and save it from destruction through population growth and industrialisation, among other threats, is received. If expectations are fulfilled, we may soon be looking at "The Third 100" – with more candidates from Namibia such as the intricate Naukluft Mountains and Nappe Complex, the Permo-Triassic succession of Mount Etjo and Waterberg with its fine record of fossil tetrapods (Mocke *et al*., 2023) or the massive Hoba Meteorite that, while not of this Earth, has become part of earth history.

Nama fossils (photos: M. Meyer)

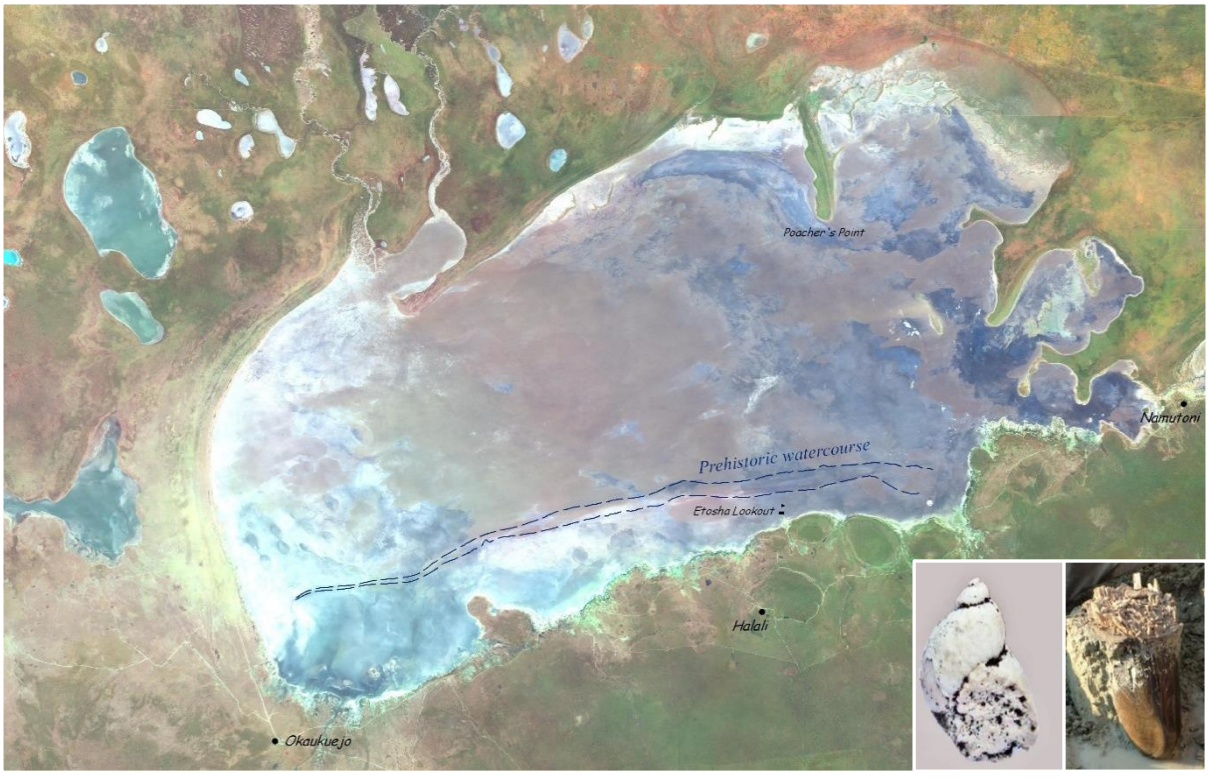

Landsat 5 image of the Etosha Pan (NASA-USGS); insets: Pleistocene landsnail (left) and mammoth tusk (right)

References

Asrat, A., Hilario, A. and Vegas, J. 2023. African Contribution to the IUGS First 100 Geological Heritage Sites. *Abstracts 29th Colloquium of African Geology*, Windhoek, Namibia, 220.

Grotzinger, J. and Miller, R. McG. 2008. Nama Group. *In*: Miller, R.McG. (Ed.). *The Geology of Namibia*, Vol. **2**, chapter 13, 229-272. Geological Society of Namibia, Windhoek.

Hoffman, P. F. and Halverson, G. P. 2008. Otavi Group of the western Northern Platform, the Eastern Kaoko Zone and the western Northern Margin Zone. *In*: Miller, R.McG. (Ed.). *The Geology of Namibia*, Vol. **2**, chapter 13, 69-136. Geological Society of Namibia, Windhoek.

Lombaard, A. F., Günzel, J. I. and Kruger, T. L. 1986. The Tsumeb lead-zinc-silver deposit S.W.A./Namibia. *In*: Anhaeusser, C.R. and Maske, S. (Eds), *Mineral Deposits of southern Africa*, Vol. **2**, 1761 - 1787. Geological Society of South Africa, Johannesburg.

Miller, R. McG. 2008. Namib Group. *In*: Miller, R. McG. (Ed.). *The Geology of Namibia*, Vol. **3**, chapter 25, 66 pp. Geological Society of Namibia, Windhoek.

Mocke, H. B., Kammerer, C. F., Smith, R. M. H. and Marsicano C. A. 2023. The first record of late Permian tetrapods from Namibia. *Palaeontologia africana*, **56**,133–141.

Pickford, M., Senut, B., Hipondoka, M., Person, A., Ségalen, L., Plet, C., Jousse, H., Mein, P., Guérin, C., Morales, J. and Mourer-Chauviré, C. 2014. Mio-Plio-Pleistocene geology and palaeobiology of the Etosha Pan, Namibia. *Communications of the Geological Survey of Namibia*, **15**, 16-68.